# Evaluation of the Dopaminergic System Using In Vivo PET Imaging and Post-Mortem Analyses in the Context of Mild Neurodegenerative and Neuroinflammatory PD Models

Pauline Roost

université PARIS-SACLAY

# EVALUATION OF THE DOPAMINERGIC SYSTEM USING IN VIVO PET IMAGING AND POST-MORTEM ANALYSES IN THE CONTEXT OF MILD NEURODEGENERATIVE AND NEUROINFLAMMATORY PD MODELS

**Thèse de doctorat de l'université Paris-Saclay**

École doctorale n°568, signalisations et réseaux intégratifs en biologie (Biosigne)
Spécialité de doctorat: Sciences de la vie et de la santé
Unité de recherche : Neurodegenerative Diseases Laboratory, UMR9199, MIRCen, CEA
Référent : Faculté des sciences

**Thèse présentée et soutenue à Le Kremlin Bicêtre, le 22/06/2020, par**

**Pauline ROOST**

## Composition du Jury

| | |
|---|---|
| **Michael SCHUMACHER**<br>Research director, UMR1195 | Président |
| **Sylvie CHALON**<br>Research director, Inserm U1253 Imagerie et cerveau | Rapportrice & Examinatrice |
| **Michel KOOLE**<br>Associate professor, Nuclear Medicine & Molecular Imaging, KU Leuven | Rapporteur & Examinateur |
| **Alexandra PETIET**<br>Researcher, ICM - UMR1127 | Examinatrice |
| **Veronique SGAMBATO**<br>Researcher, University Claude Bernard Lyon I - UMR 5229 | Examinatrice |
| **Philippe HANTRAYE**<br>Research director, MIRCen, DRF, CEA | Directeur de thèse |
| **Nadja VAN CAMP**<br>Researcher, MIRCen, DRF, CEA | Co-directrice de thèse |
| **Abhay PANDIT**<br>Research director, National University of Ireland Galway | Examinateur invité |

Thèse de doctorat

NNT : 2020UPASS086

# Acknowledgements / Dankwoord

There are multiple people that I would like to thank for their involvement in the process of my PhD research.

First of all, I would like to thank Nadja, who, as my direct supervisor, stood by me during this whole journey. I am very thankful for all the help and guidance you provided me with during the past three years, not only on a scientific level, but also personal. In short, I am very glad to have had you as my supervisor.

Next, I would like to thank everybody in MIRCen that directly or indirectly was involved in my research projects or my social life: Merci tout le monde! I would particularly like to thank: *Philippe and Emmanuel, who gave me the upportunity to be involved in the BrainMatTrain project, and who gave import scientific insights on my projects. *Marie-Laure and Cecile, for answering all my questions asked in bad French, big or small. *Martine and Mylène, for all their help with the animal experimentation. *Leopold, for all the hours we spent locked up together in the PET zone. *Didier, there is not many people who are happy when you tell them things are broken/missing (and you want a replacement 3D-printed), and for helping with all the IT problems. *Caroline and Pauline G., for answering all my question regarding histology, troubleshooting, and even helping with some of the experiments. *Marie-Claude, for sharing all your knowledge about RT-qPCR with me, but also for all scientific insights and discussions. *Anastasie, Camille, Miriam, and Mathilde, for all the great times we had talking in the office, about science and life in general. *Francesco, for surviving the last three years together, both in the lab and at home. It was hard and challenging at times, but we have both made it. I am very happy we have taken this journey together. **To all of you I say: I could not have done this without you! MERCI!

I would also like to thank all people involved in the BrainMatTrain program: ESRs, supervisors, and managers. We had great scientific interactions, but also spent great social time together all over Europe.

Next, there is some people outside MIRCEN I would like to thank: Thomas and Henriette, for trying to teach me French. Didier, Fabian, Nadya, and Lucia, for all the fun we had at dance class. YRLS boards 2019 & 2020, for showing me how international Paris can be, and how fun it is to organise big events.

Daarnaast zijn er natuurlijk ook nog een hele hoop mensen in Nederland die ik graag wil bedanken. Allereerst mijn ouders die mijn keuze om naar het buitenland te gaan voor mijn werk en opleiding altijd gesteund hebben. Bedankt voor al jullie morele steun, vooral tijdens de laatste periode van schrijven, en natuurlijk alle fysieke hulp iedere keer als ik weer ging verhuizen. Ook de rest van de familie wil ik graag bedanken voor de morele steun, maar ook dat jullie gezellig op bezoek zijn gekomen in Parijs om in mijn nieuwe leven te delen.

Lieve Mieke en Leonie, ook jullie steun heb ik hard nodig gehad de afgelopen jaren. Ik ben jullie dankbaar dat jullie nog niet hebben opgegeven en dat we nog altijd vriendinnen zijn ondanks de lange afstand. Ik ben blij met alle keren dat jullie me zijn komen opvrolijken in Parijs en alle uren die we samen achter de laptop doorgebracht hebben om te videobellen.

Als laatste: Marco. De afgelopen drie jaar ben je mijn steun en toeverlaat geweest. Ik ben heel erg blij met alle tijd die we samen hebben mogen doorbrengen in Parijs, maar in het vervolg blijf ik toch maar wat dichter in de buurt. Je t'aime.

**BEDANKT, THANK YOU, GRAZIE, DANKE, TACK, OBRIGADA, GRACIAS, MULTUMESC, BEDANKTJ, MERCI!**

## Niet-wetenschappelijke samenvatting

De ziekte van Parkinson (PD) is de op één na meest voorkomende ziekte waarbij hersencellen vergaan. PD wordt gekenmerkt door opeenhoping van het α-synucleïne eiwit, een progressief verlies van de dopamine-producerende neuronen en de aanwezigheid van ontstekingen in de neurale cellen.

In dit proefschrift heb ik het effect geëvalueerd van α-synucleïne aggregatie en milde neurale ontsteking op dopamine-neuronen in diermodellen van PD. Hiervoor heb ik een nucleaire beeldvormingtechniek gebruikt (positron emissie tomografie (PET)), en *post-mortem* analyses om de genen en eiwitten te evalueren in deze modellen.

Ik heb aangetoond dat gemuteerd α-synucleïne een gematigde maar progressieve dood van dopamine-neuronen veroorzaakt, gepaard gaande met een lichte ontstekingsreactie. Anderzijds heb ik aangetoond dat milde ontsteking van neurale cellen niet tot verlies van dopamine-neuronen leidt. PET beeldvorming visualiseerde het functionele gebrek van de dopamine neuronen, wat niet mogelijk was met de *post-mortem* analyses. Dit laat het belang van PET beeldvorming zien bij het bepalen van neuronaal verlies in diermodellen van PD.

## Non-scientific summary

Parkinson's disease (PD) is characterised by the aggregation of α-synuclein, a progressive loss of the dopamine-producing neurons, and the presence of neuroinflammation

During my PhD studies, I evaluated the impact of α-synuclein aggregation and moderate neuroinflammation on dopaminergic neurons in animal models of PD. To this end, I have used a nuclear imaging method, positron emission tomography (PET), and *post-mortem* analyses to assess the expression of different genes and proteins in these models.

I have demonstrated that mutated α-synuclein induces mild progressive death of dopamine neurons, coupled with a weak inflammatory response. Conversely, mild neuroinflammation did not lead to loss of dopamine neurons. PET imaging showed functional damage to the dopamine neurons, which was not detectable by *post-mortem* analyses. This highlights the crucial interest PET imaging to better characterise neurodegeneration in animals models of PD.

## Résumé non scientifique

La maladie de Parkinson (MP) est caractérisée par l'agrégation de l'α-synucléine, la perte des neurones qui synthétisent la dopamine (neurone DA), et une inflammation cérébrale. Pendant ma thèse, j'ai évalué les effets de l'α-synucléine et de l'inflammation modérée sur les neurones DA dans des modèles animaux de la MP. J'ai utilisé une méthode d'imagerie nucléaire, la tomographie d'émission de positons (TEP) et des analyses post mortem évaluant l'expression de différents gènes et protéines dans ces modèles.

J'ai démontré que l'α-synucléine mutée induit une mort des neurones DA, et une faible réponse inflammatoire. À l'inverse, l'inflammation modérée n'entraîne pas la mort de ces neurones. Dans les deux cas, la TEP montre de plus des atteintes fonctionnelles des neurones DA, qui ne sont pas détectées par les analyse post mortem, soulignant l'intérêt crucial de cette méthode non invasive pour mieux caractériser la dégénérescence dans les modèles animaux de la MP.

# Table of Contents

# List of Abbreviations

## List of Abbreviations

| | |
|---|---|
| **2T** | Two-tissue |
| **6-ODHA** | 6-hydroxydopamine |
| **AADC / DDC** | Aromatic L-amino acid decarboxylase or DOPA decarboxylase (DDC) |
| **ALDH1A1** | Aldehyde dehydrogenase |
| **ATP** | Adenosine triphosphate |
| **BBB** | Blood brain-barrier |
| **BPnd** | Binding potential |
| **CNTF** | Cytokine ciliary neurotrophic factor |
| **COR** | C-terminal of ROC |
| **DAT / Slc6a3** | Dopamine transporter |
| **DOPAC** | 3,4-Dihydroxyphenylacetic acid |
| **DOPAL** | 3,4-dihydroxyphenylacetaldehyde |
| **dpi** | Days post injection |
| **GFAP** | Glial fibrillary acidic protein |
| **IBA1** | Ionized calcium-binding adapter molecule 1 |
| **IL-1** | Interleukin 1 |
| **IL-6** | Interleukin 6 |
| **ITGAM / CR3** | Integrin alpha M or complement receptor 3 (CR3) |
| **LID** | Levodopa-induced dyskinesia |
| **LPS** | Lipopolysaccharide |
| **LRRK2** | Leucine-rich repeat kinase 2 |
| **MDMA** | 3,4-methylenedioxymethamphetamine or Ectasy |
| **MFB** | Medial forebrain bundle |
| **MOA-B** | Monoamine oxidase-B |
| **MPDP+** | 1-methyl-4-phenyl-2,3-dihydropyridinium |
| **MPP+** | 1-methyl-4-phenylpyridinium |
| **MPPP** | 1-methyl-4-phenyl-4-propionoxypiperidine |
| **MPTP** | 1-methyl-4-phenyl-1,2,3,6-tetrahydropyridine |
| **MRI** | Magnetic resonance imaging |
| **mRNA** | Messenger ribonucleic acid |
| **MRTM** | Multilinear reference tissue model |

| | |
|---|---|
| **NAC** | Non-amyloid component |
| **PBS** | Phosphate buffered saline |
| **RT-qPCR** | Real time quantitative Polymerase chain reaction |
| **PD** | Parkinson's disease |
| **PET** | Positron Emission Tomography |
| **PFA** | Paraformaldehyde |
| **PINK1** | PTEN homolog-induced novel kinase 1 |
| **PTEN** | Phosphatase and tensin |
| **rAAV** | Recombinant adeno-associated viral vector |
| **ROC** | Ras of complex |
| **ROS** | Reactive oxygen species |
| **siRNA** | Small interfering RNA |
| **SNr** | Substantia nigra reticulata |
| **SNpc** | Substantia nigra pars compacta |
| **SRTM** | Simplified reference tissue model |
| **STR** | Striatum |
| **TH** | Tyrosine hydroxylase |
| **TLR4** | Toll-like receptor 4 |
| **TNFα** | Tumour necrosis factor alpha |
| **TSPO / PBR** | 18 kDa translocator protein or peripheral benzodiazepine receptor (PBR) |
| **VMAT2** | Vesicular monoamine transporter 2 |
| **VTA** | Ventral tegmental area |
| **STN** | Subthalamic nucleus |
| **GPe** | External globus pallidus |
| **GPi** | Internal globus pallidus |
| **PH** | Phenylalanine hydroxylase |
| **COMT** | Catechol-O-methyltransferase |
| **HVA** | Homovanillic acid |
| **GBA1** | Glucocerebrosidase |
| **GWAS** | Gene-wide association study |
| **MAPT** | microtubule associated protein tau |
| **MSA** | Multiple system atrophy |
| **DLB** | Dementia with Lewy Bodies |
| **DR** | Dopamine receptor |
| **SNCA** | Synuclein alpha |

| | |
|---|---|
| **GTPCH1** | Guanosine triphosphate cyclohydrolase-1 |
| **GDNF** | Glial-derived neurotropic factor |
| **fVM** | Fetal ventral mesencephalon |
| **ESC** | Embryoic stem cell |
| **iPSC** | Induced pluripotent stem cell |
| **MSC** | Mesenchymal stem cells |
| **SEM** | Standard error of the mean |
| **wpi** | Weeks post-injection |
| **WT** | Wild-type |
| **CW** | Clockwise |
| **CCW** | Counter-clockwise |
| **RPM** | Rotations per minute |

# 1

# *GENERAL INTRODUCTION*

# 1. Characteristics of PD

Parkinson's disease (PD) affects 2-3% of the population over 65 years of age, resulting in over 10 million patients worldwide, which makes it the second most common neurodegenerative disorder (Poewe *et al.*, 2017). The mean age of onset of PD is 55 years of age, and the prevalence increases with age (Dauer and Przedborski, 2003). PD was named after James Parkinson, who was the first to describe the "paralysis agitans" in his essay from 1817 (Parkinson, 2002).

PD is a progressive neurological disorder that mainly affects the motor system. PD is characterised by tremor at rest, freezing, impaired balance, rigidity (passive stiffness), bradykinesia (slowness of movement), hypokinesia (reduction in amplitude of movement), akinesia (absence of unconscious movements), and stooped figure (Parkinson, 2002; Dauer and Przedborski, 2003; Cooper and Van Raamsdonk, 2018). These are displayed as hypomimia (reduction in facial expressions), hypophonia (reduced voice volume), dysarthria (speech problems), dysphagia (difficulty swallowing), micrographia (small handwriting) and slow handwriting, drooling, and smaller stride length (Dauer and Przedborski, 2003; Broadfoot *et al.*, 2019). Apart from motor symptoms, PD often also affects mental state; e.g. passiveness (lack of initiative), apathy, depression, anxiety, bradyphrenia (slowed cognitive processes), and dementia (Dauer and Przedborski, 2003; Cooper and Van Raamsdonk, 2018). Other symptoms include hyposmia (reduced smell), incontinence, constipation, and rapid eye movement sleep disorder (Cooper and Van Raamsdonk, 2018; Kouli, Torsney and Kuan, 2018). These non-motor symptoms can already start as early as 12-14 years before diagnosis, which defines the prodromal phase (Postuma *et al.*, 2012). With such a diversity of symptoms, PD is a very heterogeneous disease; many symptoms can be part of PD. A clinical diagnosis is based on bradykinesia in combination with a resting tremor or rigidity. Additionally, an asymmetric onset and responsiveness to levodopa differentiates PD from other parkinsonian syndroms (Kouli, Torsney and Kuan, 2018).

Nowadays, PD is described as a disease with slow progressive neurodegeneration which starts years before diagnosis. PD implicates multiple neuro-anatomical areas. It results from a combination of genetic and environmental factors, and manifests with a broad range of symptoms (Kalia and Lang, 2015).

The prodromal phase of PD is particularly interesting from a therapeutic standpoint. During the prodromal phase non-motor symptoms present themselves, but no clinical diagnosis can currently be made (Figure 1), diagnosis is only made when quantifiable motor- symptoms appear. Better detection and characterisation may help to start appropriate neuroprotective therapies at this early stage.

It is believed that at time of diagnosis already between 30% (Rizek, Kumar and Jog, 2016) and 50% (Fearnley and Lees, 1991), and even up to 80% (DeMaagd and Philip, 2015; Sveinbjornsdottir, 2016), of the dopaminergic neurons in the nigro-striatal pathway have perished, combined with 80% reduction of striatal dopamine levels (Marsden, 1990; Fearnley and Lees, 1991). Clinical diagnosis of PD is especially difficult in the early stages (de Lau and Breteler, 2006), this can delay a diagnosis for several years until symptoms of functional disability develop (Abbasi Gharibkandi and Hosseinimehr, 2019).

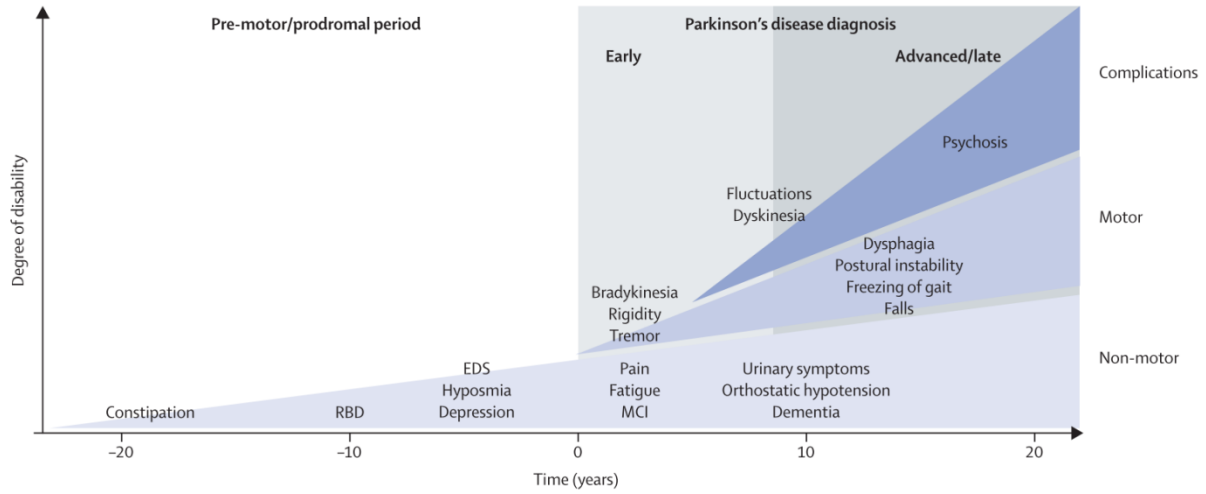


**Figure 1: Clinical symptoms and time course of PD progression. Diagnosis of PD occurs with the onset of motor symptoms, but can be preceded by a prodromal phase of over 20 years. EDS=excessive daytime sleepiness, MCI=mild cognitive impairment, RBD=REM sleep behaviour disorder. Figure from (Kalia and Lang, 2015).**

## 1.1 Dopaminergic signalling

### 1.1.1 Basal ganglia circuitry

The basal ganglia are best known for their role in motor functions (Bartels and Leenders, 2009), although they also play a role in goal-directed behaviours (DeLong and Wichmann, 2010; Haber, 2014).

The basal ganglia are a collection of interconnected subcortical nuclei. They include the striatum, substantia nigra, globus pallidus, and subthalamic nucleus (Figure 2). The substantia nigra has two separate nuclei; the GABAergic pars reticulate (SNr), and the dopaminergic pars compacta (SNpc). The dopaminergic neurons of the substantia nigra pars compacta project primarily to the striatum. The striatum is the main input structure of the basal ganglia and receives projections from the cerebral cortex, brainstem, and thalamus. The subthalamic nucleus (STN) is glutamatergic and is located between the two parts of the globus pallidus (external (GPe) and internal segments (GPi)). The subthalamic nucleus is the secondary input structure, receiving input from the cerebral cortex. The activity at the corticostriatal synapses is regulated by dopamine release from the terminals of the substantia nigra pars compacta (DeLong and Wichmann, 2010; Haber, 2014).

There are two main types of dopamine receptors

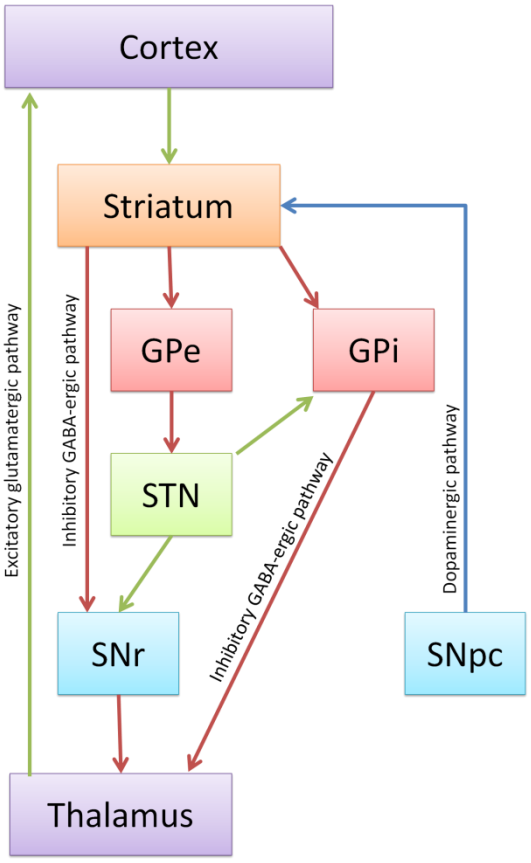


**Figure 2: Schematic representation of the basal ganglia. Exhitatory glutamatergic pathways are shown in green, and inhibitory GABA-ergic pathways in red. Dopaminergic pathways are shown in blue. GPe = globus pallidus external, GPi = globus pallidus internal, STN = subthalamic nucleus, SNr = substantia nigra reticulata, SNpc = substantia nigra pars compacta. (adaptation of *Basal ganglia diagram*, 2013)**

in the striatum; $D_1$-like and $D_2$-like receptors, their activation causing opposing effects on the basal ganglionic output. Activation of the $D_1$-like receptors by dopamine results in increased activity of the direct pathway (striatum → Gpi/SNr), leading to inhibition of GPi/SNr output neurons, and consequently to increased thalamocortical neuronal activity. Activation of the $D_2$-like receptors leads to activation of the indirect pathway; striatum → GPe → STN → thalamus, leading to disinhibition of GPi/SNr output neurons, and ultimately to greater inhibition of thalamocortical neuronal activity (DeLong and Wichmann, 2010).

### 1.1.2 Dopamine physiology

Dopamine synthesis starts in the liver, directly from tyrosine (non-essential amino acid) or indirectly from phenylalanine (essential amino acid). L-phenylalanine is converted into L-tyrosine by phenylalanine hydroxylase (PH), and tyrosine is subsequently transported into the dopaminergic neurons in the brain via an active transport mechanism. In the brain, L-tyrosine is converted into L-3,4-dihydroxyphenylalanine (L-DOPA or levodopa) through hydroxylation at the phenol ring by tyrosine hydroxylase (TH). L-DOPA is subsequently converted into 3,4-dihydroxyphenethylamine (dopamine) through decarboxylation by aromatic-L-amino acid decarboxylase (AADC; also known as DOPA decarboxylase) in the pre-synaptic terminal (Musacchio, 1975; Zahoor, Shafi and Haq, 2018).

Dopamine is metabolised after reuptake into dopaminergic neurons or glial cells. Dopamine undergoes oxidative deamination by monoamine oxidase (MAO) to produce reactive aldehyde 3,4-dihydroxyphenylacetaldehyde (DOPAL). DOPAL, in turn, is converted into 3,4-dihydroxyphenylacetic acid (DOPAC) by aldehyde dehydrogenase (ALDH) (Eisenhofer, Kopin and Goldstein, 2004). DOPAC is then degraded by the catechol-O-methyl transferase (COMT) into biologically inactive homovanillic acid (HVA) (Zahoor, Shafi and Haq, 2018).

## 1.2 Hallmarks of PD and Physiopathology

As mentioned above, Parkinson's disease is a progressive neurodegenerative disease with early prominent death of the dopaminergic neurons in the substantia nigra pars compacta (Kalia and Lang, 2015). Nevertheless, other main hallmarks of PD are the presence of Lewy bodies and inflammation.

### 1.2.1 Dopaminergic neurodegeneration

The loss of dopaminergic neurons in the substantia nigra pars compacta is the most prominent neuropathological hallmark of PD (Pienaar, Götz and Feany, 2010). The nigrostriatal dopaminergic pathway is more affected than any other (Cadet and Brannock, 1998), which is believed to stem from the sensitivity to oxidative stress (Guo *et al.*, 2018) and high density of microglial cells (Kim *et al.*, 2000). The neuronal loss within the substantia nigra pars compacta decreases the dopamine signalling in the striatum, which leads to the motor symptoms of PD (Cooper and Van Raamsdonk, 2018). However, in later stages of the disease, neurodegeneration also occurs in many other brain regions, including locus ceruleus, raphe nucleus, amygdala, and hypothalamus (Ikeda et al., 1978; Dickson, 2012), affecting cholinergic, serotonergic, and noradrenergic neurotransmitter systems (Pienaar, Götz and Feany, 2010).

### 1.2.2 Lewy pathology

In 1912 Friedrich Lewy discovered protein aggregates in brain regions outside the substantia nigra in PD patients. Later, in 1919, Konstantin Tretiakoff found similar aggregates in the substantia nigra and named them after Lewy (Trétiakoff, 1919); Lewy bodies when in the cell body, and Lewy neurites when in the processes of neurons. However, Lewy pathology is not solely restricted to the brain, but can also affect the spinal cord and peripheral nervous system (Beach *et al.*, 2010). It took until 1997 before it was discovered that the main component of Lewy bodies is α-synuclein (see 1.3.1, page 17) (Spillantini *et al.*, 1997); in a misfolded state α-synuclein becomes insoluble and aggregates (Kalia and Lang, 2015).

Lewy aggregates also contain various other proteins (including tau), amongst which some are linked to familiar forms of PD; i.e. leucine-rich repeat kinase 2 (LRRK2), parkin, ubiquitin, and UCH-L1 (Wakabayashi *et al.*, 2007). Interestingly, Lewy pathology is not always found in the brains of patients with rare genetic forms of PD, such as parkin-related PD, and non-G2019S mutated LRRK2-related PD (Poulopoulos, Levy and Alcalay, 2012).

In PD patients, Lewy bodies are commonly found in brain regions susceptible to neurodegeneration, and although generally accepted that they cause this neurodegeneration, there is also a movement suggesting that they are protective of neurodegeneration (Olanow *et al.*, 2004). It is thought that toxic α-synuclein aggregates are separated in Lewy bodies, and that they promote their degradation (Olanow *et al.*, 2004; Tanaka *et al.*, 2004). In support of this theory, *in vitro* studies have shown that cell death can precede Lewy body formation (Tompkins and Hill, 1997; Saha *et al.*, 2000). Moreover, neurons have been described as having a healthier morphology when containing Lewy bodies (Terry, 2000), and no evidence was found to support association between either Lewy body distribution or density and dopaminergic cell loss (Parkkinen *et al.*, 2011).

### 1.2.3 Inflammation

Another hallmark of PD is the presence of neuroinflammation; i.e. microglial activation, increased astrocyte and lymphocyte infiltration, and the presence of pro-inflammatory cytokines (Glass *et al.*, 2010).

Microglia are the resident innate immune cells of the brain, and play a major role in inflammatory processes. In a healthy brain they reside in a resting state that is characterized by a ramified morphology, while continuously monitoring the brain environment (Nimmerjahn, Kirchhoff and Helmchen, 2005; Glass *et al.*, 2010). In response to inflammation, microglia are activated and adopt an amoeboid morphology (Nimmerjahn, Kirchhoff and Helmchen, 2005; Cho *et al.*, 2006).

Astrocytes are abundantly present in the brain and play a role in homeostasis, provide trophic support neurons, and regalute synapses. Activated microglia can induce reactive astrocytes via secretion of pro-inflammatory cytokines (i.e. interleukin (IL)-1α, tumor necrosis factor α (TNFα), and complement component 1, q subcomponent (C1q). Reactive astrocytes lose their beneficial role in brain homestasis and instead can induce neurodegeneration (Liddelow *et al.*, 2017).

In 1988, McGeer and colleagues described for the first time the presence reactive microglia in the brains of PD patients (McGeer *et al.*, 1988). Damiar and colleagues reported an increase in glutathione peroxidase-containing cells (a subset of glial cells) surrounding the surviving dopaminergic neurons, which was inversely correlated with the amount of neuronal loss (Damier *et*

*al.*, 1993). Nagatsu and colleagues (2000) measured increased levels of various cytokines in the striatum (e.g. TNFα, IL-1β) (Nagatsu *et al.*, 2000). Finally, also activated astrocytes have been reported to accompany the Lewy pathology (Braak, Sastre and Del Tredici, 2007).

Today, it is generally believed that the immune system plays an active role, and that the neuroinflammation in PD might not only be a consequence of the ongoing neurodegeneration as initially hypothesised (Tansey and Goldberg, 2010; Cabezudo, Baekelandt and Lobbestael, 2020). However, the interplay between cytokines, neurodegeneration, and protein aggregation as cause or consequence remains largely unknown (de Lau and Breteler, 2006; Glass *et al.*, 2010; Tansey and Goldberg, 2010). One possibility is that neuronal death and the subsequent release of protein aggregates induces microglial activation. Indeed, α-synuclein can cause microglial activation, and eventually leed to a positive feedback-loop of neurodegeneration and neuroinflammation (reviewed by Roodveldt, Christodoulou and Dobson, 2008). On the other hand, the multiple hit hypothesis suggests an interaction between multiple genetic and/or environmental risk factors, including an inflammation component, is needed to trigger PD pathology (Cabezudo, Baekelandt and Lobbestael, 2020).

It is also under debate if presence of inflammatory cells is protective or deleterious. On one hand, astrocytes can protect against entry by inflammatory cells through borders or scars; on the other hand, astrocytes may also have strong pro-inflammatory potential (reviewed by Sofroniew, 2015).

## 1.3 Causes of PD / Aetiology

Parkinson's disease is a multifactorial disease (Semchuk, Love and Lee, 1993), meaning that both genetic and environmental factors play a role. The biggest risk factor for PD is age (Van Den Eeden *et al.*, 2003; Kalia and Lang, 2015; Kouli, Torsney and Kuan, 2018), with a mean age of onset of 55 years (Dauer and Przedborski, 2003). PD seems to be more prevalent in men than in women (Van Den Eeden *et al.*, 2003; de Lau and Breteler, 2006). Additionally, PD is more prevalent in Europe and the Americas, as compared to Africa, Asia, and Arabia (Van Den Eeden *et al.*, 2003; Kalia and Lang, 2015). Apart from a genetic predisposition, also environmental or occupational exposure to certain substances, as well as life style choices, can affect the risk for PD (Kalia and Lang, 2015).

### 1.3.1 Genetic

About 15% of the parkinsonian cases have a family history of PD (Deng, Wang and Jankovic, 2018). To date 23 loci have been linked to PD, termed PARK1 to PARK23. There are both autosomal dominant and recessive mutations, while some mutations are considered risk factors rather than causative (Deng, Wang and Jankovic, 2018). Even though these monogenic forms of PD are less common, the same cellular pathways are involved as in multifactorial cases (Cooper and Van Raamsdonk, 2018).

#### Dominant mutations in SNCA/PARK1/PARK4

The first gene mutation (A53T) to cause monogenic PD was discovered in 1997 in the SNCA/PARK1/PARK4 gene, which encodes α-synuclein (Polymeropoulos *et al.*, 1997). Multiple other point mutations (A53T, A53E, A30P, E46K, H50Q, G51D) (Krüger *et al.*, 1998; Zarranz *et al.*, 2004; Appel-Cresswell *et al.*, 2013; Kiely *et al.*, 2013; Proukakis *et al.*, 2013; Pasanen *et al.*, 2014) and even

duplication and triplication (Singleton et al., 2003; Chartier-Harlin et al., 2004) have now been linked to autosomal dominant PD. These mutations or increased protein expression make α-synuclein more prone to aggregation (Kalia and Lang, 2015). An overview of the use of SNCA (mutations) to model PD is discussed later on page 26. SNCA-related PD is relatively rare (Kalia and Lang, 2015), nonetheless, it led to the discovery of α-synuclein as a major component of Lewy bodies and Lewy neurites (Spillantini *et al.*, 1997). Even so, the exact function of α-synuclein remains unknown.

The primate (including human) α-synuclein sequence differs from other vertebrates by a substitution of Alanine for a Threonine at position 53 (A53T) (Hamilton, 2004). Human α-synuclein has 140 amino acids, encoded by six exons, and has three main domains; an N-terminal domain which adopts an α-helical structure upon binding to cellular membranes, a median domain called non-amyloid component (NAC) which is normally folded as an α-helix, and an acidic non-folded C-terminal domain (Snead and Eliezer, 2014; Bobela, Aebischer and Schneider, 2015). All the domains have their own roles and are essential for the structure of the protein (Snead and Eliezer, 2014). α-Synuclein is abundantly present presynaptically (Maroteaux, Campanelli and Scheller, 1988), and is thought to modulate synaptic vesicle function (Kahle *et al.*, 2002).

### Mutations in LRRK2/PARK8

The most frequent cause of monogenic PD is a mutation in the LRRK2/PARK8 gene, encoding for leucine-rich repeat kinase 2 (LRRK2). There are at least eight different pathogenic mutations in the LRRK2 gene (Kalia and Lang, 2015); of which the G2019S substitution is the most common (Healy *et al.*, 2008). LRRK2 is normally localised in membranes (Jackson-Lewis, Blesa and Przedborski, 2012), and while its normal function is not clear, there seems to be a link with mitochondria (reviewed in Winklhofer and Haass, 2010). Additionally, it is thought to be involved in neurite outgrowth (Kalia and Lang, 2015), synaptic morphogenesis (Lee *et al.*, 2012), vesicle trafficking (Sanna *et al.*, 2012), autophagy (Kalia and Lang, 2015), and protein synthesis (Kalia and Lang, 2015). Moreover, LRRK2 is highly expressed in immune cells and has been functionally linked to pathways pertinent to immune cell function, such as cytokine release, autophagy and phagocytosis (Dzamko and Halliday, 2012; Wallings and Tansey, 2019). The LRRK2 gene codes for a large protein (2527 amino acids) in the ROCO family; formed by a core signalling region (Ras of complex (ROC) and C-terminal of ROC (COR) domains) and protein-protein interaction domains (e.g. leucine-rich repeats, and WD40 domains) (Li, Tan and Yu, 2014). Interestingly, most of the disease causing mutations are localised within the catalytic domains (ROC/COR/Kinase) of LRRK2 (Healy *et al.*, 2008). The G2019S mutation leads to increased kinase activity (Kalia and Lang, 2015). The use of LRRK2 mutations to model PD will be discussed later in this chapter (page 27). For a detailed review of the putative interplay between LRRK2 and α-synuclein, the reader is referred to Cresto and colleagues (2018).

### Autosomal recessive genes

The autosomal recessive forms of PD typically have an earlier onset than classical PD (Schrag and Schott, 2006), and most are linked to mitochondrial homeostasis (McCoy and Cookson, 2012). Both homozygous and compound heterozygous mutations in these genes might result in autosomal recessive PD (Kalia and Lang, 2015).

Mutations in the PRKN/PARK2/Parkin gene (Kitada et al., 1998) account for almost half of the early-onset familial cases of PD (Lücking et al., 2000; Jackson-Lewis, Blesa and Przedborski, 2012), and there are over 100 mutations known for the Parkin gene (Lücking et al., 2000), most of which are

loss-of-function (Konnova and Swanberg, 2018). Parkin is involved in the ubiquitin proteasome system as an E3 ubiquitin ligase (Shimura et al., 2000; Zhang et al., 2000).

The gene for phosphatase and tensin (PTEN) homolog-induced novel kinase 1 (PINK1/PARK6) is the second most commonly mutated in early-onset PD (Konnova and Swanberg, 2018). Similar to Parkin, PINK1 mutations are recessive, and lead to loss-of-function (Dawson, Ko and Dawson, 2010). PINK1 is normally localised in the mitochondria (Silvestri et al., 2005), where it recruits Parkin and increases its ubiquination activity and induces Parkin-mediated mitophagy (Lazarou et al., 2013), which is a process to eliminate damaged mitochondria (Kalia and Lang, 2015).

DJ-1 is a redox sensitive molecular chaperone (Moore, Dawson and Dawson, 2006), whose mutations play a role in early-onset PD (Bonifati *et al.*, 2003); causing loss of function (Macedo *et al.*, 2003; Moore *et al.*, 2003). DJ-1 plays a role in the inhibition of α-synuclein aggregation (Shendelman *et al.*, 2004). It is expressed widely throughout the whole body, and localised in the cytosol and mitochondria (Zhang *et al.*, 2005).

#### Genetic risk factors

The biggest genetic risk factor for PD is a mutation in the GBA1 gene (Migdalska-Richards and Schapira, 2016). GBA1 mutations have reduced penetrance, thus do not cause a Mendelian form of PD, however, they can increase the risk for PD 20-30 fold (Sidransky *et al.*, 2009; Migdalska-Richards and Schapira, 2016). About 30% of GBA1 mutation carriers develop PD before the age of 80 (Migdalska-Richards and Schapira, 2016).

GBA1 encodes for β-glucocerebrosidase, a lysosomal enzyme (Beutler, 1992). Bi-allelic mutations that results in greatly reduced glucocerebrosidase enzyme activity lead to Gaucher disease, an autosomal recessive lysosomal storage disorder (Hruska *et al.*, 2008; Stoker, Torsney and Barker, 2018). Roughly 10% of patients with type 1 Gaucher disease develop PD before the age of 80 (Rosenbloom *et al.*, 2011), compared to 3-4% in the normal population (Stoker, Torsney and Barker, 2018).

In a genome-wide association study (GWAS) in PD patients, the SNCA and microtubule-associated protein tau (MAPT) locus were identified as major risk factors for PD (Simon-Sanchez *et al.*, 2009; Bandres-Ciga *et al.*, 2020). The MAPT locus has two major haplotypes, of which the MAPT*H1* haplotype is associated with an increased risk for PD. This could be due to haplotype-specific differences in expression or alternative splicing of MAPT transcripts, which can affect cellular functions at different levels, and ultimately increase PD susceptibility (Billingsley *et al.*, 2018).

In a recent GWAS around 37,700 PD patients and 1.4 million million controls were used to identify 90 independent risk factors associated with PD (Nalls *et al.*, 2019; Bandres-Ciga *et al.*, 2020).

### 1.3.2 Environmental contributors & Lifestyle

In 1983 1-methyl-4-phenyl-1,2,3,6-tetrahydropyridine (MPTP) was described to be the cause of a parkinsonian-like state of a small group of patients after injection as by-product of a designer drug (also see paragraph 2.2, page 24) (Langston *et al.*, 1983; Langston, 2017). Since it was shown that parkinsonism can be caused by a toxin, the idea arose that nigral dopaminergic neurodegeneration could also be caused by other environmental toxins (Kouli, Torsney and Kuan, 2018).

### Pesticides

Investigation of a French cohort revealed a positive association between PD and the overall use of professional pesticides, with a dose effect for the number of years used. They observed a particularly strong relation between PD and the use of organochlorine insecticides (Elbaz *et al.*, 2009). One example of an organochlorine is dieldrin, which has been shown to deplete brain dopamine levels in several animal species and increase dopamine transporter (DAT) binding in the striatum (Kanthasamy *et al.*, 2005). Additionally, a positive relationship has been shown between PD and the professional use of rotenone (mitochondrial complex I inhibitor), paraquat (inducer of oxidative stress), and other herbicides (Semchuk, Love and Lee, 1993; Tanner *et al.*, 2011).

### Heavy metals

The implication of heavy metals in PD etiology is highly debated, with several studies demonstrating relationships (Cheng *et al.*, 2015), while others do not (Jiménez-Jiménez *et al.*, 1992; Semchuk, Love and Lee, 1993; Meamar *et al.*, 2016). Of the heavy metals, iron and copper are thought to induce oxidative stress, which might underlie neuronal death (Ball *et al.*, 2019). As such, both iron and copper have been demonstrated to accelerate α-synuclein aggregation (Uversky, Li and Fink, 2001). Lead, which can cross the blood-brain barrier by mimicking calcium channels, can cause neuronal loss (Caudle *et al.*, 2012). Lastly, mercury is a neurotoxin that can cause neuronal death, however, its association with PD is still debated (Ball *et al.*, 2019).

The dietary intake of these heavy metals was found to be unrelated to PD prevalence (Mariani *et al.*, 2013). In contrast, occupational exposure to these heavy metal shows increased associated with PD (Gorell *et al.*, 1997; Coon *et al.*, 2006; Lin *et al.*, 2011)

### Lifestyle

Both cigarette smoking (Hernán et al., 2002; Ritz et al., 2007; Noyce et al., 2012; Breckenridge et al., 2016) and coffee drinking (Ascherio et al., 2001; Hernán et al., 2002; Noyce et al., 2012) have been linked to reduced incidences of PD.

It is still unclear why cigarette smoking is associated with a reduced risk of PD. One explanation is that the activation by nicotine of nicotinic acetylcholine receptors on the dopaminergic neurons are neuroprotective (Kouli, Torsney and Kuan, 2018), which has been shown in animal models (Bordia *et al.*, 2015). However, in a clinical trial there was no indication that nicotine could relieve PD symptoms (Wood, 2017). Alternatively, it could be that PD itself reduces smoking behaviour (Ritz *et al.*, 2014; Kouli, Torsney and Kuan, 2018); the reduction of dopamine levels in PD patients could make them less susceptible for addictive behaviours (Ritz *et al.*, 2014; Kouli, Torsney and Kuan, 2018). This hypothesis is supported by research showing that prodromal and PD patients had greater ease in giving up smoking compared to controls (Ritz et al., 2014). Interestingly, a significant decrease of nicotinic acetylcholine receptors was observed in the striatum and substantia nigra of PD patients that was not correlated with disease severity (Kas *et al.*, 2009).

For caffeine, as for nicotine, the exact pathway and causative roll of caffeine still need to be shown (Kouli, Torsney and Kuan, 2018). Also caffeine did not relieve clinical symptoms in PD patients in a clinical trial (Wood, 2017). Furthermore, there seemed to be marked differences between the effects in men and women; women show a weaker inverse relation between coffee and PD. This could be explained by the fact that oestrogen competitively inhibits caffeine metabolism (Ascherio *et al.*, 2004; Kouli, Torsney and Kuan, 2018).

## 1.4 Disease progression and α-synuclein spreading

### Dual hit-theory

Braak, Del Tredici and colleagues (2003) published on the temporal and spatial spreading of Lewy pathology in PD and recognized six different stages (Figure 3). In stage 1 the peripheral nervous system, olfactory system, and medulla are affected, followed by the pons and spinal cord grey matter in stage 2. Next, in stage 3, the midbrain –including the SN pars compacta-, basal forebrain, and amygdala display Lewy pathology, which spreads further to the rest of the limbic system, thalamus, and temporal cortex in stage 4. In stage 5 and 6 multiple cortical regions show Lewy pathology (Braak, Del Tredici, *et al.*, 2003; Kalia and Lang, 2015). These brain pathological stages seem to correspond to the clinical symptoms of PD: in stages 1 and 2 pre-motor symptoms occur, in stage 3 motor features appear due to nigrostriatal dopamine deficiency, and stages 4–6 correspond to the non-motor symptoms of advanced PD (Kalia and Lang, 2015). While the Braak theory initially proposes a viral pathogen as initiator of PD pathology, it has been shown that peripherally administered rotenone (an environmental toxin, also see page 19 and page 141) can induce sequential α-synuclein accumulation, inflammation, and motor dysfunction (Pan-Montojo *et al.*, 2010).

Braak, Rüb and colleagues (2003) have subsequently suggested that the stereotypic pattern of PD primarily affects cell types with a disposition for Lewy pathology; specifically, projection neurons with long, thin, incomplete or poorly myelinated axons (but not long sturdily myelinated or short-axoned nerve cells) (Braak, Rüb, *et al.*, 2003; Visanji *et al.*, 2013). It is not known why these specific neuronal types are more susceptible, and why neighbouring regions with similar cell types remain unaffected (Visanji *et al.*, 2013).

In a subsequent paper these authors hypothesized that PD might originate in the gut, and from there spread towards the brain (Braak, Rüb, *et al.*, 2003). A few years later, the dual hit-theory emerged, which states that the neurotrophic pathogen enters the brain via two routes; 1) nasal, with anterograde progression into the temporal lobe, and 2) gastric, secondary to swallowing of nasal secretions in saliva (Hawkes, Del Tredici and Braak, 2009). The nasal route would explain the early involvement of olfactory structures and the olfactory dysfunction that is often seen in early PD (Hawkes, Del Tredici and Braak, 2009). Lewy pathology has been observed in several olfactory structures, as well as projection neurons connected to the olfactory epithelium (Daniel and Hawkes, 1992; Braak, Del Tredici, *et al.*, 2003). A revised theory by Lerner and Bagic (2008) suggests not only anterograde, but also retrograde spreading of PD (Lerner and Bagic, 2008).

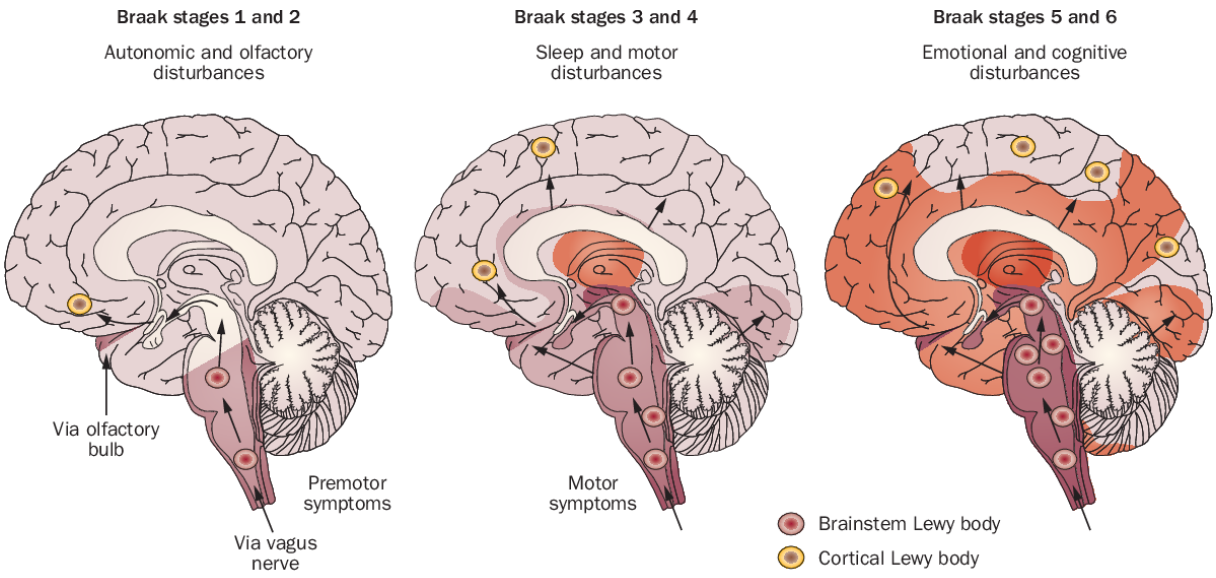


**Figure 3: Braak staging in PD patients. First the peripheral nervous system, olfactory system, and medulla are effected, followed by the pons and spinal cord grey matter. In stage 3/4 the midbrain –including the SN pars compacta-, basal forebrain, and amygdala display Lewy pathology, which spreads further to the rest of the limbic system, thalamus, and temporal cortex. In stage 5 and 6 multiple cortical regions show Lewy pathology. Figure from (Doty, 2012).**

### The gut-brain axis

In support of the theory that the gut is one of two places of origin of PD, Lewy pathology has been found throughout the gastrointestinal tract of patients (Wakabayashi *et al.*, 1988; Beach *et al.*, 2010; Shannon *et al.*, 2012). Moreover, PD patients often display non-motor symptoms related to the gastrointestinal tract (Visanji *et al.*, 2013); gastrointestinal dysfunction is common already in the early stages of PD (Pfeiffer, 2003), or even in the prodromal stages (Abbott *et al.*, 2001). The nerve cells of the gastrointestinal tract share the same vulnerabilities to Lewy pathology as the central nervous system, and could thus propagate Lewy pathology to the central nervous system via the vagal preganglionic fibres (Visanji *et al.*, 2013). In support of this, suggestive evidence was found for a potential protective effect of severing the vagal nerve against PD in humans (Svensson *et al.*, 2015; Liu *et al.*, 2017).

Additionally, dysbiosis of the gut microbiome is linked to the prodromal phase of PD. The gut microbiome is crucial for function, metabolism, and energy cycles, but it can have a neurological effect through metabolite production or the gut-brain axis. However, the specific link between the gut microbiome and PD is not clear yet (Scheperjans, Derkinderen and Borghammer, 2018; Dutta *et al.*, 2019; Yang *et al.*, 2019). Diet robustly impacts the gut microbiome; the Western diet is associated with an increased risk for PD, while the Mediterranean diet is associated with a reduced risk (Jackson *et al.*, 2019). Interestingly, the PD microbiome is associated with increased levels of lipopolysaccharide (paragraph 2.3, page 25) (Jackson *et al.*, 2019). It is hypothesised that the observed gastrointestinal permeability in PD patients could lead to increased levels of LPS in the blood, which in turn could cause neuroinflammation and ultimately neurodegeneration (Brown, 2019).

### Prion hypothesis

Lewy body-like inclusions have occasionally been found within grafted neurons after transplantation of embryonic mesencephalic neurons into the putamen of PD patients (Kordower,

Chu, Hauser, Freeman, *et al.*, 2008; Kordower, Chu, Hauser, Olanow, *et al.*, 2008; Li *et al.*, 2008). These findings suggested that Lewy body pathology can propagate from host to graft cells (Li *et al.*, 2008). Indeed, several groups have shown that injection of brain homogenates containing α-synuclein aggregates or synthetic α-synuclein fibrils into the brain of wild-type model animals led to α-synuclein pathology (Luk *et al.*, 2012; Recasens *et al.*, 2014; Shimozawa *et al.*, 2017; Melki, 2018). Based on these and other observations it is now widely believed that aggregated α-synuclein propagates and amplifies in a prion-like manner (Brundin, Melki and Kopito, 2010; Chen *et al.*, 2018; Melki, 2018).

Like in prion diseases, there is mulitple separate diseases characterised by pathological α-synuclein deposits, e.g. multiple system atrophy (MSA), dementia with Lewy Bodies (DLB) and PD. Experiments have shown differences in seed characteristics and seeding activity between patient brain extracts, which supports the hypothesis that MSA, DLB, and PD are caused by different α-synuclein strains (Figure 4), which have different functional properties, including tropism for different cell types or toxicity (Melki, 2018; Jaunmuktane and Brandner, 2019).

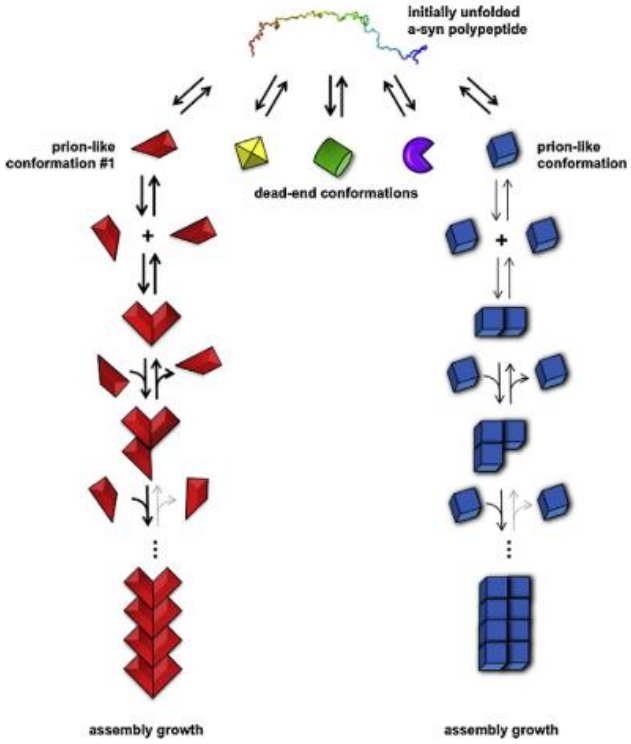


**Figure 4: Schematic representation of prion-like mechenisms for α-synuclein. α-synuclein can adopt mulitpe conformations, some of which are capable of interaction with molecules of the same conformation. These can form stable inter-molecular interactions and create assemblies that are structurally well-denined with highly specific bonds. (Figure from Melki, 2018)**

### Functional threshold theory

Zaccai and colleagues (2008) suggest that α-synuclein pathology does not follow Braak staging in around half of all PD cases (Zaccai *et al.*, 2008), indicating that Braak staging is not the only pattern of spreading for α-synuclein pathology. In fact, more recently, a different theory has emerged; the functional threshold theory (Engelender and Isacson, 2017). This theory accounts better for the neurobiology of PD symptoms since it is based on the evidence of simultaneous degeneration of the central and peripheral nervous systems (Engelender and Isacson, 2017).

This theory revolves around different vulnerabilities of brain regions, each having an individual threshold for PD pathology (e.g. α-synuclein abundance); more sensitive areas will show earlier signs of dysfunction as compared to more resistant areas. Some areas have a larger functional reserve and can compensate better for the pathology, while others will succumb and present Lewy pathology and ultimately neurodegeneration (Engelender and Isacson, 2017).

## 2. PD models

Even though, as described above, some important discoveries have been done on human samples, PD autopsy material is rare and precious. Animal models allow for study of different aspects of the disease, and explore both disease progression and evaluate possible treatment strategies. The biggest advantage however, is the possibility to study the prodromal phase with the use of slowly progressive models. At the moment, there is still no perfect model available that mimics all pathological aspects of PD. The current available models can be broadly divided in four types; 1) pharmacological models, 2) toxin-based models, 3) PD hallmark-based models, and 4) genetic-based models. A more extensive review on different animal models in PD, ranging from non-mammalian to non-human primates, can be found in the Additional Readings – Animal models of PD (page 135).

### 2.1 6-hydroxydopamine

The most-used toxin-based PD model is the 6-hydroxydopmine (6-OHDA) model, which is widely used in rodents (Ungerstedt, 1968; Thiele, Warre and Nash, 2012; Stott and Barker, 2014), pigs (Christensen *et al.*, 2018) (Table 1). 6-OHDA is an analogue of dopamine and norepinephrine (Dauer and Przedborski, 2003; Konnova and Swanberg, 2018) and is taken up preferentially by dopaminergic and noradrenergic transporters, resulting in relative cell selective toxicity (Javoy *et al.*, 1976; Jonsson, 1980). 6-ODHA-induced toxicity is caused by its accumulation in the cytosol, where it generates reactive oxygen species (ROS), inhibits mitochondrial complex I, and inactivates biological macromolecules (Cadet and Brannock, 1998; Konnova and Swanberg, 2018). A major down-side of 6-OHDA is its hydrophilic state, which makes it unable to cross the blood brain barrier, and thus requires direct injection into the brain (Dauer and Przedborski, 2003; Jackson-Lewis, Blesa and Przedborski, 2012; Jagmag *et al.*, 2016).

6-OHDA injections in the substantia nigra (pars compacta) and medial forebrain bundle (MFB) lead to rapid and complete dopaminergic neurodegeneration (Jeon, Jackson-Lewis and Burke, 1995; Cadet and Brannock, 1998; Dauer and Przedborski, 2003; Jagmag *et al.*, 2016). Striatal injections induce progressive retrograde neuronal death in the substantia nigra and ventral tegmental area (Berger, Przedborski and Cadet, 1991; Sauer and Oertel, 1994). These dopaminergic lesions are dose-dependent (Kyono *et al.*, 2011). 6-OHDA is generally injected unilaterally, since bilateral injections carry a high mortality rate (Jackson-Lewis, Blesa and Przedborski, 2012; Konnova and Swanberg, 2018). Unilateral models allow the use of the contralateral side to serve as an internal control.

### 2.2 MPTP

The neurodegenerative properties of 1-methyl-4-phenyl-1,2,3,6-tetrahydropyridine (MPTP) were first discovered in 1983 as a by-product of a designer drug (1-methyl-4-phenyl-4-

propionoxypiperidine (MPPP)) by Dr. Langston (although a single case was reported previously (Davis *et al.*, 1979)). The patients intoxicated by MPTP presented many parkinsonian motor symptoms, including rigidity, slowness of movement, postural instability, and freezing, and several non-motor symptoms, like facial seborrhoea and mild cognitive deficits. Furthermore, they all reacted to levodopa and some developed levodopa-induced dyskinesia (LID) (Davis *et al.*, 1979; Langston *et al.*, 1983; Dauer and Przedborski, 2003; Langston, 2017). PET imaging using a L-DOPA analogue (Fluorodopa, also see 4.4.2, page 40) suggested damage to the nigrostriatal pathway (Calne *et al.*, 1985). *Post-mortem* analyses showed a destruction of the substantia nigra in all cases, and a Lewy body-like inclusion in the first case only (Davis *et al.*, 1979; Langston *et al.*, 1999).

MPTP is a lipophilic compound, which can cross the blood-brain barrier. In the brain it is taken up by astrocytes (Ransom *et al.*, 1987), where monoamine oxidase-B (MAO-B) (Heikkila *et al.*, 1984) converts it to 1-methyl-4-phenyl-2,3-dihydropyridinium (MPDP+) (Dauer and Przedborski, 2003; Jagmag *et al.*, 2016; Konnova and Swanberg, 2018), followed by spontaneous oxidation into highly toxic 1-methyl-4-phenylpyridinium (MPP+) (Dauer and Przedborski, 2003). Once released by the astrocytes through organic cation transporter 3 (Cui *et al.*, 2009), MPP+ is selectively taken up by dopaminergic cells through dopamine transporter (DAT) (Javitch *et al.*, 1985), where it accumulates in the cytoplasm, binds to vesicular monoamine transporter 2 (VMAT2), and accumulates in the mitochondria (Dauer and Przedborski, 2003). Once inside the mitochondria, MPP+ blocks mitochondrial complex I (Nicklas, Vyas and Heikkila, 1985), leading to reduced ATP production, increased oxidative stress, neuro-inflammation, and ultimately cell death (Konnova and Swanberg, 2018).

MPTP is a powerful tool to model PD in both mice (Mori *et al.*, 1988) and non-human primates (Burns *et al.*, 1984; Langston, Langston and Irwin, 1984) (Table 1). Rats are resistant to MPTP toxicity (Giovanni *et al.*, 1994; Pienaar, Götz and Feany, 2010; Jagmag *et al.*, 2016; Konnova and Swanberg, 2018), as the conversion from MPTP to MPP+ occurs at the blood brain barrier in rats, preventing great influx into the brain (Riachi, LaManna and Harik, 1989; Langston, 2017). The MPTP model is the gold-standard in PD non-human primate research (Jackson-Lewis, Blesa and Przedborski, 2012; Konnova and Swanberg, 2018); it shows a striking loss of dopaminergic neurons in the substantia nigra pars compacta (Burns *et al.*, 1984), though not the ventral tegmental area (VTA) (Jacobowitz *et al.*, 1984). Additionally, relocation of α-synuclein into aggregates in the cell body has been observed in non-human primates (Forno *et al.*, 1986; Kowall *et al.*, 2000; but not mice: Jagmag *et al.*, 2016).

## 2.3 Lipopolysaccharide

As described above a hallmark of PD is the presence of neuro-inflammation (alinea 1.2.3, page 16). Lipopolysaccharide (LPS) is found on the outer membrane of gram-negative bacteria, being released physiologically as outer membrane vesicles and upon destruction of the bacteria (Brown, 2019). LPS is a potent inducer of inflammation both in peripheral tissues as well as the central nervous system via the activation of toll-like receptor 4 (TLR4), which results in NF-κB transcriptional activation of hundreds of inflammatory genes, including pro-inflammatory cytokines such as TNFα, IL-6 and pro-IL-1β (Kempuraj *et al.*, 2016; Brown, 2019). Intracerebral administration of LPS locally activates pro-inflammatory microglia and astrocytes; microglia are activated directly through interaction with TLR4, while astrocytes can also be induced indirectly through brain pro-inflammatory factors expressed by microglia (Liddelow *et al.*, 2017).

Prolonged neuroinflammation can lead to loss of dopaminergic neurons, which has been shown both *in vitro* and *in vivo* (Choi *et al.*, 2009; Khan *et al.*, 2019; Wang *et al.*, 2020). However, the dose and target region of LPS are critical factors for the outcome of the neuro-inflammatory response, thus introducing a great heterogeneity in applied experimental protocols (Table 1) (Lopes, 2016; Batista *et al.*, 2019). Generally, LPS injection is performed unilaterally in the striatum or in the substantia nigra inducing an acute and localised neuroinflammation within 24 hours that lasts up to 4 weeks (Choi *et al.*, 2009; Flores-Martinez *et al.*, 2018). Intracerebral LPS doses vary from 1µg (Pottier *et al.*, 2017; Sridharan *et al.*, 2017) to 5-10 µg (Choi *et al.*, 2009; Flores-Martinez *et al.*, 2018), and even up to 50µg (Ory *et al.*, 2015, 2016). Reports range from no observed dopaminergic neuronal loss (Hoban et al., 2013) to progressive nigrostriatal degeneration (Choi *et al.*, 2009; Deng *et al.*, 2020).

Intranigral LPS injection eventually leads to dopaminergic cell loss in the substantia nigra, albeit that different time courses have been described (Sharma and Nehru, 2015; Flores-Martinez *et al.*, 2018; Deng *et al.*, 2020). The LPS-induced inflammatory reaction in the substantia nigra is stronger than in the striatum (Herrera et al., 2000; Hoban et al., 2013), which is partly attributed to the fact that the substantia nigra has the highest concentration of microglia in the brain (Lawson et al., 1990). A study found that activated microglia express dopaminergic receptors ($D_1$-$D_4$) (Mastroeni et al., 2009), while others found that dopamine itself can modulate cellular functions of both resting-state and activated microglial cells (Fan et al., 2018), which could explain the selective vulnerability of dopaminergic neurons in PD. A reduction of extracellular dopamine concentration, following TH inhibition, was indeed shown to prevent intranigral LPS-induced activation of microglial, and loss of TH immunostaining (De Pablos et al., 2005). Additionally, human macrophages were found to express mRNA for all subtypes of dopaminergic receptors ($D_1$-$D_5$), and cytokine production in macrophages is modulated by dopamine (Gaskill et al., 2012).

**Table 1: Overview of the main toxin-based animal models for PD. This table is a simplified overview, showing the most commen uses of the models: also time window studied, dosage, and other factors can influence the pathology in the animal models. SN = substantia nigra, MFB = medial forebrain bundle, STR = striatum. (1)** (Ungerstedt, 1968; Berger, Przedborski and Cadet, 1991; Jeon, Jackson-Lewis and Burke, 1995; Maia *et al.*, 2012; Thiele, Warre and Nash, 2012). **(2)** (Burns *et al.*, 1984; Langston, Langston and Irwin, 1984; Mori *et al.*, 1988; Belloli *et al.*, 2017)**. (3)** (Hoban *et al.*, 2013; Ory *et al.*, 2015; Lopes, 2016; Flores-Martinez *et al.*, 2018; Batista *et al.*, 2019)**.**

| | Animal species | | | Location | | | | Pathology | | | |
|---|---|---|---|---|---|---|---|---|---|---|---|
| | | | | *Intracerebral* | | | | | | | |
| **Model** | ***Mouse*** | ***Rat*** | ***NHP*** | ***SN*** | ***MFB*** | ***STR*** | ***Systemic*** | ***Neuro-degeneration*** | ***Neuro-inflammation*** | **Repreducability** | **References** |
| **6-ODHA** | ✓ | ✓ | × | ++ | ++ | + | × | ++ | ± | ✓ | (1) |
| **MPTP** | ✓ | × | ✓ | × | × | × | ✓ | + | + | ✓ | (2) |
| **LPS** | ✓ | ✓ | × | ++ | × | + | ✓ | ± | ++ | × | (3) |

## 2.4 α-synuclein-based models

Alongside the A53T mutation in the SNCA gene (coding for α-synuclein) (Polymeropoulos *et al.*, 1997), multiple other mutations have been identified (Krüger *et al.*, 1998; Zarranz *et al.*, 2004; Appel-

Cresswell *et al.*, 2013; Kiely *et al.*, 2013; Proukakis *et al.*, 2013). While many models have been created using α-synuclein, its exact function is still unknown. α-synuclein is an abundantly presynaptic protein (Maroteaux, Campanelli and Scheller, 1988), that is thought to modulate synaptic vesicle function (Kahle *et al.*, 2002).

Feany and Bender (2000) have shown that expression of wild-type or mutant (A30P or A53T) α-synuclein in *Drosophila* leads to loss of the dopaminergic neurons in adult flies, as well as motor dysfunction (reversible by levodopa (Pendleton *et al.*, 2002)), and Lewy Body-like inclusions (Feany and Bender, 2000). In mice, a knockout of α-synuclein resulted in behavioural deficits as well as decreased dopamine levels in the striatum, however there was no evidence of dopaminergic cell, fibre, or synapse loss (Abeliovich *et al.*, 2000). Interestingly, α-synuclein knockout mice are resistant to MPTP (Dauer *et al.*, 2002).

Apart from SNCA mutations, SNCA duplication and triplication have been linked to autosomal dominant PD (Singleton *et al.*, 2003; Chartier-Harlin *et al.*, 2004). Overexpression of α-synuclein resulted in variable phenotypes in mice, and only a few lines were reported to have alterations in the nigrostriatal pathway (reviewd by Fleming, Fernagut and Chesselet, 2005). Interestingly, mice overexpressing α-synuclein seem more sensitive to a mixture of toxins (paraquat and maneb; 1.3.4, page 141) (Norris *et al.*, 2007).

#### Viral vector overexpression

In addition to transgenic lines, gene overexpression can be induced using viral vectors (Table 2). This has the advantage, unlike in transgenic lines, that the nigrostriatal system can be specifically targeted, expression of the vector can be dose-dependent, and is induced at a specific age. Both recombinant adeno-associated virus (rAAV) and lentivirus-based vectors have been used to overexpress SNCA and other genes in rodents (Konnova and Swanberg, 2018), with or without PD-related mutations (reviewed in Volpicelli-Daley *et al.*, 2016). Unfortunately, high expression levels – four to fivefold above normal - of α-synuclein are needed to obtain neurodegeneration (Decressac, Mattsson and Björklund, 2012), while the inflammatory response is short-lived and modest (Chung *et al.*, 2009).

#### Preformed a-synuclein fibrils

In contrast to the overexpression models of α-synuclein, preformed fibrils of α-synuclein can directly be injected into the rodent brain. These models allow the investigation of the impact and propagation of α-synuclein on the neuronal function (Volpicelli-Daley *et al.*, 2016). In both mice and rats, it has been shown that injection of α-synuclein fibrils leads to α-synuclein containing inclusions and neurodegeneration, as well as motor deficits (Luk *et al.*, 2012; Paumier *et al.*, 2015; Rey *et al.*, 2016; Abdelmotilib *et al.*, 2017; Blumenstock *et al.*, 2017; Patterson *et al.*, 2019; Yabuki *et al.*, 2020).

Moreover, some groups have used a combination of α-synuclein overexpression and preformed fibrils. This lead to Lewy body-like aggregates, more progressive dopaminergic neurodegeneration, reduced dopaminergic nerve terminal volume, aggravated motor symptoms, and long-lasting inflammation (Peelaerts *et al.*, 2015; Thakur *et al.*, 2017; Espa *et al.*, 2019).

## 2.5 LRRK2-based models

Mutations in leucine rich repeat kinase 2 (LRRK2) were first discovered to cause autosomal dominant PD in 2004 (Zimprich *et al.*, 2004). Although LRRK2 is normally localised in membranes

(Jackson-Lewis, Blesa and Przedborski, 2012), its function is not clear, but there seems to be a link with mitochondria, autophagy, endocytosis, and many other cellular processes (reviewed by Winklhofer and Haass, 2010; Berwick *et al.*, 2019). The most common PD-related mutations in the LRRK2 gene are G2019S (Kachergus *et al.*, 2005) and R1441C/G (Dusonchet *et al.*, 2011; Konnova and Swanberg, 2018). These pathogenic mutations lead to hyperactivation of the LRRK2 kinase domain (Alessi and Sammler, 2018).

Transgenic *Drosophila* with a non-functional truncated version of LRRK2 showed no abnormalities in dopaminergic neurons (Wang *et al.*, 2008), while over-expression leads to dopaminergic neurodegeneration and levodopa-reversible motor deficits (Liu *et al.*, 2008). Over-expression of G2019S mutant LRRK2 caused a more severe phenotype (Liu *et al.*, 2008). Knockout mice have abnormal accumulation and aggregation of proteins, including α-synuclein (Jagmag *et al.*, 2016). Knock-out rats, unlike mice, show no significant dopaminergic cell loss, inhibited proinflammatory response, and inhibited rAAV-mediated α-synuclein expression (Ness *et al.*, 2013; Daher *et al.*, 2014). Similarly, LRRK2 transgenic rats (human wild-type LRRK2 or human mutated LRRK2: G2019S, R1441C or R1441G) did not show neurodegeneration in the substantia nigra, however, in many cases they did show behavioural deficits (Walker *et al.*, 2014; Lee *et al.*, 2015; Shaikh *et al.*, 2015; Sloan *et al.*, 2016). Conversely, overexpression of human G2019S LRRK2 in adulthood did generate significant dopaminergic neuronal loss (Dusonchet *et al.*, 2011; Zhou *et al.*, 2011).

**Table 2: Overview of the use of α-synuclein overexpressing models using viral vector approaches in literature. The first line (bold) indicates the AAV2/6-PGK-A53T-α-synuclein model that was studied at 15 weeks post-injection in the submitted paper (page 108). AAV = adeno virus-associated vector, LV = lentivirus. CBA = chicken β-actin, CMV = cytomegalovirus, PGK = phosphoglycerate kinase, WPRE = woodchuck hepatitis virus posttranscriptional regulatory element. WT = wildtype. pi = post-injection. nm = not mentioned.**

| Viral Vector | | | | | | | |
|---|---|---|---|---|---|---|---|
| ***Vector Type*** | ***Promoter & Enhancer*** | ***α-Synuclein Type*** | **Timepoint pi** | **Cell death in SN** | **Fibre loss in striatum** | **α-Aggregation** | **Reference** |
| ***AAV2/6*** | ***PGK*** | ***A53T*** | **15 weeks** | **30%** | **nm** | **+** | ***(Cresto et al., in progress)*** |
| AAV2/6 | Synapsin/WPRE | WT | 3-16 weeks | 42-80% | 30-60% | + | (Decressac *et al.*, 2012) |
| AAV2/6 | Synapsin/WPRE | WT | 4-12 weeks | ns | ns-33% | + | (Phan *et al.*, 2017) |
| AAV2/5 | Synapsin | WT | 24 weeks | 50% | 50% | + | (Mulcahy *et al.*, 2012) |
| AAV2/5 | Synapsin | WT | 18 weeks | 40% | 30% | + | (Mulcahy *et al.*, 2013) |
| AAV2/5 | CBA/CMV | WT | 4-8 weeks | 35-90% | 42% | + | (Gombash *et al.*, 2013) |
| AAV2/5 | CBA | WT | 4-15 weeks | ns-50% | nm | + | (Sanchez-Guajardo *et al.*, 2010) |
| AAV5 | nm | WT | 4-12 weeks | ns-60% | ns-64% | + | (Gorbatyuk *et al.*, 2008) |
| rAAV | CBA/CMV | WT | 3-8 weeks | 23-55% | 10-50% | + | (Kirik *et al.*, 2002) |
| | | A53T | | | | + | |
| LV | PGK | WT | 5 months | 35% | 15% | + | (Lo Bianco *et al.*, 2002) |
| | | A53T | | 24% | ns | + | |
| AAV2 | Synapsin | A53T | 4-24 weeks | ns-56% | nm | nm | (Chung *et al.*, 2009) |
| AAV2/7 | Synapsin/CMV | A53T | 4-29 days | 60-80% | nm | + | (Van der Perren *et al.*, 2015) |
| AAV2/7 | Synapsin/CMV | A53T | 9 weeks | 95% | nm | + | (Crabbé *et al.*, 2019) |

Recently, it has was shown by our lab that rAAV-mediated overexpression of truncated mutant (G2019S) LRRK2 in the rat substantia nigra caused dopaminergic neurodegeneration, suggesting the mutant kinase domain is sufficient to induce neuronal loss (Cresto *et al.*, 2020).

**Combination strategies (lrrk2&a-syn)**

Overexpression of mutant LRRK2 in A53T mutated α-synuclein transgenic mice accelerated the PD neuropathology and promoted α-synuclein aggregation. Conversely, downregulation of LRRK2 was shown to suppress α-synuclein aggregation and slowed the neuropathology (Lin *et al.*, 2009). Cresto *et al*. (2018) have recently written an extensive review on the growing evidence for an interaction between LRRK2 and α-synuclein. While the underlying mechanisms for interaction between LRRK2 and α-synuclein are not clear, there is compelling evidence that the two proteins may act in concert to trigger dopaminergic neurodegeneration. As a consequence, therapeutic

targeting of both proteins could slow down the disease process in patients with LRRK2 mutations but also in those with sporadic forms of PD (Cresto *et al.*, 2018).

# 3. Towards a cure

Even though PD has first been described over 200 years ago, there is still no curative treatment to this day (Kalia and Lang, 2015; Fahn, 2018). There are drugs available that help improve motor function, even though they have problematic side-effects in time (Stoker, 2018; Zahoor, Shafi and Haq, 2018). In tandem with drugs, there is the possibility of invasive deep brain stimulation (DBS), which can reduce the need for medication and reduce motor symptoms (Dallapiazza *et al.*, 2018). Lastly, to restore dopamine delivery in the brain in a more physiological way, gene therapy and cell grafting strategies have gained interest. Even though clinical trials with regenerative medicine have run into a number of difficulties, e.g. lack of efficacy, and ethical barriers (Stoker, 2018), one of the aims of the BrainMatTrain program[1,2] was to improve cell graft survival by employing hydrogels as a delivery support.

As previously described, PD is characterised by a selective loss of the dopaminergic neurons in the substantia nigra pars compacta, which leads to a dopamine deficiency in the striatum (Dauer and Przedborski, 2003). Most treatment strategies aim to supplement dopamine in the striatum (Zahoor, Shafi and Haq, 2018). However, dopamine cannot cross the BBB, and must therefore be synthesised within the central nervous system (Zahoor, Shafi and Haq, 2018).

## 3.1 Pharmacological dopamine increase

### 3.1.1 Levodopa

Currently, the most used treatments are based on levodopa (Zahoor, Shafi and Haq, 2018), the dopamine precursor that can cross the BBB, in contrast to dopamine (Samii, Nutt and Ransom, 2004; Zahoor, Shafi and Haq, 2018). In the brain, levodopa is converted into dopamine by AADC (Musacchio, 1975).

In 1957, Carlsson and colleagues showed that levodopa (L-dopa), a naturally occurring L-isomer of the amino acid D,L-dihydroxyphenylalanine, was able to restore the levels of dopamine. For this experiment rabbits were treated with reserpine to deplete all three catecholamines; interestingly L-dopa restored only dopamine levels, leaving the levels of adrenaline and noradrenaline almost untouched, while a precursor of serotonin did not elevated any catecholamine's level (Carlsson, Lindqvist and Magnusson, 1957). The important discoveries of Carlsson were rewarded with the Nobel Prize in Physiology or Medicine in 2000, together with Paul Greengard and Eric R. Kandel, for effectively proving the link between loss of dopamine and

[1] http://www.curamdevices.ie/curam/research/eu-projects/currentprojects/h2020---marie-curie/brainmattrain/

[2] The BrainMatTrain project is funded by the European Union Horizon 2020 Programme (H2020-MSCA-ITN-2015) under the Marie Skłodowska-Curie Initial Training Network and Grant Agreement No. 676408.

Parkinsonism. Carlsson suggested that dopamine was involved in PD and that L-dopa could restore levels of dopamine in the PD brain. In 1960, Ehringer and Hornykiewicz confirmed there was a neostriatal dopamine deficiency in *post-mortem* PD brains (translation Ehringer and Hornykiewicz, 1998). Thanks to Hornykiewicz and Birkmayer, Carlsson's findings were rapidly translated into human testing, with the aim of restoring the missing dopamine. From 1961, levodopa was partially administered to PD patients but many reports were fairly sceptical about its therapeutic effect (Tolosa et al., 1998). Additionally various concerns were raised due to the gastrointestinal side effects caused by administration of even tiny doses. A solution to the problems was given by George Cotzias in 1969: he developed an oral levodopa intake based on high dosage together with a very slow release over time (Cotzias, Papavasiliou and Gellene, 1969). Since then, levodopa has become the major therapeutic against PD's motor symptoms.

Generally, levodopa administration rapidly shows a clinical effect, which can lasts for several hours. As the disease advances, the clinical effect becomes less prominent and the effects wear off faster, necessitating increased dosage and frequency of administration. Increasing the dosage leads to occurrence of adverse side-effects (Fahn, 2018; Zahoor, Shafi and Haq, 2018). Some of these side-effects stem from the peripheral conversion of levodopa into dopamine, which can be counteracted by combined administration of levodopa and peripheral AADC blockers, like benserazide and carbidopa. These cannot cross the BBB, but selectively prevent the peripheral conversion of levodopa to dopamine, and thus reduce the peripheral side effects (Silva *et al.*, 1997). Other side-effects result in significant motor complications such as levodopa-induced dyskinesia (LID) and severe on-off motor fluctuations. These can be handled by reducing the levodopa dose, making the right dosage of levodopa a fine balance to find (Zahoor, Shafi and Haq, 2018). Alternatively, research projects are aimed to identify molecules that reduce LID (e.g. Aron Badin *et al.*, 2013). Non-motor side-effects of levodopa include gastrointestinal disturbances (like nausea and vomiting), and anxiety and hallucinations, due to extra-nigral effects of dopamine (Kalia and Lang, 2015; Fahn, 2018; Zahoor, Shafi and Haq, 2018).

### 3.1.2 Dopamine degradation inhibitors

#### Monoamine Oxidase B inhibitors

Monoamine Oxidase B (MAO-B) inhibitors work through inhibition of dopamine metabolism, in order to increase the level of endogenous dopamine in the striatum (Zahoor, Shafi and Haq, 2018), and to relieve motor symptoms (Goldenberg, 2008). To delay the onset of complications with levodopa use, levodopa-sparing initial therapy can be considered, using MAO-B inhibitors or dopamine agonists (Goldenberg, 2008; Kalia and Lang, 2015). However, the effects of these are debatable (Lang and Marras, 2014; PD Med Collaborative Group *et al.*, 2014). MAO-B inhibitors are generally well tolerated, but can cause gastrointestinal side-effects by itself, and a myriad of other less-common adverse effects (Goldenberg, 2008).

#### Catechol-O-methyl transferase inhibitors

Catechol-O-methyl transferase (COMT) inhibitors are another way to limit dopamine degradation and preserving endogenous dopamine (Goldenberg, 2008). They are mostly used in combination with levodopa, since they have a limited effect on PD symptoms on their own. COMT inhibitors are especially effective in patients with wearing-off problems of levodopa, since COMT inhibitors increase the half-life and brain delivery of levodopa (Zahoor, Shafi and Haq, 2018). Since

COMT inhibitors can lead to amplification of levodopa-induced side-effects, they often necessitate a reduction in levodopa dose. Additionally, COMT inhibitors come with their own side-effects (Zahoor, Shafi and Haq, 2018).

### 3.1.3 Dopamine agonists

Dopamine agonists stimulate the dopaminergic system by binding to the dopamine receptors, and thus do not need to be converted into dopamine (Samii, Nutt and Ransom, 2004). While dopamine agonists are less effective in controlling motor symptoms of PD, they can be useful in patients with minor symptoms, patients who do not tolerate levodopa, or in combination with levodopa therapy (Zahoor, Shafi and Haq, 2018). Commonly used are ropinirole, pramipexole, and rotigotine. Apomorphine is less commonly used but can be very useful as additional medication in patients with severe motor fluctuations (Goldenberg, 2008; Zahoor, Shafi and Haq, 2018). Some studies suggest that dopamine agonists additionally have a mild neuroprotective effect (reviewed by Olanow, Jenner and Brooks, 1998). However, dopamine agonist treatment comes with severe side-effects, including nausea and vomiting, insomnia, constipation, fainting, hallucinations, and sleepiness (Samii, Nutt and Ransom, 2004; Goldenberg, 2008). Another important side-effect is the development of impulse control disorder, which occurs in 15-20% PD patients taking dopamine agonists (Weintraub *et al.*, 2010; Poletti *et al.*, 2013; Zahoor, Shafi and Haq, 2018). Impulse control disorder entails a wide range of behaviours, including hypersexuality, gambling, binge eating, compulsive shopping, and compulsive writing (Weintraub and Claassen, 2017). On the other hand, stopping with or reducing the dose of dopamine agonists can lead to dopamine agonist withdrawal syndrome (Weintraub and Claassen, 2017), which also has psychological consequences (Zahoor, Shafi and Haq, 2018).

### 3.1.4 Non-dopaminergic mechanisms

Besides pharmacological drugs that act on the dopaminergic system, as described above, there are also PD drugs that act through non-dopaminergic mechanisms, for example anticholinergics. The loss of dopaminergic neurons disturbs the normal balance between dopamine and acetylcholine in the brain. Anticholinergic drugs act as antagonist for cholinergic receptors and thereby reduce the activity of acetylcholine, this can lead to restoration of the balance (Zahoor, Shafi and Haq, 2018). Anticholinergics were the first pharmacological agents used as treatment for PD, but since the discovery of levodopa they are little used (Brocks, 1999). Anticholinergics are most useful to relief tremors and muscle stiffness, and can even be used as monotherapy in the early stages of tremor-dominant PD (Zahoor, Shafi and Haq, 2018). They can cause many side-effects, one of which is dry mouth, which is actually beneficial for patients who experience drooling (Goldenberg, 2008).

Conversely, nicotine has been shown to protect against nigrostriatal damage (Ryan *et al.*, 2001; Huang *et al.*, 2009) and improve LID in PD models (Huang *et al.*, 2011; Quik *et al.*, 2013). Nicotine binds to nicotinic acetyncholine receptors, and AQW051 is a partial agonist for the nicotinic acetyncholine receptors. Even though AQW051 was shown to significantly reduce LID in MPTP-treated monkeys without compromising the beneficial effects of levodopa (Di Paolo *et al.*, 2014), AQW051 did not significantly reduce dyskinesia or parkinsonian severity in PD patients (Trenkwalder, Berg, *et al.*, 2016).

Other targets of interest are serotonin receptors and glutamate receptors. Sarizotan is a 5-HT1A agonist with additional affinity for $D_3$ and $D_4$ receptors, which was shown to inhibit levodopa-induced turning in 6-OHDA treated rats in a dose-dependent manner (Gerlach *et al.*, 2011). Mavoglurant (AFQ056) is a glutamate receptor antagonist with debatable outcome. It showed reduced LID without affecting levodopa therapy in two studies (Berg *et al.*, 2011; Stocchi *et al.*, 2013), but failed to reduce LID in a third study (Trenkwalder, Stocchi, *et al.*, 2016).

**Conclusion**

The drugs that have been discussed above are used to control the motor symptoms of PD, but long-term use of dopaminergic therapies results in significant adverse effects (Zahoor, Shafi and Haq, 2018; Moriarty *et al.*, 2019). Thus there is a requirement to develop better means of restoring striatal dopamine (Moriarty *et al.*, 2019). Additionally, the dopaminergic treatments do not alter the course of the disease, thus there is a need for treatments that are able to slow down progression of the disease (Zahoor, Shafi and Haq, 2018; Moriarty *et al.*, 2019).

## 3.2 Deep brain stimulation

As described above, levodopa can be accompanied by severe dyskinesias and other side-effects after long-term use. In these patients deep brain stimulation might be considered, which may allow increased control of the motor symptoms and a reduction of levodopa dose (Zahoor, Shafi and Haq, 2018). Deep brain stimulation is a surgical technique in which electrodes are implanted in a target brain region. An impulse generator gives tiny electrical stimuli to the brain to disrupt or modulate neural signalling (Okun, 2012). The positive therapeutic outcome has been shown by several clinical trials; demonstrating motor improvements, long-lasting effects, and general improvement of life quality (Groiss *et al.*, 2009).

Deep brain stimulation has been in used for over 70 years, but has also greatly evolved over time. The first deep brain stimulation electrode was implanted in 1948 in the caudate nucleus to treat depression and anorexia in a PD patients (Malek, 2019). However, Benabid (1987) has performed pioneering work for modern day deep brain stimulation (Malek, 2019).

## 3.3 Gene therapy

Apart from the drugs described above, that aim to restore dopamine levels in the brain, gene therapy is being tested, generally to achieve endogenous dopaminergic restoration in a more continuous fashion (Zahoor, Shafi and Haq, 2018). Gene therapy uses viral vectors, not for the creation of PD models as described above (2.4, page 26), but to introduce a beneficial gene (Bjorklund, 2018; Hitti *et al.*, 2019).

Adeno-associated viral vectors (AAVs) are non-integrating vectors, which limits the risks of insertional mutagenesis that can occur during viral vector integration (Mukherjee and Thrasher, 2013). Their main drawback is the relatively limited size of the genetic cargo, meaning that only one gene of the dopamine synthesis pathway can be incorporated (Moriarty *et al.*, 2019). An AAV coding for AADC has been shown to successfully express AADC in MPTP-lesioned non-human primates, leading to long-term conversion of levodopa to dopamine. In combination with levodopa administration this resulted in long-term improvement of clinical rating scores, lower levodopa requirements, and improved [$^{18}$F]FMT uptake (Bankiewicz *et al.*, 2006). Subsequent phase I trials also

found improved clinical parameters and increased [$^{18}$F]FMT PET uptake (Christine *et al.*, 2009; Muramatsu *et al.*, 2010).

In contrast to AAVs, lentiviral vectors are integrating vectors, carrying a much larger capacity for genetic cargo (Moriarty *et al.*, 2019). This characteristic is exploited to restore endogenous dopamine production through medial spiny neurons by providing all the required building blocks (Bjorklund, 2018; Aron Badin *et al.*, 2019; Hitti *et al.*, 2019); i.e. genes encoding the rate-limiting enzymes in dopamine synthesis: AADC, TH, and guanosine triphosphate cyclohydrolase-1 (GTPCH1) (Palfi *et al.*, 2014). Striatal injection of this triple-gene lentiviral vector was shown to results in functional improvements in both 6-OHDA-lesioned rats (Azzouz *et al.*, 2002) and MPTP-lesioned non-human primates (Jarraya *et al.*, 2009). This was translated into ProSavin (OXB-101; Oxford Biomedia, UK), which was found well tolerated and improved motor behaviour in PD patients in a phase I/II trial (Palfi *et al.*, 2014, 2018). More recently, this lentiviral vector has been optimised (Stewart *et al.*, 2016), and subsequently tested in MPTP-lesioned non-human primates (Aron Badin *et al.*, 2019). This OXB-102 is currently in clinical trials under the name AXO-Lenti-PD (Lewis, 2018).

Alternatively, gene therapy is also being explored as a delivery system for neuroprotection. Viral vectors coding for glial-cell-derived neurotrophic factor (GDNF) or neurturin (its naturally occurring analogue) have been tested to slow dopaminergic neurodegeneration (Wang *et al.*, 2002; Marks *et al.*, 2008, 2010; Warren Olanow *et al.*, 2015).

## 3.4 Cell grafting approaches

Another way to ensure endogenous dopamine production is by introducing exogenous dopaminergic cells into the striatum. In this context, cell grafting approaches have great potential as regenerative treatment (Stoker, 2018). Several strategies have been proposed and are in various stages of preclinical and clinical testing (Moriarty *et al.*, 2019).

The first prove of concept studies showing the potential of brain cell grafting in the context of PD appeared in the late 70's (Perlow *et al.*, 1979; Björklund *et al.*, 1981). Björklund and colleagues (1981) grafted fetal ventral mesencephalon (fVM) tissue in 6-ODHA-lesioned rats and observed improved motor symptoms (Björklund *et al.*, 1981). The first human trials with human fVM cells started in the late 1980s and showed promising results (Lindvall *et al.*, 1990; reviewed in Barker, Drouin-Ouellet and Parmar, 2015). Even though fVM cells were shown the be effective in treating the critical features of PD, there are many ethical and logistical barriers for widespread use, e.g. unpredictable and inadequate supply of fetal tissue (Barker, Drouin-Ouellet and Parmar, 2015; Stoker, 2018; Moriarty *et al.*, 2019). These initial studies have spurred the search for renewable sources of dopamine-producing cells (Stoker, 2018; Moriarty *et al.*, 2019).

Embryonic stem cell (ESC) lines are isolated from the early blastocyst, and can be generated from surplus human embryos derived from *in vitro* fertilisation procedures (Thomson *et al.*, 1998). This is thought to lead to smaller ethical barriers as compared to the use of fetal tissue (Barker and de Beaufort, 2013). ESCs can be reprogrammed to midbrain dopaminergic neuronal progenitor cells with high efficiency, which have been shown to improve motor deficits in 6-OHDA-lesioned rats (Grealish *et al.*, 2014). The first clinical trials with ESC-derived dopaminergic neuron progenitors are currently ongoing (NeuroStemCellRepair, TRANSEURO, and NYSTEM-PD) (reviewed by Barker *et al.*, 2017).

Induced pluripotent stem cells (iPSCs) are derived through reprogramming of somatic cells, such as fibroblasts, into pluripotent cells, which can then be converted into dopaminergic neuron

progenitor cells (Takahashi *et al.*, 2007). Grafting of human iPSC-derived dopaminergic neuron progenitors into MPTP-lesioned non-human primates showed graft cell survival and functional integration, hence, spontaneous movement recovery (Kikuchi *et al.*, 2017). These preclinical studies lead to clinical trials using iPSC-derived dopaminergic neuron progenitors (CiRA trial and Summit for PD trial) (reviewed by Barker *et al.*, 2017). A major disadvantage of using autologous iPSCs is that any genetic defect of the host, will also be present in the grafted cells (Moriarty *et al.*, 2019).

Finally, bone marrow-derived mesenchymal stem cells (MSCs) are multipotent cells that can be differentiated into TH-positive cells. Grafting of MSCs was shown to improve motor symptoms in 6-ODHA-lesioned mice (Offen *et al.*, 2007). Differentiation into dopaminergic neurons has proven to be challenging (Moriarty *et al.*, 2019), but not impossible (Trzaska, Kuzhikandathil and Rameshwar, 2007). It has been suggested that MSCs themselves have anti-inflammatory and paracrine activity, resulting in a neuroprotective effect. This could make MSC grafts useful even without differentiation into dopaminergic neurons (Kim *et al.*, 2009). A small open-label clinical trial using MSC grafts in PD patients has shown short-term safety and hinted at improved motor scores (Venkataramana *et al.*, 2010).

## 4. Positron Emission Tomography Imaging

Positron emission tomography (PET) imaging is used for clinical diagnosis, monitoring disease progression, evaluation of (neuroprotective) therapies, and drug occupancy studies both in patients (Thobois, Guillouet and Broussolle, 2001), and preclinical settings (Sahin *et al.*, 2014).

PET imaging relies on the use of radiolabelled molecules, termed radiotracers, that diffuse freely through the body and selectively bind to specific biological targets (Van Camp, Bramoullé and Hantraye, 2011). PET can be used to monitor receptors (Ishida *et al.*, 2005), transporters (Sérrière *et al.*, 2014), neurotransmitter synthesis and enzymes (Becker *et al.*, 2017), intracellular proteins (Ory *et al.*, 2015), and aggregated proteins (Franzmeier *et al.*, 2020) *in vivo* (Figure 5) (Van Camp, Bramoullé and Hantraye, 2011; Abbasi Gharibkandi and Hosseinimehr, 2019; Herfert *et al.*, 2019). Of all modalities to image the brain *in vivo* PET imaging has the highest sensitivity and allows quantitative evaluation (Herfert *et al.*, 2019), thus providing valuable information.

A big advantages of PET is its translational potential; it can be used on a wide spectrum of species, from humans to rodents (Zheng *et al.*, 2012; Ma *et al.*, 2015; Parkinson *et al.*, 2016; Matthews *et al.*, 2018), and even down to insects (Currie, 2019). Clinical and preclinical imaging can learn from each other due to the high translational value of PET imaging. Preclinical imaging has the possibility to compare with *post-mortem* studies, which is more complicated in human studies (but possible (Sabri *et al.*, 2015)). The main advantage of preclinical imaging, however, is the possibility to study the prodromal phase of diseases like PD.

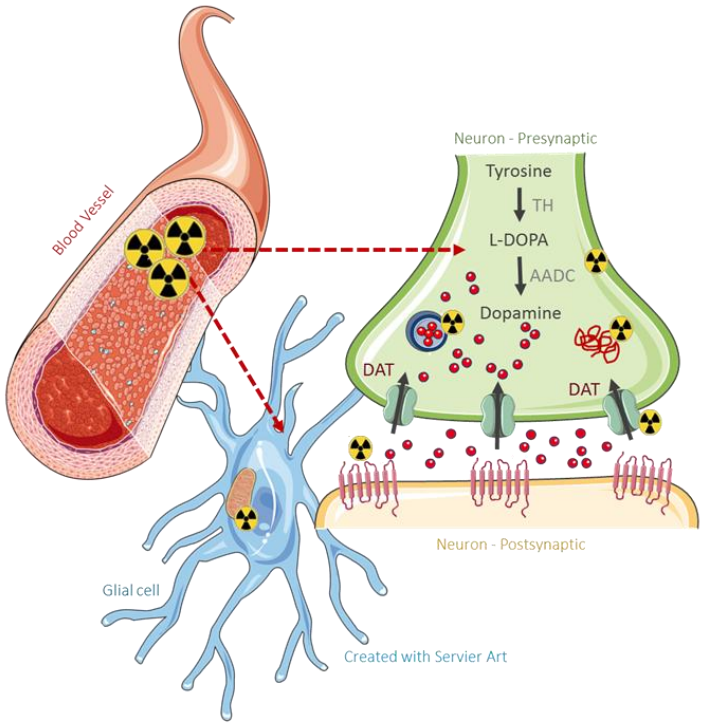


**Figure 5: Schematic overview of PET imaging targets for PD. A PET radiotracer is injected intravenously and diffuse freely through the body. Radiotracers can selectively bind to elements in the dopamine synthesis (AADC), neurotransmitter vesicles (VMAT2), protein aggregates, presynaptical transporters (DAT), post-synaptical receptors ($D_2R$), or glial mitochondrial proteins.**

## 4.1 Principles of PET imaging

PET imaging utilises a positron-emitting radioisotope linked to a molecule, together forming the radiotracer (Van Camp, Bramoullé and Hantraye, 2011). This radioisotope undergoes radioactive decay in the form of positron emission, which subsequently travels a short distance, dependent on the initial emission energy and the medium through which it is travelling. Upon interaction with an electron there is an annihilation event, which gives rise to the emission of two 511keV gamma ray photons that are emitted in almost exactly opposite directions, with a directional uncertainty of about ±0.5°. Detection of the annihilation event happens through simultaneous detection of these photons by opposite detectors, termed coincidence detection (Figure 6) (Cherry and Gambhir, 2001; Miller *et al.*, 2008; Van Camp, Bramoullé and Hantraye, 2011). The time-window for coincidence detection, called the coincidence window, is traditionally 5-10 ns and based on the time it takes to cross the field of view of the scanner (3 ns) (Van Camp, Bramoullé and Hantraye, 2011).

The raw data collected by a PET scanners is thus a list of these coincidence events, representing a line in space, and flagged with a time stamp (Van Camp, Bramoullé and Hantraye, 2011). Coincidence detection can also detect photons that do not stem from the same annihilation event. These accidental coincidences arise when two separate annihilation events cause two unrelated photons to hit opposing detectors within the coincidence window. These accidental, and false, coincidences need to be corrected for in order to prevent overestimation or mislocalisation of the isotope concentration (Van Camp, Bramoullé and Hantraye, 2011). Another important correction is for photon attenuation, which reduces the number of coincidences and can thus underestimate the signal (Chow, Rannou and Chatziioannou, 2005).

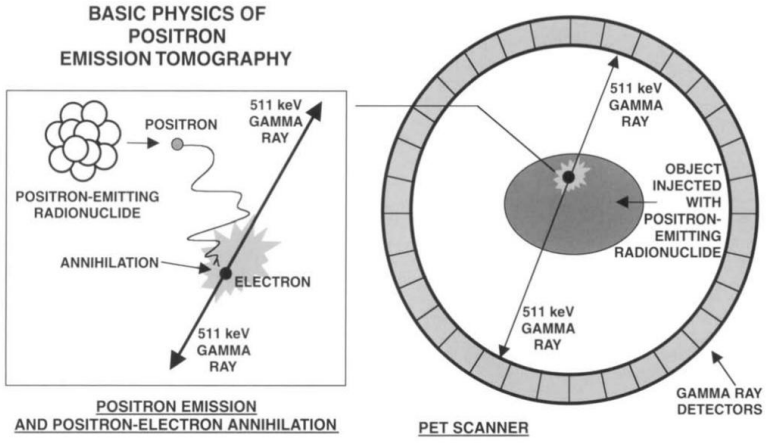


**Figure 6: Schematic representation of positron emission tomography imaging. Positrons are emitted from the radionuclide and annihilate upon interaction with electrons, giving rise to gamma ray photon emission in opposite directions. Detection of the annihilation event happens through simultaneous detection of these photons by opposite detectors, termed coincidence detection. Figure from Cherry and Gambhir (2001).**

## 4.2 Advantages and disadvantages of PET imaging

PET imaging has several advantages over other *in vivo* imaging techniques. First of all PET imaging is very versatile; radiotracers against many different substances exist (See paragraph 4.4, page 39). Additionally, PET imaging is a very translational tool that can be used in many different animal species (Cherry and Gambhir, 2001; Van Camp, Bramoullé and Hantraye, 2011; Herfert *et al.*, 2019). PETs *in vivo* nature allows for longitudinal study design, which allows one to follow disease or therapy progression, as well as a minimisation of animal numbers (Cherry and Gambhir, 2001; Herfert *et al.*, 2019).

PET imaging is very sensitive and can detect nanomolar concentrations of radiotracer (Van Camp, Bramoullé and Hantraye, 2011), with high specificity and high resolution (Abbasi Gharibkandi and Hosseinimehr, 2019). Since PET imaging is a truly quantitative technique (Cherry and Gambhir, 2001; Miller *et al.*, 2008; Abbasi Gharibkandi and Hosseinimehr, 2019), it can give information about physiological and biochemical events by monitoring the distribution and concentration of the radiotracer in the body over time (Cherry and Gambhir, 2001; Miller *et al.*, 2008). It thus provides metabolic information rather than structural information (Miller *et al.*, 2008). And lastly, it can do so without interfering in the biological activity of the molecule of interest (Miller *et al.*, 2008).

One of the main challenges of PET imaging is the short half-lives of the radioisotopes (Miller *et al.*, 2008; Abbasi Gharibkandi and Hosseinimehr, 2019), which necessitate rapid synthesis methods. The labelled probe has to be synthesised, purified, analysed, and formulated within timescale of roughly three isotope half-lives (Miller *et al.*, 2008; Van Camp, Bramoullé and Hantraye, 2011), which corresponds to 60 minutes for [$^{11}$C] and only 6 minutes for [$^{15}$O]. This is less of an issue for [$^{18}$F], which has a half-life of 110 minutes (Miller *et al.*, 2008). Within the synthesis time, also the radionuclide purity needs to be ensured, which can require extra purification steps (Abbasi Gharibkandi and Hosseinimehr, 2019). These technical challenges also hinder the development and optimisation of new probes (Cherry and Gambhir, 2001).

A major disadvantage of PET imaging is the radioactive nature of the technique and the high costs that are paired with it (Van Camp, Bramoullé and Hantraye, 2011; Abbasi Gharibkandi and Hosseinimehr, 2019). These arise from the heavy infrastructure (Miller *et al.*, 2008; Van Camp, Bramoullé and Hantraye, 2011), and the many different human competences that are required; including chemists, physicists, biologists, physicians, and imaging processing specialists (Van Camp, Bramoullé and Hantraye, 2011). PET imaging calls for cyclotron facilities for radioisotope production, radiochemical laboratories with shielded hot cells and automated chemical units for radioligand preparation, and PET scanners, preferably all in close proximity to limit synthesis time and time to imaging (Miller *et al.*, 2008; Van Camp, Bramoullé and Hantraye, 2011). A part of this heavy infrastructure is needed to reduce exposure to radioactivity for all involved parties (Van Camp, Bramoullé and Hantraye, 2011).

Lastly, PET imaging in small animals has inherent physical limitations that affect the accuracy of quantification (Van Camp, Bramoullé and Hantraye, 2011); which are described above (4.1 Principles of PET imaging). Additionally, PET imaging has a limited time resolution which challenges the detection of fast molecular and functional changes (Herfert *et al.*, 2019). These complex biological processes, fast or slow, are described by very simplified pharmacokinetical models, which must be taken into account for data interpretation (Herfert *et al.*, 2019).

## 4.3 Radiotracer properties

When producing a new radiotracer, there are several things to take into account, e.g. the radioligand production time, ability to pass the blood-brain barrier (BBB) while its radiometabolites should not, and interference with biological processes (Van Camp, Bramoullé and Hantraye, 2011).

The ability of a radiotracer to cross the BBB is determined by it lipophilicity, molecular weight, cross-sectional area, hydrogen-bonding capacity, formal charge (Pike, 2009; Van Camp, Bramoullé and Hantraye, 2011). Moderate lipophilicity is sufficient for good cerebral uptake, while still ensuring low non-specific binding. High lipophilicity has the disadvantage of favouring binding to blood proteins, which reduced the tracer free fraction in blood plasma (Pike, 2009). Passive entry into the brain is promoted by a low molecular weight (Pike, 2009), a small cross-sectional area (Fischer, Gottschlich and Seelig, 1998; Seelig, 2007), a low hydrogen-bonding capacity (Pike, 2009), and lack of a formal charge (Seelig, 2007). A radiotracer's ability to stay in the brain is a combination of its capacity for passive entry versus its susceptibility for expulsion by drug efflux pumps (Raub, 2006; Pike, 2009). The radiotracer should thus be poor substrate for drug efflux pumps, like P-glycoprotein (Van Camp, Bramoullé and Hantraye, 2011).

Radiotracers are vulnerable to metabolisation. Ideally, this metabolism happens outside the brain, and produces radiometabolites that cannot cross the BBB due to lower lipophilicity with low or no interaction with the target protein (Pike, 2009), these radiometabolites should not accumulate in the liver or any other organs, where they can cause irradiation issues; ideally they are excreted via the urinary tract (Kristensen and Nørbygaard, 1984). The metabolisation of a radiotracer can be determined through *ex vivo* analyses (Pike, 2009; for example Peyronneau *et al.*, 2012).

PET imaging aims to study the normal functioning of the body, meaning that when using a PET tracer it should not affect the biology of the brain. Therefore, radiotracers are used at tracer doses, ~5% of receptor occupancy, and not at pharmacological doses. The specific activity (the ratio between activity and mass) has to be taken into account when deciding on the injected dose to assure tracer dose. However, in the generation of Focus 220 scanners, radiotracer dose needs to

compensate for a loss of sensitivity in rodent studies, due the increase resolution needed for their small brains (Cherry and Gambhir, 2001), resulting in a 25-fold higher dose as compare to humans.

Lastly, animals are generally anaesthetised for PET imaging, which can cause interference between the anaesthetic and the radiotracer, e.g. FDG-PET and xylazine, which can introduce variability if the anaesthesia is not constant between animals.

The two most common PET isotopes are [$^{11}$C] and [$^{18}$F], with a half-life of 20 minutes and 110 minutes, respectively (Abbasi Gharibkandi and Hosseinimehr, 2019). Due to its short half-life, [$^{11}$C] radiotracers can only be used synthesised on-site. The longer half-life of $^{18}$F makes is suitable for use at imaging centres that do not have on-site cyclotron (Abbasi Gharibkandi and Hosseinimehr, 2019). However, a major disadvantage of [$^{18}$F] labelled radiotracer is the occurrence of defluorination, which produced an [$^{18}$F] ion that binds extremely well to bone tissue, including skull (Pike, 2009). The resulting accumulation of radioactivity in the skull is problematic for subsequent quantification; together with the spatial resolution of PET imaging it results in a partial volume effect, i.e. a 'spill-over' in the adjacent brain tissue. This can be avoided by choosing proper labelling sites (Pike, 2009).

## 4.4 PET imaging targets in PD

As mentioned above, PET tracers can be used to monitor receptors, transporters, neurotransmitter synthesis and enzymes, intracellular proteins, and aggregated proteins *in vivo* (Figure 5) (Van Camp, Bramoullé and Hantraye, 2011; Abbasi Gharibkandi and Hosseinimehr, 2019; Herfert *et al.*, 2019). Here, the most relevant targets in the context of PD will be discussed, with a focus on tracers that were used in the present study.

### 4.4.1 Glucose metabolism

[$^{18}$F]2-fluoro-2-deoxy-D-glucose ([$^{18}$F]FDG) is the most frequently used tracer in clinical PET imaging, but has also widely been used in animal studies (Cherry and Gambhir, 2001). [$^{18}$F]FDG visualises regional glucose metabolism, which has shown to be altered in many diseases and disorders (Phelps, 2000), and can be used in humans and many different animal species (Cherry and Gambhir, 2001).

In humans, a PD related pattern of glucose metabolism measured with [$^{18}$F]FDG has been reported. This corresponds to relative increased metabolism of the thalamus, globus pallidus/putamen, cerebellum and pons, and relative hypometabolism of the occipital, temporal, parietal, and frontal cortices (Eidelberg *et al.*, 1994; Ma *et al.*, 2007; reviewed in Meles *et al.*, 2017, 2020; independent study by Matthews *et al.*, 2018). A correlation was observed between this pattern and PD patient cognitive skills (Trošt, Perovnik and Pirtošek, 2019).

Similarly, in MPTP monkeys (paragraph 2.2, page 24) a correlation between altered [$^{18}$F]FDG pattern and motor deficits was observed (Ma *et al.*, 2012). In nigral 6-OHDA lesioned rats (see paragraph on 6-hydroxydopamine, page 24) significant glucose hypo-metabolism was observed in the ipsilateral sensory motor cortex using [$^{18}$F]FDG-PET (Casteels *et al.*, 2008). The multivariate pattern approach, as used by Eidelberg and colleagues (1994), has been further developed and applied in rat models of PD. Devrome and colleagues (2019) observed a PD specific pattern of glucose metabolism in an adeno-associated viral vector based α-synuclein rat model. This pattern overlapped to a large extent with the human PD related pattern (Devrome *et al.*, 2019). In a similar viral vector-mediated overexpression model of PD, bilateral hypermetabolism was observed in the

striatum at 2wpi, ipsilateral nigral hypermetabolism at 4wpi, ipsilateral striatal hypometabolism at 6wpi, and contralateral striatal hypermetabolism at 9wpi (Crabbé *et al.*, 2019). Preclinical [$^{18}$F]FDG-PET imaging can support the validation of disease specific brain patterns of glucose metabolism.

### 4.4.2 L-aromatic amino acid decarboxylase (AADC) enzymatic activity

AADC is the second enzyme in the biosynthetic pathway of several monoamine neurotransmitters; dopamine, norepinephrine, and serotonin. AADC rapidly converts L-DOPA to dopamine, which can be subsequently converted to norepinephrine or serotonin (DeJesus *et al.*, 2005).

L-3,4-dihydroxy-6-[$^{18}$F]fluoro-phenylalanine ([$^{18}$F]FDOPA) is a commonly used PET tracer in PD patient imaging (Ruottinen *et al.*, 1995) and visualises dopamine synthesis, storage and turnover (Garnett, Firnau and Nahmias, 1983). The chemical structure of [$^{18}$F]FDOPA is closely related to L-DOPA, and undergoes all the same metabolic steps; decarboxylation by L-aromatic amino acid decarboxylase (AADC), storage by vesicular monoamine transporters (VMAT), and catabolism by monoamine oxidase and monoamine oxidase and catechol-O-methyl-transferase (COMT) (Melega *et al.*, 1991; Endres *et al.*, 1997). However, AADC and COMT are abundantly present in the peripheral organs, such as liver and kidney (Rahman, Nagatsu and Kato, 1981; Männistö, 1998). Peripheral metabolisation of [$^{18}$F]FDOPA by COMT results in 3-O-methyl-[$^{18}$F]FDOPA, which can cross the BBB and thus reduce signal-to-background ratio and lower image contrast. Either plasma metabolite analysis or peripheral COMT inhibitors (e.g. entecapone, tolcapone, or opicapone) are therefore required for [$^{18}$F]FDOPA quantification (Ruottinen *et al.*, 1995; Becker *et al.*, 2017). Blocking of peripheral AADC (via e.g. carbidopa or benserazide) prior to [$^{18}$F]FDOPA administration is required to inhibit peripheral metabolism of [$^{18}$F]FDOPA in PD patients (Melega *et al.*, 1991; Ruottinen *et al.*, 1995; Li *et al.*, 2014), and non-human primates (Melega *et al.*, 1991; Pate *et al.*, 1993; Dejesus *et al.*, 2001).

In PD patients, [$^{18}$F]FDOPA showed reduced uptake in the caudate and putamen (Holtbernd *et al.*, 2015; Akamatsu *et al.*, 2017; Daryl J. Wile *et al.*, 2017), and the substantia nigra was clearly visualised (Akamatsu *et al.*, 2017). Furthermore, efforts are being undertaken to increase quantification methods, for example by integrating blood metabolomics (Glaab *et al.*, 2019) or applying other quantification methods (Alves *et al.*, 2017).

In rats [$^{18}$F]FDOPA was shown to successfully visualise unilateral 6-ODHA lesions; peripheral COMT inhibitors were combined with peripheral AADC inhibitors for these studies. (Kyono *et al.*, 2011; Walker, Dinelle, Kornelsen, Lee, *et al.*, 2013; Walker, Dinelle, Kornelsen, McCormick, *et al.*, 2013; Becker *et al.*, 2017). As in non-human primate, a significant correlation between [$^{18}$F]FDOPA and striatal dopamine levels was observed in rats (Kyono *et al.*, 2011; Walker, Dinelle, Kornelsen, Lee, *et al.*, 2013). However, [$^{18}$F]FDOPA was unable to discriminate between a partial and complete 6-OHDA lesion (Becker *et al.*, 2017).

Alternatively, 6-[$^{18}$F]fluoro-m-tyrosine ([$^{18}$F]FMT) has a 10-fold greater affinity for AADC than [$^{18}$F]FDOPA and is not a substrate for COMT (DeJesus *et al.*, 1997). [$^{18}$F]FMT is transformed by AADC in 6-[$^{18}$F]-m-tyramine ([$^{18}$F]FMTA) in the blood plasma, and is subsequently oxidized to 6-[$^{18}$F]fluoro-m-hydroxyphenylacetic acid ([$^{18}$F]FHPAA) by mono-amine oxidase. Even though these two metabolites cannot cross the BBB, peripheral inhibition of AADC is still necessary (via e.g. carbidopa or benserazide) (Endres *et al.*, 1997; Becker *et al.*, 2017).

In a clinical setting, it was shown that [$^{18}$F]FMT-PET imaging inversely correlated with motor scores of PD patients (Gallagher *et al.*, 2011). Compared to [$^{18}$F]FDOPA, [$^{18}$F]FMT was also found to have higher extrastriatal uptake in regions with specific uptake (such as amygdala, pallidum, thalamus, and hippocampus), which might be useful for the examination of non-motor symptoms (Li *et al.*, 2014). In mice, like [$^{18}$F]FDOPA, [$^{18}$F]FMT failed to clearly visualise the mouse striatum (Honer *et al.*, 2006).

To the best of our knowledge, only a single study so far has been conducted using [$^{18}$F]FMT in rats. Becker and colleagues (2017) have shown that [$^{18}$F]FMT can distinguish between partial and complete 6-OHDA lesioned rats, which was not discernible using [$^{18}$F]FDOPA. However, in contrast to the human and macaque studies, inhibition of peripheral AADC activity was necessary for both [$^{18}$F]FMT and [$^{18}$F]FDOPA. The study suggests thus that [$^{18}$F]FMT could be more sensitive to detect dopaminergic lesions, and can be used to investigate presynaptic dopamine integrity and AADC activity. This lesion most likely has to exceed 25% loss of dopaminergic terminals to be detectable with [$^{18}$F]FMT (Becker *et al.*, 2017).

### 4.4.3 Dopamine transporter

Dopamine transporter (DAT) is expressed on the presynaptic membrane in the synaptic terminal of dopaminergic neurons. Several cocaine analogues exist as radioligand targeting DAT (Abbasi Gharibkandi and Hosseinimehr, 2019; Ikeda *et al.*, 2019). In clinics, DAT-SPECT (using [$^{123}$I]FP-CIT) is used widely for the differential diagnosis of PD and other neurodegenerative parkinsonism from essential tremor, drug-induced parkinsonism, or other neurological diseases that do not involve the nigrostriatal dopaminergic system (Brooks, 2016; Varrone and Pellecchia, 2018; Ikeda *et al.*, 2019). Examples of DAT-PAT radioligands are [$^{18}$F]LBT999 (Dollé *et al.*, 2006; Chalon *et al.*, 2019) and [$^{18}$F]FE-PE2I (Schou *et al.*, 2009; Varrone *et al.*, 2009). DAT-PET is becoming a valuable clinical tool to replace DAT-SPECT; in a clinical study [$^{18}$F]FE-PE2I was found to yield excellent basic diagnostic differentiation in early-stage PS, at least as good as [$^{123}$I]FP-CIT (Jakobson Mo *et al.*, 2018), while a clinical trial to compare [$^{18}$F]LBT999 to [$^{123}$I]FP-CIT is planned to start in 2020 (NCT04265209). I will focus here on [$^{18}$F]LBT999 since this radioligand was used in my PhD research.

(E)-N-(4-fluorobut-2-enyl)-2β-carbomethoxy-3β-(4'-tolyl)nortropane, was first utilised as an $^{11}$C radiotracer ([$^{11}$C]LBT999). In baboons it showed a high and rapid uptake mainly localised in striatal regions (Chalon *et al.*, 2006). The fluorinated version ([$^{18}$F]LBT999) can be synthesized using either two-step (Dollé *et al.*, 2006) or one-step radiosynthesis (Dollé *et al.*, 2007).

In healthy volunteers [$^{18}$F]LBT999 was shown to have high symmetric uptake in the caudate and putamen, and low uptake in the cerebellum (Arlicot *et al.*, 2017). In non-human primates, [$^{18}$F]LBT999 showed a similar pattern; high uptake in the caudate and putamen, moderate uptake in the midbrain, and low uptake in the cortex and cerebellum (Saba *et al.*, 2006). Furthermore, [$^{18}$F]LBT999 showed reduced uptake in both the caudate and putamen in early PD patients as compared to controls. Using striatal ratios it was even possible to differentiate patients from controls (Santiago-Ribeiro *et al.*, 2017).

In rats, [$^{18}$F]LBT999 showed specific binding to DAT and allowed quantification with high reproducibility, sensitivity, and specificity in the striatum. In the nigral area the variability was higher and the reliability lower (Sérrière *et al.*, 2014). Thereafter, the same group has shown that DAT density, as seen by [$^{18}$F]LBT999, was reduced in 6-OHDA lesioned rats (Sérrière *et al.*, 2015; Vetel *et*

*al.*, 2019). Grealish and colleagues (2014) have taken it one step further and have shown that [$^{18}$F]LBT999 is sensitive enough to observe functional improvement after cell grafting in 6-OHDA lesioned rats (Grealish *et al.*, 2014).

### 4.4.4 Vesicular monoamine transporter 2

VMAT2 has a critical role in maintaining catecholamine and serotonin levels in central nervous system. VMAT2 is expressed in all monoaminergic neurons of the brain, including those expressing dopamine, serotonin (5-HT), norepinephrine, epinephrine, and histamine. In 2006, VMAT2-PET imaging was proposed as a potential biomarker for PD (Bohnen et al., 2006).

[$^{11}$C]fluoropropyl-(+)-dihydrotetrabenazine is a well characterised radiotracer for vesicular monoamine transporter II (VMAT2) (reviewed by Kilbourn and Koeppe, 2019). [$^{18}$F]fluoropropyl-(+)-dihydrotetrabenazine ([$^{18}$F]DTBZ, also termed [$^{18}$F]AV-133) is the $^{18}$F-version of this radiotracer (Kung *et al.*, 2007). VMAT2 transports dopamine, and norepinephrine and serotonin, from the cytoplasm to the secretory vesicles (Schuldiner, 1994). [$^{18}$F]DTBZ was shown to have a high specific binding ratio and metabolic stability (Kilbourn *et al.*, 2007).

In healthy volunteers, [$^{18}$F]DTBZ showed the highest brain uptake levels in the striatum (Lin *et al.*, 2013). [$^{18}$F]DTBZ demonstrated decreased binding potential in the striatal regions of PD patients (Okamura *et al.*, 2010; Lin *et al.*, 2014). Subsequently, Hsiao and colleagues (2014) showed that this decrease in PD patients, and thus the decrease in VMAT2, was inversely correlated with disease severity (Hsiao *et al.*, 2014).

In 6-OHDA lesioned baboons [$^{18}$F]DTBZ showed a reduction of VMAT2 in the lesioned striatum, which was confirmed by autoradiography (Zhu *et al.*, 2012). In the 6-OHDA lesioned rat, [$^{18}$F]DTBZ showed a clear and definitive loss of VMAT2 binding in the ipsilateral striatum (Wang *et al.*, 2010). [$^{18}$F]DTBZ has been used to validate a novel PD rat model (Weng, Huang, *et al.*, 2017), while in the MPTP mouse model the radiotracer has been used to investigate therapeutic outcomes (Weng, Chen, *et al.*, 2017).

In an AAV2/6-Synapsin/WPRE-WT-α-synuclein rat model, [$^{11}$C]DTBZ showed asymmetrical striatal binding in the absence of dopaminergic neurodegeneration in the substantia nigra, while S129-phosphorylated α-synuclein was observed in the dopaminergic terminals (Phan *et al.*, 2017). This indicates that DTBZ is sensitive enough to detect early synaptic dysfunction caused by α-synuclein overexpression.

### 4.4.5 Dopamine receptors

While previous targets are located at the presynaptic side of the dopaminergic synapse, $D_2$- and $D_3$- receptors ($D_2R$/$D_3R$) are located at the postsynaptic side. Dopaminergic neuronal loss induces a dopamine depletion in the synapse and subsequent increase of $D_2R$ binding sites and affinity (Mach and Luedtke, 2018). Therefore, $D_2R$ PET ligands are of interest to evaluate restoration of dopamine levels at the level of the synapse after dopamine replacement therapies (for example Palfi *et al.*, 2014; for example Fukai *et al.*, 2019).

The preferential ligand to image $D_2R$ is [$^{11}$C]raclopride, which is in direct competition with endogenous dopamine. In PD patients, [$^{11}$C]raclopride binding is reduced due to a combination of upregulation of $D_2R$/$D_3R$ and reduced occupancy by endogenous dopamine (Arena and Stoessl, 2016).

Alternatively, (S)-N-[(1-allyl-2-pyrrolidinyl)methyl]-5-(3-[$^{18}$F]fluoropropyl)-2,3-dimethoxy-benzamide ([$^{18}$F]fallypride) is another dopamine $D_2$- and $D_3$- receptor (Mukherjee *et al.*, 1999) antagonist first described by Mukherjee and colleagues (1995). They showed high striatal uptake of [$^{18}$F]fallypride in rats and specific displacement by haloperidol in macaque brain (see page 140) (Mukherjee *et al.*, 1995). Subsequently the same group demonstrated that specific binding of [$^{18}$F]fallypride is reduced after amphetamine-induced dopaminergic release (Mukherjee *et al.*, 1997), through direct competition with dopamine for binding to the $D_2$R and $D_3$R (Abbasi Gharibkandi and Hosseinimehr, 2019).

[$^{18}$F]fallypride has been successfully used to study the $D_2$R and $D_3$R changes in the striatum in PD patients (Fisher *et al.*, 2013; Stark, Smith, Lin, *et al.*, 2018; Stark, Smith, Petersen, *et al.*, 2018). Unlike [$^{11}$C]raclopride, [$^{18}$F]fallypride is also capable of identifying extrastriatal dopamine receptors (de Paulis, 2003; Elsinga, Hatano and Ishiwata, 2006; Stark, Smith, Petersen, *et al.*, 2018). However, recently Karalija and colleagues (2019) have demonstrated reliable extrastriatal [$^{11}$C]raclopride binding in older adults (Karalija *et al.*, 2019).

In rats, [$^{18}$F]fallypride showed increased brain uptake in the ipsilteral to a 6-ODHA lesion, indicating $D_2$R and $D_3$R upregulation (Choi *et al.*, 2012). Mann and colleagues (2018) confirmed these results and continued by showing with [$^{18}$F]fallypride that botulinum neurotoxin A can reverse the effect of 6-OHDA (Mann *et al.*, 2018).

### 4.4.6 Serotonin

Alternatively, biomarkers could be used to predict the progression of PD and the occurrence of non-motor symptoms. The serotonin system is a very interesting target for this since it is involved in several non-motor symptoms of PD, like depression, anxiety, and apathy (Dujardin and Sgambato, 2020). Moreover, Millot and colleagues (2020) have shown that serotonergic lesioning in non-human primates aggravates MPTP-induced parkinsonian motor-symptoms. It must be noted, that, to a lesser extent, also dopaminergic neurons where lesioned using MDMA (Millot *et al.*, 2020).

Much like DAT, the serotonin transpoter regulates the concentration of free serotonin in the synaptic cleft (Leung, 2004). One example of a radioligand to visualise serotonin transporter binding is [$^{11}$C]N,N-Dimethyl-2-(2-amino-4-cyanophenylthio)benzylamine ([$^{11}$C]DASB) (Wilson *et al.*, 2000). Using [$^{11}$C]DASB, it was found that apathetic PD patients show greater serotonergic alterations compared to non-apathetic patients, indicating that serotonergic degeneration has a prominent role in neuropsychiatric symptoms of early PD (Maillet *et al.*, 2016).

### 4.4.7 TSPO imaging in the context of PD

18kDa translocator protein (TSPO) is expressed on the outer mitochondrial membrane of activated microglial and astrocytes (Papadopoulos *et al.*, 2006; Venneti, Lopresti and Wiley, 2006), where it is part of the mitochondrial transition pore. TSPO is expressed in astrocytes, microglia, macrophages but also by endothelial cell, and in peripheral organs (Banati, 2002; Bonsack and Sukumari-Ramesh, 2018). Increased densities of activated microglia and astrocytes during neuroinflammatory events result in higher regional densities of TSPO (Furube *et al.*, 2018), making this protein the PET imaging biomarker of neuroinflammation (Chauveau *et al.*, 2009; Owen and Matthews, 2011; Abbasi Gharibkandi and Hosseinimehr, 2019).

[$^{11}$C](R)-PK11195 is the first generation radioligand that targets TSPO, which has been used since the 80's, however, the clinical usefulness is limited due to low brain bioavailability, non-specific binding, and the relatively short half-life of $^{11}$C (Best *et al.*, 2019). In PD patients, overall increased [$^{11}$C](R)-PK11195 binding was observed in the pons, basal ganglia (including substantia nigra) and frontal and temporal cortical regions, which remained stable over 2 years (Gerhard *et al.*, 2006; reviewed by Bartels and Leenders, 2007; Kang *et al.*, 2018).

Low specific binding and quantification issues of [$^{11}$C](R)-PK11195 have led to the development of a whole generation of new ligands, so called 2$^{nd}$ generation ligands. However, in humans, a polymorphism in TSPO has been demonstrated to underlie different binding affinities of second generation ligands to 18kDa TSPO (Bonsack and Sukumari-Ramesh, 2018; Best *et al.*, 2019; Werry *et al.*, 2019), which has not been observed in rodents.

N,N-diethyl-2-(2-(4-(2[18F]-fluoroethoxy)phenyl)5,7dimethylpyrazolo[1,5a]pyrimidin-3-yl)acetamide ([$^{18}$F]DPA714) is a second generation radioligand that targets TSPO, developed by James and colleagues (2008). Over the last ten years, different research groups within the CEA have validated [$^{18}$F]DPA714; from rodents (Chauveau *et al.*, 2009) to non-human primates (Lavisse, Inoue, *et al.*, 2015; Van Camp *et al.*, 2019), and into humans (Lavisse, García-Lorenzo, *et al.*, 2015; García-Lorenzo *et al.*, 2018; Wimberley *et al.*, 2018). Even though the TSPO PET signal is mostly attributed to activated microglia, more recently it was demonstrated that also activated astrocytes contribute significantly to the [$^{18}$F]DPA714 PET signal (Lavisse *et al.*, 2012; Van Camp *et al.*, 2019). Other studies underlined this finding by showing that both activated microglia and astrocytes are positive for TSPO (Ory *et al.*, 2015; Pannell *et al.*, 2020).

In rats, multiple groups have used [$^{18}$F]DPA714 to image LPS-based neuroinflammatory models of different strengths, and suggesting different quantification methods (Ory *et al.*, 2015, 2016; Sridharan *et al.*, 2017; Vieira *et al.*, 2018). In a non-human primate model of neuroinflammation, a clear correlation between TSPO expression, as measured by optical density, and binding of [$^{18}$F]DPA was observed. Furthermore, [$^{18}$F]DPA714 showed a strong colocalisation with CD86$^{+}$ microglia, and in a lesser extend with GFAP$^{+}$ astrocytes (Lavisse, Inoue, *et al.*, 2015). PET imaging in healthy volunteers suggested that [$^{18}$F]DPA714 is a promising radioligand with good stability and expected biodistribution (Arlicot *et al.*, 2012; Lavisse, García-Lorenzo, *et al.*, 2015); high binding in the thalamus and low binding in the cerebellum (Lavisse, García-Lorenzo, *et al.*, 2015), similar to the distribution in non-human primates (Lavisse, Inoue, *et al.*, 2015).

To the best of our knowledge, the use of [$^{18}$F]DPA714 in PD patients has not been published yet. However, Terada and colleagues have reported significant increases of $BP_{nd}$ in the occipital, temporal and parietal cortex of PD patients using [$^{11}$C]DPA713, which was increased even further 1 year later (Terada *et al.*, 2016). Similarly, other studies using [$^{11}$C](R)-PK11195 have shown increased binding levels in the pons, basal ganglia (including substantia nigra and striatum), and frontal and temporal cortical regions (Ouchi *et al.*, 2005; Gerhard *et al.*, 2006; Edison *et al.*, 2013; Iannaccone *et al.*, 2013), which remained stable over 2 years (Gerhard *et al.*, 2006).

# Context and aims of the PhD Thesis

EVALUATION OF THE DOPAMINERGIC SYSTEM USING *IN VIVO* PET IMAGING AND *POST-MORTEM* ANALYSES IN THE CONTEXT OF MILD NEURODEGENERATIVE AND NEUROINFLAMMATORY PD MODELS

## Scientific context: BrainMatTrain program

Even though cell replacement therapy has great potential, there is still suboptimal cell survival, differentiation, and reinnervation of host tissue. Studies report a <20% survival rate for grafted fetal tissue and <10% for grafted human iPSC-derived dopaminergic neuron progenitor cells (Castilho, Hansson and Brundin, 2000; Bruggeman et al., 2019). Biomaterials may have great potential to overcome these problems with cell-based therapies and might propel the field forward. Biomaterials can be utilised to provide physical support during implantation and differentiation, as well as to deliver relevant tropic factors to both grafted and host tissue (Bruggeman et al., 2019). Biomaterials of interest are hydrogels; 3D networks of hydrated polymers (Bruggeman et al., 2019). Hydrogels are one of two main components of the extracellular matrix (Frantz, Stewart and Weaver, 2010), making them well-suited to mimic the extracellular environment (Bruggeman et al., 2019). Indeed, GDNF-containing hydrogels were found to increase survival, striatal re-innervation, and functional efficacy of grafted fVM cells in 6-OHDA-lesioned rats (Moriarty, Pandit and Dowd, 2017; Moriarty et al., 2019).

"Development of Biomaterial-based Delivery Systems for Parkinson's Disease- An Integrated Pan-European Approach", BrainMatTrain, was an Intensive Training Network program financed under the Marie-Sklowdoska-Curie Actions, which financed the current PhD work. The goal of the BrainMatTrain project[3,4] was to develop a multi-modal collagen-based hydrogel that incorporates both neuroprotective and anti-inflammatory moieties to help improve graft survival in a PD environment. BrainMatTrain, which has officially finished December 2019, was an interdisciplinary project to study the use of biomaterials from fundamental to translational preclinical research, and up to commercial development.

Within this network I have focused on the improvement and characterisation of rodent models and their *in vivo* biomarkers, with the ultimate aim to follow the therapeutic efficacy of the multi-modal hydrogels *in vivo*. In order to achieve this, I have worked closely together with Francesco Gubinelli on the characterisation of the models and their biomarkers. Additionally, I have visited our partners at Lund University to gain more insight into the technical difficulties that come with cell grafting in rodent models.

[3] http://www.curamdevices.ie/curam/research/eu-projects/currentprojects/h2020---marie-curie/brainmattrain/

[4] The BrainMatTrain project is funded by the European Union Horizon 2020 Programme (H2020-MSCA-ITN-2015) under the Marie Skłodowska-Curie Initial Training Network and Grant Agreement No. 676408.

## Aim of the PhD Thesis

As described above, the brain pathology of Parkinson's disease is characterized by a progressive dopaminergic neurodegeneration, accumulation of α-synuclein aggregates, and the presence of neuroinflammation. To this day there is no treatment that can slow or stop PD progression; treatment only exists to alleviate the symptoms. Animal models are often used to learn more about disease progression and in search for novel treatments. As discussed above, there are many different animal models that can be employed to model specific traits of PD, ranging from neurotoxic and neuroinflammatory-causing substances to PD-related gene overexpression.

PD is a progressive disease with a long prodromal phase that emerges later in life. Especially the prodromal to early, mild stages of PD are ideal targets for treatments to slow or stop PD progression. Even though this represents an important phase within the physiopathology of PD, only few imaging studies exists on mild models of PD revealing the course of dopamine pathology.

The "Neurodegenerative Diseases Laboratory" of MIRCen evaluates neurodegeneration, protein aggregation, neuroinflammation, and genetic predisposition and their interaction using different models ranging from cell cultures to viral-vector induced rodent and primate models. At MIRCen we have access to several techniques to study our models, including *in vivo* MR and PET imaging, behavioural assessment, and *post-mortem* immunohistochemistry and RT-qPCR.

Behavioural studies are widely accessible in preclinical research and therefore, first choice to evaluate neuronal loss *in vivo*, even though, moderate neuronal loss does not induce a pronounced behavioural phenotype and requires sensitive behavioural tests that are consistently performed. PET imaging offers the advantage to image dopaminergic neuronal loss *in vivo* and has been put forward as the translational imaging technique in both preclinical and clinical studies. However, preclinical PET imaging in these mild rodent models is highly challenging; neuronal loss is only moderate, and thus the choice of image post-processing will be crucial to obtain optimal sensitivity of detection. Preclinical rodent studies offer the access to *post-mortem* analysis, which allows validation of *in vivo* results. The strength, and the major challenge within this project, was to combine *in vivo* behavioural analyses and PET imaging with *post-mortem analysis*, which were all performed on the same animals. With the combibation of these tools, we aimed for an extensive comprehension of *in vivo* imaging markers.

**In this PhD thesis, I aimed to evaluate *in vivo* the effects of 1- α-synuclein overexpression, 2- α-synuclein and LRRK2 co-expression, and 3- mild neuroinflammation, on the dopaminergic system and dopaminergic neuronal cell loss.**

**To this end, PET imaging and behavioural studies have been selected as the main *in vivo* tools. *In vivo* data were validated by *post-mortem* techniques evaluating gene- (by RT-qPCR) and protein-expression (by immunohistochemistry).**

# 2

# *METHODOLOGY AND IMPROVEMENTS*

## 1. Statistical analysis

Data are presented as mean ± standard error of the mean (SEM), unless stated otherwise. Data is presented as %-change or as relative difference (Δ%), further referred to as asymmetry or asymmetry ratio. While %-change infers a directionality of the difference as compared to the contralateral hemisphere, relative difference does not give a directionality, and can thus be used with varying contralateral data.

$$\%\ change = \frac{(ipsilateral - contralateral)}{contralateral}\ x\ 100$$

$$Asymmetry\ ratio = \ \Delta\% = \frac{|\ ipsi - contra\ |}{(ipsi + contra) * 0.5}\ x\ 100$$

The number of rats is indicated by *n*. Statistical analysis was performed using Statistica 13 software (Statsoft; Tulsa, USA). Prior to analysis, the data were assessed for normality and homogeneity of variance. Difference between the injected and non-injected side were analysed using the student t-test. If multiple groups were compared an ANOVA test was used, followed by Scheffé post-hoc analysis. Spearman correlation analyses were performed using R software. Annotations used to indicate level of significance are as follows: *P < 0.05, **P < 0.01, ***P < 0.001.

## 2. Animals

All animal experimental procedures were performed in accordance with the French regulation (French Act Rural Code R 214/87-131; authorization n°B 92-032-02) and complied with Standards for Humane Care and Use of Laboratory Animals of the Office of Laboratory Animal Welfare (OLAW – n°A5826-01) and the European Union (EU Directive 2010-63/EEC). All experimental procedures performed in this PhD work received approval from the local ethical committee (CETEA n°44), and the French Ministry of Education and Research (approvals SYNCHNEURO: …, LRRKSYN: APAFIS#1372-2015080415269690v02, NEUROMODEL: APAFIS#389-2015032716213569 0v02). All efforts were made to minimize animal suffering and animal care was supervised by veterinarians and animal technicians skilled in rodent healthcare and housing.

All animals used for the presented studies are male Sprague Dawley rats (JANVIER; St Berthevin, France), which arrived with a mean weight of ~280 grams, and acclimatised one week before start of any study. Rats were randomly allocated to experimental groups.

### 2.1 Housing

Rats were housed in a temperature-controlled (22±1°C, humidity 50%) room maintained on a 12/12 hour light/dark cycle. Food and water were provided ad libitum. Animals were housed, if possible, in pairs in standard individual ventilated rat cages with either corn cob or wood chip bedding. Enrichment was provided in the form of tissue paper, and a wooden chewing block.

### 2.2 Anaesthesia & monitoring

All experimental procedures, except behavioural testing, have been performed under general anaesthesia. Overall, anaesthesia was induced with 4% isoflurane (Iso-Vet; Coumon d'Auvergne,

France) in 100% $O_2$. To prevent corneal desiccation, ophthalmic ointment was regularly applied on the eyes during all procedures.

For stereotactic injections, anaesthesia was maintained with an intrapereotoneal (*i.p.*) injection of a mixture of ketamine (75 mg/kg; Imalgène 1000; Merial, Lyon, France) and xylazine (5 mg/kg; Rompun™; Bayer Animal Health). As analgesia, lidocaine (Xylovet; Ceva Santé Animale, Libourne, France; 7 mg/kg) was administered subcutaneously under the scalp prior to the stereotactic surgery. After surgical intervention, anaesthesia was reversed by subcutaneous injection of atipamezole (0,5 mg/kg; Antisedan; Vetoquinol, France).

For *in vivo* PET imaging and MR imaging studies, maintenance of anaesthesia was assured with 1.5-2.5% isoflurane in $O_2$.

During stereotactic injection and PET imaging, body temperature was monitored with a rectal probe and a feedback coupled heating blanket (Homeothermic Blanket System; Harvard Apparatus Ltd.), while using regulated water flow in the MRI bed during magnetic resonance (MR) imaging. Respiratory rate was monitored during MR imaging using PC SAM software (Small Animal Instruments, Stony Brook, USA), or using a home-made respiration monitoring system and an oxygen saturation/heartbeat monitoring system (PureSAT® 2500A VET; Nonin, USA or CapnoTrue® AMP; Bluepoint Medical, Germany) during PET imaging.

## 2.3 Stereotactic surgery

Anaesthetised rats were placed on the stereotactic frame and injected using 34-gauge blunt-tip canula linked to a 10 µl Hamilton syringe (Hamilton; Reno, USA) by a polyethylene catheter and a micro pump (Micro4 Controller; WPI Inc.). After injection the needle was left in place for an additional 5 minutes and then slowly withdrawn.

At the end of the surgical procedure, the site of incision was cleaned and the scalp was closed using Michel wound clips. After anaesthesia reversal, rats were rehydrated with a subcutaneous injection of warm saline (10 ml/kg) and left in a ventilated heating box (28°C) until they fully recovered from anaesthesia. Post-surgery analgesia was insured by the administration of paracetamol (1.6 mg/ml; Doliprane) in the drinking water for 48 hours.

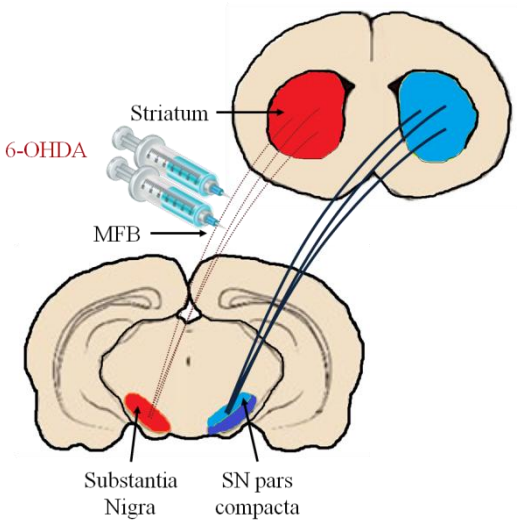


**Figure 7: Schematic overview of our complete lesion model.** 6-OHDA is unilaterally injected in two separate locations near the MFB, connecting the substantia nigra and striatum.

### 2.3.1 Complete lesion model: 6-OHDA

The gold-standard rat model for Parkinson's disease (PD) is the 6-hydroxydopmine (6-OHDA) model. As stated above (Chapter 1: 2.1, page 24), 6-OHDA has been used since the sixties (Ungerstedt, 1968), and it can cause rapid and complete neurodegeneration if injected into the medial forebrain bundle (MFB) (Cadet and Brannock, 1998). Here, we used this widely studied complete lesion model to train the experimenter and evaluate, validate, and where needed, improve our methods, for the use on milder PD models.

To induce a severe unilateral dopaminergic lesion, 6-ODHA (Sigma-Aldrich, France) was injected in the MFB (Figure 7). 6-OHDA was injected into two separate locations at a rate of 0.5 µl/min with a final mass of 17.5 µg of 6-OHDA per rat; 2*2.5 µl 6-OHDA solution at a concentration of 3.5 µg/µl, diluted in phosphate buffered saline (PBS). 6-OHDA was unilateral injected into the right MFB at the following stereotactic coordinates (Paxinos and Watson, 1998): anteroposterior -3.8/-4.4 mm inter-aural, mediolateral -1.6/-1.4 mm from bregma, and ventral -7.8/-8.0 mm from the dura, with the tooth bar set at -3.9 mm.

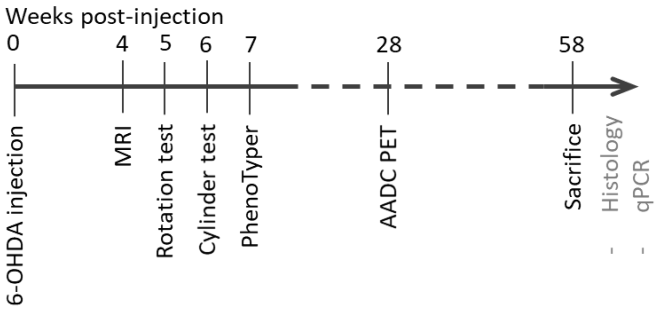


**Figure 8: Schematic overview of timeline for our complete lesion model.**

### The complete lesion model for validation and optimisation

For validation and optimisation of novel and existing techniques, six 6-OHDA rats have been used for behavioural testing, PET imaging, immunohistochemistry, and real-time quantitative PCR (RT-qPCR) (Figure 8). The apomorphine-induced rotation test was performed at 5 weeks post-injection (wpi), the cylinder test at 6wpi, and the PhenoTyper test at 7wpi. AADC-PET imaging was performed at 6 months post-injection. All animals were sacrificed at 17 months post-injection. Immunohistochemistry was performed using primary antibodies directed against dopamine transporter (DAT), ionized calcium-binding adapter molecule 1 (IBA1), tyrosine hydroxylase (TH), vesicular monoamine transporter 2 (VMAT2), and S129-phosphorylated α-synuclein (pS129-α-syn), for further details see section 6.2, page 71. For RT-qPCR primers were used against aromatic L-amino acid decarboxylase (AADC), DAT, IBA1, TH, and VMAT2, for further details see section 6.3, page 75.

Data is presented as %-change and as relative difference (Δ), further referred to as asymmetry or asymmetry ratio.

## 2.3.2 Mild dopaminergic lesion model: α-synuclein overexpression

Previously, our lab developed a viral vector-induced α-synuclein overexpressing rodent PD model; overexpressing either A53T mutant human α-synuclein protein (see Chapter 5, page 108, Cresto et al., *submitted*) or WT human α-synuclein (unpublished data) in the substantia nigra ($2.5x10^{10}$ viral particles). In order to aggravate and/or accelerate this model, in the context of my PhD, we doubled the viral vector dose, as well as the number of injection sites per substantia nigra; thus increasing the viral genome count four-fold.

For AAV production, plasmids constructs were packaged into AAV2/6 capsids as previously described (Berger *et al.*, 2015). AAVs coded for WT or A53T α-synuclein, under the control of the PGK promotor. Briefly, viral particles were produced by transient co-transfection of HEK-293T cells with an adenovirus helper plasmid (pXX6-80), an AAV packaging plasmid carrying the rep2 and cap8 genes, and the AAV2 transfer vector containing the above-mentioned expression (WT or A53T-α-synuclein) cassettes. Seventy-two hours after transfection, recombinant vectors were purified and

concentrated from the cell lysate and supernatant by ultracentrifugation on an iodixaniol density gradient, followed by dialysis against PBSMK (0.5 mM MgCl2 and 1.25 mM KCl in PBS). Concentration of the vector stocks was estimated by quantitative PCR following the method described by Aurnhammer and colleagues (2012) and expressed as viral genomes per ml of concentrated stocks (vg/ml).

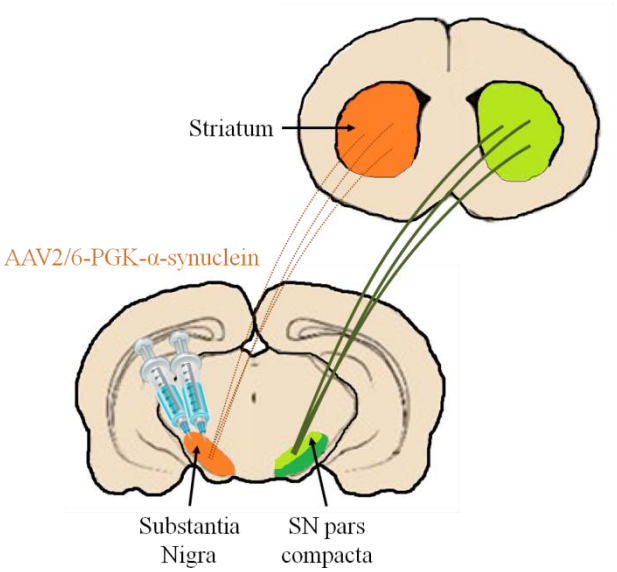


**Figure 9: Schematic overview of our mild dopaminergic lesion model.** AAVs coding for WT or A53T α-synuclein are unilaterally injected into two sites of the substantia nigra**.**

Recombinant AAVs coding for either wild-type (WT) or A53T mutated human α-synuclein were injected into the left substantia nigra of rats, at a rate of 0.25 µl/min, using a double needle injection approach (Figure 9). A total of 6 µl of viral vector solution was injected per rat, evenly divided over the two injection sites. Viruses were injected at a concentration of $5.0x10^{10}$ viral particles per injection site, giving a final concentration of $1.0x10^{11}$ viral particles per rat.

The following stereotactic coordinates (Paxinos and Watson, 1998) were used: anteroposterior +2.4/+3.4 mm inter-aural, mediolateral +2.0 mm from bregma, and ventral -7.8 mm from the skull, with the tooth bar set at -3.3 mm. The coordinates were verified on age-matched animals prior to stereotactic injection with AAV2/6-PGK-α-synuclein, using blue dye injection and subsequent slicing of frozen brains.

In Chapter 5 (page 108), the synergistic effect of A53T-α-synuclein and leucine-rich repeat kinase 2 (LRRK2) overexpression on the survival of dopaminergic neurons in the substantia nigra is evaluated. For this, AAVs coding for A53T-α-synuclein was co-injected with AAVs coding for GFP, G2019S-ΔLRRK2 or DK-ΔLRRK2 (dead kinase) at the same stereotactic coordinates. Further details on the LRRK2 vectors can be found in the paper included in Chapter 5.

### 2.3.3 Neuroinflammation model: LPS

Lipopolysaccharide (LPS) from *Escherichia coli* can cause a systemic or local neuroimflammatory response, as previously described in Chapter 1: 2.3, page 25. Although LPS is an established model for neuroinflammation, it has only recently been developed and validated in our lab, in collaboration with my colleague Dr. Gubinelli (PhD 2016-2019), in the context of the BrainMatTrain project.

LPS (L2880, Sigma-Aldrich, France) was diluted with PBS to reach a concentration of 5 µg/µl. Each animal was unilaterally injected in the left striatum with 2 µl of solution, hence 10µg of LPS per rat, at a rate of 0.5 µl/min (Figure 10). The following stereotactic coordinates were applied (Paxinos and Watson, 1998): anteroposterior +0.5 mm from bregma, mediolateral +3 mm from bregma, and ventral -4.3 mm from the dura, with the tooth bar set at -3.3 mm.

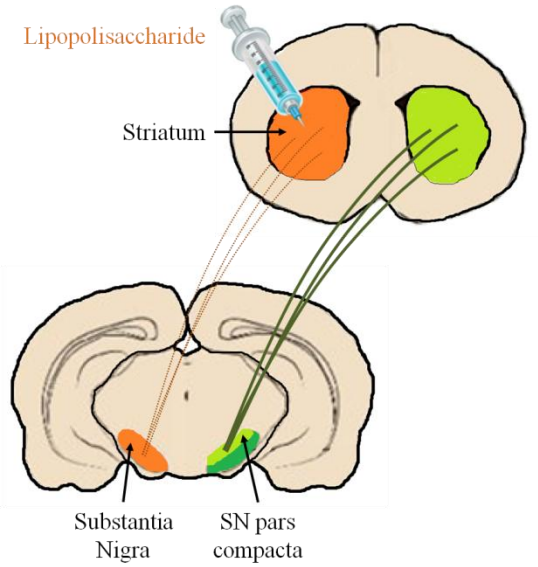


**Figure 10: Schematic overview of our neuroimflammatory model.** LPS is unilaterally injected into the striatum.

## 3. Behavioural analyses

Prior to all behavioural testing, the animals were habituated to experimenter's handling and interaction during a 5-day habituation period, during 2 minutes every day. All behavioural experimentation was recorded using a small camera and EthoVision XT software (Noldus Information Technology, Wageningen, the Netherlands).

### 3.1 Apomorphine-induced rotation test

Apomorphine is a non-selective dopamine agonist, which binds to both $D_1$ and $D_2$-receptors (Schwarting and Huston, 1996; Millan et al., 2002), resulting in rotational behaviour in unilateral dopaminergic lesion models. Literature suggests that a severe unilateral lesion (>80-90% dopaminergic nerve terminal loss (Hudson *et al.*, 1993; Schwarting and Huston, 1996)) or a large dopamine depletion (>95%; (Chang *et al.*, 1999)) are required to induce rotational behaviour after apomorphine administration. Below this threshold rotational behaviour will not occur.

For this test we used the Rotameter set-up (Panlab-Harvard Apparatus, Spain), which can hold up to 4 rats at the same time, and was placed in a operator-separate room with lighting at 90 lux. The individual bowls were separated from each other by opaque plastic walls (±30 cm), while an infrared camera was mounted above the bowls to observe the rats from the operator-separate control room. Apomorphine (10 mg/ml; Sigma-Aldrich, France) was diluted 1:10 in saline to create a stock solution of 1 mg/ml. Each rat received an *i.p.* apomorphine injection while awake, with a dose of 0.75 mg/kg. Rats were immediately placed in the Rotameter harness, and counting started as soon as all rats were placed in the Rotameter apparatus. Clockwise and counter-clockwise rotations were recorded for 60 minutes, after which rats were placed back in their home cages and surveyed for another 30 minutes. Clockwise rotations were subtracted from counter-clockwise rotations to arrive at the net counter-clockwise rotations.

#### 3.1.1 Preliminary evaluation in a complete lesion model

Whilst the amphetamine-induced rotation test has previously been employed in the lab with rat PD models, apomorphine has not been used before. The general setup of the apparatus and

analysis method is the same; however, the time-window of assessment of the rotations has a crucial impact on the evaluation of the results, as demonstrated below.

Comparison of clockwise (CW) and counter-clockwise (CCW) rotations over a 60 minute period demonstrated significant more counter-clockwise rotations (+2489±515%; Δ179±7%; n=6; p=0.0007). We observed that the average counter-clockwise rotations per 3-minute interval dropped drastically after 39 minutes (Figure 11A). The elimination half-life of apomorphine is 28 minutes (Symes, Lal and Soukes, 1976), which corresponds with this observation. Therefore, it has been decided to assess only the first 30 minutes of the apomorphine-induced rotation test.

Comparison of clockwise and counter-clockwise rotations over the first 30 minute period resulted in an even larger difference of +8746±2874%, or a relative difference of Δ194±2% (n=6; p=0.0003). Even though the total and net number of rotations decreased (Figure 11B), the RPM values increased (Figure 11C). The test indicates that our 6-OHDA animals have a severe lesion, which was later on confirmed by histological assessment (section 6.2.6, page 73).

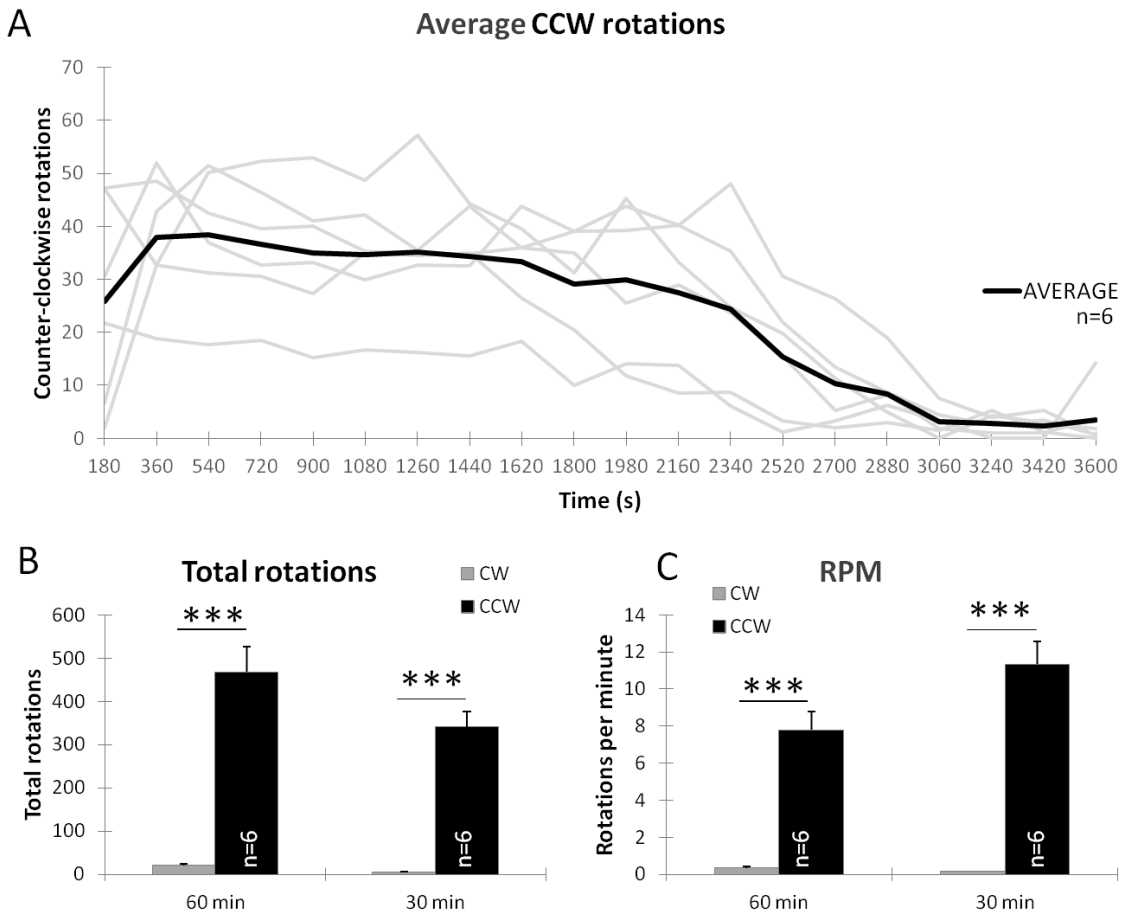


**Figure 11: Behavioural assessment with apomorphine-induced rotation test in 6-OHDA rat model at 5wpi. A)** Counter-clockwise rotations per animal (grey) and group average (black) over time. **B)** Group average total clockwise (grey) and counter-clockwise (black) rotations over a 60 minute period (left) or the first 30 minute period (right). **C)** Group average rotations per minute for total clockwise (grey) and counter-clockwise (black) rotations over a 60 minute period (left) or the first 30 minute period (right). Results are expressed as means ± the standard error of the mean (SEM). Paired student t-test **p<0.01, ***p<0.001.

## 3.2 Spontaneous forelimb use: Cylinder test

The cylinder test evaluates forelimb usage by counting the number of touches by the forepaws - either left, right, or simultaneous - with the wall of a clear glass cylinder (5L, Ø20 cm). The animals were placed in the glass cylinder in an operator-separate room (lights at 90 lux), with a video camera placed below the cylinder. The animals were recorded during 5 minutes. Video recordings were analysed by counting the number of contacts with the wall of the clear glass cylinder, for each forepaw, alone or simultaneous. The number of impaired forelimb contacts – contralateral to the injection – was expressed as a percentage of total forelimb contacts, as described in the paper by Gombash and colleagues (Gombash et al., 2013);

$$Gombash = \frac{(contra + \frac{1}{2} * simultaneous)}{(contra + ipsi + simultaneous)}$$

Control rats should score around 50% in this test. For statistical analyses a student t-test with unequal variance was performed against this hypothetical 50% score. Literature has shown that forelimb use is significantly correlated with striatal TH levels, as seen by optical density measurements (Gombash *et al.*, 2013).

### 3.2.1 Preliminary evaluation in a complete lesion model

The cylinder is frequently used in our lab to study unilateral PD models (unpublished data).

We confirmed that in healthy control groups, rats have an average Gombash score that is not significantly different from the hypothetic 50% score (Figure 12, 49%; WT: n=15; p=0.50). In the complete 6-ODHA model, the cylinder test showed significantly reduced use of -54±9% of the contralateral forepaw at 6wpi (Figure 12; n=6; p=0.0019), or a left-right asymmetry ratio of (Δ116±18%). These data correspond to what has previously been published on the cylinder test in a complete 6-ODHA lesion model (Decressac, Mattsson and Björklund, 2012).

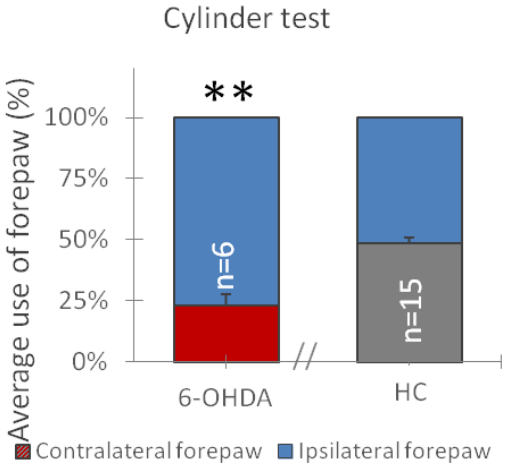


**Figure 12: Behavioural assessment with cylinder test in 6-OHDA rat model at 6wpi and healthy controls.** Average percentage of contralateral (red/grey) and ipsilateral (blue) forepaw contacts with the cylinder during 5 minutes. Student t-test with unequal variance was performed against the hypothetical 50% score. Results are expressed as means ± the standard error of the mean (SEM). Student t-test with unequal variance **p<0.01.

## 3.3 Spontaneous locomotor activity: PhenoTyper

Spontaneous locomotor activity was recorded in PhenoTyper cages (Noldus Information Technology, Wageningen, the Netherlands). The PhenoTyper is an instrumented home cage in which rodent behaviour is automatically monitored through a video-based observation system. The cages are 45 cm x 45 cm x 45 cm, and are made of transparent Perspex walls with an opaque black Prespex

floor covered with grey cellulose-based bedding (Cellu-Dri, Technilab-BMI BV, the Netherlands). Cages are equipped with a water bottle and feeding station, with *ad libitum* food and water provided. Each cage also contains a top unit with built-in hardware for video tracking (digital infrared-sensitive video camera and infrared lights). Six PhenoTyper cages were connected via two sequential Quad units to a single computer. Rats were introduced into the PhenoTyper cages at 10h00, during the light phase, and monitored for 23 consecutive hours. Ethovision XT (Noldus Information Technology, Wageningen, the Netherlands) was used for data acquisition and for analysis. The following parameters were assessed: total distance moved, mean velocity, and time spend moving.

### 3.3.1 Preliminary evaluation in a complete lesion model

In MIRCen, the PhenoTyper cages have been used before in Alzheimer disease models (unpublished data), but they have never been used in a PD model.

Here, we compared spontaneous movement over 23 hours in 6-OHDA rats (n=6) with healthy age-matched controls (n=3), using PhenoTyper cages (Noldus Information Technology, Wageningen, the Netherlands). We did not observe any significant differences in total distance moved (Figure 13A; n=6/2; p=0.342), mean velocity (Figure 13B; n=6/2; p=0.343), or time spend moving (Figure 13C; n=6/2; p=0.788).

Sgroi and colleagues (2014) claim that locomotor activity in 6-OHDA animals (10µg in 4 µl ascorbic acid 0.1%) stabilised 2 weeks post-injection. But, they do not report if locomotor activity differed before and after surgery. To the best of our knowledge, significant differences in locomotor behaviour using PhenoTyper cages have only been reported after levodopa treatment (Nikolaus *et al.*, 2014; Sgroi, Kaelin-Lang and Capper-Loup, 2014). This makes spontaneous locomotor activity tracking using the PhenoTyper not an ideal analysis technique for our models. We have therefor not used it in subsequent studies.

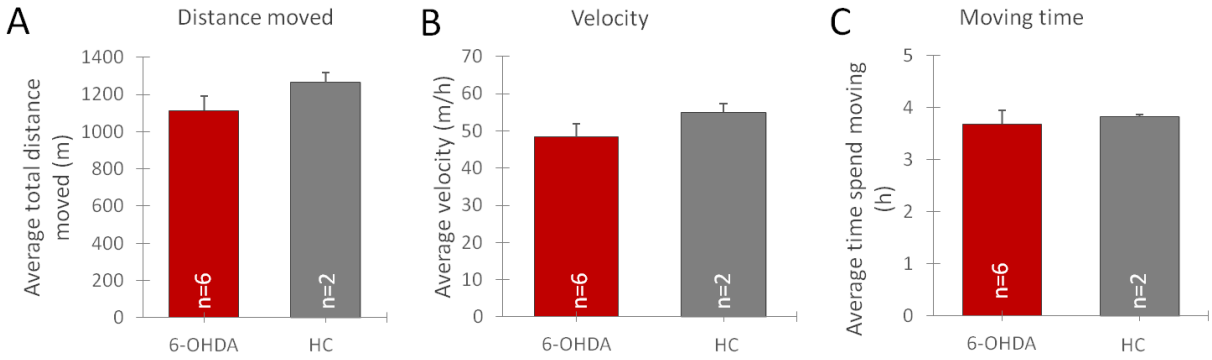


**Figure 13: Behavioural assessment with PhenoTyper activity cages in 6-ODHA rats and healthy control rats at 7wpi. A)** Group averages for 6-OHDA (red) and healthy controls (grey) of total distance moved in meters during 23 hours. **B)** Average velocity in m/h during 23 hours. **C)** Average time spend moving in hours during 23 hours. Results are expressed as means ± the standard error of the mean (SEM). Student t-test, non-significant.

## 3.4 Forelimb akinesia: Adjusting step test

The adjusting step test allows assessing asymmetry in motor abilities. The adjusting step test was performed after the example of Olsson and colleagues (1995). Briefly, rats are held by the torso fixing one forelimb, while the other forepaw touches the table. Rats are then moved across the table

by an experienced experimenter at a speed of around 5 sec/m, sequentially in the forehand and backhand direction. This is repeated until at least two good runs are recorded for both forelimbs, with a maximum of 5 minutes per rat. Video recordings are analysed at a lower speed to count the number of steps for each trial. An average of four trials per forepaw was used for statistical analysis:

$$\frac{\sum contralateral\ steps}{\sum ipsilateral\ steps + \sum contralateral\ steps}$$

The adjusting step test has previously succesfully been used in our lab on PD models (unpublished data). Olsson and colleagues (1995) showed that, in a 6-OHDA rat model, the contralateral forepaw is severely affected in the adjusting step test, in both the backhand and forehand direction, which resulted in a dragging paw when the rats was moved sideways by the experimenter (Olsson *et al.*, 1995). Even though one study suggested that large depletion of striatal dopamine is necessary before rats can no longer make the adjusting steps (Chang *et al.*, 1999), more recent literature suggests that the adjusting step test is capable to detect partial lesion, and might be more sensitive than the cylinder test. Rats injected with preformed fibrils, inducing 48% loss of TH-positive neurons in the ipsilateral substantia nigra, showed reduced use of the contralateral forepaw in the adjusting step test but no in the cylinder test (Patterson *et al.*, 2019).

We have used the adjusting step test in the WT and A53T-α-synuclein model, results of which are presented and discussed in Chapter 3 (page 86).

## 3.5 Sensorimotor integration: Vibrissae-evoked forelimb-placing test

The vibrissae-evoked forelimb-placing test allows assessing sensorimotor integration. The test was performed after the example of Schallert and colleagues (2000). Rats were held in the similar grip as for the adjusting steps test, while vibrissae were stimulated by brushing the edge of a table by a forward movement. In a control animal, this quickly elicits an ipsilateral forepaw touch on the table; animals with a unilateral lesion will show impaired limb placing ability, but no deficit on the unimpaired side. One session contains three successful trials on every side, or a maximum test time of three minutes. The outcome score is calculated as a percentage of touches or misses on total attempts:

$$\frac{number\ of\ successful\ runs}{total\ runs} \times 100\%$$

The vibrissae-evoked forelimb-placing test has, to the best of my knowledge, never been performed in our lab before.

Schallert and colleagues (2000) have demonstrated that 6-OHDA lesioned rats, with 88% reduction of dopamine concentration in the striatum, show a severe significant deficit using the vibrissae-evoked forelimb-placing test (Schallert *et al.*, 2000). In a Huntington disease model, Lelos and colleagues (2016) observed a significant motor deficit using the vibrissae-evoked forelimb-placing test, but not using the cylinder test, suggesting higher sensitivity of the vibrissae-evoked forelimb-placing test compared to the cylinder test (Lelos *et al.*, 2016).

We have used the adjusting step test in the WT and A53T-α-synuclein model, results of which are presented and discussed in Chapter 3 (page 86).

## 3.6 Conclusion and choice of behavioural tests

To the best of our knowledge, only a few studies have reported on the use of the PhenoTyper in PD models, showing only relevant results after levodopa treatment. In our hands, the PhenoTyper did not demonstrate any significant deficits in spontaneous locomotor activity in the complete 6-OHDA lesion model, and thus we do not expect to detect any spontaneous deficits in milder lesion models. Therefore, we have not further evaluated this test in any of the other models.

Even though the apomorphine-induced rotation test showed very promising results in the 6-OHDA model, it is known from literature that a large lesion or severe dopamine depletion are required for this test to show significant turning behaviour. Since we do not expect such an extensive lesion in our α-synuclein overexpression models, we have opted not to use it for the models evaluated in this PhD study.

The cylinder test is easy to put in place, robust and little time-consuming. For these reasons, this was the behavioural test of choice. According to literature, the adjusting step test and vibrissae-evoked forelimb-placing test have good potential to identify mild lesions and motor deficits, with a higher sensitivity as compared to the cylinder test. Therefore, we have included these tests in the evaluation of α-synuclein overexpression models (Chapters 3, 4, and 5).

# 4. Magnetic resonance Imaging

## 4.1 MR acquisition

For each study, anatomical 3-dimensional (3D) $T_2$-weighted MR images were acquired on a separate group of age-matched animals using a horizontal 11.7 T scanner (Bruker, Ettlingen, Germany) and ParaVision 6 software (Bruker, Germany). Animals were fixed in prone position in a MRI-compatible stereotactic rat frame to prevent head motion. 3D T2-weighted images were acquired using a turbo-spin echo sequence with the following parameters: TE, 45 ms; 17 echo averages; TR, 10000 ms; in-plane resolution 200x200 µm; 100 slices with 300 µm thickness; resulting in an acquisition time of 20 min.

## 4.2 Image processing

Image processing was performed using PMOD® software (PMOD 3.804; PMOD Technologies LLC, Switzerland). All processes were performed by the same operator for all animals.

### 4.2.1 Creation of MRI template

MRI templates of age-matched animals (Figure 14) were created to the example of Vállez Garcia and colleagues (2015). This was performed for the studies of Chapters 3 and 4(Early timepoint: n=4; bw=580±11g, Late: n=8; body weight (bw)=484±8g), Chapter 5(n=4; bw≈567g), and Chapter 6 (n=3; bw=450±20g).

Briefly, a brain mask was applied to individual T2-weighted MR images. These masked MR images were then automatically co-registered to a representative image using rigid transformations using the FuseIt module of PMOD® software. Next, the co-registered images were averaged into a single image. This averaged image was subsequently mirrored in axial orientation. This mirrored image was then automatically co-registered to the initial averaged image using the FuseIt module of

PMOD® software. Finally, the average-MR-image and the co-registered-mirrored-average-MR-image were averaged into a single image, resulting in the final MRI template.

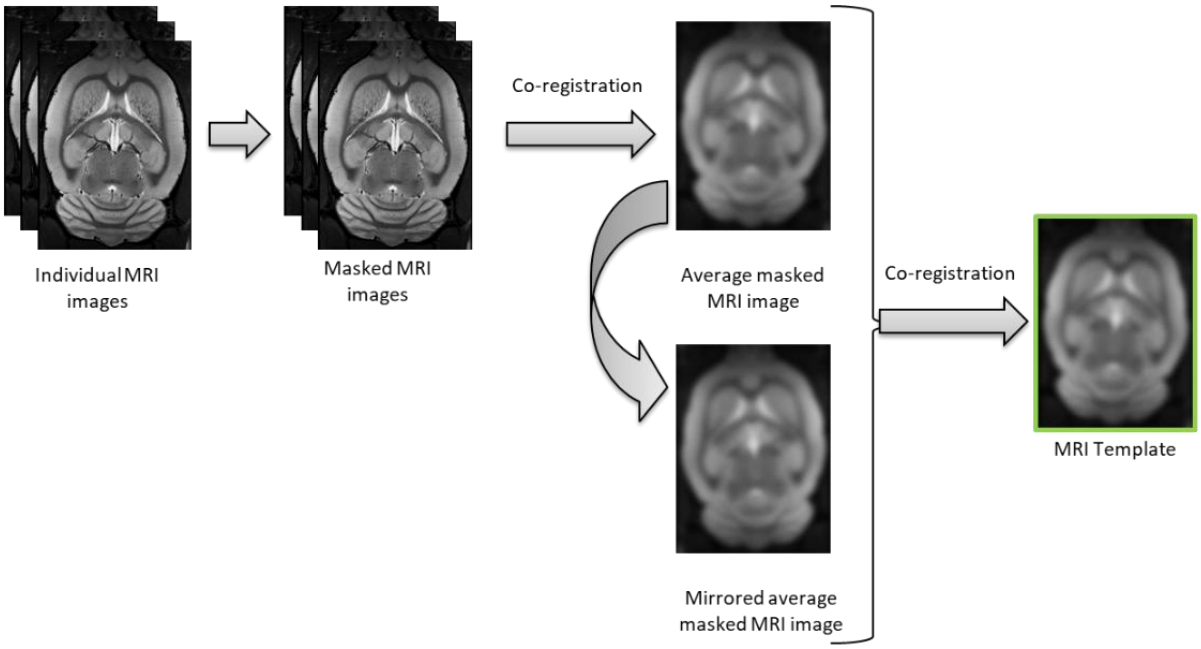


**Figure 14: Schematic representation of the creation of the MRI template.** First, all individual MRI are masked. Subsequently masked images were co-registered to a representative image using rigid transformations and averaged. This average MRI was mirrored, and co-registered to the original average MR image. Lastly, the mirrored and original averaged MR image were averaged again, created our final MRI template.

### 4.2.2 Co-registration of Atlas to MRI template

To define anatomical areas of interest, an existing MRI Atlas was adapted to the home-made MRI templates that were created for each individual study (Figure 15). To this end, the home-made MRI template was automatically co-registered to the T2-weighted MRI template of the Schiffer/PMOD Rat Brain Atlas, using affine transformations in the FuseIt module of PMOD® software (Schiffer *et al.*, 2006). The inverse transformation was subsequently used to place the Schiffer/PMOD Rat Brain Atlas (Schiffer *et al.*, 2006) on our MRI template.

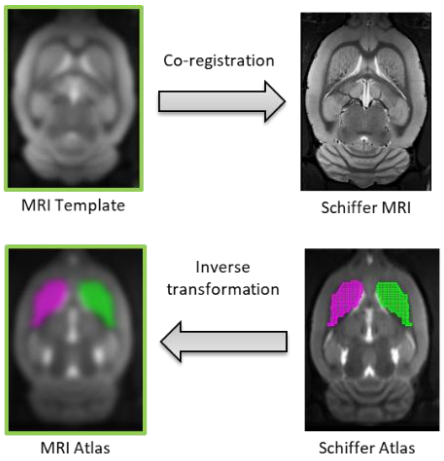


**Figure 15: Schematic representation of co-registration of the Schiffer rat brain atlas to the MRI template.**

### 4.2.3 Creation of BrainMask

To mask outer-brain signal on PET images, a BrainMask was created based on the Schiffer/PMOD Rat Brain Atlas (Schiffer *et al.*, 2006). For this, the individual regions of interest (ROIs) were fused into one large ROI covering the whole brain, which was subsequently dilated by 2 pixels. This BrainMask has corresponding localisation to the home-made MRI templates.

# 5. Positron Emission Tomography

## 5.1 Radioligand synthesis

### 5.1.1 6[$^{18}$F]fluoro-L-m-tyrosine

6-$^{18}$F-fluoro-L-m-tyrosine ([$^{18}$F]FMT) is a PET tracer that is metabolised by aromatic L-amino acid decarboxylase (AADC), which is involved in the production of dopamine (Chapter 1: 4.4.2, page 40). [$^{18}$F]FMT was synthesized as described by Lemaire and colleagues (2015). Briefly, the radiosynthesis of [$^{18}$F]FMT was realised using a multi-step approach after $^{18}$F substitution of a small deactivated aromatic ring. Its conversion into an $^{18}$F-fluorobenzyl halide compound was followed by the enantioselective formation of a new chiral carbon-carbon bond by phase transfer catalysis. Subsequent hydrolysis and HPLC purification afforded [$^{18}$F]FMT with a radiochemical yield of 30 ± 5% (decay corrected; mean±95% confidence interval). At the end of synthesis the enantiomeric purity was ≥ 96%, the specific activity was more than 555 GBq/µmol and the radioactivity concentration more than 1.1 GBq/mL.

[$^{18}$F]FMT injected volume was diluted in physiological water, and the average injected volume was 1 ml (range 0.5-1.7 ml). The injected doses (ID), body weight, and benserazide dose per study are shown in Table 3.

**Table 3: Overview of experimental parameters for [$^{18}$F]FMT PET imaging.** The column for "animals scanned" shows the total number of animals successfully scanned per group, and in brackets the number quantifiable PET scans.

| *Chapter* | *Group* | *Animals scanned* | *Average ID (MBq)* | *ID range (MBq)* | *Body weight (g)* | *Benserazide dose (mg/kg)* |
|---|---|---|---|---|---|---|
| *Ch 2* | 6-ODHA | 4 (4) | 48±3 | 41-54 | 612±12 | 5.14±0.05 *i.v.* |
| *Ch 3* | WT | 4 (3) | 40±1 | 36-43 | 579±23 | 9.99±0.20 |
| *Ch 4* | Early A53T | 7 (4) | 45±4 | 31-61 | 542±12 | 9.95±0.04 |
| *Ch 3 and 4* | Late A53T | 4 (2) | 43±2 | 40-46 | 589±21 | 11.24±1.2 |
| *Ch 4 add.* | Late A53T | 6 (5) | 49±1 | 43-53 | 569±15 | 9.98±0.10 |

### 5.1.2 [$^{18}$F]LBT999

8-((E)-4-fluoro-but-2-enyl)-3β-p-tolyl-8-aza-bicyclo[3.2.1]octane-2β-carboxylic acid methyl ester ([$^{18}$F]LBT999) binds reversibly to dopamine transporter (DAT), responsible for presynaptical dopamine reuptake (Chapter 1: 4.4.3, page 41). [$^{18}$F]LBT999 was synthesized as described by Dollé and colleagues (2007). Briefly, LBT999 was labelled with 18F at its 4-fluo-2-butenyl element via direct substitution of the chloro-analog. The mixture was purified by HPLC using ammonium acetate and the desired fraction was collected and diluted in water. [$^{18}$F]LBT999 was trapped using a light cartridge, eluted with ethanol, and subsequently diluted with 0.9% NaCl. The radiochemical yields of $^{18}$F were about 30-40%, and a radiochemical purity of >90%. Before usage, the tracer was diluted in 0.9% NaCl to have a maximum ethanol content of 15%.

[$^{18}$F]LBT999 was diluted in physiological water and the average injected volume was 0.8 ml (range 0.5-1.1 ml). Since [$^{18}$F]LBT999 is eluted with ethanol, dilutions needed to be made to not

exceed 15% of ethanol. The injected doses (ID), body weight, RAS, and ethanol dose per chapter are shown in Table 4.

**Table 4: Overview of experimental parameters for [$^{18}$F]LBT999 PET imaging.**

| *Chapter* | *Group* | *Animals scanned* | *Average ID (MBq)* | *ID range (MBq)* | *Body weight (g)* | *Injected mass (nmoles)* |
|---|---|---|---|---|---|---|
| *Ch 3* | WT | 3 | 60±1 | 58-62 | 566±21 | 7.86±3.26 |
| *Ch 4* | Early A53T | 6 | 46±2 | 40-52 | 546±15 | 9.90±4.0 |
| *Ch 3 and 4* | Late A53T | 4 | 57±2 | 54-63 | 590±21 | 7.55±2.54 |
| *Ch 5* | A53T/GFP | 7 | 52±2 | 45-62 | 565±22 | 4.46±0.82 |
| | A53T/GS | 7 | 52±3 | 45-66 | 587±14 | 3.44±0.81 |
| | A53T/DK | 7 | 53±3 | 39-61 | 580±13 | 6.16±1.71 |
| | PBS | 5 | 49±3 | 39-56 | 538±27 | 6.67±1.99 |

### 5.1.3 [$^{18}$F]DPA714

[$^{18}$F]DPA714[N,N-diethyl-2-(2-(4-(2-[18F]fluoroethoxy)phenyl)-5,7-dimethylpyrazolo[1, 5-a]pyrimidin-3-yl)acetamide] ([$^{18}$F]DPA714) binds to 18kD translocator protein (TSPO), located on the outer membrane of mitochondria, and upregulated during inflammatory events (Chapter 1: 4.4.7, page 43). [$^{18}$F]DPA714 was synthesised according to procedures previously reported (Damont *et al.*, 2008; James *et al.*, 2008). Briefly, DPA714 was labelled with $^{18}$F at its 2-fluoroethyl moiety using atosyloxy-for-fluorine nucleophilic aliphatic substitution, using a commercially available GE TRACERLab FX-FN synthesizer (GE Medicam Systems; Buc, France) (Kuhnast *et al.*, 2012). [$^{18}$F]DPA714 was formulated in physiological saline containing less than 10% of ethanol at a concentration of 61±13 MBq/mL (2.46±1.65 nmol/mL; mean±SD). Radiochemical purity of [$^{18}$F]DPA714 was greater than 99% and specific radioactivity ranging from 100 to 165 GBq/µmol (n=3; mean±SD).

[$^{18}$F]DPA714 injected volume was varied to compensate for changes in activity and diluted in physiological water; average injected volumes was 1.2 ml (range 1.0-1.5 ml). Since [$^{18}$F]DPA714 is eluted with ethanol, dilutions needed to be made to not exceed 15% of ethanol. The injected doses (ID), body weight, RAS, and ethanol dose per chapter are shown in Table 5.

**Table 5: Overview of experimetal parameters for [$^{18}$F]DPA714 PET imaging.**

| *Chapter* | *Group* | *Animals scanned* | *Average ID (MBq)* | *ID range (MBq)* | *Body weight (g)* | *Injected mass (nmoles)* | *Ethanol concentration (%)* |
|---|---|---|---|---|---|---|---|
| *Ch 6* | LPS | 9 | 61±4 | 39-82 | 375±5 | 2.46±0.46 | 12±1 |

## 5.2 Image acquisition and reconstruction

PET image aqcuisition was performed on a MicroPET® Focus 220 system (resolution: 1.5 × 1.5 × 1 mm; Siemens, France). Animals were placed within the scanner using a home-made stereotactic-like frame compatible with PET acquisition in prone position. Radioligands were injected into the tail vein, using an injection pump (Pump11 Elite; Harvard Apparatus Ltd.), at a rate of 1 mL/min *via* a 26-gauge catheter.

A dynamic emission scan was started simultaneously with the intravenous bolus injection of [$^{18}$F]FMT, [$^{18}$F]LBT999, or [$^{18}$F]DPA714, and lasted 60 min, 90 min, or 90 min, respectively. The data were acquired in list-mode. The time coincidence window was set to 6 ns, and the levels of energy discrimination were set to 350-650 keV.

For image reconstruction, PET data was normalised for detector inhomogeneities, corrected for scatter, attenuation, and radioactivity decay, and reconstructed using Fourier rebinning and ordered subset expectation maximization 2D (16 subsets and 4 iterations). The following 24 timeframes were used for 90 min scans: 4 x 15 sec; 4 x 30 sec; 2 x 60 sec; 5 x 2 min; 3 x 5 min; 6 x 10 min, while the last 3 timeframes were eliminated for 60 min scans.

**Table 6: List of timepoints for manual blood sampling**

| *Timepoint (min)* | *Amount (µL)* |
|---|---|
| 00:05 | 50 |
| 00:10 | 50 |
| 00:15 | 50 |
| 00:30 | 50 |
| 00:45 | 50 |
| 01:00 | 50 |
| 01:15 | 50 |
| 01:30 | 50 |
| 01:45 | 50 |
| 02:00 | 50 |
| 03:00 | 50 |
| **05:00** | **500** |
| 07:30 | 50 |
| **10:00** | **500** |
| **15:00** | **500** |
| 20:00 | 50 |
| **30:00** | **500** |
| 40:00 | 50 |
| 50:00 | 50 |
| **60:00** | **500** |
| 70:00 | 50 |
| 80:00 | 50 |
| **90:00** | **500** |

## 5.3 Arterial input function and metabolite analysis

Metabolite corrected arterial input functions were measured in a separate group of animals (n=3), only for the [$^{18}$F]DPA714 study. Blood samples (≈50 µL) were collected at selected timepoints (see Table 6) from the femoral artery to establish [$^{18}$F]DPA714 arterial kinetics of the whole blood, and plasma. First, whole blood samples were counted using a gamma counter (Wizard 2480; PerkinElmer, France), and next radioactivity was measured in cell-free plasma (≈20 µL) after centrifugation (5 min, 2054 g, 4°C),

Larger samples (500 µL) were collected at 5, 10, 20, 40, 60 and 90 min after radiotracer injection for further metabolite analysis (Peyronneau et al., 2013). Briefly, the cartridge (60-mg HLB Oasis SPE cartridge; Waters) was conditioned with 1 mL of acetonitrile and equilibrated with 5 mL of purified water. Plasma samples (200 µL) were diluted to 400 µL with an aqueous solution containing 4% hydrochloric acid. The radioactivity was measured in the resulting solution, which was directly applied to the HLB cartridge. The cartridge was then sequentially washed with 1 mL of water and acetonitrile /water (35/65, v/v) solution. [$^{18}$F]DPA714 was finally eluted with 1 mL of acetonitrile. The radioactivity was measured in all the collected fractions as well as in the cartridge. The radioactivity due to unchanged [$^{18}$F]DPA714 was expressed

as the percentage of the sum of radioactivity found in the eluted fractions or as the fraction of the initial radioactivity measured in each plasma sample (Peyronneau et al., 2013).

For each individual animal, the parental fraction was fitted using a 1-exponential decay function, and then applied to plasma input function. Time activity curves (TACs) of the parental [$^{18}$F]DPA714 plasma fraction were expressed in standard uptake values (SUV). Parent [$^{18}$F]DPA714 plasma exposure was estimated in all tested conditions by calculating the area under the curve (AUC) from 0 to 90 min. AUC expressed in SUV x min is inversely correlated to [$^{18}$F]DPA714 plasma clearance (Cl = dose/AUC).

## 5.4 Image processing

Image processing was performed using PMOD® software (PMOD 3.804; PMOD Technologies LLC, Switzerland), by the same operator for all animals.

### 5.4.1 Image pre-processing and segmentation

Dynamic PET images were summed ([$^{18}$F]FMT: 60 min, [$^{18}$F]LBT999: 5 min, and [$^{18}$F]DPA714: 90 min), and subsequently smoothed with a Gaussian filter (1x1x1mm) and cropped (20*15*30mm). The resulting summed-images were manually co-registered onto the MRI template (paragraph 4.2.1, page 57) using only rigid transformations (PET2MRI) (Figure 16).

Next, the inverse affine transformations (revPET2MRI) where used to place the MRI Atlas (4.2.2, page 58) and MRI BrainMask (4.2.3, page 58) on the raw dynamic PET image, hence without altering the PET images. The voxels outside of the BrainMask were masked to reduce outer-brain signal. Segmentation based on the MRI Atlas was used for all subsequent analyses.

These image pre-processing steps were executed using alternatively PVIEW and PFUSIT modules of the PMOD® software.

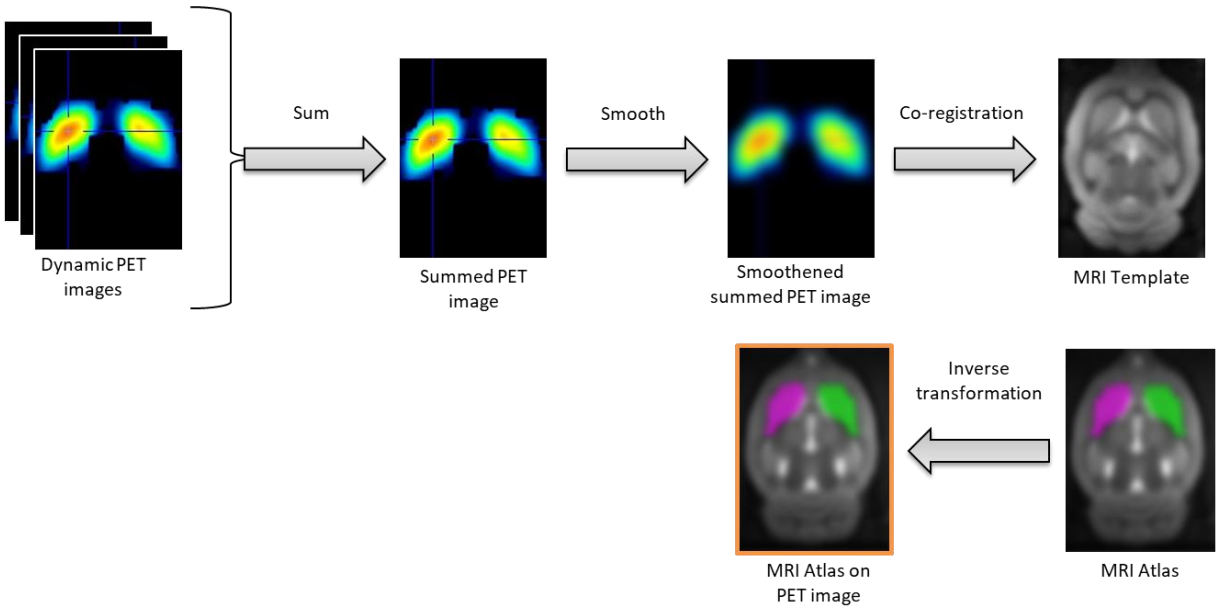


**Figure 16: Schematic representation of PET image pre-processing and segmentation.** Individual dynamic PET images were first summed and subsequently smoothened. Next, the summed-smoothened individual PET images were co-registered to

our MRI template using rigid transformations. The inverse transformation was used to place the MRI atlas on the (raw dynamic) PET data without altering the PET image.

### 5.4.2 Relative quantification

Relative quantification was performed using the VIEW module of PMOD® software. Time activity curves (TACs), representing the radioligand uptake in VOIs over time, were extracted from dynamic PET images and expressed in standard uptake values (SUV, Figure 17):

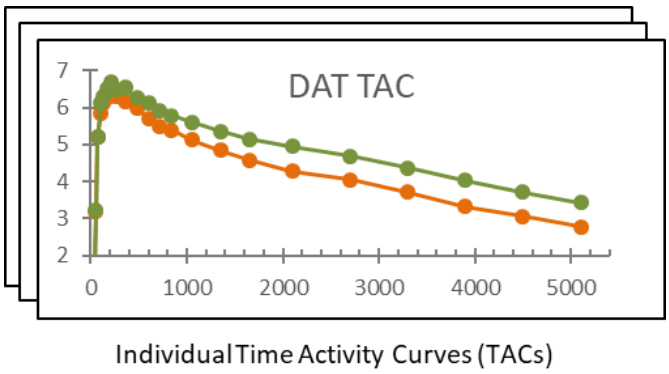


$$SUV = \frac{mean\ VOI\ values\ (\frac{Bq}{mL})}{injected\ dose\ (Bq)/body\ weight\ (g)}$$

**Figure 17: Representative example of DAT PET Time Activity Curve (TAC).** The vertical axis represents SUV values, and the horizontal axis time (s).

In a subsequent step, average SUV was calculated within a specified timeframe corresponding to pseudo-equilibrium uptake of the radioligand; and relative SUV values can be calculated as the ratio of SUV in a VOI relative to the SUV uptake within the (pseudo-) reference region. The reference region being defined as the region that does not express the target of interest, and which displays similar radioligand uptake and distribution as the VOI.

This relative quantification method has been successfully employed previously in our lab in rodent studies for both [$^{18}$F]LBT999 (Grealish et al., 2014) and [$^{18}$F]DPA714 (Lavisse et al., 2012). However, during this PhD, we have used absolute quantification methods with the aim to be more sensitive and precise in our quantification, which was not previously done for any of these tracers in rodents in our lab.

### 5.4.3 Absolute quantification

TACs were used for subsequent absolute quantification through kinetic modelling. We chose to calculate quantitative parametric images using the PXMOD module of PMOD® software, in which the pixel intensity corresponds to the quantitative measure. Though less sensitive than quantification based on individual regional TACs, this allows to; evaluate eventual regional changes and offers the possibility of voxel-based analysis (Chapter 5).

Overall, we have chosen simplified quantification methods based on (pseudo-) reference regions; for [$^{18}$F]FMT and [$^{18}$F]LBT999 simplified quantification methods have been extensively evaluated (Eberling *et al.*, 2007; Sérrière *et al.*, 2014). As reported in literature, the cerebellum was used as the reference region for [$^{18}$F]FMT and [$^{18}$F]LBT999 quantification.

Quantification of TSPO is more complex; firstly, since there is no reference region available that does not express TSPO, and secondly, TSPO-PET ligands have complex blood pharmacokinetics. Previous studies by Ory and colleagues (Ory *et al.*, 2016) demonstrated the contralateral striatum is a better pseudo-reference region than the cerebellum. However, there is no clear consensus whether simplified quantification methods are equally or more sensitive than full quantification using metabolite-corrected plasma input curves. Therefore, we conducted a pilot study for [$^{18}$F]DPA714.

We aimed to evaluated the feasibility of simultaneous PET imaging and whole blood measurements. The findings for this pilot study will be described in section 5.5.2 (page 68).

### Patlak plot - [18F]FMT

The Patlak plot is a graphical analysis method suitable for systems with irreversible trapping of the radiotracer (Patlak, Blasberg and Fenstermacher, 1983; Peters, 1994). The Patlak plot can be used if the plasma activity is known, resulting in a plot of the transformed TAC against a "normalised time" (PMOD, 2009d):

$$\frac{C_{tissue}(t)}{C_p(t)} = K\frac{\int_0^t C_p(\tau)d\tau}{C_p(t)} + V$$

However, we did not have information on the plasma activity and therefore had to use the reference region method, which was the cerebellum. A prerequisite for the reference region is that the tracer is not irreversibly being trapped (Patlak and Blasberg, 1985). In the Patlak reference plot, the plasma data is then replaced by the TAC of the reference tissue. The slope of the linear regression now has the following relation with the equilibrium constant $K_{eq}$ (PMOD, 2009d):

$$slope = K = \frac{k_2 k_3}{(k_2 + k_3)(1 - k_{eq})}$$

The Patlak graphical reference plot has also been successfully applied on rat [$^{18}$F]FMT data by Becker and colleagues (Becker *et al.*, 2017).

### Logan plot - [18F]LBT999

The Logan plot is a second graphical analysis method, but unlike the Patlak plot, it is specific for reversible receptor systems (Logan *et al.*, 1990). The Logan plot can be used if the plasma activity is known (PMOD, 2009c):

$$\frac{\int_0^t C_{tissue}(\tau)d\tau}{C_{tissue}(t)} = K\frac{\int_0^t C_p(\tau)d\tau}{C_{tissue}(t)} + V$$

However, for the final study, we did not collect plasma activity information, and had to use the Logan reference tissue method (Logan *et al.*, 1996). This is possible since the distribution volume ratio (DVR) can directly be calculated from the graphical method using data from a reference region (C'(t)) and an average tissue-to-plasma clearance ($k'_2$):

$$\frac{\int_0^t C_{tissue}(\tau)d\tau}{C_{tissue}(t)} = DVR\frac{\int_0^t C'(\tau)d\tau + \frac{C'(t)}{k'_2}}{C_{tissue}(t)} + int'$$

In this case DVR is the regression slope and the intercept int' which is constant after equilibration time t* (PMOD, 2009b).

PXMOD was first allowed to find the best fit, with liberty in the equilibration time t*. Next, the average equilibration time t* per group was calculated and forced for absolute quantification of each single pixel.

Previously, Sérrière and colleagues (2014) have compared several methods of analysis for [$^{18}$F]LBT999 PET imaging, and successfully used the Logan reference tissue model, amongst others, in healthy rats (Sérrière *et al.*, 2014).

**$MRTM_0$ - [$^{18}$F]DPA714**

Previously, Ory and colleagues (2015) have used the simplified reference tissue model (SRTM) (Lammertsma AA and Hume SP, 1996) to quantify [$^{18}$F]DPA714 PET data (Ory *et al.*, 2015). In a subsequent paper, Ory and colleagues (2016) suggest that full kinetic modelling is possible using SRTM or multi-linear reference tissue model (MRTM) with the contralateral striatum as the reference region, and a scan duration of at least 90 minutes (Ory *et al.*, 2016).

However, in our experiments we did not meet this last constraint; due to time limitations our scan lasted 60 minutes. In order to select the most suitable model, I have therefore reanalysed three existing 90 minutes [$^{18}$F]DPA714 PET data sets (Lavisse *et al.*, 2012) using the SRTM and MRTM model as suggested by Ory and colleagues (2016), and compared the results to quantification of the same datasets, but only using the first 60 minutes of data acquisition. This comparison revealed that Ichise's non-invasive plot ($MRTM_0$ (Ichise *et al.*, 1996)) at 60 minutes showed BPnd values closest to SRTM and MRTM at 90 minutes; data correlated well, even though there was a slight underestimation.

$MRTM_0$ is based on the Logan plot and has been developed for receptor studies. The model requires a region without receptors and a receptor-rich region and assumes that the non-displaceable distribution volumes are equal in those regions (Ichise *et al.*, 1996; PMOD, 2009a), which we have found in the contralateral and ipsilateral striatum, respectively.

If the Logan plot is applied for both TACs of the receptor-lacking and receptor-rich region, the input curve can be eliminated and the following expression is found:

$$\frac{\int_0^t C_{tissue}(\tau)d\tau}{C_{tissue}(t)} = \frac{V}{V'}\frac{\int_0^t C'(\tau)d\tau}{C_{tissue}(t)} + \frac{V}{V'k'_2}\frac{C'_{tissue}(t)}{C_{tissue}(t)} + int'$$

V and V' are the total distribution volumes of $C_{tissue}(t)$ and $C'_{tissue}(t)$, $k'_2$ is the clearance constant, and int' is the intercept which is constant after equilibration time t* (Ichise *et al.*, 1996; PMOD, 2009a).

PXMOD was first allowed to find the best fit, with liberty in the equilibration time t*. Next, the average equilibration time t* per group was calculated and forced for absolute quantification of each single pixel.

Absolute quantification based on automated arterial input measurements simultaneous to [$^{18}$F]DPA714 PET imaging are described in detail on page 68, where a pilot study is described.

### 5.4.4 Image post-processing and segmentation

The resulting [$^{18}$F]FMT parametric images were smoothed (2x2x2mm) before further processing, but not the [$^{18}$F]LBT999 or [$^{18}$F]DPA714 images. The "revPET2MRI" transformation was applied to put the atlas on parametric images in order to extract the average Ki or BPnd values per VOI from the MRI atlas.

To illustrate the results per study, averaged parametric images have been created per group. To that end, the individual parametric images were moved to MRI template space, using the PET2MRI transformation described above. Next, the parametric PET images were averaged and

subsequently fused to the MRI template. In doing so, the orignial PET data have not been modified or transformed before absolute quantification, but only for the rendering of an average quantified PET image.

## 5.5 Methodological improvements

### 5.5.1 [$^{18}$F]FMT

As explained previously, (Chapter 1: 1.1.2, page 15) L-DOPA is converted into dopamine by the AADC enzyme (Musacchio, 1975), and ultimately degraded by COMT into a biological inactive molecule (Eisenhofer, Kopin and Goldstein, 2004). [$^{18}$F]FDOPA (Chapter 1: 4.4.2, page 40) is closely related to L-DOPA and undergoes the same metabolic steps (Melega *et al.*, 1991; Endres *et al.*, 1997); [$^{18}$F]FDOPA is completely metabolized by peripheral AADC and COMT, resulting in radioactive metabolites that can cross the BBB. Peripheral metabolism has to be blocked in order to achieve brain uptake of [$^{18}$F]FDOPA (Ruottinen *et al.*, 1995; Kyono *et al.*, 2011; Walker, Dinelle, Kornelsen, Lee, *et al.*, 2013; Walker, Dinelle, Kornelsen, McCormick, *et al.*, 2013; Becker *et al.*, 2017). However, this does not eliminate the formation of [$^{18}$F]FDOPA metabolites in the brain.

In contrast to [$^{18}$F]FDOPA, [$^{18}$F]FMT (Chapter 1: 4.4.2, page 40) has the advantage of being a substrate for AADC, but with only minimal affinity for COMT (Jordan *et al.*, 1997). Therefore, it is considered that [$^{18}$F]FMT does not require the use of COMT inhibitors prior to PET imaging (Barrio *et al.*, 1996; DeJesus *et al.*, 1997). However, we found that blocking with benserazide, a peripheral AADC inhibitor, was not successful in almost 30% of the animals (6 out of 20) in [$^{18}$F]FMT PET scans, leaving us unable to perform absolute quantification in these animals. This led us to investigate the several parameters that could influence the efficacy of benserazide; anaesthesia and injection route.

#### Pilot study on intravenous injection of benserazide in a complete lesion model

Our first aim was to evaluate if blocking of peripheral AADC could be more efficient after intravenous administration. However, to the best of our knowledge, little is known about the toxicity of benserazide after intravenous injection; therefore, in a pilot study (n=4) we injected only 5mg/kg of benserazide intravenously 30 minutes before radiotracer injection. In the bulk of our experiments, we injected animals ~30 minutes before radiotracer injection intraperitoneally with 10mg/kg of benserazide, after the example of Becker and colleagues (Becker *et al.*, 2017).

Quantification of [$^{18}$F]FMT PET imaging using the cerebellum as the reference region (section 5.4.3, page 63) showed that Ki values were not different from studies using intraperitoneal injection of benserazide (Chapter 3, n=4/5; p=0.10). Average Ki value of the striatum contralateral to 6-OHDA injection after intraperitoneal benserazide injection was 0.012±0.001, while intravenously it was 0.010±0.002 (contralateral to AAV2/6-PGK-WT/A53T-α-synuclein injection).

A significant decrease of -58±3% of AADC enzymatic rate in the ipsilateral caudate putamen was observed as compared to the contralateral caudate putamen (Figure 18A; Δ81±6%; n=4; p=0.0017) in 6-OHDA rats.

It was therefore concluded that chancing the injection route of benserazide had no beneficial effect on peripheral AADC inhibition by benserazide, and thus the intraperitoneal injection of benserazide would be used in future experiments.

### AADC quantification in extrastriatal brain regions

In addition to the striatum, we also observed significant left-right differences in several extrastriatal regions: hypothalamus (Figure 18A, -33±6%; Δ40±8%; n=4; p=0.021), thalamus (-18±3%; Δ20±4%; p=0.029), and cortex (-20±4%; Δ23±5%; p=0.002).

Previously, Honer and colleagues (2006) observed highest radioactivity concentrations in the striatum, followed by the thalamic nuclei and the substantia nigra in MPTP mice (Honer *et al.*, 2006). Taken together with our data, this indicates that [$^{18}$F]FMT could possibly quantify extrastriatal brain regions, however, this was outside the scope of the PhD work (Li *et al.*, 2014).

### Pilot study on different anaesthesia regimes in a complete lesion model

Secondly, we aimed to evaluate if the AADC inhibition by benserazide would be impacted by isoflurane. To that end, we evaluated if another anaesthesia regime, under continuous medetomidine infusion, could improve success rate of [$^{18}$F]FMT PET imaging. Medetomidine (Domitor) was first subcutaneous injected as a bolus (0.05 mg/kg) after anaesthetic induction by isoflurane, and subsequently perfused (0.1 mg/kg/h). Benserazide injection protocol was equal to described above: 5mg/kg of benserazide intravenously injected 30 minutes before radiotracer injection.

Quantification of [$^{18}$F]FMT PET imaging using the cerebellum as the reference region (section 5.4.3, page 63) showed no significant differences between the use of isoflurane (ki=0.013±0.002) and medetomidine (Ki=0.011±0.002) (Figure 18B, n=4; p=0.42).

### Conclusion

Taken together, intravenous administration of benserazide or medetomidine anaesthesia do not improve the blocking rate of peripheral AADC using benserazide. Thus, we have continued to use the same parameters for our studies as suggested by Becker and colleagues (Becker *et al.*, 2017).

In future experiments, it should be tested if peripheral inhibition of COMT increases the success rate of quantifiable [$^{18}$F]FMT PET scans.

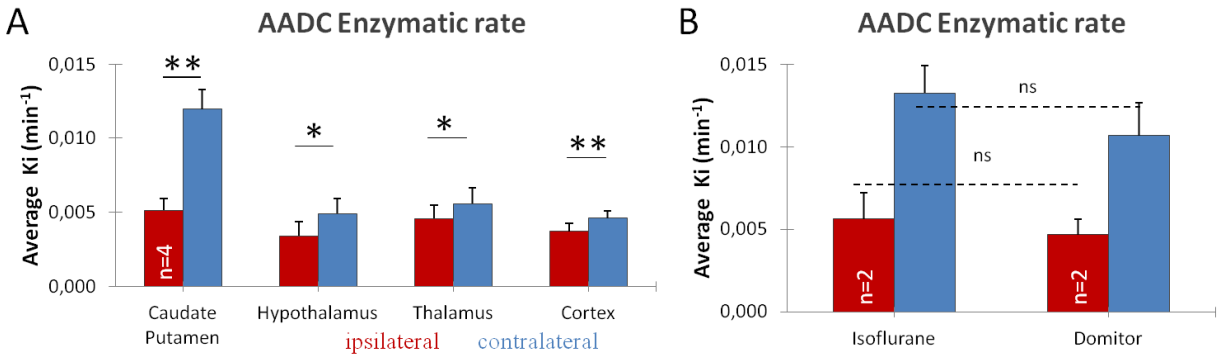


**Figure 18: AADC-PET analysis on 6-OHDA complete lesion model using isoflurane and medetomidine anaesthesia at 28wpi. A)** Average AADC enzymatic rate per indicated brain area for the ipsilateral (red) and contralateral (blue) striatum. **B)** Average AADC enzymatic rate per type of anaesthesia. Results are expressed as means ± the standard error of the mean (SEM). Paired student t-test. *p<0.05, **p<0.01.

### 5.5.2 [$^{18}$F]DPA714

#### Pilot study on automated arterial input measurements simultaneous to [$^{18}$F]DPA714 PET imaging

**Aims**

Previously, it has been suggested by Napieczynska and colleagues (2018) that online recording of the blood radioactivity through an arteriovenous shunt allows precise measurement of the arterial input function (AIF) without losing the blood volume. Furthermore, combining the continuous data acquisition with a single manually collected blood sample was suggested to be the most accurate approach for subsequent quantitative data analysis (Napieczynska *et al.*, 2018). Our aim here was to evaluate the feasibility of simultaneous acquisition of PET images and the arterial input function after [$^{18}$F]DPA714 injection using the commercially available Twilite system (Swisstrace; Zurich, Switzerland), to the example of [$^{18}$F]FDG PET experiments (Weber *et al.*, 2002). Specifically, in this pilot study, we aimed to 1) measure the plasma to blood conversion function, and 2) compare the "gold-standard" manual AIF with the automated input function, and 3) identify dispersion or other parameters.

**Experimental setup**

A commercially available Twilite system (Swisstrace; Zurich, Switzerland) was used to measure the whole blood concentration of [$^{18}$F]DPA714 (Figure 19). We used the same experimental setup as previously described (Weber *et al.*, 2002). Briefly, polyethylene catheters (PE20; prefilled with 50 UI/mL heparinized saline) were implanted, under isoflurane anaesthesia in 100% oxygen, in the femoral artery and vein of five animals to create an arteriovenous shunt. A continuous blood flow through the shunt was assured using a peristaltic pump (Ismatec®, Germany) at a standard flow rate of 0.332ml/min. At the arterial side, the PE20 catheter was placed in a cassette that entered the coincidence detector; at the venous side, butterfly catheters allowed for radiotracer injection in the arteriovenous shunt using an automated injection pump, and withdrawal of blood samples. Whole blood concentration of the radioligand was continuously measured online using PMOD® software (PMOD 3.804; PMOD Technologies LLC, Switzerland). Additional blood samples (500µL) were manually withdrawn from the shunt at 5, 10, 20, 40, 60 and 90 min after injection to count in parallel, and on the same animal, the whole blood and plasma concentration, and to determine the parental fraction of [$^{18}$F]DPA714 as described above (paragraph 5.3, page 61).

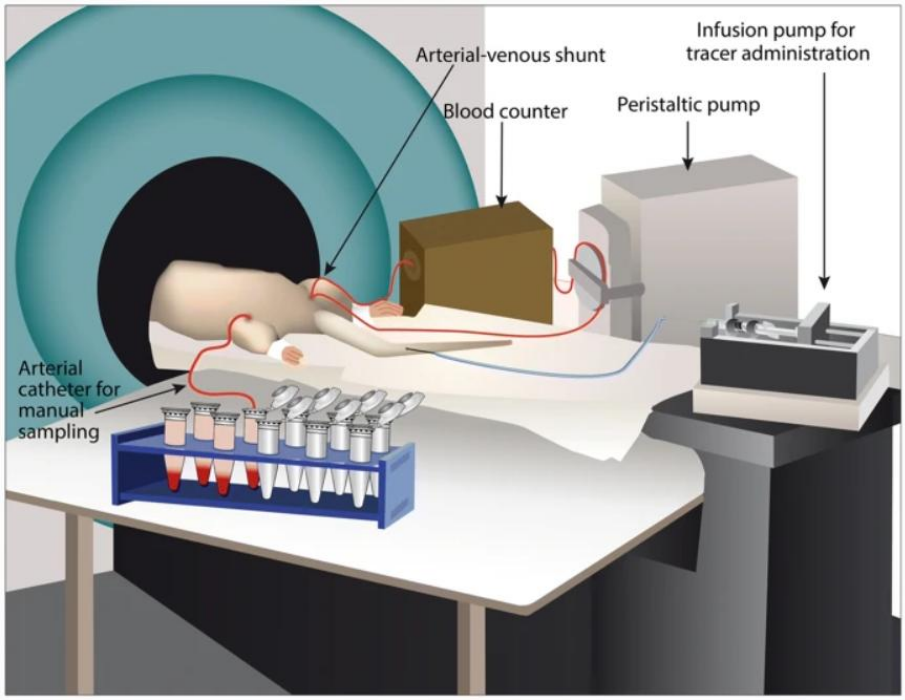


**Figure 19: Schematic illustrations of an online blood counter setup and manual blood sampling to obtain an arterial input function from a rat.** After the start of the PET acquisition, the radiotracer is injected via an infusion pump as a fast bolus, and the activity in the whole blood is counted using an online blood counting system. For this, a catheter is placed in the femoral artery of the animal and subsequently passes through the blood counter, in which the radioactivity from the blood is counted. The peristaltic pump ensures a constant and continuous blood flow through the arterial-venous shunt. Manual blood sampling can be conducted using an arterial catheter to correct the blood curve for the plasma free fraction and the contribution from metabolites. Image from Herfert and colleagues (2019).

## Results

### *Plasma to whole blood conversion*

The parental fraction was highly consistent for the three animals. [$^{18}$F]DPA714 metabolises rapidly with only 50% of the parental fraction present 30 minutes post-tracer injection, and 20% 90 minutes after injection (Figure 20A).

Blood input curves were highly consistent amongst the three animals (Figure 20B), with the whole-blood input function displaying larger area under the curve (AUC) compared to the plasma input curve (Figure 20). The Plasma over Blood (PoB) curves showed up to almost tenfold higher uptake in the whole blood compared to the plasma, which equilibrated during the 90 minutes period to almost equally whole-blood plasma ratios. This PoB ratio is much lower as compared to the NHP, but similar to what we know for mice (unpublished data). Note that the time points for metabolite sampling created an important noise in the whole-blood curves. This is most probably due to an error in the decay correction, as sampling of the larger blood volumes required more time. Here, we used the onset of the blood sampling for decay correction, which results in overestimation of the whole-blood signal if sampling takes longer than the other samples. This creates an important noise in the PoB curve, and a more correct decay correction should be taken into account for future experiments. The dashed grey line (Figure 20D) is a rough estimate of what could be expected for a plasma to whole-blood conversion function. Despite high consistent input functions between the three animals, we observed a high variability in the PoB ratios. This variability, together with the noise in the whole blood curves, did not allow estimating a proper fit for the PoB curve.

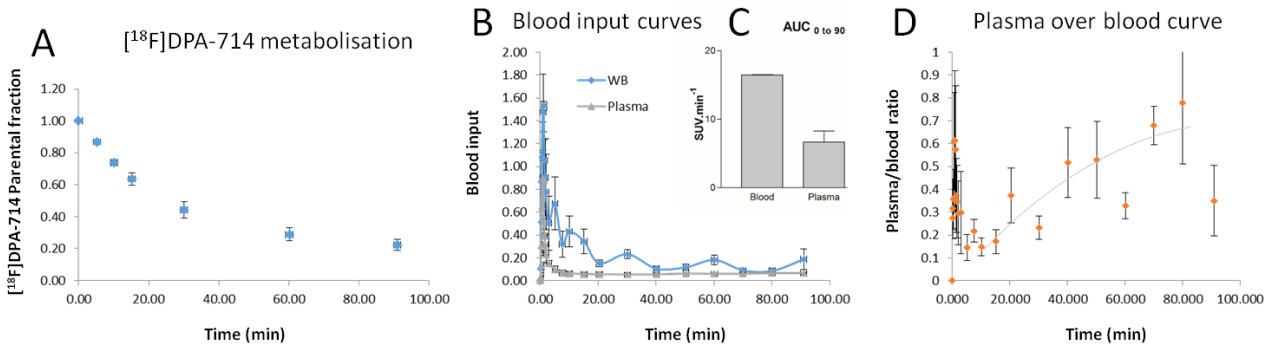


**Figure 20: Plasma to whole blood conversion. A)** [$^{18}$F]DPA714 metabolisms shown as the parental fraction over time**. B)** Blood input curve in SUV for whole blood (blue) and plasma (grey) over time. C) Calculation of the total area under the curve for graph B. **D)** Plasma over blood curve. Results are expressed as means.

***Comparison of the manual and the automated input function***

Of the four automated input acquisitions tested, the first three displayed serious coagulation in the arteriovenous shunt already at 30 minutes after tracer injection, despite heparinization of the catheters. Shortening of the arteriovenous shunt to almost half its length and reducing the death volume wherever possible, combined with a rigorous heparinization protocol (flushing every 15 minutes), allowed for a full 90 minutes automated acquisition of the whole blood input function.

The peak of the automated input curve was higher than the peak obtained by manual blood sampling (Figure 21). However, the peak width was broader, indicating that dispersion effects occur, which need to be corrected for. More problematically, the tail of the whole-blood input curve, acquired over the entire 90 minute period, showed increasing noise over time, strongly suggesting that [$^{18}$F]DPA714 was sticking to the PE20 tubing.

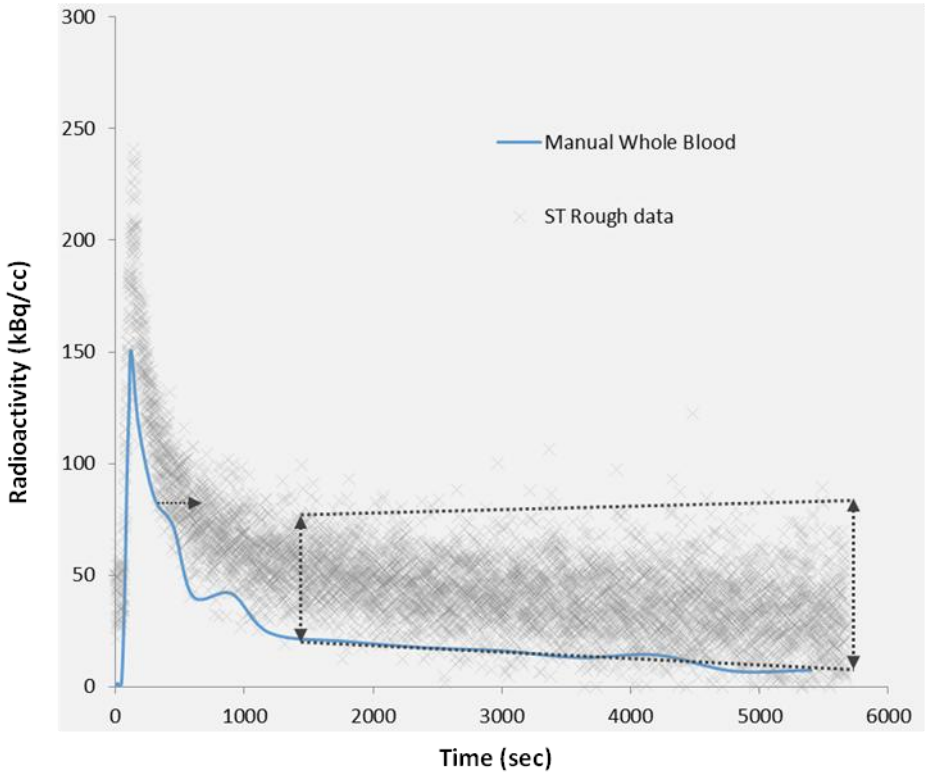


**Figure 21: Comparison of the manual (blue) and the automated input function (grey).** The radioactivity (kBq/cc) plotted over time (s). Results are expressed as means.

**Discussion**

We conducted a first pilot experiment to evaluate the feasibility of simultaneous blood sampling and PET imaging using the [$^{18}$F]DPA714 radioligand. With this pilot experiment, we obtained preliminary data, which are the basis for future experiments required to further develop this tool.

First, we observed that whole blood to plasma conversion data shows a high variability amongst animals. These preliminary data suggest that manual blood samples for each animal are required to scale each whole blood to plasma conversion correctly. These results are in concordance with the suggestion of Napieczynska and colleagues (2018) combining the continuous data with a single manually collected blood sample is the most accurate approach for the data analysis (Napieczynska *et al.*, 2018).

Secondly, these preliminary data showed that the implication of the Twilite system for the collection of automated [$^{18}$F]DPA714 input functions requires large methodological improvements; such as the evaluation of other catheter materials (e.g. Teflon), denoising algorithms (suggested by Santangelo, 2018), and correction for dispersion. The development of these technical aspects were out of the scope of my PhD.

Taken together, it was decided to perform absolute quantification based on the reference tissue model as previously described by Ory and colleagues (2015, 2016), and detailed previously on page 65.

# 6. *Post-mortem* studies

## 6.1 Brain tissue collection

All animals were ultimately sacrificed for subsequent immunohistological and biochemical analyses. Animals were deeply anaesthetized with 4% isoflurane before receiving a lethal dose of pentobarbital (180 mg/kg; Hexagon). Animals were then transcardially perfused with 280 ml 4% paraformaldehyde (PFA) in 0.01 M PBS at a rate of 28 ml/min. The brains were collected and post-fixated for 24h in 4% PFA at +4°C and transferred to a 30% sucrose solution in PBS for cryoprotection. All brains were cut into 40 µm coronal sections using a freezing microtome (CM1900, Leica, Germany). Serial sections of the striatum and substantia nigra were stored at -20°C in antifreeze solution (30% sucrose, 30% ethylene glycol in PBS) until use.

## 6.2 Immunohistological analyses and quantification

### 6.2.1 Immunohistochemistry

For free-floating immunohistochemistry, sections were incubated for 20 min with 0.3% $H_2O_2$ in PBS. Where necessary, antigen retrieval protocol was executed before $H_2O_2$ incubation; 20min at 85° in citrate (pH 6.0). After rinsing sections were incubated 1 h in blocking solution containing 4.5% normal goat serum (NGS) in PBS with 0.2% Triton™ X-100 (PBST). Sections were subsequently transferred into primary antibody solution (in 3% NGS in PBST) for incubation overnight at 4°C (unless otherwise stated). After rinsing, sections were incubated with the appropriate secondary antibody (Vector Laboratories) diluted to 1:1000 into blocking solution for 1 h at room temperature followed by 1 h incubation in Vectastatin ABC Kit (Vector Laboratories) and revelation using the DAB

Peroxidase Substrate Kit with nickel (Vector Laboratories). The following day, sections were dehydrated in consecutive ethanol baths (50%, 70%, 96%, absolute) and xylene before sealing the cover slip with Eukitt mounting medium.

We used primary antibodies directed against S129 phosphorylated α-synuclein (pS129-α-syn; 1:5.000; ab51253; Abcam), DAT (antigen retrieval; 1:200; AB1766; Chemicon), GFAP (1:10.000; Z0334; DAKO), IBA1 (1:3.000; 019_19741; WAKO), TH (2 night incubation; 1:2.000; MAB318; Millipore), Vimentin (1:2.000; IF01; Calbiochem), and VMAT2 (3 night incubation; 1:5.000; 496-515; Calbiochem).

### 6.2.2 Stereology

Stereological cell counting was performed using the optical fractionator principle on a Leica microscope (DM6000B & CTR6500, Leica, Germany). The amount of $TH^+$ neurons per substantia nigra was calculated using Mercator Software (Explora Nova, France). Squares (100 x 100 µm) were randomly systematically placed 80 µm apart in the manually outlined substantia nigra. Quantification was performed on serial sections separated by 200 µm covering the whole substantia nigra (anterior to posterior).

### 6.2.3 Optical density

The stained sections were digitalised using an ImageScanner III (GE Healthcare, USA) with Epson scan software (Epson, USA) at 2400dpi. Subsequent analysis was performed using Fiji-ImageJ software (open source, GitHub). In Fiji-Image the images were first transformed to 8-bit format and the scale was set. The area of interests were manually outlined for every section, including a blank region per microscope slide. The build-in function of Fiji-ImageJ was subsequently used to provide the light intensity per area of interest. Lastly, staining intensity was measured as optical density after background subtraction using the formula displayed below:

$$[OD] = log10\left(\frac{\max light\ intensity}{measured\ light\ intensity\ sample}\right) - log10\left(\frac{\max light\ intensity}{measured\ light\ intensity\ blank}\right)$$

### 6.2.4 Immunofluorescence

The protocol for immunofluorescence is similar to the one for immunohistochemistry. Briefly, after rinsing sections were incubated 30 minutes in blocking solution containing 4.5% normal goat serum (NGS) in PBS with 0.2% Triton™ X-100. Sections were subsequently transferred into primary antibody solution (in 3% NGS in PBST) for incubation overnight at 4°C. After rinsing, sections were incubated with the appropriate secondary antibody (Invitrogen) diluted to 1:1000 into blocking solution for 1 hour at room temperature. Subsequently, sections were stained for DAPI for 5 minutes at room temperature and mounted in fluorescent mounting medium. We used primary antibody against IBA1 (1:1000; 019_19741; WAKO).

### 6.2.5 Fluorescent intensity

The fluorescently stained sections were digitalised using laser confocal microscopy (SP8, Leica, Germany. Subsequent analysis was performed using Fiji-ImageJ software (open source, GitHub). The images were first converted to 8-bit format and the scale was set, subsequently the area of interest

was delineated. The fluorescent intensity was obtained using the standard intensity measurement in Fiji-ImageJ.

### 6.2.6 Preliminary evaluation in a complete lesion model

**Tyrosine hydroxylase**

TH immunohistochemistry was performed after the example of (Cresto *et al.*, 2020). Even though TH immunohistochemistry had been employed successfully before, I have attempted to increase penetrance of the antibody by using pre-treatments of the tissue (EDTA or citrate at 85°C) and by increasing incubation time. However, none of this yielded a better result than achieved with the protocol described by Cresto and colleagues (2020).

The density of TH-positive cells was first assessed using optical density analyses following immunohistochemistry in the substantia nigra (Figure 23A), the density of TH-positive fibres was assessed using optical density analysis in the striatum (Figure 23B). This showed a significant decrease of 50%, equal to an asymmetry of Δ67% of TH density in the substantia nigra (-50±3%; Δ67±6%; n=6; $p<0.001$), and a significant decrease of 77%, equal to an asymmetry of Δ129% of TH-positive fibre density in the striatum (-77±6%; Δ129±14%; n=6; $p<<0.001$).

These data suggest that the loss of dopaminergic fibres in the striatum is larger than the reduction of dopaminergic cells in the substantia nigra. Although surprising, this could be in line with research by Phan and colleagues (2017), who observed synaptic dysfunction before neurodegeneration in a α-synuclein overexpression model (Phan *et al.*, 2017). Nevertheless, others suggest more equal dopaminergic neurodegeneration in the substantia nigra and striatal TH fibre loss (Decressac, Mattsson and Björklund, 2012).

More likely, this phenomenon is induced by the less sensitive method of assessing dopaminergic neuronal loss through $TH^+$ optical density in the substantia nigra instead of cell counting *via* unbiased stereology. This is supported by our behavioural results (paragraph 3.1, page 52); the presence of rotational behaviour in the apomorphine-induced rotation test suggests a severe unilateral lesion (>80-90% dopaminergic nerve terminal loss; (Hudson *et al.*, 1993; Schwarting and Huston, 1996)). Indeed, using a different data set (from Chapter 4), comparison between results obtained through stereology and those obtained through TH optical density in the substantia nigra showed only a weak correlation between the two measures (Figure 22), even though both showed a significant asymmetry between ipsilateral and contralateral side. It also appeared that optical density underestimates the loss of TH-positive neurons. Thus, although optical density analysis is much less time consuming, we recommend using unbiased stereological techniques for assessment of TH-positive neurons in the substantia nigra.

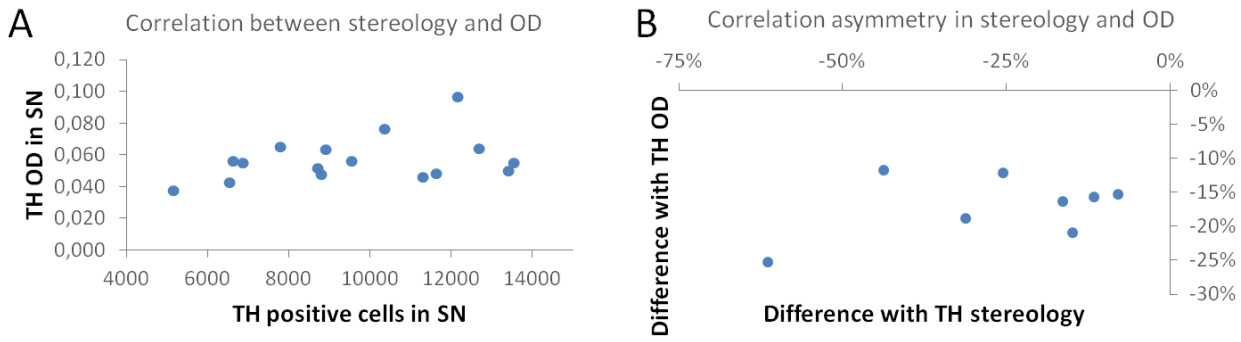

**Figure 22: Graphs showing correlation between TH stereology and optical density in the substantia nigra. A)** Correlation per animal per substantia nigra between the amount of TH-positive cells as measured by stereology, and the TH optical density. **B)** Correlation between the left/right differences between measurements taken by stereology and optical density. Each point is an individual animal. Correlation calculated with Spearman correlation, non-significant.

### S129phosporylated-α-synuclein

The antibody against S129-phosphorylated α-synuclein has previously been employed in our lab, thus no further optimisation of the protocol was required.

Here, we have shown no significant signal corresponding to S129phosporylated-α-synuclein in 6-OHDA injected animals, in either the substantia nigra nor in the striatum.

### Inflammation markers

All immunohistochemistry against markers for inflammation has been performed after the example of (Gubinelli, 2019). We have also attempted to performed immunohistochemistry against TSPO, however we have not succeeded in finding an antibody that worked in our hands.

Here, analysis in the striatum of IBA1 as an inflammatory marker revealed no significant increase in 6-OHDA animals (Figure 23F; n=6; p=0.09). Thus, we can say that there is no major inflammatory events going in the 6-OHDA model 1 year after injection, even though there is broad neurodegeneration.

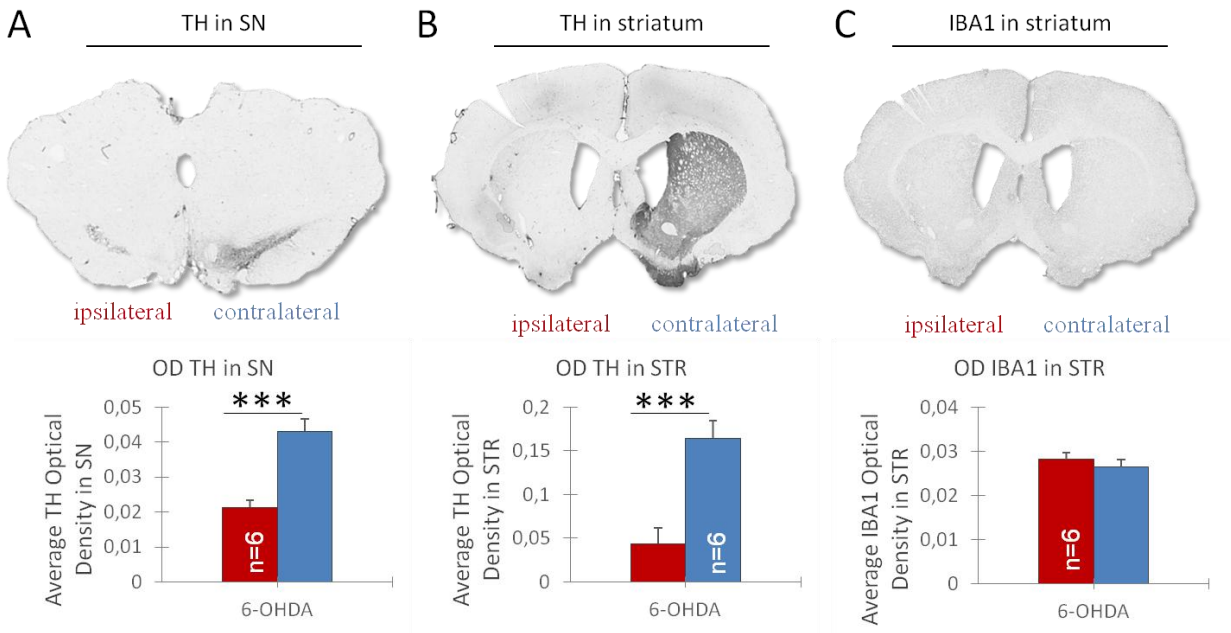


**Figure 23: Histological evaluation of the effect of a complete 6-OHDA lesion on TH and IBA1 in both the substantia nigra and striatum. A)** Average TH optical density in ipsilateral (red) and contralateral (blue) substantia nigra and representative histological image. **B)** Average TH optical density in the striatum. **C)** Average IBA1 optical density in the striatum. Representative images are taken from a single animal. Results are expressed as means ± the standard error of the mean (SEM). Paired student t-test ***p<0.001.

### Dopaminergic system

While all antibodies to visualise the dopaminergic system have been employed before in our lab, none had been used in rat PD models. Therefore, pilot stainings were performed to determine the optimum concentration, incubation time, and pre-treatment. While this was straightforward for VMAT2 (3 night incubation; 1:5.000; 496-515; Calbiochem), it proved more difficult for DAT, a high antibody concentration and rigorous pre-treatment was required with citrate (pH 6.0 at 85°C; 1:200;

AB1766; Chemicon). We have also attempted to perform immunohistochemistry against AADC, however we have not succeeded in finding an antibody that worked in our hands.

In the 6-OHDA model, the large scale dopaminergic neurodegeneration and fibre loss is accompanied by a strong reduction in DAT protein density (Figure 24A; Δ77±7%; n=6; p=0.003). Additionally, we observed a considerable reduction of VMAT density in the striatum (Figure 24B; Δ95±5%; n=6; p<0.001).

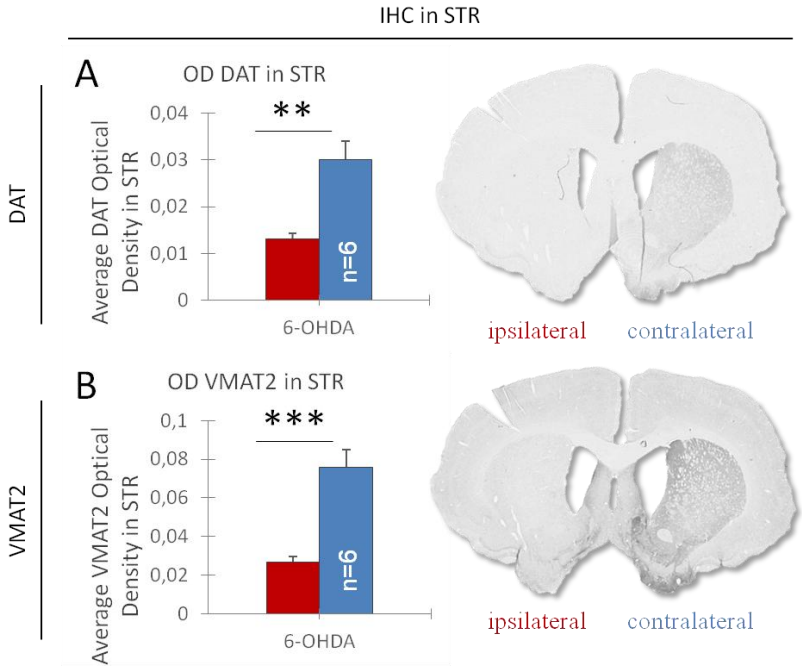


**Figure 24: Histological evaluation of the effect of a complete 6-OHDA lesion on the dopaminergic system in the striatum. A)** Average DAT optical density in the ipsilateral (red) and contralateral (blue) striatum and a representative histological image. **B)** Average VMAT2 optical density. Representative images are taken from a single animal. Results are expressed as means ± the standard error of the mean (SEM). Paired student t-test **p<0.01, ***p<0.001**.**

## 6.3 Real-time quantitative PCR

For transcriptomic analysis, striata and substantia nigra was first dissected by hand from the coronal 40 µm sections, using a surgical scalpel and a binocular microscope. These were then used to extract mRNA using E.Z.N.A.® FFPE RNA Kit (Omega Biotek, Georgia, USA) following the supplier's heat extraction guidelines. mRNA levels were measured using Nanodrop (ThermoFischer Scientific), and quality was validated using Bioanalyzer (Agilent). mRNA was then reverse-transcribed into cDNA using SuperScript™VILO™ cDNA Synthesis Kit (Vilo Life Technologies).

RT-qPCR was performed using iTaq™ Universal SYBR® Green Supermix (Bio-Rad) and primers (Eurofin Genomics) specific to different targets on 0.35-1 ng of cDNA, using 10 nM of primers (see Table 7). Reactions were run in triplicates in 384-well PCR plates (Bio-Rad or 4Titute), using a mix of cDNA and a household gene (Ppia or Rplp0) primer as an inter-plate control.

Data were analysed using Bio-Rad CFX Maestro software (Bio-Rad). Cycle threshold (Ct) values were generated in regression mode. Results are shown as relative normalised expression.

**Table 7: List of primers used for RT-qPCR**

| Gene/Primer | Forward sequence | Reverse sequence |
|---|---|---|
| **Ppia / Cyclo (housekeeping)** | ATGGCAAATGCTGGACCAAA | GCCTTCTTTCACCTTCCCAAA |
| **Rplp0 (housekeeping)** | CAGGCGTCCTCATTAGAG | ATCTGCTGCATCTGCTTGGAG |
| **Hprt1 (housekeeping)** | GGACCTCTCGAAGTGTTGGATAC | CCCTGAAGTGCTCATTATAGTCAA |
| **AADC / DDC** | GTGACCTCTGGTGGCAATGA | GCTTTCTGCTGTGTCCCGAT |
| **DAT / Slc6a3** | GCCCATTTATGCGACCTACAA | CCAGTGACGCAGCGTGA |
| **GFAP** | AATGACTATCGCCGCCAAC | CTCCTGGTAACTCGCCGACT |
| **IBA1** | CCAGCCTAAGACAACCAGCGTC | GCTGTATTTGGGATCATCGAGGAA |
| **TH** | GCCCTACCAAGATCAAACCTAC | GGCGCTGGATACGAGAG |
| **TNFα** | AAATGGGCTCCCTCTCATCAGTTC | TCTGCTTGGTGGTTTGCTACGAC |
| **TSPO / PBR** | CAGTGTCCTTCACGGAGCAG | CGGGTACCCAGGATTGAGAC |
| **Vimentin** | GCAAAGCAGGAGTCAAACGA | AATTCTCTTCCATTTCACGCATCT |
| **VMAT2** | CAGTCACAGGCGAGCCAGAGT | AGCAGCGCAAGGAACACGAT |

## Preliminary evaluation in a complete lesion model

### Dopaminergic system

Although RT-qPCR against TH and VMAT has been used before in our lab, AADC and DAT had not been investigated before. Multiple primers for each target were designed by an expert in our lab, and subsequently I identified the most suitable one.

Here, significant differences were shown in mRNA levels for all tested dopaminergic markers between the ipsilateral and contralateral substantia nigra after 6-OHDA injection into the MFB (Figure 25). Both TH (Δ197%; n=4/6; p<<0.001) and AADC (Δ163%; n=2/6; p<<0.001) are involved in dopamine synthesis (Chapter 1: 1.1.2, page 15), while DAT is for presynaptic dopamine reuptake (Δ197%; n=3/6; p<<0.001), and VMAT is for intercellular transport (197%; n=4/6; p<<0.001).

### Inflammation markers

Although most inflammation markers had already been validated and used by Dr. Gubinelli (2019) in his PhD thesis, I have identified the most suitable option for use against TSPO. These inflammation markers are used in Chapter 6.

Here, there is no significant difference in IBA1 mRNA levels between the ipsilateral and contralateral substantia nigra 1 year after 6-OHDA injection into the MFB (Figure 25; n=3/6; p=0.30).

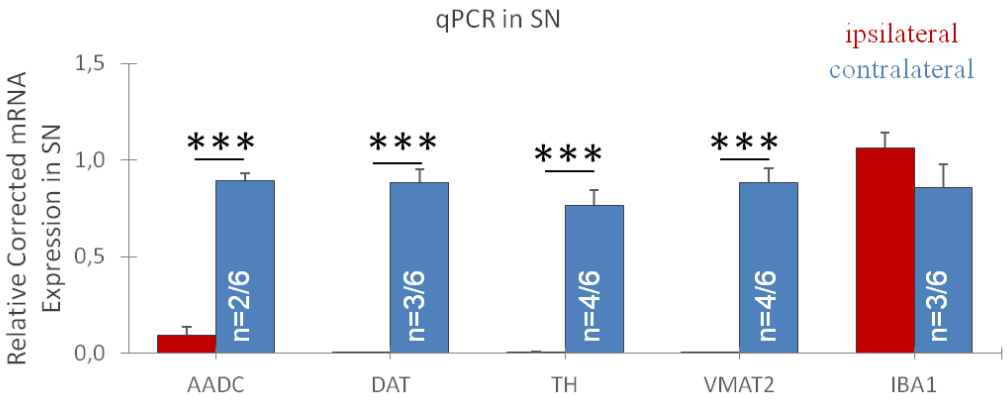

**Figure 25: mRNA levels of dopaminergic and inflammatory markers in the substantia nigra in 6-OHDA animals.** mRNA levels in the ipsilateral (red) and contralateral substantia nigra (blue) in intra-MFB 6-OHDA lesioned rats as measured by RT-qPCR. Results are expressed as means ± the standard error of the mean (SEM). Student t-test ***p<0.001.

### Correlation between different markers

Pairwise Spearman correlation analysis, between different measures including left-right side, demonstrated different associations between *post-mortem* dopaminergic markers, FMT-PET imaging and behaviour. The results of this analysis are graphically represented in a correlation plot, in which the color corresponds to the strength and sign of the correlation (Figure 26). Expression of all dopaminergic markers are correlated; especially the association between TH and VMAT is strong (r=0.98). Surprisingly, whilst immunohistochemistry did not show any significant neuroinflammation in the SN, IBA1 expression showed relatively mild inverse association with the dopaminergic markers I*n vivo* measures, FMT-PET and gombash score correlate positively with dopaminergic expression markers, and inversely with the expression of Iba1. Even though these data must be considered with caution –*the unilateral complete 6OHDA model induces an "off/on" situation in the affected/healthy nigrostriatal system*- this approach will be applied in future studies.

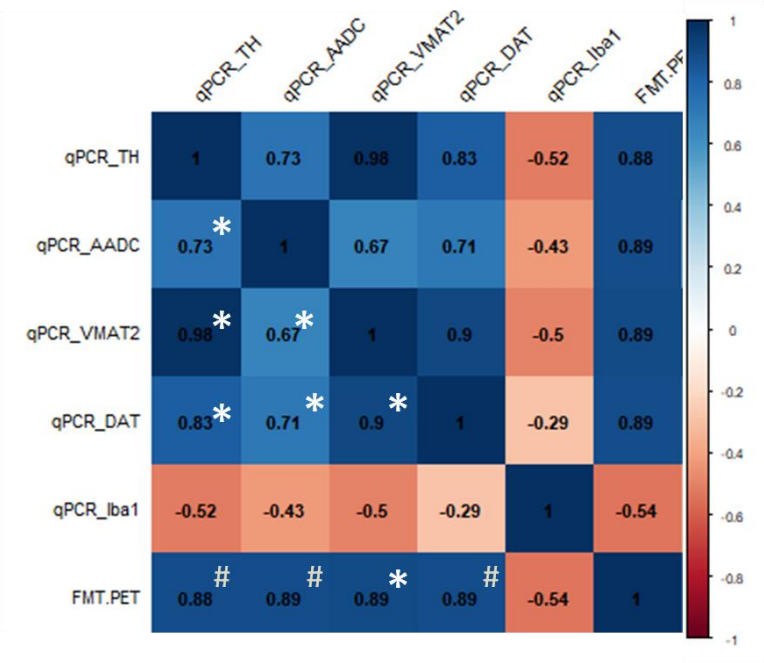


**Figure 26: Spearman correlation between *in vivo* data and different *post-mortem* data. Spearman correlation coefficients are marked in the corresponding case; blue signifies a positive association, while red signifies a negative association. * p<0.01, # p<0.05.**

# 3

# *RESULTS ON COMPARISON OF TWO α-SYNUCLEIN OVEREXPRESSING RAT MODELS*

## 1. Background and aims

As shown previously in the introduction (Table 2), several groups have published on the overexpression of wild-type (WT) or A53T-α-synuclein in the substantia nigra using viral vectors. These have shown varying degrees of dopaminergic cell death in the substantia nigra and fibre loss in the striatum, while all showed α-synuclein pathology. However, to the best of our knowledge, not many studies have compared overexpression of WT-α-synuclein to overexpression of A53T-α-synuclein.

In our lab, two AAV2/6 viral vectors have been developed under the PGK promoter encoding WT and mutant A53T human α-synuclein protein (AAV2/6-PGK-WT-α-synuclein and AAV2/6-PGK-A53T-α-synuclein). Cresto and colleagues (in progress) have injected AAV2/6-PGK-A53T-α-synuclein unilaterally in the substantia nigra and showed significant dopaminergic neurodegeneration in the substantia nigra only occurs 15 weeks post-injection. Dopaminergic neurons often displayed accumulation of pS129-α-synuclein and stained positive for ThioS, suggesting the formation of aggregates. In addition, a 40% decrease of dopaminergic neurons was observed in the substantia nigra at 15 weeks post-injection (wpi), and consequenlty 20% less use of the contralateral forepaw in the cylinder test.

Nevertheless, an incubation time of 15 weeks post-injection makes this model less optimal to evaluate therapeutic strategies. In order to accelerate this timeline, we increased the viral vector dose, as well as the number of injection sites per hemisphere, using a double injection strategy. As a result the viral genome count was four-fold.

**Here, we aimed to evaluate the impact of viral vector-induced expression of wild-type or mutant-A53T α-synuclein on the survival of dopaminergic neurons in the nigrostriatal pathway. For this, we used *in vivo* behavioural analyses and dopaminergic PET markers, which were compared with *post-mortem* analyses measuring neuronal death and α-synuclein aggregation.**

## 2. Study design

Fifteen rats were unilaterally injected in the substantia nigra with a viral vector overexpressing wild-type (WT-α-syn; n=7) or mutated (A53T-α-syn; n=8) human α-synuclein, using a double injection approach (AAV2/6-PGK-WT-α-synuclein or AAV2/6-PGK-A53T-α-synuclein; 2x5.00E+10 vgc).

Animals were studied 10 to 12 weeks post injection (wpi; Figure 27) with PET imaging, using a ligand substrate for aromatic L-amino acid decarboxylase (AADC) (6[$^{18}$F]fluoro-L-m-tyrosine ([$^{18}$F]FMT)), or a ligand for dopamine transporter (DAT), [$^{18}$F]LBT999. Anatomical MRI scans were performed for PET coregistration and quantification. Behavioural evaluation was performed using the cylinder test, adjusting steps test, and vibrissae test. The *in vivo* studies were followed by *post-mortem* stereology for tyrosine hydroxylase (TH)-positive cells in the substantia nigra.

Statistical analyses were performed using paired student t-tests to compare the ipsilateral and contralateral side in imaging studies, RT-qPCR, and immunohistochemical analyses, while for behavioural analysis a student t-test with unequal variance was used to compare against the hypothetic 50% value (chapter). All data were calculated as asymmetry ratios, according to the following formula:

$$Asymmetry\ ratio = \ \Delta\% = \frac{|\ ipsi - contra\ |}{(ipsi + contra) * 0.5}\ x\ 100$$

$$\%\ change = \frac{(ipsilateral - contralateral)}{contralateral}\ x\ 100$$

More detailed information about the methods can be found in Chapter 2.

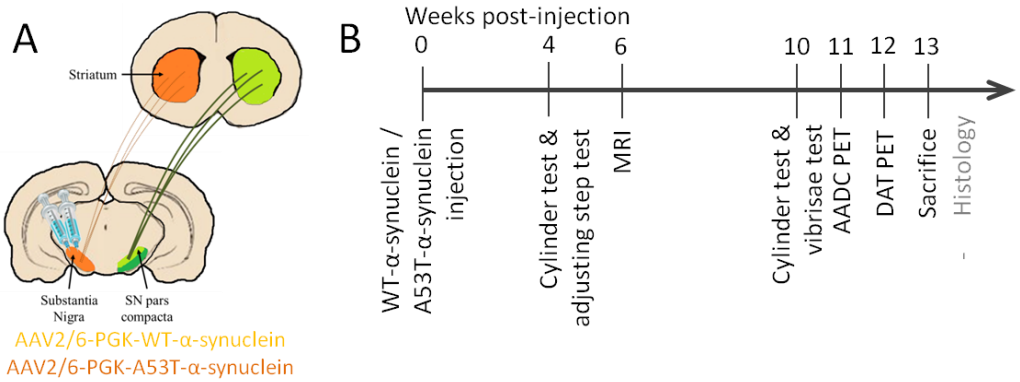


**Figure 27: Schematic overview of the study design. A) Animals were injected with either AAV2/6-PGK-WT-α-synuclein or AAV2/6-PGK-A53T-α-synuclein in the substantia nigra using a double injection approach. B) Timeline of the different experimental analyses.**

# 3. Results

## 3.1 Behavioural analysis

Using the cylinder test, we observed a modest but significant motor deficit in the WT-α-synuclein group at 4 weeks post injection (wpi) (Figure 28 left; Δ39±12%; n=7; p=0.041), which could not be demonstrated at 10wpi (n=7; p=0.20). On the contrary, the A53T-α-synuclein group presented a statistically significant asymmetry in forepaw use at 4wpi (Figure 28 right; Δ45±7%; n=8; p<0.001), which was even more pronounced at 10wpi (Δ79±22%; n=8; p=0.034).

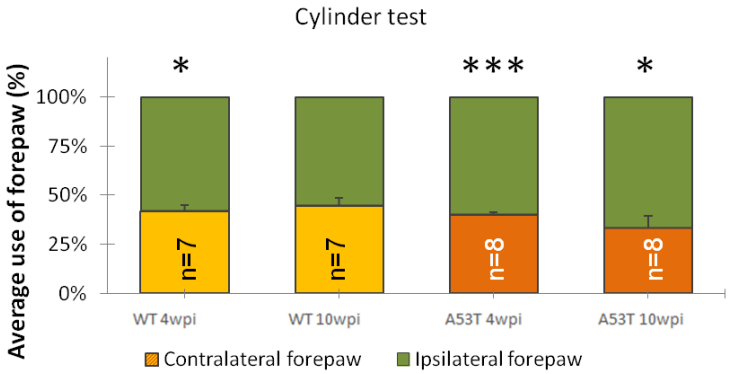


**Figure 28: Behavioural analysis using the cylinder test at 4 and 12wpi for both the WT- and A53T-α-synuclein groups. Relative use of the contralateral (yellow/orange) and ipsilateral forepaw (green). Results are expressed as means ± the standard error of the mean (SEM). Student t-test with unequal variance *p<0.05, ***p<0.001.**

## 3.2 PET imaging of the dopaminergic system

Averaged parametric Ki images representing the AADC enzymatic rate in the striatum are shown in Figure 29 for both the WT-α-synuclein group (Figure 29A) and the A53T-α-synuclein group at 10-12wpi (Figure 29B). We did not observe a significant asymmetry in AADC metabolism between the striata ipsilateral and contralateral to AAV-injection for the WT-α-synuclein group (Figure 29C; n=3; p=0.32). A trend was observed for the A53T-α-synuclein group, although it did not reach statistical significance (n=2).[5]

Averaged parametric images representing non-displaceable binding potential ($BP_{nd}$) of [$^{18}$F]LBT999 to DAT in the striatum 10-12wpi in WT-α-synuclein and A53T-α-synuclein groups are shown in figures Figure 29D and Figure 29E, respectively. The A53T-α-synuclein group showed significant asymmetry in DAT binding between the ipsilateral and contralateral striatum (Figure 29F; Δ54±8%; n=4; p=0.003). In the WT-α-synuclein groups the left-right asymmetry in DAT binding was smaller, with a larger heterogeneity (Δ32±13%), not reaching the significance level (n=3; p=0.051).

[5] Due to the difficulties in blocking with benserazide, a pepipheral AADC inhibitor, we could not perform absolute quantification in all scanned animals (n=4). More details can be found in chapter 2, page 66.

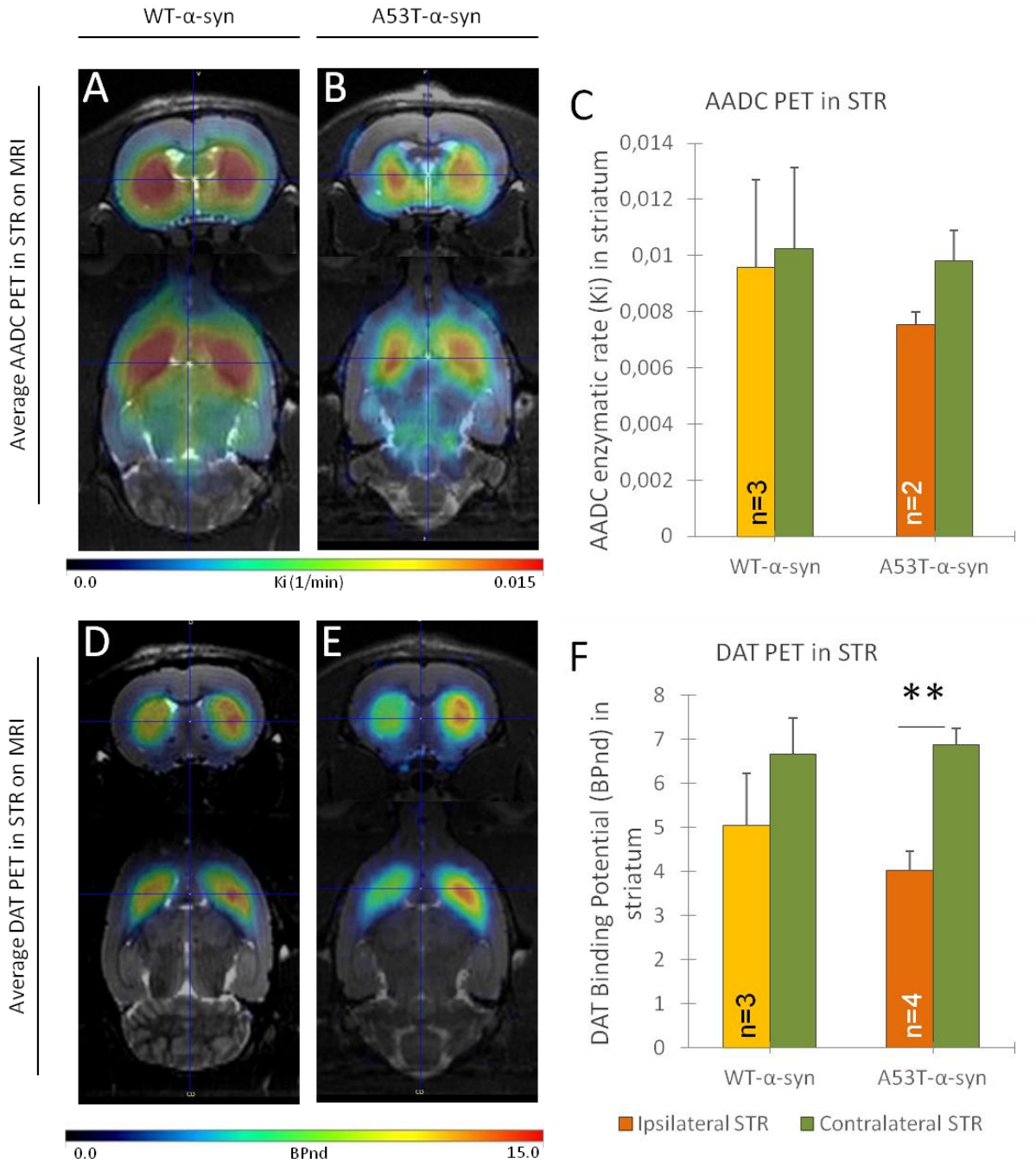


**Figure 29: *in vivo* PET analyses of both the WT- and A53T-α-synuclein groups using [$^{18}$F]FMT (AADC) and [$^{18}$F]LBT999 (DAT). A) Average of quantified AADC-PET images for the WT-α-synuclein and B) A53T-α-synuclein animals. C) AADC enzymatic rate for ipsilateral (yellow/orange) and contralateral striata (green) for both WT- and A53T-α-synuclein injected animals at 11wpi. D) Average of quantified DAT-PET images for the WT-α-synuclein and E) A53T-α-synuclein animals. F) DAT non-displaceable binding potential for ipsilateral and contralateral striata for both WT- and A53T-α-synuclein injected animals at 12wpi. Results are expressed as means ± the standard error of the mean (SEM). Paired student t-test **p<0.01**

## 3.3 *Post-mortem* analysis of neurodegeneration [6]

The number of TH-positive cells in the SN was assessed by unbiased stereology. This revealed no significant difference for animals injected with WT-α-synuclein (Figure 30 left; n=7; p=0.31). For animals injected with A53T-α-synuclein we observed a significant asymmetry of Δ33% in the number of TH-positive cells in the injected SN as compared to the contralateral SN (Figure 30 right; Δ33±10%; n=8; p=0.009).

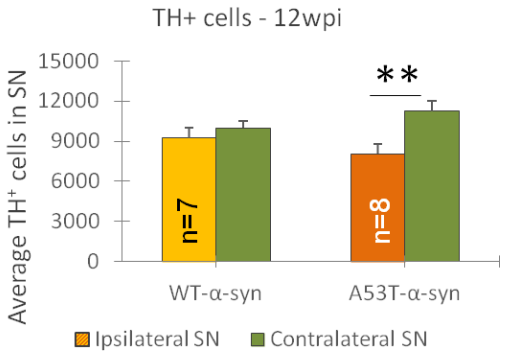


**Figure 30: Stereological analysis of the amount TH-positive neurons in the substantia nigra. Average number of cells counted by stereology for ipsilateral (yellow/orange) and contralateral striata (green) for both WT- and A53T-α-synuclein injected animals. Results are expressed as means ± the standard error of the mean (SEM). Paired student t-test **p<0.01.**

# 4. Discussion

### Behaviour

At 4wpi, we observed a significant asymmetry in forepaw use in the cylinder test for both the WT-α-synuclein and A53T-α-synuclein group. This transient reduction in contralateral forepaw use might be due to side-effects of the stereotactic surgery, rather than being an effect of the WT-α-synuclein overexpression. This is underlined by the fact that the motor deficits in both the WT-α-synuclein and A53T-α-synuclein group are very similar at 4wpi (WT: Δ39±12%, A53T: Δ45±7%), while this motor deficit is no longer seen at 12wpi in the WT-α-synuclein group, and increases for the A53T-α-synuclein group. This disappearance of a motor deficit at 12wpi in the WT-α-synuclein group is probably due to recovery after surgery. For the A53T-α-synuclein group the deficit remains at 12wpi and tends to aggravate when compared to the 4 week timepoint.

At the early timepoint after surgery, it might be difficult to discern between the effect of the surgery and/or injection, and that of the overexpression of WT or A53T-α-synuclein overexpression. Indeed in the present experiments we did not test the impact of the surgery on the performance of the rat during the cylinder test. However, Dr Cresto reported in her PhD dissertation that intranigral injection of PBS does not results in behavioural asymmetry in the cylinder test at 15wpi. In line with this, transduction of the substantia nigra with AAV-PGK-WT/G2019-LRRK2 does not induce significant

[6] Due to the global situation concerning COVID-19, analysis of pS129-α-synuclein for the WT-α-synuclein animals has been temporarily put on hold.

asymmetry either. Similarly, in the first series of experiments that were published (Cresto *et al.*, 2020), the motor performance of rats intranigrally injected with AAVs coding for LRRK2 indicated no asymmetry when assessed with the CatWalk system (Noldus), suggesting that AAV-injections at the titers used here do not produce major aspecific asymmetric use of the forepaws. However, it cannot completely be ruled out that at 4wpi the mild asymmetry seen in the WT-α-synuclein group is at least in part due to the injection procedure. To test the effects of the stereotaxic surgery our results should have been compared to non-injected and PBS-injected animals.

At 12wpi, the lack of a motor deficit for the WT-α-synuclein group cannot likely be explained by habituation to, or lack of interest for, the behavioural tests. Since the cylinder test is based on the ratio between left and right forepaw use, this cannot affect the outcome measure. However, a significant reduction of overall touches was observed for both groups (for more detailed information see the Supplementary data, Figure 31 (page 86)). The absence of asymmetry in this group at 12 wpi suggests that if an initial "dysfunction" of nigral neurons had occurred at 4 weeks, compensatory mechanisms prevailed to restore "normal" neuronal functions.

In conclusion, the motor asymmetry seen after AAV injection is with high probability induced by the transgene and its neurotoxic effects on neuronal function and /or neurogeneration.

### AADC-PET imaging

We were not able to demonstrate a significant asymmetry in the A53T-α-synuclein group, even though our results are suggestive for an asymmetric AADC enzymatic activity in the A53T-α-synuclein group. Different reasons can be put forward. First, we could only quantify AADC enzymatic activity in a small number of animals, due to insufficient blocking of peripheral AADC activity with benserazide, resulting in a low statistical power of this study. Next, there is a low signal to background-ratio in our [$^{18}$F]FMT PET images (Figure 29A,B). Smoothing of the PET images was required to enable quantification of $K_i$; this might have caused a loss of sensitivity in our quantification. The interanimal variability of the effect of benzerazide in rats is not explained so far, but represent another difficulty to use FMT in rat models.

To the best of our knowledge, only a few studies exist using [$^{18}$F]FMT PET imaging in rodent PD models (Honer *et al.*, 2006; Becker *et al.*, 2017). Honer and colleagues (2006) were unable to demonstrate dopaminergic neuronal loss, in a MPTP mouse model, using [$^{18}$F]FMT PET imaging. This might be attributed to the spill-in effect from surrounding brain regions displaying high radiotracer uptake, such as the basal brain areas, which possibly represent thalamic nuclei and/or basal ganglia (e.g. substantia nigra) (Honer *et al.*, 2006). Becker and colleagues (2017) have used [$^{18}$F]FMT to study both the complete and partial 6-OHDA lesion models. They observed a significant decrease in [$^{18}$F]FMT uptake in the ipsilateral striatum as compared to the contralateral striatum for both the complete and partial 6-ODHA model (Becker *et al.*, 2017). It must be noted that the partial lesion has a 72% loss of dopamine content in the striatum, as compared to 99% reduction in the full lesion group, making it still a very severe model. Becker and colleagues could not demonstrate a significant difference between their partial and complete lesion (Becker *et al.*, 2017).

[$^{18}$F]FDOPA, another PET tracer widely used to measure AADC enzymatic activity, has so far never been used in α-synuclein overexpression models. Nonetheless, in the complete 6-OHDA lesion model, Walker and colleagues (2013) showed that [$^{18}$F]FDOPA PET quantification was correlated with dopamine metabolite concentration (Walker, Dinelle, Kornelsen, Lee, *et al.*, 2013). Kyono and

colleagues (2011) used varying degrees of the partial 6-OHDA lesion model and showed a significant correlation between [$^{18}$F]FDOPA uptake and dopamine concentration (Kyono *et al.*, 2011).

### DAT-PET imaging

We demonstrate a significantly decreased binding of [$^{18}$F]LBT999 to DAT in the A53T-α-synuclein group, but not in the WT-α-synuclein group. Comparison of *in vivo* with *post-mortem* data showed an asymmetry ratio of Δ54% compared to Δ34% neuronal loss. Van der Perren and colleagues (2015) have demonstrated a gradual decrease of DAT binding using [$^{18}$F]-FECT PET imaging in their α-synuclein overexpression model. They show a ~50% decrease of DAT binding after ~60% reduction of TH-positive cells in the substantia nigra (Van der Perren *et al.*, 2015 AAV2/7-CMV/Synapsin- A53T-α-synuclein).

[$^{18}$F]LBT999 has never been used in α-synuclein overexpression models before, though, it has succesfully been used in the partial 6-OHDA model. Sérrière and colleagues (2015) have demonstrated a significant decrease in DAT binding in the ipsilateral striatum using [$^{18}$F]LBT999 (Sérrière *et al.*, 2015). Vetel and colleagues (2019) used [$^{18}$F]LBT999 to characterize a novel 6-OHDA lesion model; they showed a reproducible ~64% decrease in DAT binding in the striatum associated with a ~64% reduction of TH-positive cells in the substantia nigra (Vetel *et al.*, 2019). Grealish and colleagues (2014) have taken it one step further and have used [$^{18}$F]LBT999 to observe functional improvement after cell grafting in 6-OHDA lesioned rats (Grealish *et al.*, 2014).

Taken together, our results suggest that the DAT tracer [$^{18}$F]LBT999 is more sensitive to detect mild dopaminergic neuronal loss as compared to the AADC substrate [$^{18}$F]FMT. The increased signal to noise-ratio and easier usage make [$^{18}$F]LBT999 the preferred radiotracer of the two studied here. Additionally, [$^{18}$F]LBT999 has been extensively studied in rodent and non-human primate models, showing an ability to precisely quantify dopaminergic neuron loss and even assess the beneficial effects of therapeutic approaches (Grealish *et al.*, 2014; reviewed by Chalon *et al.*, 2019).

### Neuronal loss

In the present study, we did not observe any dopaminergic neuron loss in the substantia nigra after the expression of AAV2/6-PGK-WT-α-synuclein at 12wpi. In contrast, we demonstrated that overexpression of AAV2/6-PGK-A53T-α-synuclein lead to -27±6% of neuronal loss at 12wpi (asymmetry: Δ33±10%). Several other research groups have also reported on AAV-based overexpression of WT and A53T-α-synuclein in the substantia nigra, leading to various degrees of dopaminergic neuron loss in the substantia nigra and fibre loss in the striatum (Table 2).

The lack of a motor deficit for the WT-α-synuclein was consistent with results from the *post-mortem* analyses, which showed no significant loss of dopaminergic neurons in the substantia nigra. Literature has shown that WT-α-synuclein overexpression not always induces significant dopaminergic cell death (Sanchez-Guajardo *et al.*, 2010; Phan *et al.*, 2017). Even so, multiple groups have shown neurodegeneration after overexpression of WT-α-synuclein (Decressac, Mattsson and Björklund, 2012; Gombash *et al.*, 2013). Since the resulting phenotype is mild as compared to A53T-α-synuclein overexpression, it might be possible that the selected timepoint of this study was too early. For future experiments, it would thus be beneficial to study multiple, more distant, timepoints (e.g. 16, 20, and 24 weeks post-injection).

Interestingly, although in most cases deficits induced with WT-α-synuclein are smaller than with A53T-α-synuclein, at least one group showed the reverse; Lo Bianco and colleagues (2002)

observed more dopaminergic cell and fibre loss after WT-α-synuclein overexpression using lenti-viral vectors with a PGK promoter as compared to A53T-α-synuclein overexpression.

Van der Perren and colleagues (2015), using AAV2/7-CMV/Synapsin-A53T-α-synuclein expression in the sunstantia nigra, demonstrated significant dopaminergic cell loss in the substantia nigra (up to 80%) at 10wpi, leading to a significant motor deficit in the cylinder test (-50%) (Van der Perren *et al.*, 2015). The dopaminergic neurodegeneration we have observed in our experiments is much smaller than that found by other groups. However, the severity of the model also highly depends on the viral vector (e.g. AAV2, AAV6, AAV2/6), its promoter (e.g. PGK, CBA), and its enhancer elements (e.g. WPRE), the viral vector load, injection volume, and injection site and coordinates.

### Conclusion

In conclusion, we have shown that A53T-α-synuclein overexpression, but not WT-α-synuclein, is able to generate neuronal loss and dopamine deficiency 12 weeks post-injection, which is detectable *in vivo* by DAT-PET imaging and the cylinder test, and *post-mortem* by $TH^+$ stereology. The double injection AAV2/6-PGK-A53T-α-synuclein model results in a shorter time-window to develop a behavioural deficit and dopaminergic neuron loss in the substantia nigra, which makes this model more interesting for the evaluation of potential new therapeutic strategies.

Interestingly, we observed larger asymmetry with DAT PET (Δ54±8%) than in neuronal loss (-27±6%; Δ33±10%), suggesting additional downregulation of DAT protein. We further aim to characterize this model longitudinally, and to identify dopaminergic synaptic compensation mechanisms.

## 5. Supplementary behavioural data

### Longitudinal evaluation of cylinder test

Longitudinal evaluation of the cylinder test revealed that the WT-α-synuclein and A53T-α-synuclein animals had a significant lower amount of total touches at 10wpi as compared to 4wpi (WT: Δ69±11%; n=7; p<0.001, A53T: Δ53±15%; n=8; p=0.002). Interestingly, on an individual level, we observe that while for some rats of the WT-α-synuclein group the motor symptoms seem to aggravate, for others they diminish or even disappear over time (Figure 31).

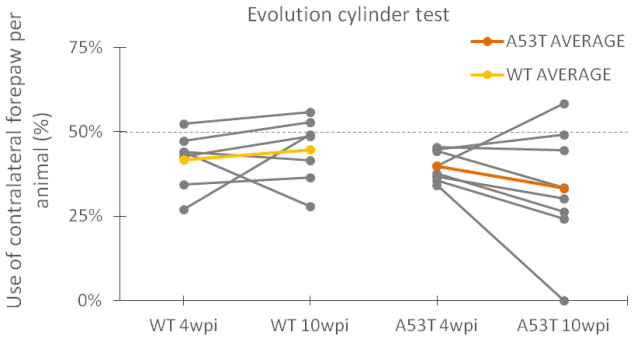


**Figure 31: Use of the contralateral forepaw per animal at both 4wpi and 12wpi. Every line show the evolution of a single animal.**

### Adjusting steps test and vibrissae test

Neither the WT-α-synuclein nor the A53T-α-synuclein group showed a behavioural deficit using the adjusting step test at 4wpi (Figure 32B, WT: n=7; p=0.19, A53T: n=8; p=0.07) or the vibrissae test at 10wpi (Figure 32C, WT: n=7; p=0.52, A53T: n=8; p=0.07).

We did not observe a behavioural deficit using the adjusting steps test. However, Gombash and colleagues (2013) and Decressac and colleagues (2012) showed a significant deficit in their respective WT-α-synuclein models before positive outcome of the cylinder test (Decressac, Mattsson and Björklund, 2012; Gombash *et al.*, 2013), suggesting that the adjusting steps test is more sensitive as compared to the cylinder test to detect motor symptoms in PD models. The discrepancy between our results and literature might be explained by the low replicability for the adjusting steps test in our hands. Indeed, the angle of the forepaw-restriction hold was decidedly variable between animals and runs. This inconsistency caused more false negatives since rats were not sufficiently stimulated to make the adjusting steps. The improve this, the rats could be trained longer beforehand to get accustomed to the forepaw-restriction hold, making it easier for the experimenter. Furthermore, a treadmill could be employed (as described by Chang *et al.*, 1999), which would equalise the speed and make the experimenter stationary, which could also make this test easier to perform consistently.

Similarly, like the adjusting steps test, the vibrissae test is experimenter-dependent, and therefore very variable in its execution, mainly in terms of hold, angle, and distance to the table. The lack of reproducibility induces a lack of sensitivity; hence, these tests were not used for further studies.

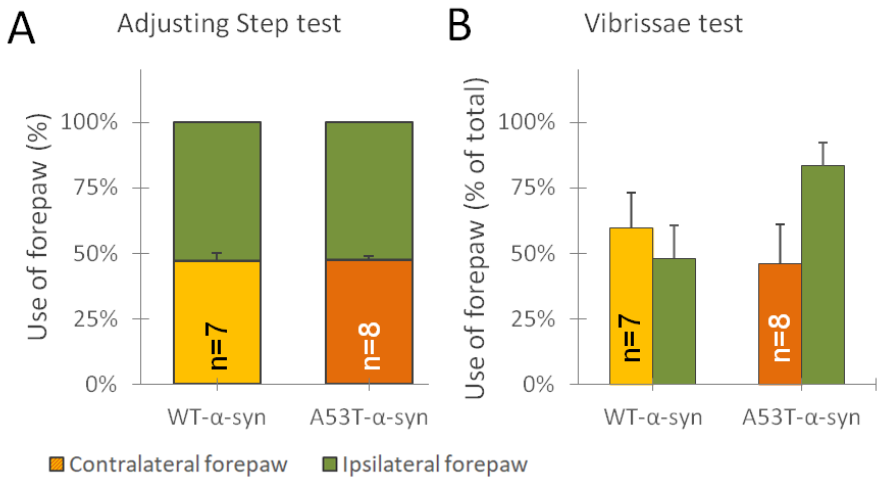


**Figure 32: Percentage of successful forepaw use in A) the Adjusting steps test and B) the Vibrissae test. Relative use of the contralateral (yellow/orange) and ipsilateral forepaw (green). Results are expressed as means ± the standard error of the mean (SEM). Paired student t-test, non-significant.**

# 4

# *RESULTS ON A MILD PROGRESSIVE NEURODEGENERATION MODEL*

# Part i. Evaluation of α-synuclein-induced neurodegeneration

## 1. Background and aims

Previously, we have compared two pathologically relevant rodent PD models based on overexpression of wildtype (WT) or A53T-mutant human α-synuclein protein in the substantia nigra through viral vectors (Chapter 3). This work has shown that A53T-α-synuclein, but not WT-α-synuclein, is able to generate neuronal loss and dopamine deficiency at 12 weeks post-injection (wpi). We demonstrated changes in the dopaminergic system *in vivo* through DAT-PET imaging corresponding to dopaminergic neuronal loss shown with *post-mortem* by $TH^+$ stereology.

**In the present study, we continued the evaluation of the double injection AAV2/6-PGK-A53T-α-synuclein model, with a focus on the effect of α-synuclein accumulation on the dopaminergic projection neuron. To that end, we performed extensive comparison of *in vivo* and *post-mortem* data.**

**In addition to the previously discussed 12 week timepoint (Chapter 3), we evaluated neuronal loss in the substantia nigra and the projection neurons at an earlier timepoint (8wpi), and added PBS control animals. In addition to the previous chapter, *post-mortem* analyses were completed with more extensive immunohistochemical analyses and RT-qPCR.**

## 2. Study design

Four cohorts of rats ($n_{total}$=32) were unilaterally injected in the SN with AAV2/6 viral vector coding for mutated (A53T) human α-synuclein (AAV2/6-PGK-A53T-α-synuclein; 2x5.00E+10 vgc) or with PBS (Figure 33A). Animals were evaluated at an early (n=2x8; 6-8 weeks post-injection (wpi)) or the late timepoint (n=2x8; 10-13wpi) (Figure 33B). The late A53T-α-synuclein cohort consist of the same animals as described in Chapter 3 (page 79). At each timepoint, the same animals underwent *in vivo* behaviour and PET imaging, and *post-mortem* immunohistological and RT-qPCR analyses.

PET imaging was performed using 6-[$^{18}$F]fluoro-L-m-tyrosine ([$^{18}$F]FMT) - a substrate for AADC, and [$^{18}$F]-LBT999 ([$^{18}$F]LBT) - a radioligand for dopamine transporter (DAT). AADC enzymatic rate (Ki) and DAT binding ($BP_{ND}$) were calculated using Patlak and Logan graphical methods respectively, employing the cerebellum as a reference region. For behavioural analysis, rats underwent the cylinder test during 5 minutes, in which contralateral and ipsilateral forepaw use was compared. Immediately after the *in vivo* studies, rats were sacrificed for histological studies and biochemical analyses. RT-qPCR studied gene expression of hydroxylase (TH), ionised calcium-binding adaptor molecule 1 (IBA1), aromatic L-amino acid decarboxylase (AADC), dopamine transporter (DAT), vesicular monoamine transporter 2 (VMAT2) in the substantia nigra. Immunohistochemical studies evaluated protein expression of hydroxylase (TH), phosphorylated serine 129 α-synuclein (pS129-α-syn), IBA1, DAT, VMAT in the substantia nigra and/or striatum. More detailed information about the methods can be found in Chapter 2.

Statistical analyses were performed using paired student t-tests to compare the ipsilateral and contralateral side in imaging studies, RT-qPCR, and immunohistochemical analyses, while for behavioural analysis a student t-test with unequal variance was used to compare against the hypothetic 50% value. All data is presented as asymmetry data:

$$Asymmetry\ ratio = \ \Delta\% = \frac{|\ ipsi - contra\ |}{(ipsi + contra) * 0.5}\ x\ 100$$

$$\%\ change = \frac{(ipsilateral - contralateral)}{contralateral}\ x\ 100$$

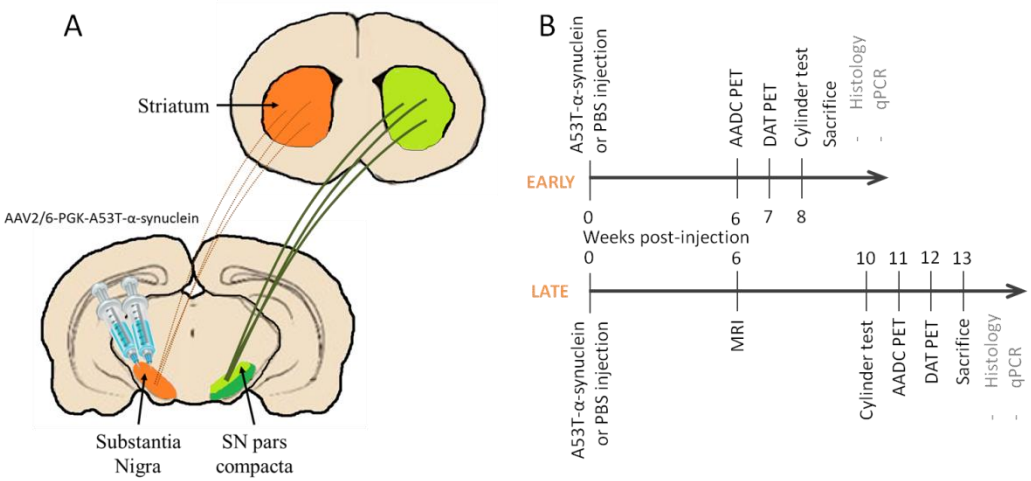


**Figure 33: Schematic overview of study design. A) AAV2/6-PGK-A53T-α-synuclein or PBS is injected in the substantia nigra in two locations. Data are collected from the substantia nigra and the striatum. B) Schematic overview of time schedule for the experiment. Rats were studied at 6-8wpi (early) or 10-13wpi (late).**

# 3. Results

## 3.1 Behavioural analysis

The cylinder test revealed a clear motor deficit at both the early (Figure 34, Δ76±23%; n=7; p=0.025) and the late timepoint (Δ79±22%; n=8; p=0.034) after AAV2/6-PGK-A53T-α-synuclein injection. Neither the early (n=8; p=0.32), nor the late PBS injected animals (n=8; p=0.14) show a significant motor deficit.

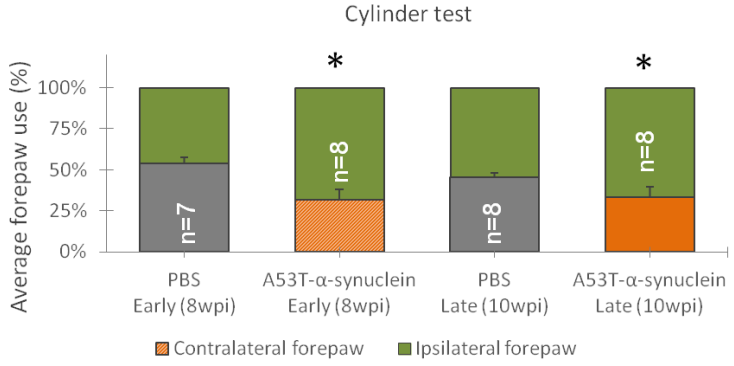


**Figure 34: Behavioural analysis using the cylinder test at the early (8wpi) and late (10wpi) timepoints for both the A53T-α-synuclein groups and PBS groups. Relative use of the contralateral (greey/orange) and ipsilateral forepaw (green). Results are expressed as means ± the standard error of the mean (SEM). Student t-test with unequal variance *p<0.05.**

## 3.2 PET imaging of the dopaminergic system

At the early timepoint, FMT-PET imaging did not show any significant left-right asymmetry in AADC enzymatic activity in the striatum after AAV2/6-PGK-A53T-α-synuclein injection, as we have previously shown for the late timepoint (Figure 35A,B, Early: n=4; p=0.25, Late: n=2).

In contrast, the significant asymmetry in DAT binding potential in the ipsilateral versus contralateral striatum was also observed at the early timepoint in A53T-α-synuclein rats (Figure 35C,D, Δ33±7%; n=6; p=0.027), as we have previously shown for the late timepoint (Δ54±8%; n=4; p=0.003).

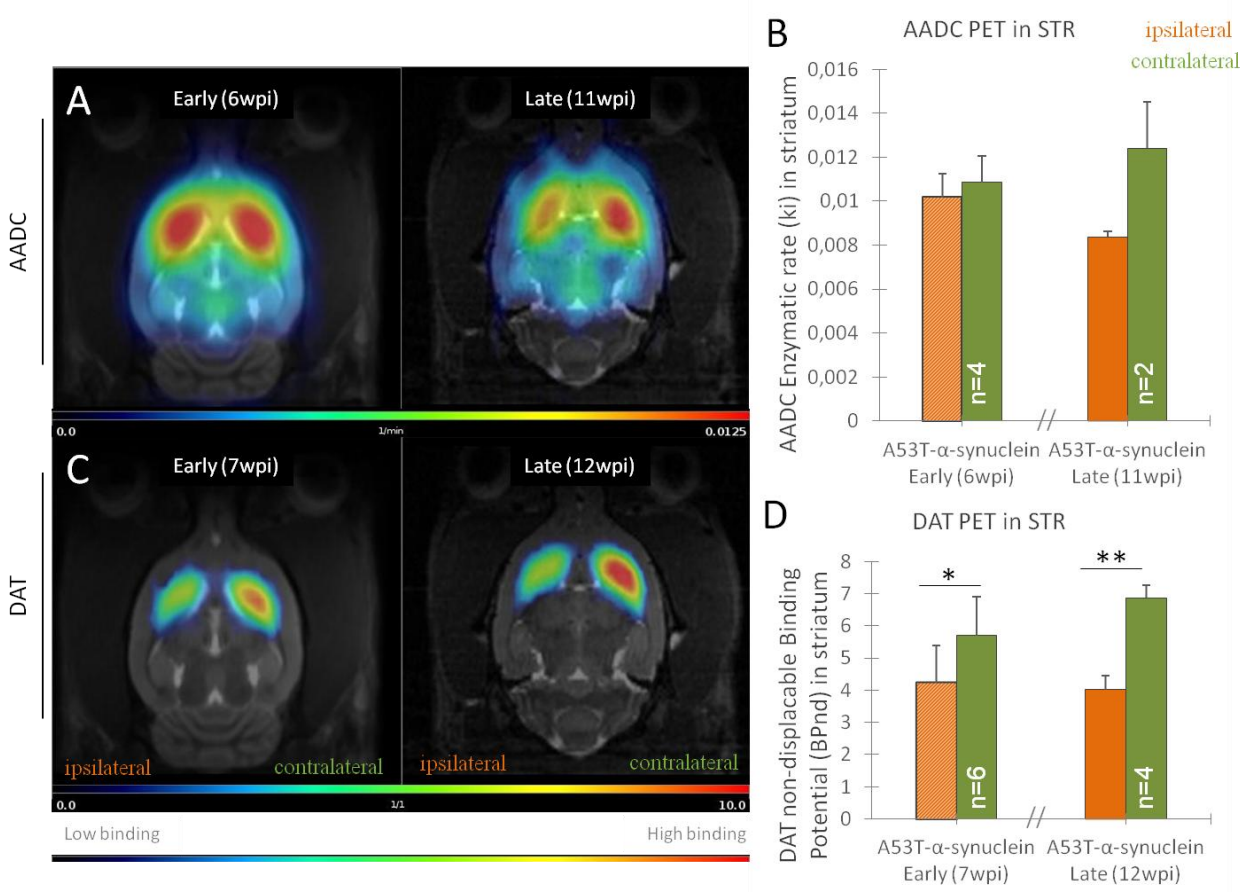


**Figure 35: *in vivo* PET analyses of A53T-α-synuclein animals, at both the early and late timepoint, using [$^{18}$F]FMT (AADC) and [$^{18}$F]LBT999 (DAT). A) Average of quantified AADC-PET images for the early (left) and late timepoint (right) of A53T-α-synuclein injected animals. B) AADC enzymatic rate for ipsilateral (orange) and contralateral striata (green) for both early and late timepoints after A53T-α-synuclein injection. C) Average of quantified DAT-PET images for the A53T-α-synuclein animals, at both the early (left) and late timepoint (right). D) DAT non-displaceable binding potential for ipsilateral and contralateral striata for A53T-α-synuclein injected animals, at both the early and late timepoint. Results are expressed as means ± the standard error of the mean (SEM). Paired student t-test *p<0.05, **p<0.01.**

## 3.3 *Post-mortem* analyses: α-synuclein, inflammation, and the dopaminergic system

### pS129-α-synuclein accumulation

We observed the presence of pS129-α-synuclein protein in the substantia nigra at the early timepoint after AAV2/6-PGK-A53T-α-synuclein injection as compared to the contralateral side (Figure

36A,B, Δ71±12%; n=7; p=0.004), and a smaller, but still significant, accumulation at the late timepoint (Δ34±9%; n=8; p=0.012).

The late PBS groups did not show a significant accumulation of pS129-α-synuclein in the substantia nigra (n=8; p=0.28).

### Tyrosine hydroxylase

At the early timepoint, we observed a significant difference of TH-positive positive neurons between the ipsilateral and contralateral substantia nigra after AAV2/6-PGK-A53T-α-synuclein injection, as measured by unbiased stereological counting (Figure 36C,D, Δ17±5%; n=6; p=0.013). At the late timepoint after AAV2/6-PGK-A53T-α-synuclein injection the difference in TH-positive neurons between the ipsi- and contralateral substantia nigra was stronger, as measured by unbiased TH stereology (Δ33±10%; n=8; p=0.009). This coincided with a borderline significant asymmetry of TH protein in the striatum at the late timepoint (Figure 36E,F, Δ40±12%; n=8; p=0.056). RT-qPCR showed no significant difference in TH mRNA levels in the substantia nigra at either timepoint after AAV2/6-PGK-A53T-α-synuclein injection (Figure 36G, Early: n=7/6; p= 0.13, Late: n=4/6; p=0.16).

The early PBS group did not show a significant asymmetry in TH-positive positive neurons in the substantia nigra, as measured by unbiased stereological counting (n=4; p=0.98). Neither did we observe a significant asymmetry in TH protein in the striatum at the early timepoint, as measured by optical density (n=8; p=0.51), nor at the late timepoint for PBS rats (n=8; p=0.44). RT-qPCR showed no significant difference in TH mRNA levels in the substantia nigra at either timepoint after PBS injection (Early: n=8/8; p=0.20, Late: n=8/8; p=0.99).

### Neuroinflammation [7]

At the early timepoint we demonstrated a minor but significant increase of IBA1 protein in the substantia nigra after AAV2/6-PGK-A53T-α-synuclein injection (Figure 36H,I, Δ6±2%; n=7, p=0.010). This result was not confirmed by RT-qPCR, which did not show significantly increased IBA1-mRNA expression in the substantia nigra at the early timepoint (Figure 36J, n=7/7, p=0.27). At the late timepoint, however, we did observe a significant increase of IBA1 mRNA levels (Δ38%; n=3/6; p=0.025).

With RT-qPCR we did not observe a significant difference at either the early timepoint (n=8/8; p=0.72), nor at the late timepoint for the PBS injected animals (n=8/8; p=0.88).

[7] Due to the global situation concerning COVID-19, IBA1 immonhistological analysis at 12wpi has been delayed.

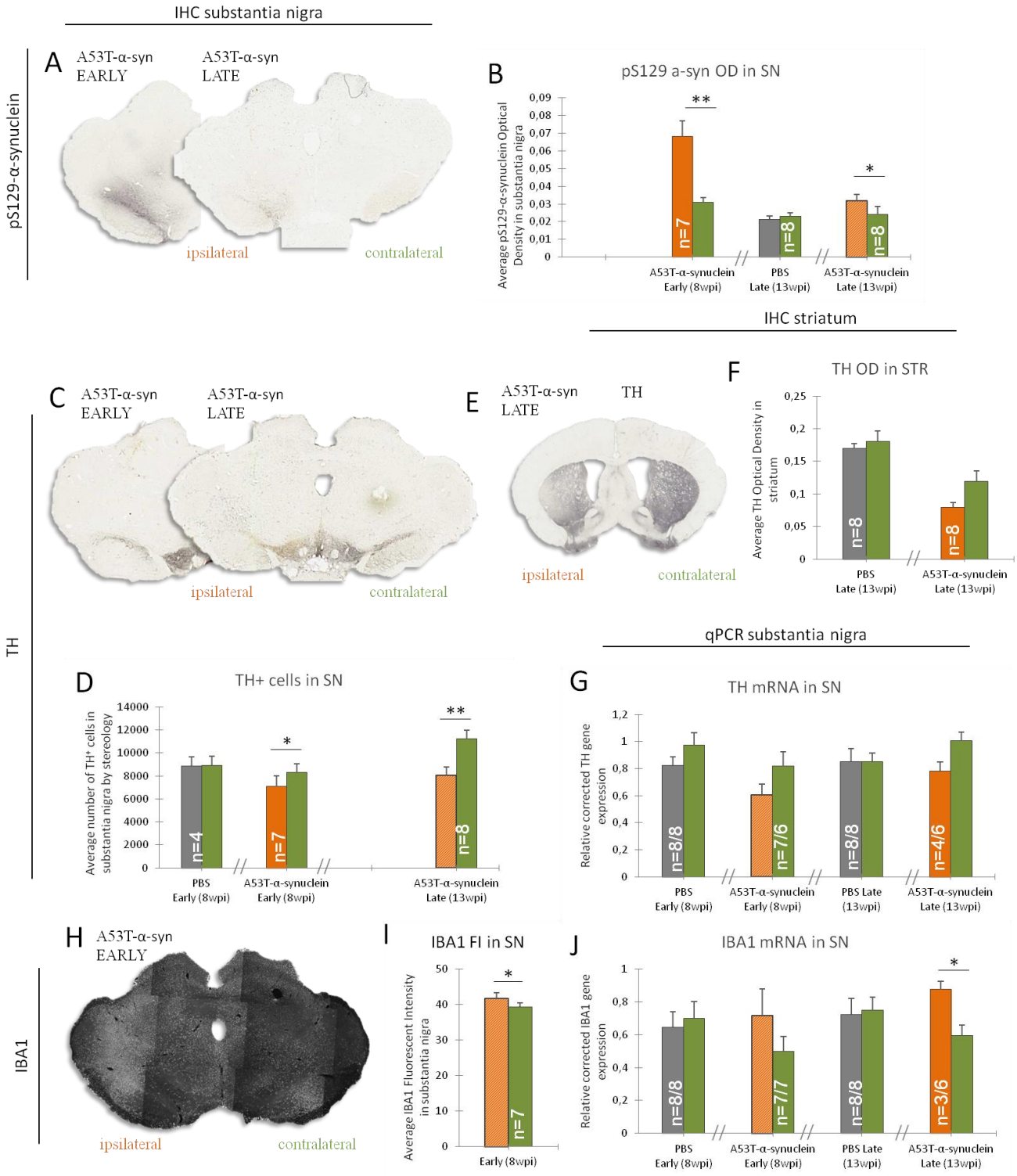


**Figure 36:** ***Post-mortem*** **analyses of the pS129-α-synuclein, neuroinflammation, and neurodegeneration in the substantia nigra and striatum. A) Representative immunohistochemical images of pS129-α-synuclein staining. B) Quantification of optical density of pS129-α-synuclein staining in the ipsilateral (grey/orange) and contralateral (green) substantia nigra. C) Representative immunohistochemical image of TH staining in the striatum. D) Representative immunohistochemical images of TH staining, and E) quantification through unbiased stereological counting. F) Relative TH mRNA expression levels in the substantia nigra. G) Quantification using optical density measurements. H) Representative immunofluoresence image of IBA1 staining, and I) quantification through fluorescent intensity in the substantia nigra. J) Relative IBA1 mRNA expression levels in the substantia nigra. Results are expressed as means ± the standard error of the mean (SEM). Paired student t-test *p<0.05, **p<0.01.**

### Aromatic L-amino acid decarboxylase

We did not measure an asymmetry in AADC mRNA expression in the substantia nigra after AAV2/6-PGK-A53T-α-synuclein injection using RT-qPCR at the early timepoint (**Fout! Verwijzingsbron niet gevonden.**A, n=7/7; p=0.36). At the late timepoint, however, we do observe a significant difference in AADC mRNA levels between the ipsilateral and contralateral substantia nigra (Δ25%, n=3/6, p=0.043).

For PBS injected animals we did not observe a significant asymmetry in AADC mRNA expression in the substantia nigra using RT-qPCR at either the early (n=8/7; p=0.67), nor at the late timepoint (n=8; p=0.42).

### Dopamine transporter

At the early timepoint after AAV2/6-PGK-A53T-α-synuclein injection, we did not observe a significant asymmetry in DAT mRNA expression in the substantia nigra (**Fout! Verwijzingsbron niet gevonden.**D, n=7/7; p=0.17), nor in DAT protein levels in the striatum (**Fout! Verwijzingsbron niet gevonden.**B,C, n=7; p=0.13). However, at the late timepoint, we did demonstrate a significant left/right difference in DAT mRNA levels in the substantia nigra (Δ30%; n=4/5; p=0.027) and DAT protein levels in the striatum (Δ29±6%; n=8; p=0.005).

For the PBS groups we did not observe significant asymmetry in DAT mRNA expression in the substantia nigra at either timepoint (Early: n=8/7; p=0.93, Late: n=8/8; p=0.45). Similarly, we did not observe significant asymmetry in DAT protein levels in the striatum after PBS injection (Early: n=8; p=0.42, Late: n=8; p=0.71).

### Vesicular monoamine transporter 2

We did not observe a significant asymmetry in VMAT2 mRNA levels in the substantia nigra at the early timepoint after AAV2/6-PGK-A53T-α-synuclein injection (**Fout! Verwijzingsbron niet gevonden.**G, n=7/6; p=0.47), while there was a significant asymmetry at the late timepoint (Δ42%; n=4/5, p=0.024). However, we did not demonstrate a significant left/right difference in VMAT2 protein levels in the striatum at the early timepoint (**Fout! Verwijzingsbron niet gevonden.**E,F, n=7; p=0.16) nor the late timepoint in the A53T-α-synuclein animals (n=8; p=0.34).

In the early PBS group we observed a small, but significant asymmetry in VMAT2 mRNA expression in the substantia nigra (Δ18%; n=8/8, p=0.045), while at the late timepoint we did not observe asymmetry (n=8/8; p=0.95). Similarly, we did not observe significant asymmetry in VMAT2 protein levels in the striatum after PBS injection (Early: n=8; p=0.65, Late: n=8; p=0.47).

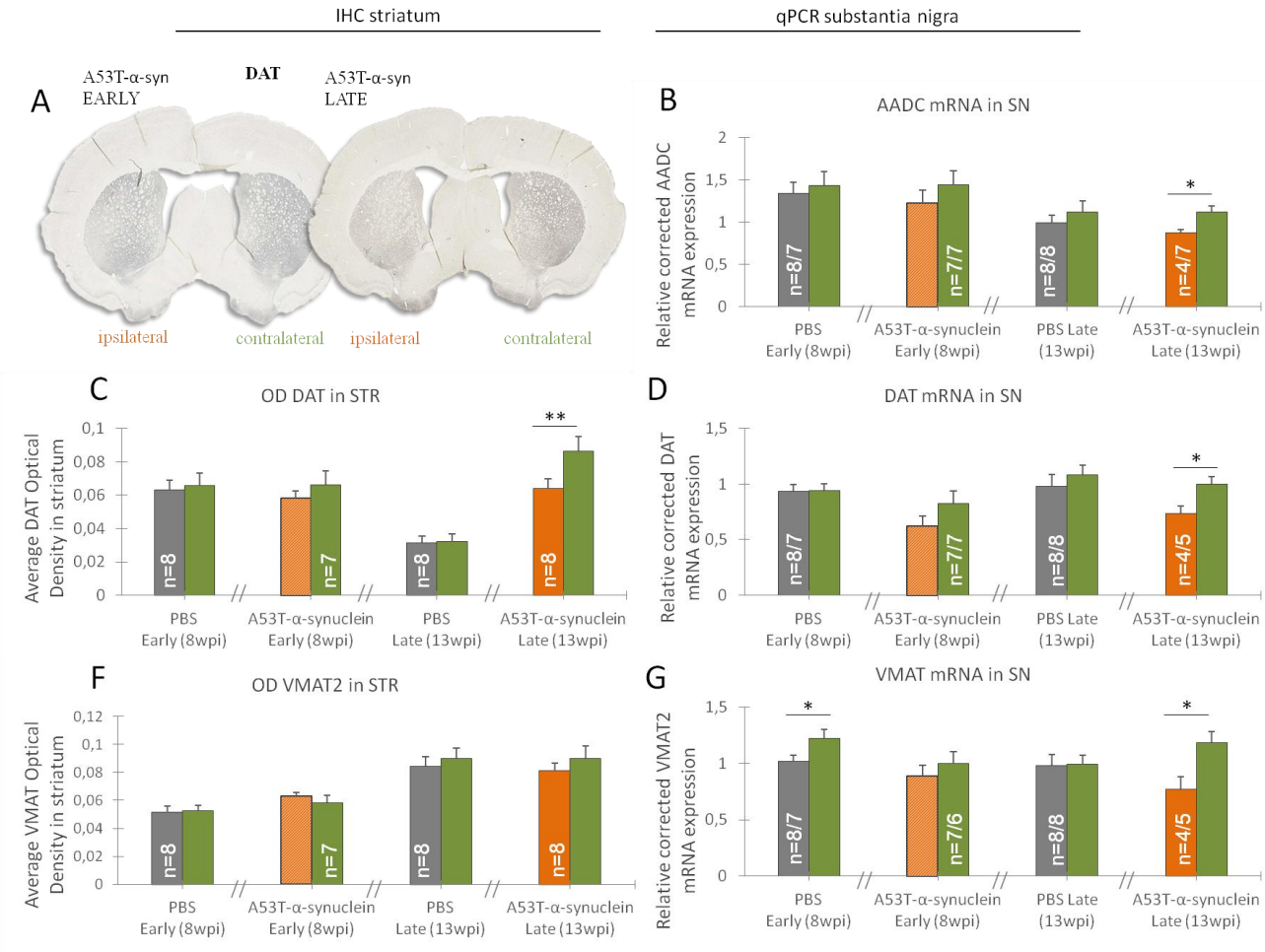


**Figure 37: *Post-mortem* analyses of the dopaminergic system in the substantia nigra and striatum. A) Representative immunohistochemical images of DAT staining in the striatum, and C) quantification using optical density measurements of the ipsilateral (green/orange) and contralateral (green) striatum. B) Relative AADC mRNA expression levels in the substantia nigra. D) Relative DAT mRNA expression levels in the substantia nigra. E) Representative immunohistochemical images of VMAT2 staining in the striatum, and F) quantification using optical density measurements. G) Relative DAT mRNA expression levels in the substantia nigra. Results are expressed as means ± the standard error of the mean (SEM). Paired student t-test *p<0.05, **p<0.01.**

### Correlation between *post-mortem* data and PET imaging

At the early timepoint after AAV2/6-PGK-A53T-α-synuclein injection we observed positive associations between the different *post-mortem* dopaminergic makers (Figure 38C), while they showed a moderate negative association with IBA1 expression. *In vivo* DAT-PET showed weak associations with the *post-mortem* dopaminergic markers. Interestingly, however, DAT-PET showed a strong negative association with IBA1 expression at the early timepoint. At the late timepoint we observe the same overall pattern (Figure 38D). Notably, the associations between *post-mortem* dopaminergic markers and IBA1 expression seem stronger, while the association between *in vivo* DAT-PET and IBA1 expression seems weaker.

In the PBS group at the early timepoint we observed a less distinct pattern of associations (Figure 38A). While at the late timepoint we again observe positive associations between *post-mortem* dopaminergic markers and a mild negative association with IBA1 expression (Figure 38B).

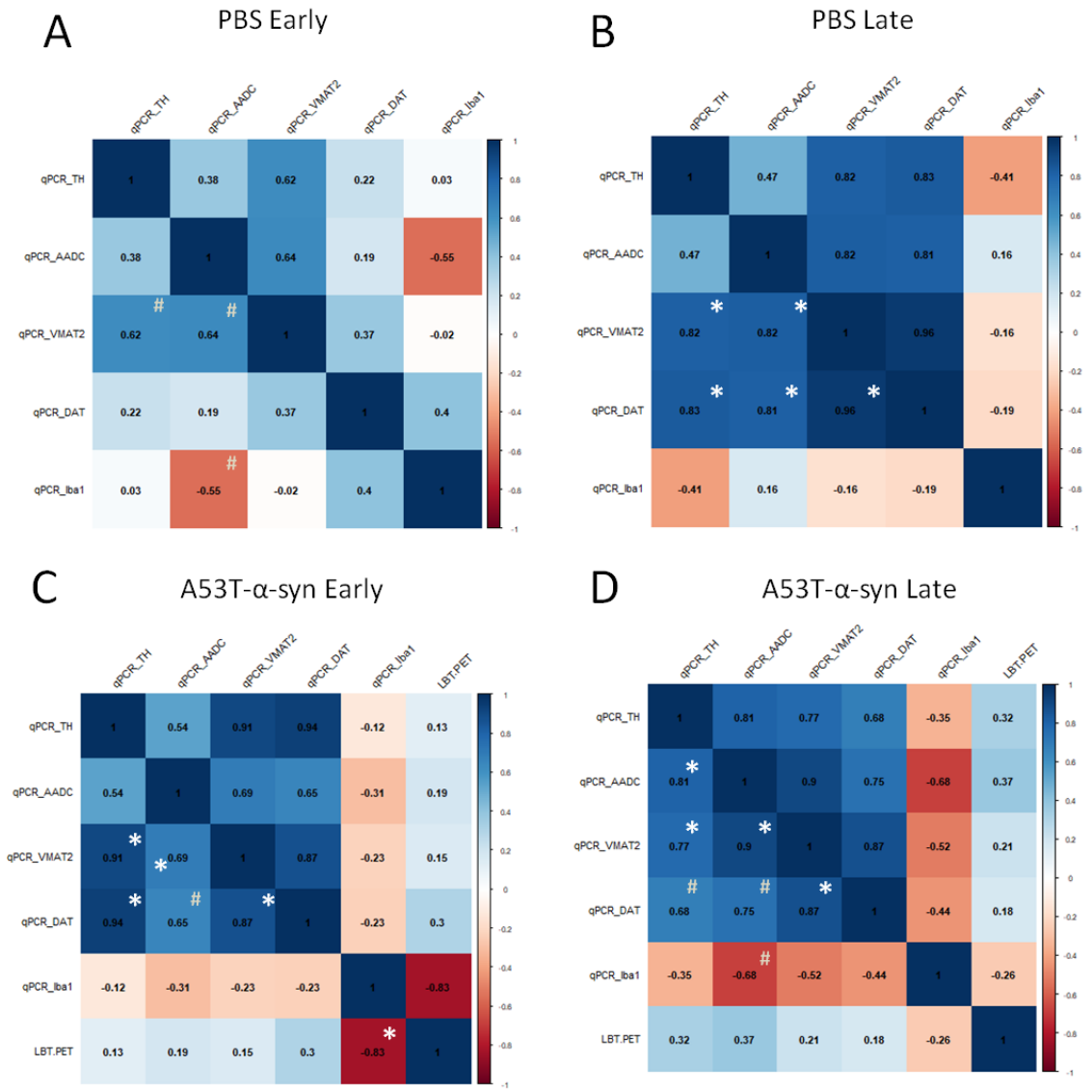


**Figure 38: Spearman correlation between *in vivo* data and different *post-mortem* data. A) Shows the early PBS group, while B) shows the late PBS group. C) Shows the early AAV2/6-PGK-A53T-α-synuclein injection group, while D) shows this group at the late timepoint. Spearman correlation coefficients are marked in the corresponding case; blue signifies a positive associations, while red signifies a negative associations. * p<0.01, # p<0.05.**

## 4. Discussion

### Behavioural analysis

With this work, we aimed to evaluate the progression of neuronal loss in the substantia nigra and the dopaminergic system in our double injection AAV2/6-PGK-A53T-α-synuclein model. Using behavioural testing a motor deficit was shown at the early timepoint that remained stable at the late timepoint, with equal strength and variability. The severity of the motor deficit was mild comparable to what we observed in a complete lesion model of 6-ODHA (Δ116±18%, Chapter 2: 3.2.1, page 54). Our double AAV2/6-PGK-A53T-α-synuclein injection displayed a comparable motor deficit at 8wpi as measured in a rAAV2/7-CMV-A53T-α-synuclein model at 3wpi, reported by Van der Perren and colleagues (2015). However, unlike our model, these authors performed a longitudinal study in the same animals and showed a progressive increase of the motor deficit (-25% at 3wpi, -50% at 4wpi) (Van der Perren et al., 2015). The lack of evolution of the motor deficit between the 8wpi and 12wpi group cannot be attributed to a plateau-effect, since our 6-OHDA data, confirmed by others (Schallert et al., 2000), shows that the use of the contralateral forepaw in the cylinder test can reduce much below what we have observed in the double injection AAV2/6-PGK-A53T-α-synuclein model. Lastly, it could be that the cylinder test lacks sensitivity to demonstrate the differences between our two groups. Van der Perren and colleagues (2015) used a similar induction method, but their model develops much faster and stronger, making the differences between timepoints larger. To circumvent the question of sensitivity, the corridor test could be included in future studies. Although it measures sensorimotor integration, it is said to be highly sensitive to deficits in the dopaminergic system in PD rat models (Dowd *et al.*, 2005; Fitzsimmons, Moloney and Dowd, 2006).

### PET imaging of the dopaminergic system

With AADC-PET we did not observe a significant loss of dopaminergic fibre, despite a clear trend as discussed in Chapter 3. In literature it has been suggested that AADC could be affected by compensation mechanisms in order to increase the amount of dopamine available in the synapse (Lee et al., 2000; Blesa et al., 2017; Kaasinen and Vahlberg, 2017); and thus raise synaptic dopamine levels. However, our data showed no change in AADC-mRNA expression levels at the early timepoint. At the late timepoint we observed a significant asymmetry for left/right AADC-mRNA expression, which is most probably due to a decrease of the AADC mRNA level in the ipsilateral striatum rather than an increase in the contralateral striatum. Even so, since there is translational and post-translational modification, there are still multiple ways in which final protein concentration can be modified (e.g. Chang, Mues and Hyland, 1996; Duchemin *et al.*, 2000). Thus, a lack of compensation mechanism at the mRNA expression level does not conclusively show that there is no AADC compensation mechanisms at all. Since PET imaging shows the accumulation of all previous processes, it could still be that the lack of asymmetry we observe with AADC-PET imaging is due to a combination of a reduced number of nerve terminals and a functional increase of AADC protein.

We have shown a significant left-right asymmetry in DAT binding using PET imaging. The difference in left-right binding (Δ54±8%) was markedly larger at the late timepoint as compared to the early timepoint (Δ33±7%), which coincides with increasing size of the dopaminergic lesion. However, DAT-PET shows a much larger asymmetry at the late timepoint (Δ54±8%) than suggested by the loss of dopaminergic neurons alone (Δ33±10%). DAT regulates synaptic dopamine levels; and thus, reduced DAT expression increases the amount of dopamine available in the synapse. DAT is

thought to compensate for dopaminergic neuronal loss in the substantia nigra and the accompanying loss of dopaminergic fibres in the striatum (Lee et al., 2000). At the late timepoint, we indeed observe an asymmetry in DAT mRNA and protein levels in the substantia nigra and striatum, respectively. Thus, our results at the late timepoint are in concordance with the idea of DAT compensation.

At the early timepoint, we do not observe such an compensatory effect of either DAT mRNA or protein levels. However, DAT-PET still shows a much larger asymmetry (Δ33±7%) than the loss of dopaminergic neurons (Δ17±5%) suggests. Recently it has been shown that extracellular monomeric and fibrillar α-synuclein can potentiate DAT binding and pre-endocytic clustering of DAT on the cell surface, thereby facilitating DAT endocytosis and down-regulating its transporter activity (Kobayashi *et al.*, 2019).

Down-regulation of striatal DAT has also been suggested after intra-MFB 6-OHDA injection in rats (Sossi et al., 2009). Conversely, striatal DAT binding was increased during the premotor phase in MPTP-treated non-human primates (Vezoli et al., 2014). Other studies observed no compensation mechanisms for striatal DAT in MPTP-treaded monkeys (Bezard et al., 2001), mice (Bezard et al., 2000), or the partial 6-OHDA lesion rat model (Dentresangle et al., 2001).

Using PET imaging in PD patients a greater reduction in DAT binding was observed as compared to AADC activity ([$^{18}$F]DOPA) or VMAT2 binding; suggestive of a down-regulation of DAT in the striatum (Lee *et al.*, 2000; Adams *et al.*, 2005; Daryl J Wile *et al.*, 2017). Additionally, a down-regulation of DAT mRNA in the striatum has been reported (Uhl et al., 1994; Joyce et al., 1997). Interestingly, reduced DAT binding can already be observed during the prodromal phase, using PET imaging, possibly reflecting prodromal compensatory mechanisms (Adams *et al.*, 2005; Stoessl, 2007; Daryl J Wile *et al.*, 2017).

### Neuronal loss & α-synuclein aggregation

Here we have injected a viral vector coding for A53T-α-synuclein into the substantia nigra, which led to significant dopaminergic neuronal loss in the substantia nigra at 8wpi (-15±4%, Δ17±5%), as measured by unbiased TH$^+$-stereology. This loss of dopaminergic neurons was mild compared to a complete lesion 6-ODHA model (-93.6±1.2%) (Decressac, Mattsson and Björklund, 2012). Our model is also milder compared to other viral vector overexpression models of α-synuclein. Decressac and colleagues (2012) showed around 70% loss of the dopaminergic neurons in a WT-α-synuclein model (Decressac, Mattsson and Björklund, 2012; AAV2/6-Synapsin/WPRE-WT-α-synuclein), while Van der Perren and colleagues (2015) showed around 70% loss in their A53T-α-synuclein overexpression model already at 2.5wpi. However, this last group also described a low vector dose model, which is much more in line with the size of the reduction of TH$^+$ cells we observe, which is around 30% at 12wpi (Van der Perren *et al.*, 2015; AAV2/7-Synapsin/CMV-A53T-α-synuclein). This demonstrates that besides the construction of the viral vector, also the titer plays a major role.

In the striatum, we have observed an almost significant reduction of TH-fibres at the late timepoint, while we observed significant neuronal loss in the substantia nigra (-27±6%, Δ33±10%). Decressac and colleagues (2012) demonstrated an almost equal reduction in striatal fibres as in dopaminergic cells in the substantia nigra. Noteworthy, our model seems to affect mostly the distal side of the striatum (visual observation), while Decressac's model seems to affect the medial striatum (Decressac, Mattsson and Björklund, 2012). This difference is most probably due to different

stereotactic injection coordinates in the substantia nigra, engaging different areas in the striatum (Haber, 2014).

Overall, we have shown here that our model progresses over time, with both an increase in the loss of $TH^+$ neurons in the substantia nigra and $TH^+$ fibres in the striatum.

In our studies, the loss of dopaminergic neurons in the substantia nigra was accompanied by an increase of α-synuclein phosphorylated at serine 129. Previously, studies have shown that approximately 90% of α-synuclein in Lewy Bodies is phosphorylated at serine 129 (Van der Perren *et al.*, 2015). At the early timepoint we also observed increased levels of pS129-α-synuclein in the striatum, which might suggest relocation or even spreading of α-synuclein aggregates (Gerfen and Bolam, 2010). Similarly, Van der Perren and colleagues (2015) observed dopaminergic neuronal loss and striatal fibre loss after nigral overexpression of α-synuclein (Van der Perren *et al.*, 2015).

Interestingly, we observed a larger increase of pS129-α-synuclein in both the substantia nigra and the striatum at the early timepoint as compared to the late timepoint, which might be attributed to neuronal loss. Nevertheless, Van der Perren and colleagues (2015) observed an initial increase in the percentage of aggregate positive cells which remained stable at later timepoints despite the occurance of severe neuronal loss (Van der Perren *et al.*, 2015).

We observed a small but significant inflammation at the early timepoint in the substantia nigra, which was not measurable by RT-qPCR. At the late timepoint we observed an upregulation of IBA1 mRNA in the substantia nigra using RT-qPCR. Previously, Chung and colleagues (2009) observed early microglial activation in the striatum, but not in the substantia nigra, after α-synuclein overexpression in the substantia nigra (Chung *et al.*, 2009).

Taken together the decrease of pS129-α-synuclein and the increase of inflammation over time, we hypothesize that neurodegeneration is mainly driven by α-synuclein overexpression at our early timepoint. Neuroinflammation seems to occur secondary to neuronal death. Based on their results, Chung and colleagues (2009) suggested that neuroinflammation is involved already before neuronal death occurs in their AAV2-Synapsin-A53T-α-synuclein model, and forms a positive feedback-loop to aggravate neurodegeneration (Chung *et al.*, 2009). However, they did not report on α-synuclein aggregation in their model.

## Conclusion

Here, we evaluated double injection of AAV2/6-PGK-A53T-α-synuclein as a rat PD model at two different timepoints. We have shown progressive loss of dopaminergic neurons in the substantia nigra, in combination with increasing neuroinflammation. The *in vivo* PET imaging and *post-mortem* analyses support the presence of potential DAT compensation mechanisms. Future research will have to unveil whether these compensation effects occur at the ipsilateral and/or contralateral synapse.

# Part ii. Exploration of compensation mechanisms in mild neurodegenerative models

## 5. Background and aims

We have previously suggested that compensation effects might impact PET imaging markers. **Here, we aimed to identify whether these compensation mechanisms occur at the ipsilateral and/or contralateral hemisphere.**

Since the analyses of the data are still ongoing, we have decided not to integrate the data obtained in this additional A53T-α-synuclein overexpressing group with the previous study. Unbiased stereological assessment is still ongoing [8] and should give confirmation of the lesion size and compatibility of these complementary data.

## 6. Study design

In parallel to the PBS 10-12wpi (reported above), one cohort of animals (n=10) was injected in the substantia nigra with AAV2/6 viral vector coding for mutated (A53T) human alpha-synuclein (n=10) or with PBS (n=8) (Figure 39A). Animals were evaluated at the late timepoint (Figure 39B; n=18; 10-12wpi). Animals underwent *in vivo* behaviour and PET imaging, and *post mortem* immunohistological and RT-qPCR analysis. The late PBS is the same as shown above, while the A53T-α-synuclein is a new cohort; the *post-mortem* analyses were performed at the same time to be able to compare. More detailed information about the methods can be found above (page 100) and in Chapter 2.

Statistical analyses were performed using paired student t-tests to compare the ipsilateral and contralateral side in imaging studies, RT-qPCR, and immunohistochemical analyses, while for behavioural analysis a student t-test with unequal variance was used to compare against the hypothetic 50% value. All data are presented as asymmetry ratios, calculated using the following formula:

$$Asymmetry\ ratio = \ \Delta\% = \frac{|\ ipsi - contra\ |}{(ipsi + contra) * 0.5}\ x\ 100$$

$$\%\ change = \frac{(ipsilateral - contralateral)}{contralateral}\ x\ 100$$

[8] Unbiased stereology is ongoing, but halted due to the current COVID-19 pandemic and consequent confinemt.

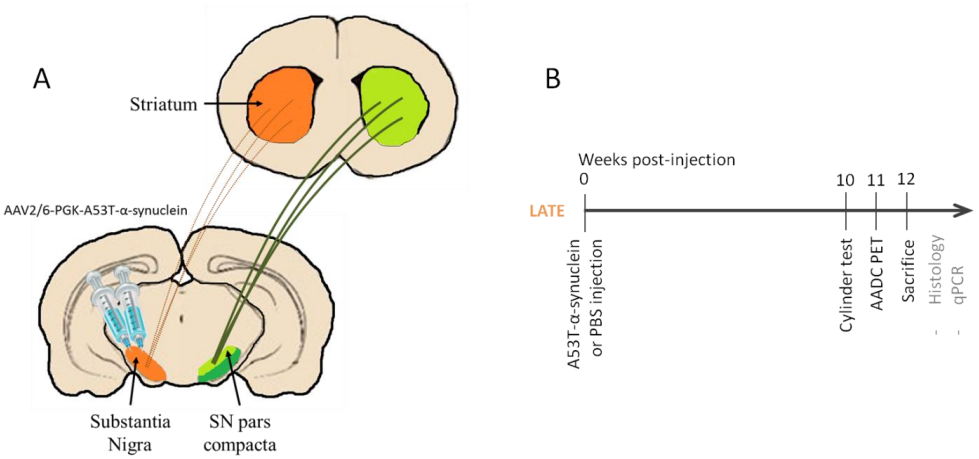


**Figure 39: Schematic overview of study design. A) AAV2/6-PGK-A53T-α-synuclein or PBS is injected in the substantia nigra in two locations. Data are collected from the substantia nigra and the striatum. B) Schematic overview of time schedule for the experiment.**

# 7. Results

## 7.1 Behavioural analysis

Using the cylinder test, we observed significant deficits in spontaneous forepaw usage after AAV2/6-PGK-A53T-α-synuclein injection (Figure 40, Δ36±10%; n=8; p=0.013), while the PBS injected group showed no motor deficit (n=8; p=0.14).

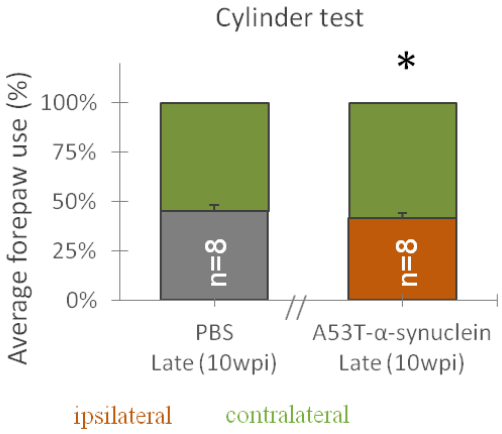


**Figure 40: Behavioural analysis using the cylinder test at late timepoint (10wpi) for both the A53T-α-synuclein and PBS groups. Relative use of the ipsilateral (grey/brown) and contralateral forepaw (green). Results are expressed as means ± the standard error of the mean (SEM). Student t-test with unequal variance *p<0.05.**

## 7.2 PET imaging of the dopaminergic system

Using [$^{18}$F]FMT-PET imaging, we did not observe significant left-right asymmetry in AADC enzymatic activity in the striatum after AAV2/6-PGK-A53T-α-synuclein injection (Figure 41A, B, n=5; p=0.10).

Interestingly, if we combine these data with the previously obtained data for the late timepoint, we observe a small but significant asymmetry (Δ13±4%; n=7; p=0.030).

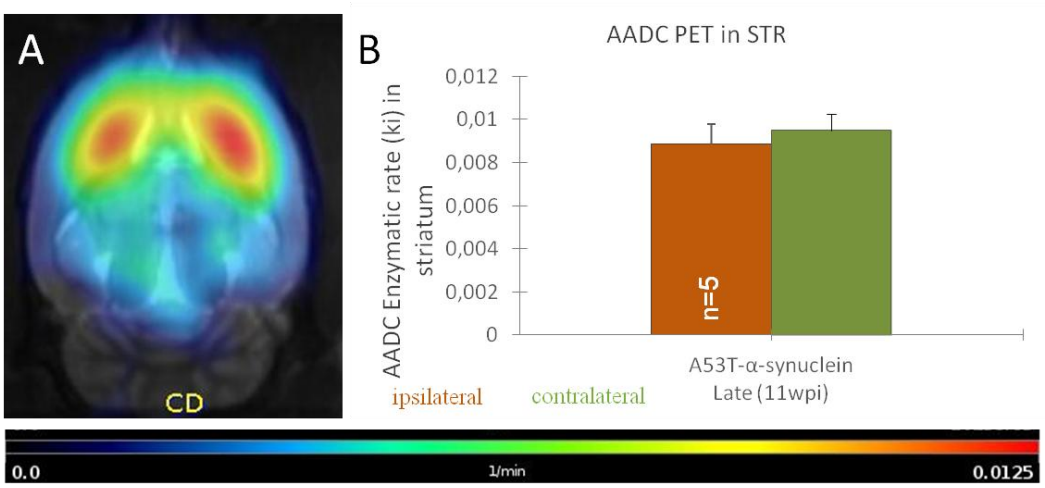


**Figure 41: *in vivo* PET analyses of A53T-α-synuclein animals, at 11wpi, using [$^{18}$F] (AADC). A) Average of quantified AADC-PET images of A53T-α-synuclein injected animals. B) AADC enzymatic rate for ipsilateral (brown) and contralateral striata (green) 11 weeks after A53T-α-synuclein injection. Results are expressed as means ± the standard error of the mean (SEM). The colour scale represent Ki (1/min). Paired student t-test, non-significant.**

## 7.3 Post-mortem analyses: α-synuclein, inflammation, and the dopaminergic system

### pS129-α-synuclein accumulation

We demonstrated a significant increase of pS129-α-synuclein protein in the substantia nigra of A53T-α-synuclein injected animals (Figure 42A, Δ57±16%; n=9; p=0.007). As expected, in the PBS group at the late timepoint we did not observe a significant difference (n=8; p=0.28). Similarly, in the striatum there was a significant increase of pS129-α-synuclein in A53T-α-synuclein injected animals (Figure 42B, Δ13±3%; n=9; p=0.006). In the PBS group at the late timepoint we did not observe a significant asymmetry (n=8; p=0.08); interestingly, there was a significant difference between the ipsilateral PBS-injected animals and contralateral A53T-α-synuclein injected animals (Δ23%; n=8/9; p=0.013).

### Tyrosine hydroxylase

Using optical density to rapidly estimate the amount of TH-positive cells in the substantia nigra, we did not observe a significant asymmetry after either A53T-α-synuclein injection (Figure 42C, n=9; p=0.50; non-parametric) or PBS injection (n=8; p=0.08; non-parametric). In the striatum, we did not observe any TH asymmetry at the late timepoint using optical density analysis for A53T-α-synuclein (Figure 42E, n=9; p=0.28) or PBS injected animals (n=8; p=0.44). RT-qPCR showed a significant asymmetry in TH mRNA expression in the substantia nigra in the A53T-α-synuclein injected animals (Figure 42D, Δ29%; n=8/8; p=0.008), while there was no asymmetry in PBS animals (n=8/8; p=0.99).

### Neuroinflammation

In the striatum, we did not observe any asymmetry for IBA1 at the late timepoint after A53T-α-synuclein injection (Figure 42G, n=9; p=0.20) or PBS injection using optical density analysis (n=8; p=0.44). Using RT-qPCR we observed no significant asymmetry in IBA1 levels in the substantia nigra in the A53T-α-synuclein or PBS group (Figure 42F, A53T: n=8/8; p=0.25, PBS: n=8/8; p=0.30).

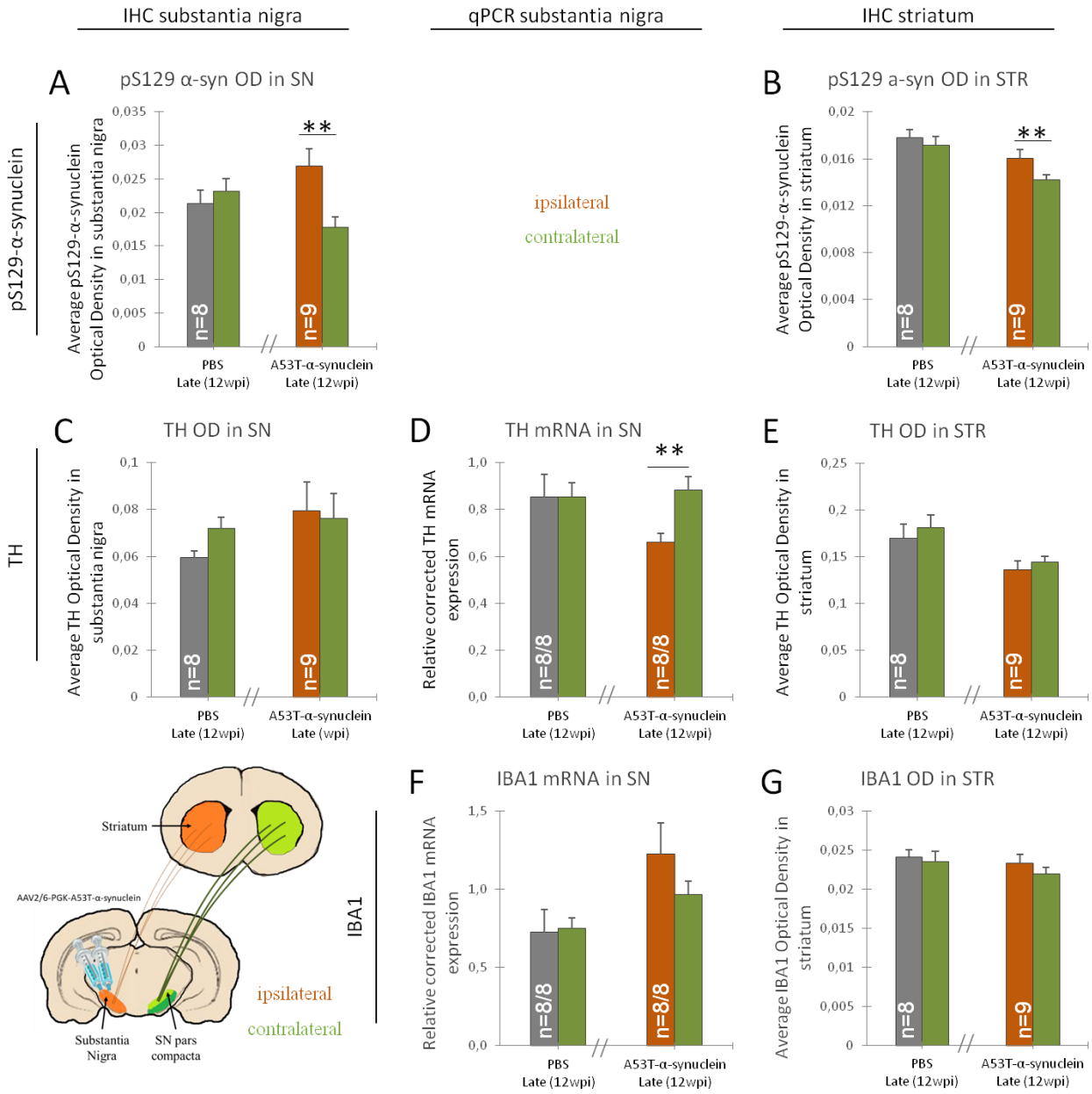


**Figure 42: *Post-mortem* analyses of the pS129-α-synuclein, neuroinflammation, and neurodegeneration in the substantia nigra and striatum. A) Quantification of immunohistochemical pS129-α-synuclein staining in the ipsilateral (grey/brown) and contralateral (green) substantia nigra, and B) in the striatum, both assessed with optical density measurements. C) Stereological quantification of immunohistochemical TH staining in the substantia nigra. D) Relative TH mRNA expression levels in the substantia nigra. E) Optical denstity quantification of immunohistochemical TH staining in the striatum. F) Relative IBA1 mRNA expression levels in the substantia nigra. G) Optical denstity quantification of immunohistochemical TH staining in the striatum. Results are expressed as means ± the standard error of the mean (SEM). Paired student t-test **p<0.01.**

### Aromatic L-amino acid decarboxylase

Using RT-qPCR we did not observe a significant asymmetry in AADC mRNA expression in the substantia nigra of A53T-α-synuclein animals (Figure 43A, n=8/8; p=0.062) nor in PBS injected animals (n=8/8; p=0.42).

### Dopamine transporter

We did not observe a significant asymmetry in DAT protein levels in the striatum for A53T-α-synuclein injected animals (Figure 43C, n=9; p=0.30), nor for the PBS injected animals (n=8; p=0.71). RT-qPCR showed significant asymmetry of DAT mRNA expression levels in the substantia nigra in A53T-α-synuclein injected animals (Figure 43B, Δ20%; n=8/8; p=0.042), while PBS animals showed no asymmetry (n=8/8; p=0.45).

### Vesicular monoamine transporter 2

We did not show any significant asymmetry in VMAT2 protein levels in the striatum after A53T-α-synuclein injection (Figure 43E, n=9; p=0.20), nor after PBS injection (n=8; p=0.47). Similarly, using RT-qPCR, we did not observe significant asymmetry in VMAT2 mRNA expression in the substantia nigra for A53T-α-synuclein injected animals (Figure 43D, n=8/8; p=0.33), nor for PBS injected animals (n=8/8; p=0.95).

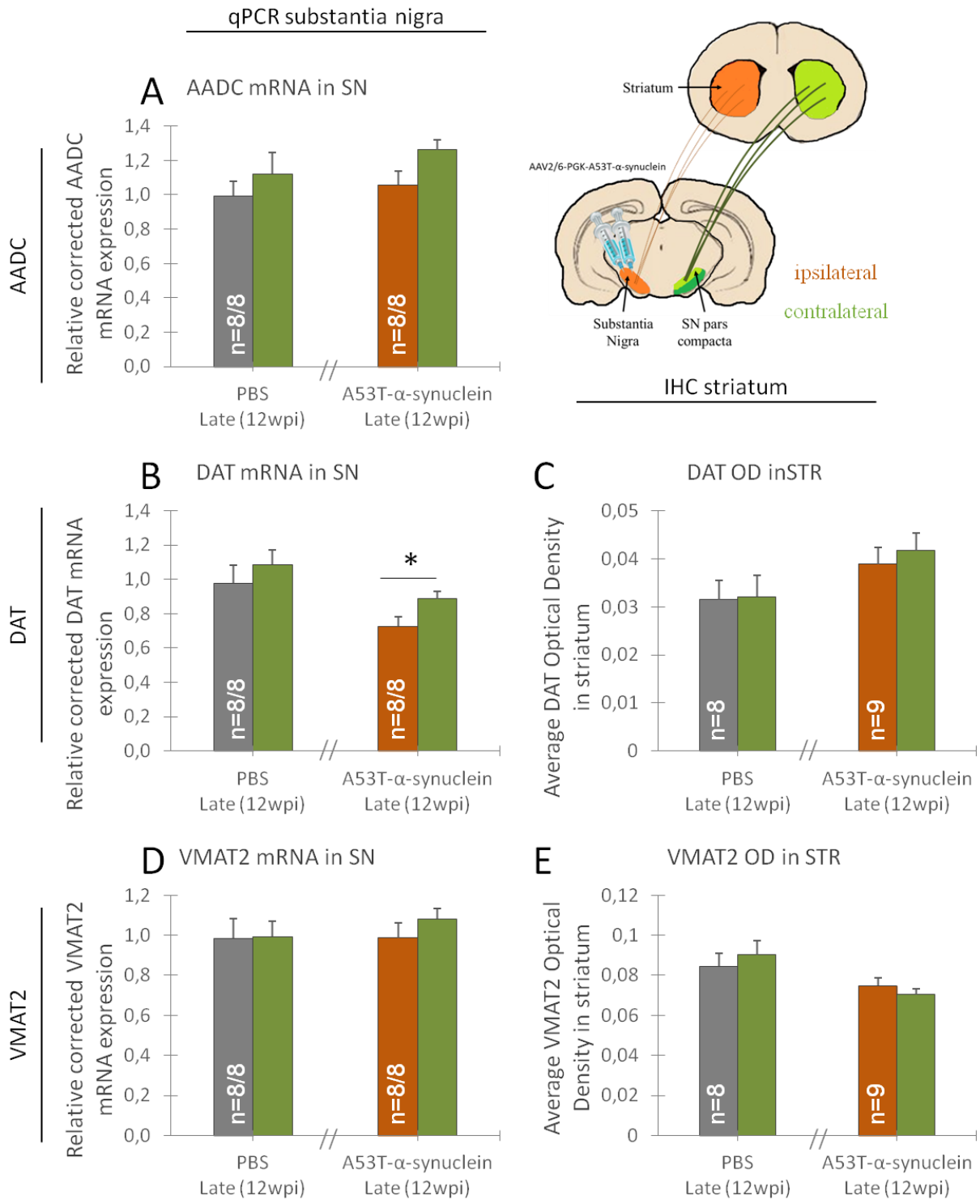


**Figure 43:** ***Post-mortem*** **analyses of the dopaminergic system in the substantia nigra and striatum. A) Relative AADC mRNA expression levels in the ipsilateral (grey/brown) and contralateral (green) substantia nigra. B) Relative DAT mRNA expression levels in the substantia nigra. C) Quantification of immunohistochemical DAT staining in the striatum, as assessed with optical density measurements. D) Relative VMAT2 mRNA expression levels in the substantia nigra. E) Quantification of immunohistochemical VMAT2 staining in the striatum, as assessed with optical density measurements. Results are expressed as means ± the standard error of the mean (SEM). Paired student t-test *p<0.05.**

## 8. Discussion

With this work we aimed to study the above observed compensation effect in more detail. We used our double injection AAV2/6-PGK-A53T-α-synuclein rat model at the late timepoint (10-12wpi), and PBS injected animals as a control. Using behavioural testing we observed a motor deficit for A53T-α-synuclein rats, while the PBS injected rats did not show a motor deficit. Conversely, using *in vivo* AADC-PET imaging we did not observe a significant asymmetry. Using *post-mortem*, we demonstrated significant presence of phosphorylated α-synuclein in both the substantia niga and striatum, and a reduction of TH mRNA in the substantia nigra. We did not observe neuroinflammation, as assessed by IBA1 mRNA and protein levels, nor did we observe significant changes in AADC and VMAT2 protein density in the striatum, or VMAT2 mRNA expression in the substantia nigra.

Previsously, we have also shown a motor deficit at 10-13wpi after nigral AAV2/6-PGK-A53T-α-synuclein injection. Morever, previously we had already observed an increase in pS129-α-synuclein protein density in the substantia nigra, and an asymmetry in DAT mRNA expression in the substantia nigra. Conversely, again we did not demonstrate asymmetry using AADC-PET, nor did we observe asymmetry in IBA1 mRNA expression in the substantia nigra or TH and VMAT2 protein density in the striatum.

However, we have previously demonstrated asymmetry in AADC and VMAT2 mRNA expression in the substantia nigra, as well as DAT protein density in the striatum, which we were unable to replicate here. Thus, we were unable to conclusively show the presense of DAT compensation mechanisms here. The lack of compensation mechanisms in our current experiment might be explain by the lack of dopaminergic neuron loss in the substantia nigra. However, a less sensitive method of analysis was used due to a lack of time. As shown in Chapter 2: 6.2.6 (page 73), optical density underestimates neuronal loss as compared to unbiased stereological counting. It is therefore not conclusive that there is indeed no neurodegeneration in the nigrostriatal pathway. Further research by way of unbiased stereology will be done to answer this question.

### Conclusion

Here, we aimed to investigate whether the previously observed compensation mechanisms occur at the ipsilateral and/or contralateral hemisphere. However, we were not able to demonstrate any compensation mechanism. Further research has to show if the neuronal loss in the new cohort is comparable to the first cohort.

Nevertheless, a very mild PD model, like described here, might be reflective of a prodromal phase, thus making it very interesting for research on neuroprotective agents; the dopaminergic neurons are suffering, but have not perished yet. Additionally, this mild model might be used the research the interplay between A53T-α-synuclein overexpression and other PD-related gene mutations, e.g. the putative enhancing effect of the A53T-α-synuclein mutation and LRRK2 (Cresto et al., 2018).

# 5

# *RESUTLS ON THE INTERPLAY BETWEEN LRRK2 AND α-SYNUCLEIN*

## 1. Background and aims

Leucine-rich repeat kinase 2 (LRRK2) is a kinase of which rare mutations have shown to cause autosomal dominant PD (Chapter 1: 2.5, page 27). The overlap between clinical phenotypes associated with mutations in SNCA and LRRK2 suggests that these proteins play an important role in both sporadic and genetic PD (Cresto *et al.*, 2018). Our lab is interested in the potential synergistic interaction between α-synuclein and LRRK2 and their role in the susceptibility to develop PD. Conversely, inhibition of LRRK2 kinase activity is envisioned as one of the main therapeutic targets in PD.

The main mode of action of LRRK2 is through its kinase domain; rendered constitutively active through the G2019S. Previously, it was shown by the team of Emmanuel Brouillet from our lab that overexpression of the C-terminal domain of LRRK2 alone did not affect dopaminergic neuronal survival at 6 months post-injection, while the constituently active G2019S form of LRRK2 resulted in a significant reduction of 30% of TH-positive neurons in the substantia nigra of rats (AAV2/9-PGK/WPRE-ΔLRRK2$^{WT/G2019S}$) (Cresto *et al.*, 2020). In Chapter 4, we have shown that A53T-α-synuclein overexpression results in significant dopaminergic neurodegeneration in the rat substantia nigra. The hypothesis is that mutated G2019S-LRRK2 increases the toxicity of A53T-α-synuclein overexpression. Previous studies performed in our lab at 15wpi have demonstrated that G2019S-ΔLRRK2 alone did not produce significant dopaminergic neurodegeneration. Co-overexpression of A53T-α-synuclein and G2019S-ΔLRRK2 induced a greater dopaminergic neurodegeneration than overexpression of A53T-α-synuclein alone. These results show that the effect of exacerbated A53T-α-synuclein toxicity by G2019S-ΔLRRK2 overexpression might be due to cell-autonomous mechanisms involving the the LRKK2 kinase domain. Alternatively, the interplay between A53T-α-synuclein and LRRK2 might be due to non-cell-autonomous mechanisms, such as neuroinflammation.

This study was subsequently repeated using AAV2/6-PGK-A53T-α-synuclein model as characterized in Chapter 4. The post-mortem data at 6wpi complementing the existing 15wpi data have been summarised in a paper entitled "*The C-terminal fragment of LRRK2 with the G2019S substitution increases the neurotoxicity of mutant A53T α-synuclein in dopaminergic neurons in vivo*", which was submitted to Translational Neurodegeneration (page 148). For this work, I was involved in the experiment conducted at 6 weeks post-injection; I have assisted with the stereotactic injections, and with the transcranial perfusions, cut all the brains, and contributed to the immunohistochemical analyses.

In the present chapter, we aimed to evaluate if DAT-PET imaging allows to discriminate A53T-α-synuclein-induced dopaminergic neuron loss from that induced by co-overexpression of A53T-α-synuclein and G2019S-ΔLRRK2.

## 2. Study design

Briefly, four cohorts of rats ($n_{total}$=48) were unilaterally injected in the SN with AAV2/6 viral vector coding for mutated (A53T) human α-synuclein in combination with a viral vector coding for GFP, G2019S-LKKR2 or a dead-kinase form of LRRK2 (DK-LRRK2); control animals were injected with PBS (Figure 44A,B). Animals were evaluated at the early timepoint (n=4x12; 6-8 weeks post-injection (wpi, Figure 44C). Animals underwent *in vivo* behaviour and PET imaging, and *post-mortem* immunohistological evaluation.

For behavioural analysis, rats were subjected to the cylinder test for 5 minutes, in which contralateral and ipsilateral forepaw use was compared. PET imaging was performed using [$^{18}$F]LBT999 - a radioligand for dopamine transporter (DAT). DAT binding ($BP_{ND}$) was calculated using Logan's graphical method, employing the cerebellum as a reference region. Immediately after the *in vivo* studies, rats were sacrificed for histological studies. Immunohistochemical studies evaluated protein expression of tyrosine hydroxylase (TH). Unbiased stereology was performed by a single experimenter, due to time constraints, not all contralateral substantia nigras were counted. More detailed information about the methods can be found in Chapter 2, and in the submitted paper (page 148).

Inter-group statistical analyses were performed using repeated measures ANOVA, to compare the ipsilateral and contralateral side across all groups in imaging studies and immunohistochemical analyses. For post-hoc analyses between groups, Fisher's least significant difference test (LSD) was used. For behavioural analysis ANOVA was used to compare against the Gombash score of the PBS group. Within-group statistical analyses were performed using paired student-tests to compare the ipsilateral and contralateral side within groups in imaging studies and immunohistochemical analyses. Data are presented as asymmetry ratios:

$$Asymmetry\ ratio = \Delta\% = \frac{|\ ipsi - contra\ |}{(ipsi + contra) * 0.5}\ x\ 100$$

$$\%\ change = \frac{(ipsilateral - contralateral)}{contralateral}\ x\ 100$$

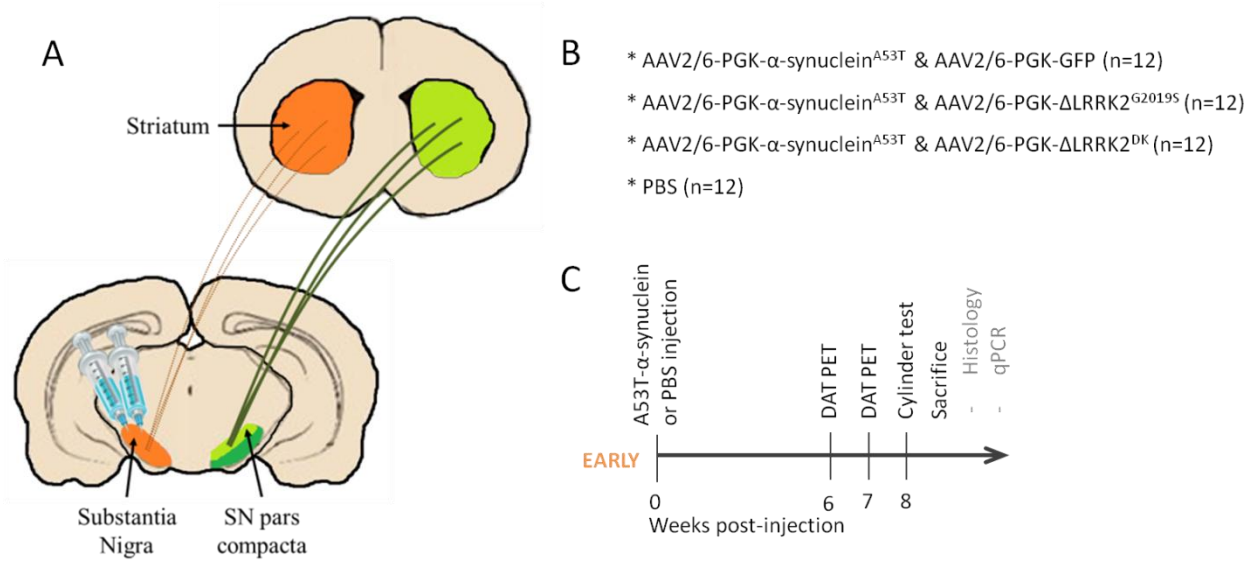


**Figure 44: Schematic overview of study design. A) Viral vectors or PBS is injected in the substantia nigra in two locations. Data are collected from the substantia nigra and the striatum. B) Representation of viral vectors used for the different experimental groups. C) Schematic overview of time schedule for the experiment. Rats were studied at 6-8wpi (early).**

# 3. Results

## 3.1 Behavioural analysis

The cylinder test (Figure 45A) revealed a significant difference from the PBS group for the A53T/GFP (Δ62±17%; n=12; p=0.005) and A53T/GS group (Δ58±10%; n=12; p=0.021), but not the A53T/DK group (n=12; p=0.37). Noteworthy, the A53T/GFP group was also significantly different from the A53T/DK group (Δ41±10%; n=12; p=0.044).

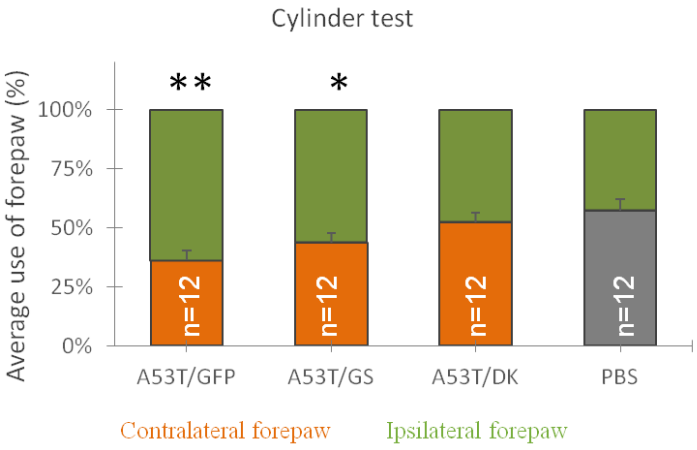


**Figure 45: Behavioural analysis using the cylinder test at 8wpi for all experimental groups and the PBS group.Relative use of the contralateral (orange/grey) and ipsilateral forepaw (green). Results are expressed as means ± the standard error of the mean (SEM). ANOVA with Scheffé post-hoc, *p<0.05, **p<0.01.**

## 3.2 PET imaging of the dopaminergic system

### Ipsi- and contralateral $BP_{nd}$ measures between groups

We did not demonstrate a group effect or a left-right effect in the DAT non-displaceable binding potential in the striata after expression of the different viral vectors in the substantia nigra (Figure 46; n=7/7/7/5; p=0.21). Surprisingly, we observed a high variability in $BP_{nd}$ between different vector groups.

However, if we compare the ipsilateral and contralateral hemisphere of each group individually, we a statistically significant asymmetry in the A53T/GFP (Δ21±2%; n=7; p=0.001), A53T/GS (Δ15±3%; n=7; p=0.003), and A53T/DK groups (Δ17±4%; n=7; p=0.003), but not the PBS group (n=5; p=0.25).

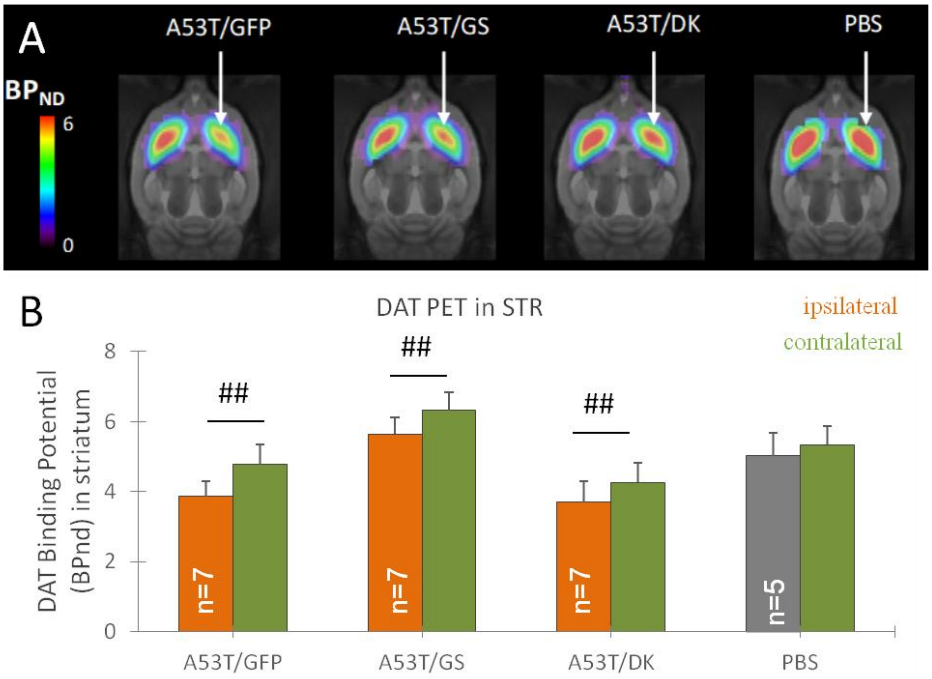


**Figure 46: *in vivo* PET analysis of all experimental groups and PBS group using [$^{18}$F]LBT999 (DAT). A) Average of quantified DAT-PET images for experimental groups and PBS animals. B) DAT non-displaceable binding potential for ipsilateral (orange/grey) and contralateral striata (green). Results are expressed as means ± the standard error of the mean (SEM). ANOVA did not show significant differences. Within group paired student t-test ##p<0.01 in intragroup comparision.**

### $BP_{nd}$-ratio between groups

To account for the variability in $BP_{nd}$ between vector groups, we calculated the $BP_{nd}$-ratio, using the contralateral striatum as a control side (Figure 47). Despite the absence of a significant difference between $BP_{nd}$-ratios, we observed a trend similar to the behavioural data, showing the lowest $BP_{nd}$-ratio for A53T/GFP (0.81±0.02), followed by A53T/GS (0.86±0.03), A53T/DK (0.87±0.03), and PBS (0.94±0.04). As the $BP_{nd}$-ratios were derived from $BP_{nd}$-measures from the entire striatum, these data were suggestive of local and modest $BP_{nd}$ changes.

However, if we compare the ipsilateral over contralateral ratio of each group individually to the hypothetical 1 value, we observe statistically significant differences in the A53T/GFP (n=7; p<<0.001), A53T/GS (n=7; p=0.002), and A53T/DK groups (n=7; p=0.004), but not the PBS group (n=5; p=0.16).

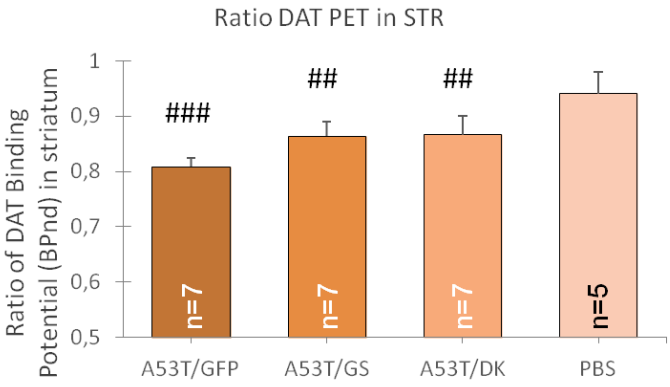

**Figure 47: DAT-PET $BP_{nd}$-ratio per group. Ratio was calculated by division of the average $BP_{nd}$ of the ipsilateral striatum by the average $BP_{nd}$ of the contralateral striatum. Results are expressed as means ± the standard error of the mean (SEM). ANOVA did not show significant differences. Within group paired student t-test with unequal variance, ##p<0.01, ###p<0.001 in intragroup comparisons.**

## 3.3 Post-mortem analysis: neurodegeneration

Dopaminergic neuronal loss was assessed by unbiased stereology in the injected and non-injected substantia nigra, performed by a single operator. We did not observe stastically significant dopaminergic neuronal loss in the injected substantia nigra of the experimental groups as compared to the PBS group, using one-way ANOVA (Figure 48, A53T/GFP: n=12; p=0.84, A53T/GS: n=12; p=0.61, A53T/DK: n=12; p=0.52). However, if we compare the ipsilateral and contralateral hemisphere of each group individually, we observe stastically significant asymmetry in both the A53T/GS (Δ21%; n=12/5; p=0.035) and A53T/DK groups (Δ30%; n=12/4; p=0.008), but not the A53T/GFP group (n=12/6; p=0.21) or PBS (n=12/7; p=0.49).

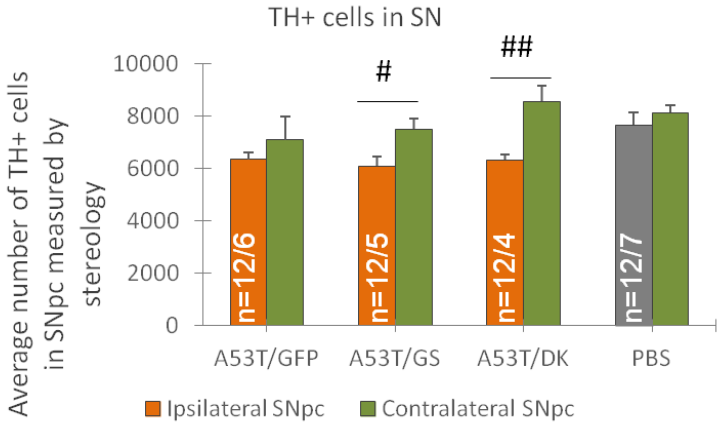


**Figure 48: *Post-mortem* analysis of neurodegeneration in the substantia nigra. Quantification of the number of TH-positive cells in the ipsilateral (orange/gre) and contralateral substantia nigra (green) using unbiased stereological counting. Results are expressed as means ± the standard error of the mean (SEM). ANOVA did not show significant differences. Within group paired student t-test #p<0.05, ##p<0.01, in intragroup comparisons.**

# 4. Discussion

In addition to the *post-mortem* study submitted, we have evaluated the synergistic effect of G2019S-ΔLRRK2 or DK-ΔLRRK2 and A53T-α-synuclein overexpression *in vivo* in the substantia nigra. G2019S-ΔLRRK2 co-overexpression with A53T-α-synuclein did not induce a larger behavioural deficit than observed after co-overexpression of A53T-α-synuclein and GFP. Similarly, the DAT-$BP_{nd}$-ratio was not more different in the G2019S-ΔLRRK2 co-overexpression group. Combined overexpression of A53T/DK induced a behavioural phenotype close to PBS animals, even though DAT-$BP_{nd}$-ratio was comparable to the G2019S-ΔLRRK2 group. Our results show that DAT-$BP_{nd}$-ratios globally followed the same pattern as the cylinder test showed. Surprisingly, the *post-mortem* data obtained by unbiased $TH^+$ stereology showed an opposite pattern; a tendency for increased dopaminergic neurodegeneration after co-overexpression of A53T-α-synuclein and G2019S-ΔLRRK2 or DK-ΔLRRK2. Since viral vector load was equal in all groups, these results suggest an interplay between ΔLRRK2 and A53T-α-synuclein toxicity. These findings support the hypothesis from the paper (appendix 2,

page 148); the C-terminal domain of G2019S-LRRK2 (G2019S-ΔLRRK2) is sufficient to augment the toxic effects of A53T-α-synuclein through a cell-autonomous mechanism involving the catalytic activity of its kinase domain. Furthermore, the effect of G2019S-ΔLRRK2 upon A53T-α-synuclein toxicity is likely specific or a particular interplay between these two proteins, and the crosstalk occurs within the same neurons. However, the results also indicdate that even in an experimental condition where the two proteins are expressed in high levels (approximately 5-50 fold the level of endogenous α-synuclein and LRRK2, respectively), the effect of G2019S-ΔLRRK2 on A53T-α-synuclein is moderate. Thus, it is reasonable to speculate that in a condition with physiological levels of expression of LRRK2 and α-synuclein, the cell-autonomous crosstalk between the two proteins might be of moderate importance in dopaminergic neurons. Non-cell autonomous mechanisms involving interaction of dopaminergic neurons with neighbouring glial cells and immune cells may have more important roles in patients and transgenic animal models (Cresto *et al.,* in progress).

Discrepancies between *in vivo* and *post-mortem* data might be due to several compensation mechanisms. $TH^+$ stereology seems to suggest an increase of TH-positive neurons in the contralateral substantia nigra, which could be explained by an increase in TH expression per cell, resulting in greater visibility and thus a bias in TH stereological counting. Little is known about TH compensation effects in the substantia nigra. RT-qPCR analyses measuring at the mRNA levels of TH in the substantia nigra could elucidate this question. A few older reports have described TH compensation mechanisms in the substantia nigra in MPTP mice and humans. Greenwood and colleagues (1991) showed that in MPTP-treated mice cytoplasmic TH protein was increased, resulting in stable levels of dopamine and DOPAC even with the presence neuronal loss (Greenwood *et al.*, 1991). Joyce and colleagues (1997) demonstrated loss of TH protein in the substantia nigra of PD patients, accompanied by a severe loss of neurons expression TH and DAT mRNA. Remaining neurons showed a shift to higher concentrations of TH mRNA, but a shift to lower concentrations of DAT mRNA per cell (Joyce *et al.*, 1997).

The discrepancy between *in vivo* and *post-mortem* data could also suggest that ΔLRRK2 itself impacts different cell mechanisms at a functional level, influencing DAT-$BP_{nd}$-ratios and behavioural phenotype, but not influence neuronal cell death. In support of this view, Zhou and colleagues (2011) have shown that temporal overexpression of G2019S-LRRK2 impairs DAT-mediated dopamine reuptake. However, they did not observe a direct interaction between DAT and G2019S-LRRK2 (Zhou *et al.*, 2011). Morevover, two studies described reduced DAT-binding using PET imaging in asymptomatic LRRK2 mutation carriers (Adams *et al.*, 2005; Nandhagopal *et al.*, 2008), thus indicating that LRRK2 might influence DAT binding, but does not influence neuronal death. Interestingly, Penney and colleagues (2016) demonstrated compensation mechanisms in neuro-muscular junctions of the fruitfly after post-synaptic LRRK2 overexpression; enhancement of presynaptic neurotransmitter release by increasing the size o the release ready pool of vesicles (Penney *et al.*, 2016).

We cannot exclude compensation mechanisms of the contralateral hemisphere contributing to inter-animal or inter-group differences. Assessment of DAT protein levels in the striatum and mRNA expression in the substantia nigra, using immunohistochemical and biochemical techniques, respectively, could give more conclusive information about potential DAT compensation mechanisms in co-overexpression models of LRRK2 and α-synuclein.

We have shown that overexpression of A53T-α-synuclein, both alone and in combination with G2019S-ΔLRRK2, led to a significant motor deficit as measured with the cylinder test. Conversely, combined overexpression of A53T-α-synuclein and DK-ΔLRRK2 does not lead to a significant motor deficit. This could suggest that the dead kinase form of ΔLRRK2 might be neuroprotective. Others, indeed, observed that a dead kinase form of LRRK2 alone reduced neuronal toxicity (Greggio *et al.*, 2006; Smith *et al.*, 2006). Additionally, LRRK2 knock-out rats show reduced neurodegeneration after α-synuclein overexpression compared to wild-type rats (Daher *et al.*, 2014). In a subsequent paper Daher and colleagues (2015) suggested that a LRRK2 kinase inhibitor has neuroprotective effects in wild-type rats overexpressing α-synuclein (Daher *et al.*, 2015). These findings highlight the potential of LRRK2 as a putative therapeutic neuroprotective target.

Finally, we have explored different methods to analyse the acquired DAT-PET data; "standard" $BP_{nd}$ quantification, $BP_{nd}$-ratios. Using $BP_{nd}$ quantification we were not able to show between-group differences, but we did observe a tendency for within-group asymmetry. To account for the variability in absolute $BP_{nd}$ values we have calculated $BP_{nd}$-ratios. A next step could be to use statistical parametric mapping.

Previously, Casteels and colleagues (2006) used statistical parametric mapping in 6-OHDA rats to demonstrate severe hypometabolism in the ipsilateral sensorimotor cortex, using [$^{18}$F]FDG, and a striatal decrease in DAT availability, using [$^{18}$F]FECT (Casteels *et al.*, 2006). Moreover, statistical parametric mapping has been used to quantify and map abnormalities in DAT activity in early PD patients (Ma *et al.*, 2002). More recently, Wang and colleagues (2017) have demonstrated the use of statistical parametric mapping using [$^{11}$C]β-CFT (DAT), [$^{11}$C]Raclopride ($D_2R$), and [$^{18}$F]FDG (glucose metabolism). They conclude that statistical parametric mapping of static PET/CT scan data is potentially very usefull for clinical use (Wang *et al.*, 2017).

## Conclusion

Taken together, these data are indicative of an interplay between ΔLRRK2 and A53T-α-synuclein toxicity. Moreover, they point towards an important role for the kinase domain of LRRK2 in this synergistic toxicity. This makes LRRK2, especially its kinase domain, an interesting target for therapeutic strategies. Future studies could shed more light on the role of compensation mechanism in this co-overexpression model.

## 5. Supplementary data: Voxel-wise $BP_{nd}$-ratio changes between groups

In an attempt to pick up local, intra-striatal $BP_{nd}$-ratio changes, we calculated parametric $BP_{nd}$-ratio images. To that end, we flipped each individual image, co-registered both flipped and non-flipped images, and finally divided the original by the co-registered flipped image. The striatum contralateral to the injection side was masked (Figure 49A). SPM analysis using ANOVA was performed on the masked $BP_{nd}$-ratio images of the ipsilateral striatum. Nevertheless the local differences lacked statistical power to reach a significance level of $p<0.001$ (Figure 49B, no correction for multiple comparisons, no cluster size). Nevertheless, T-score images reflect same tendency as observed with overall BPnd ratios. Additionnally, T-score images show that BPnd is not homogeneously decreased over the entire striatum, underlying the interest of voxel-wise analysis. The results are highly suggestive of regional differences between groups, and warrent further investigation.

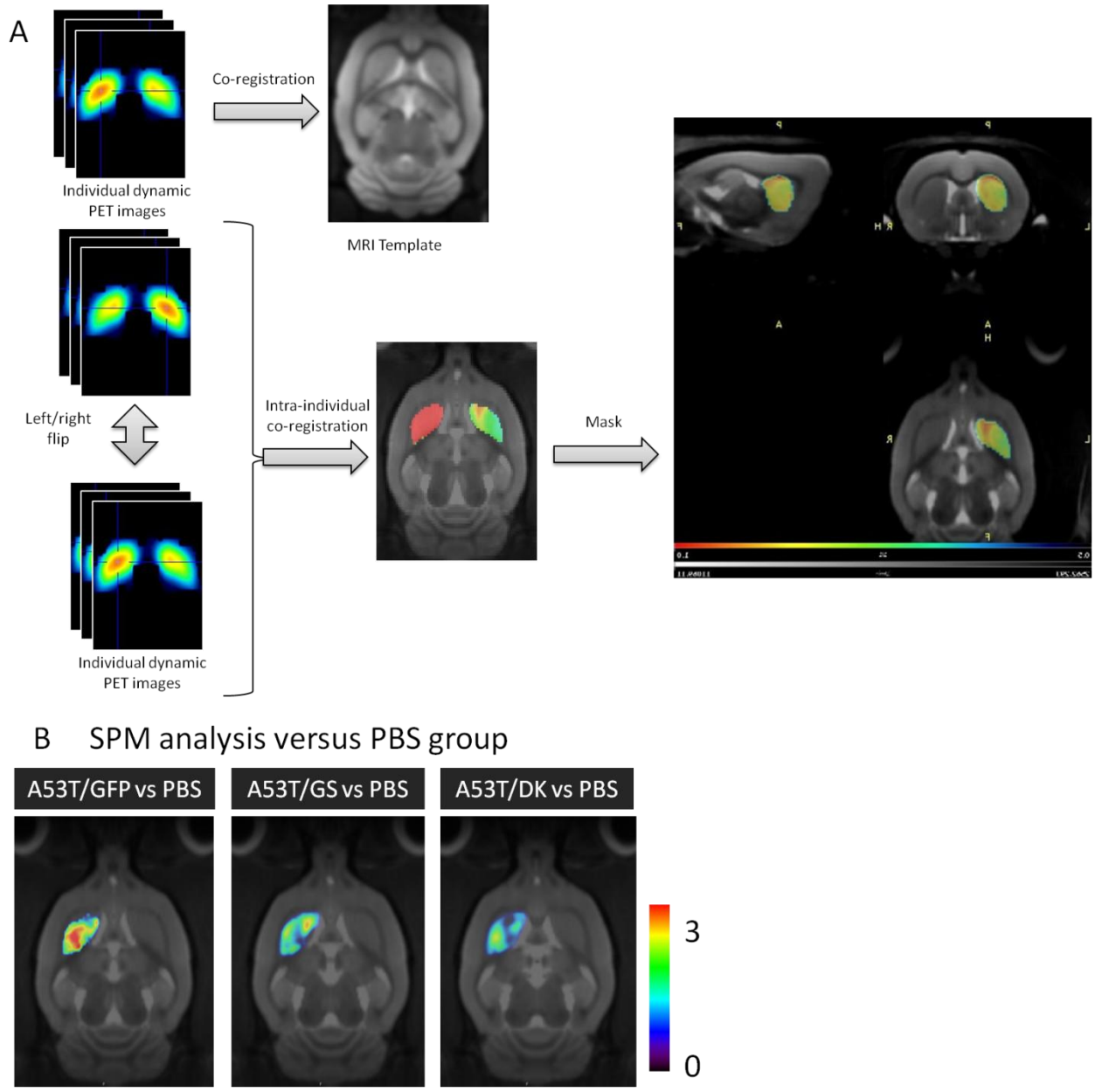


**Figure 49: Voxel-wise DAT-PET $BP_{nd}$-ratio changes. A) Creation of the voxel-wise DAT-PET $BP_{nd}$-ratio images per rat. B) T-maps created by SPM showing voxel-wise analysis of the DAT-PET $BP_{nd}$-ratio images versus the PBS group. Non-significant.**

# 6

# *RESULTS ON NEUROINFLAMMATION AND NEURODEGENERATION*

## 1. Background and aims

Besides dopaminergic cell loss in the substantia nigra, a second hallmark of Parkinson's Disease (PD) is the presence of neuro-inflammation, more specifically activated microglial cells (McGeer et al., 1988). Nevertheless, it remains a major question in PD whether neuro-inflammation is a consequence or a cause of dopaminergic cell loss (Tansey and Goldberg, 2010). In a healthy situation, glial cells support neuronal viability, while in an activated state they are responsible for pro- and anti-inflammatory responses (Kim *et al.*, 2000). Literature suggests that glial activation and peripheral pro-inflammatory mediators contribute to the pathogenesis of PD (Kempuraj *et al.*, 2016).

As outlined in the introduction, LPS can be considered as the model of choice to evaluate neuroinflammation induced neurodegeneration on the dopaminergic neurons. Susceptibility of dopaminergic neuronal loss is dependent on the injected dose, administration route and location, and the time-window during which the model is evaluated. This model is generally used to validate new PET radioligands for neuroinflammation (Ory *et al.*, 2015; Pottier *et al.*, 2017; Sridharan *et al.*, 2017; Berdyyeva *et al.*, 2019), or to evaluate neuroprotective or anti-inflammatory strategies.

**Here, we aimed to characterize the neuro-inflammatory response and its impact on the dopaminergic neurons in a moderate intrastriatal LPS model, before induction of dopaminergic neurodegeneration. To that end, we combined *in vivo* PET imaging and *post-mortem* analyses.**

## 2. Study design

Twelve adult male Sprague Dawley rats were injected unilaterally in the striatum with 10 µg lipopolysaccharides (LPS; Figure 50A), and were studied using *in vivo* PET imaging and *post-mortem* techniques. Animals underwent PET imaging at 5 or 7 days post injection (dpi), and were sacrificed immediately after completion of the PET scan (Figure 50B).

*In vivo* PET imaging was performed using a ligand for translocator protein (TSPO); [$^{18}$F]DPA714[N,N-diethyl-2-(2-(4-(2-[18F]fluoroethoxy)phenyl)-5,7-dimethylpyrazolo[1,5-a]pyrimidin-3-yl)acetamide] ([$^{18}$F]DPA714) during 60 minute long continuous scans (n=9).

Immunohistochemistry was performed using primary antibodies directed against ionized calcium-binding adapter molecule 1 (IBA1), glial fibrillary acidic protein (GFAP), vimentin, dopamine transporter (DAT), and tyrosine hydroxylase (TH). RT-qPCR was performed using primers for aromatic L-amino acid decarboxylase (AADC), DAT, GFAP, IBA1, TH, tumour necrosis factor alpha (TNFα), 18 kDa translocator protein (TSPO), vimentin, and vesicular monoamine transporter 2 (VMAT2).

More detailed information on the methodology can be found in Chapter 2.

Statistical analyses were performed using paired student t-tests to compare the ipsilateral and contralateral side in imaging studies, RT-qPCR, and immunohistochemical analyses. Inflammation markers are presented as %-change, while dopaminergic marker data are presented as asymmetry ratios:

$$Asymmetry\ ratio = \Delta\% = \frac{|\ ipsi - contra\ |}{(ipsi + contra) * 0.5}\ x\ 100$$

$$\%\ change = \frac{(ipsilateral - contralateral)}{contralateral}\ x\ 100$$

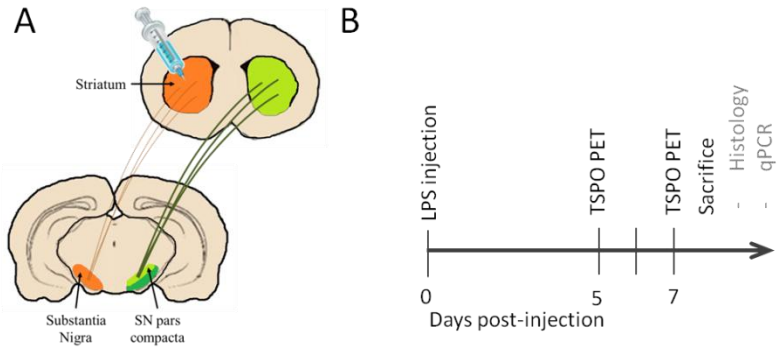


**Figure 50: Schematic overview of study design. A) LPS is injected in the striatum, and data are collected from both striata. B) Schematic overview of time schedule for the experiment. Rats were studied at 5-7dpi.**

# 3. Results

## 3.1 *In vivo* and *post-mortem* analyses of neuroinflammation

PET imaging using [$^{18}$F]DPA714, a ligand for 18kD translocator protein (TSPO; Figure 51A), demonstrated a significant increase of the binding potential (BPnd) (Figure 51B; +262±74%; n=9; p=0.0011) in the LPS-injected striatum as compared to the contralateral non-injected side at 5 (n=3) or 7dpi (n=6). These results were coherent with those obtained by RT-qPCR, showing increased TSPO mRNA expression in the ipsilateral striatum (Figure 52B; +236%; n=12/11; p<<0.001).

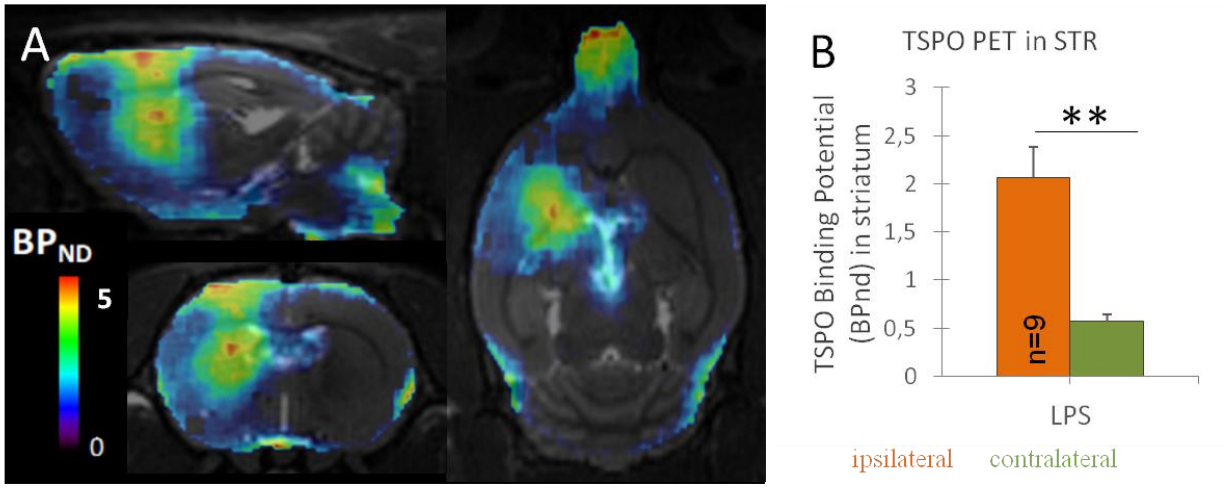


**Figure 51: *In vivo* analysis of TSPO as neuroinflammation marker in the striatum. A) Average quantified TSPO-PET images in non-displacable binding potential in different orientations. B) Quantification of TSPO-PET imaging in the striatum. The ipsilateral striatum (orange) and the contralateral striatum (green) at 7 days post-LPS injection. Results are expressed as means ± the standard error of the mean (SEM). Paired student t-test **p<0.01.**

*Post-mortem* analyses of other inflammatory markers revealed a drastic increase in the density of activated microglia in the injected striatum using anti-IBA1 immunohistochemistry (Figure 52C; +322±25%; n=12; p<<0.001). These results were underlined by RT-qPCR, showing increased IBA1 mRNA expression in the ipsilateral striatum (Figure 52D; +371%; n=12/11; p<<0.001). Additionally, we observed an increased density of activated reactive astrocytes in the LPS-injected striatum

(Vimentin: Figure 52E; n=12; p<0.001, GFAP: Figure 52G; +107±11%; n=12; p<<0.001). These findings were consistent with those obtained by RT-qPCR, showing increased expression of vimentin and GFAP mRNA in the ipsilateral striatum (Vimentin: Figure 52F; n=12/10; p<<0.001, GFAP: Figure 52H; +181%; n=12/10; p<<0.001). In parallel, mRNA expression of the pro-inflammatory cytokine TNFα was strongly increased in the ipsilateral striatum (Figure 52I; +277%; n=11/11; p<<0.001).

A more comprehensive study of neuro-inflammation in this same LPS model was performed by my colleague Dr Gubinelli in the context of his PhD dissertation (Gubinelli, 2019), which is added in the supplementary data (page 127).

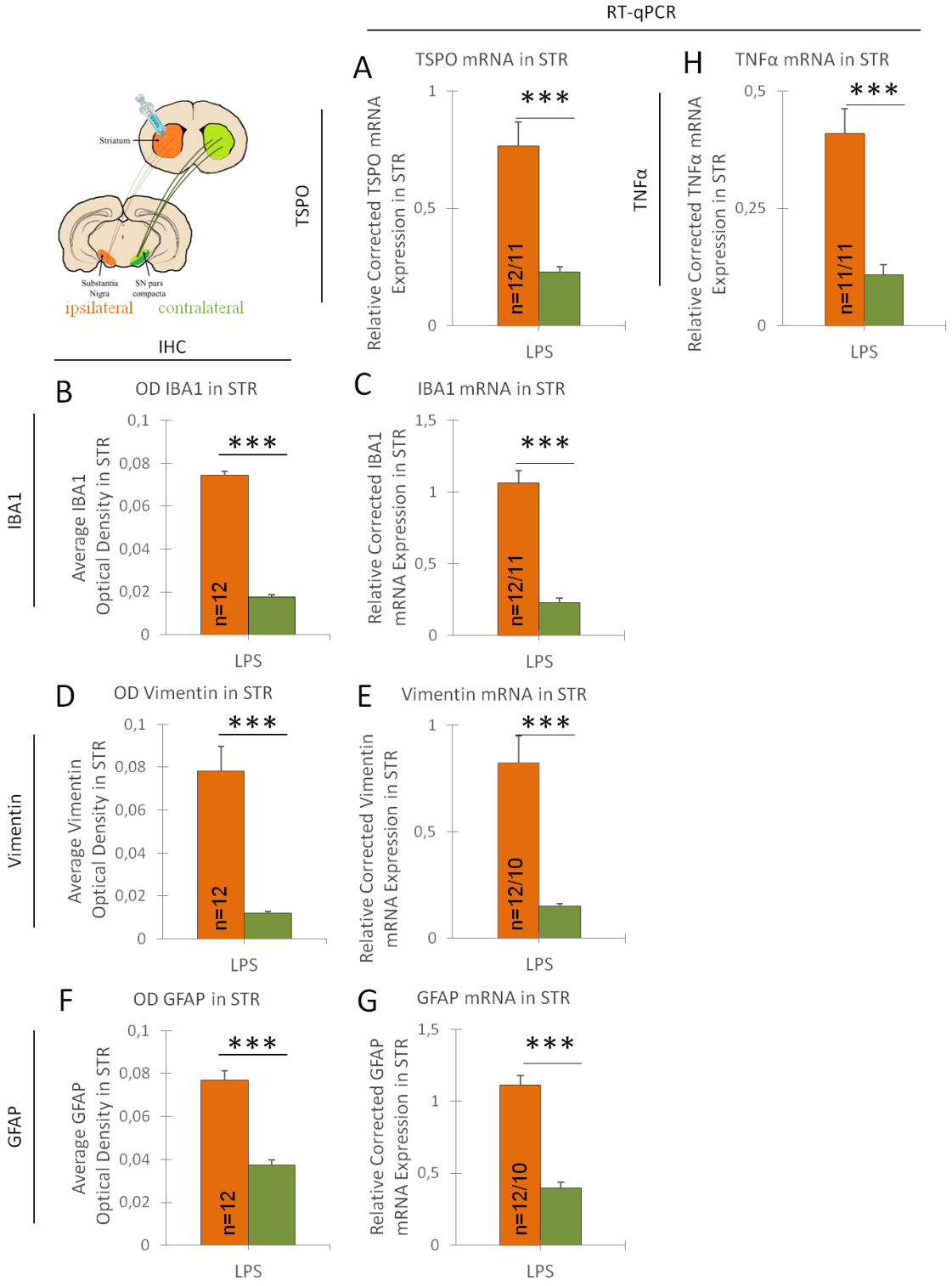


**Figure 52: *Post-mortem* analyses of neuroinflammation markers in the striatum. A) Relative TSPO mRNA expression levels in the striatum. B) Quantification of optical density of IBA1 staining in the striatum. C) Relative IBA1 mRNA expression levels in the striatum. D) Quantification of optical density of vimentin staining in the striatum. E) Relative vimentin mRNA expression levels in the striatum. F) Quantification of optical density of GFAP staining in the striatum. G) Relative GFAP mRNA expression levels in the striatum. H) Relative TNFα mRNA expression levels in the striatum. The ipsilateral striatum (orange) and the contralateral striatum (green) at 7 days post-LPS injection. Results are expressed as means ± the standard error of the mean (SEM). Paired student t-test ***p<0.001.**

## 3.2 *Post-mortem* analyses: dopaminergic system

Although we were unable to quantify TH fibre loss in the striatum due to technical difficulties using immunohistochemistry, we observed a small, but significant decrease of TH mRNA of Δ28% in the injected striatum using RT-qPCR (Figure 53A; n=10/11; p=0.045).

Nevertheless, preliminary results obtained by Dr. Gubinelli at 30dpi indicated that there was neither a loss of TH fibre loss in the striatum (Figure 53B; n=9; p=0.060), nor a reduction in the number of TH-positive neurons in the substantia nigra *pars compacta* as measured by unbiased stereology (Figure 53C; n=6/8; p=0.26; unpaired student t-test).

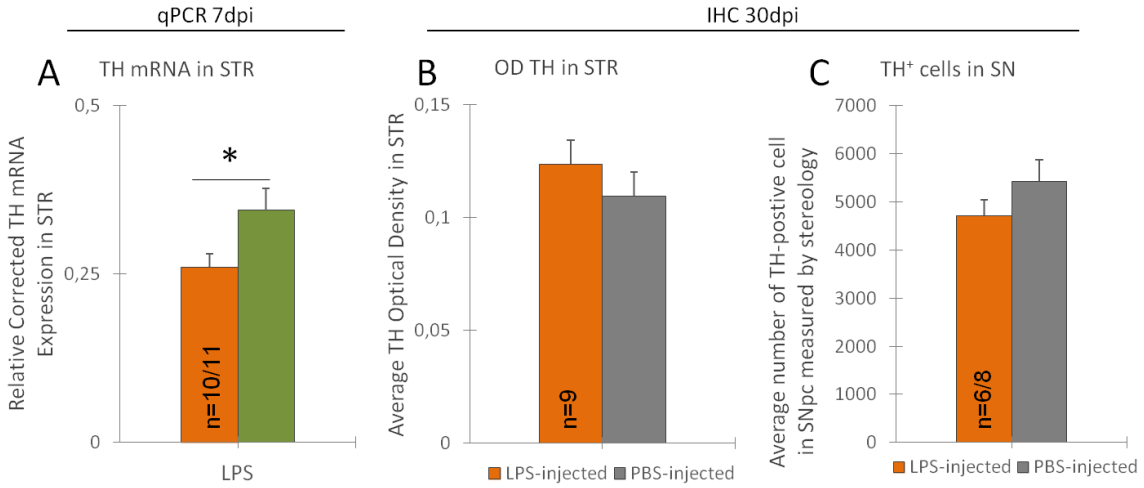


**Figure 53: *Post-mortem* analyses of dopaminergic neurodegeneration markers. A) Relative TH mRNA expression levels in LPS injected striata (orange) or the contralateral side (green) at 7dpi. B) Quantification of TH through optical density in the striatum following LPS (orange) or PBS injection (grey) at 30dpi. C) Quantification of TH-positive cells in the substantia nigra through unbiased stereology following LPS (orange) of PBS injection (grey) at 30dpi. Results are expressed as means ± the standard error of the mean (SEM). A) Paired student t-test *p<0.05, B,C) unpaired student t-test, non-significant.**

Immunohistological evaluation of the dopaminergic system did not reveal any significant asymmetry in the density of DAT protein in the LPS-injected striatum (Figure 54A; n=12; p=0.75). RT-qPCR analysis of DAT mRNA expression in the striatum confirmed these results (Figure 54B; n=3/3; p=0.50). It must be noted that the experimental number for the DAT RT-qPCR analysis was slightly lower due to some technical difficulties. Neither did we observe a significant asymmetry in AADC mRNA expression (Figure 54C; n=9/9; p=0.29), nor for VMAT2 mRNA expression in the striatum at 7dpi (Figure 54D; n=11/11; p=0.14).

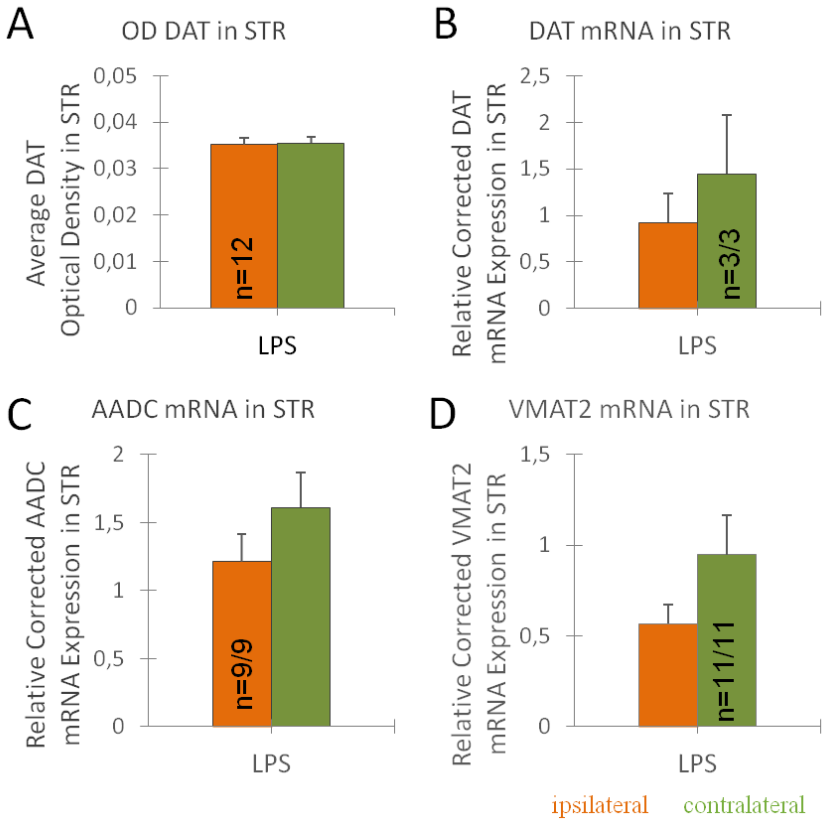


**Figure 54:** ***Post-mortem*** **analyses of dopaminergic markers in the striatum. A) Quantification of DAT through optical density in LPS injected striata (orange) or the contralateral side (green) at 7dpi. Relative B) DAT, C) AADC, and D) VMAT2 mRNA expression levels in the striatum following LPS injection at 7dpi. Results are expressed as means ± the standard error of the mean (SEM). Unpaired student t-test, non-significant.**

## 3.3 Correlation between *in vivo* and *post-mortem* data

Spearman correlation analysis of between *post-mortem* measures and *in vivo* individual TSPO-$BP_{nd}$ data showed postive associations between all different inflammation related markers (Figure 55A). Interestingly, expression of TNFα was highly correlated with expression of GFAP (r=0.96, Figure 55A,B), IBA1 (r=0.80, Figure 55A,B), and TSPO (r=0.81, Figure 55A,C). Consitent with these observations, TSPO-$BP_{nd}$ showed positive associations with the expression of inflammatory markers ($r_{BP\text{-}TSPO}$= 0.9, $r_{BP\text{-}TNF\alpha}$= 0.85, $r_{BP\text{-}GFAP}$= 0.84, $r_{BP\text{-}Iba1}$= 0.85, Figure 55A,C).

Amongst the dopaminergic expression markers only AADC and TH showed a positive association (Figure 55A,E). Additionally, expression of VMAT2, AADC, and TH showed comparable negative associations with the expression of inflammation-related markers, including $BP_{nd}$ (Figure 55A,D).

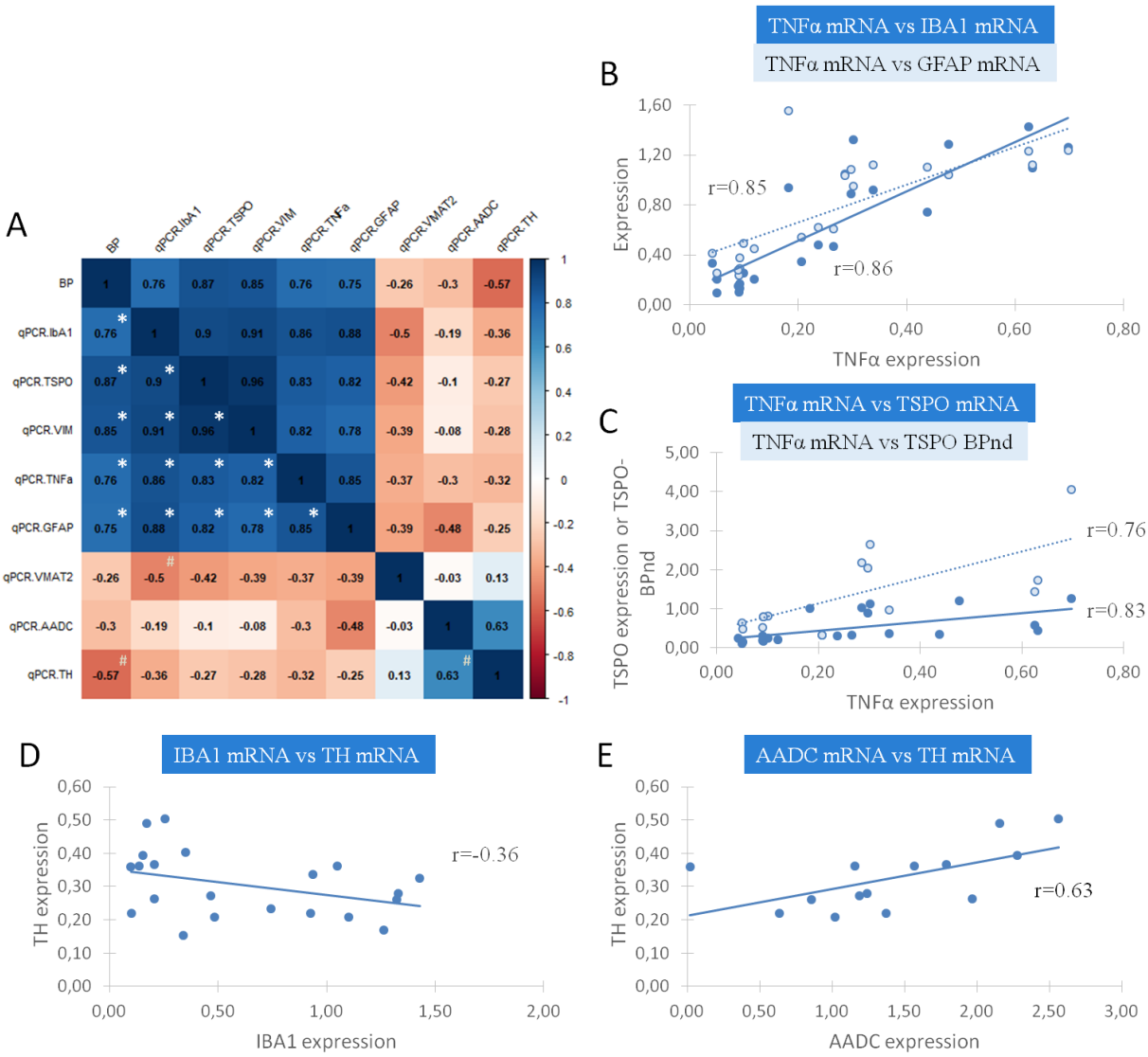


**Figure 55: Spearman correlation between *in vivo* individual PET $BP_{nd}$ data and *post-mortem* expression data. A) Spearman correlation coefficients are marked in the corresponding case; blue signifies a positive correlation, while red signifies a negative correlation. * p<0.01, # p<0.05. B) Correlation graph between expression of GFAP (light blue/red) and IBA1 (dark blue), and TNFα. C) Correlation graph between TSPO-$BP_{nd}$ (light blue/red) and TSPO expression (dark blue), and TNFα. D) Correlation graph between TH and IBA1. E) Correlation graph between TH and AADC.**

# 4. Discussion

### Inflammation in a striatal LPS model

We observed significantly increased TSPO binding *in vivo,* using [$^{18}$F]DPA714 PET imaging in the LPS-injected striatum at 5-7dpi. A likely interpretation of LPS-induced TSPO changes is an increase in the number of TSPO-expressing microglia as suggested in the peripheral induced LPS mouse model (Furube *et al.*, 2018). In line with this, it was shown in the LPS model using fluorescence-activated cell sorting on radioligand-treated tissue that not the radioactivity per microglial cell was increased, but the number of microglia per gram of tissue increased (Tournier *et al.*, 2019). However, we cannot attribute the observed [$^{18}$F]DPA714 PET signal to microglia alone, since Lavisse and colleagues (2012) have shown that also reactive astrocytes overexpress TSPO and have a role in the [$^{18}$F]DPA714 PET

signal. Additionaly, our *post-mortem* data showed that LPS-induced neuroinflammation does not only lead to an increased density of activated microglia, but to increased densities of reactive astrocytes as well, which is in line with previous reports, showing that LPS-induced proinflammatory microglia can activate astrocytes (Liddelow *et al.*, 2017). Ory and co-workers (2015) and Herera and colleagues (2000) reported on the presence of GFAP positive cells with low TSPO immunoreactivity in the periphery of the LPS-induced neuroinflammatory lesion (Herrera *et al.*, 2000; Ory *et al.*, 2015). Here we show, using a mild model of neuroinflammation, that astrocytes are present within the LPS-induced neuroinflammatory lesion, even though to a lesser extend than the presence of microglia. In addition, we showed a strong association between the expression of TSPO- and astrocytic markers.

These reactive astrocytes and microglia produce neurotoxic molecules which, in turn, can damage the blood-brain barrier (BBB) integrity (reviewed by Sofroniew, 2015). Indeed, Ory and colleagues (2015), who studied a high-dose (50µg) LPS-induced inflammation model, demonstrated a loss of BBB integretry at the LPS-injected hemisphere at 7 days post-injection using dynamic contrast enhanced MRI. Even though we have not performed *in vivo* or *ex vivo* analyses of BBB integrity, Ory and colleagues (2015) have shown that despite BBB disruption in their model, it does not affect tracer uptake during PET imaging. They have demonstrated that TSPO binding and BBB breakdown followed different patterns, whilst *in vivo* PET data and *post-mortem* autoradiography data were positively correlated (Ory et al., 2015).

It is known that activated microglia can have both beneficial and deleterious effects on neuronal survival (Liu and Bing, 2011; Kalia and Lang, 2015). The latter is attributed to the production of a variety of neurotoxic factors including interleukin-1 (IL-1), IL-6, tumour necrosis factor alpha (TNFα), nitric oxide, prostaglandin E2, and superoxide (Kim and Joh, 2006). These factors might cause neuronal damage, which, in turn, induces microglial activation, leading to a positive reinforcement loop (Streit, Walter and Pennell, 1999; Liu and Bing, 2011).

We observed a strong increase of TNFα mRNA expression in the ipsilateral striatum. This proinflammatory cytokine is expressed by reactive microglia, which in turn activate astrocytes, but also by infiltrating macrophages. CD68 protein is highly expressed by circulating macrophages and tissue macrophages (e.g. microglia) (Holness and Simmons, 1993). Ory and colleagues (2015) observed CD68-positive cells in the ipsilateral striatum (Ory *et al.*, 2015), while Herrera and colleagues (2000) observed many integrin alpha M (ITGAM)-positive cells with macrophage morphology in the core of the lesion (Herrera *et al.*, 2000). This corresponds to the results presented here on TNFα mRNA, in combination with increased mRNA levels for TNFα and ITGAM shown by Mr. Gubinelli (2019), this confirms that, at least part of, the macrophages contribute to the observed PET signal.

### Dopaminergic markers

TH mRNA can normally be found in the striatum, in the axons of dopamine synthesising neurons (Melia *et al.*, 1994; Aschrafi *et al.*, 2017). Our transcriptomic data revealed a small decrease of TH expression in the synaptic terminals of the striatum after striatal LPS injection, while preliminary data obtained at 30 days post-injection did not show any dopaminergic neurodegeneration, consistent with other studies using 10 µg striatal LPS-injection (Hoban *et al.*, 2013). Additionally, we observed negative associations with the inflammatory expression markers. These data are suggestive of neuroinflammation-induced suffering of the dopaminergic afferents.

We did not observe a reduction in striatal DAT protein levels, nor for striatal DAT, AADC, or VMAT mRNA levels. Nevertheless, we observed negative associations between the expression of TH, AADC, and VMAT2 and the inflammatory markers (e.g. IBA1, GFAP, and TNFα).

Previously, it has been shown that intranigral LPS injection induces reduced DAT mRNA expression in the substantia nigra (De Pablos *et al.*, 2005), while again others suggest increased DAT activity in the nucleus accumbens and medial prefrontal cortex after peripheral LPS injection (van Heesch *et al.*, 2014).

Interestingly, Herrera and colleagues (2000) found increased levels of dopamine and DOPAC in the LPS-injected striatum (Herrera *et al.*, 2000), while many others found increased levels of dopamine and/or DOPAC in several other brain regions after peripheral LPS administration (Dunn, 1992; Lavicky and Dunn, 1995; Borowski *et al.*, 1998; MohanKumar, MohanKumar and Quadri, 1999; van Heesch *et al.*, 2014). This could be explained by increased dopamine turnover, which can be be evaluated by measuring the dopamine concentration over DOPAC and HVA concentrations. An increased dopamine turnover could indicate increased TH activity and/or levels. Indeed, Nolan and colleagues (2000) demonstrated increased activity of TH after systemic LPS injection (Nolan *et al.*, 2000). However, this is in discrepancy with our results and of others (De Pablos *et al.*, 2005), since we observed a small decrease of TH mRNA expression. Nevertheless, TH activity can be regulated independently by mRNA phosphorylation.

Others have reported on the associations between inflammation markers and markers for the dopaminergic system. A PET study in asymptomatic MPTP non-human primates demonstrated a decrease in VMAT $BP_{nd}$ which was associated with an increase in TSPO levels as shown with [$^{11}$C]PK11195. It was suggested that decreased VMAT2 is an early pathogenic event which might precede nigrostriatal degeneration (Chen *et al.*, 2008). Furthermore, Glaab and colleagues (2019) observed both metabolic changes associated with inflammation and voxel-wise changes using [$^{18}$F]FDOPA-PET in PD patients (Glaab *et al.*, 2019).

## Conclusion

In conclusion, we have used [$^{18}$F]DPA714 PET imaging to show increased TSPO binding in a LPS-induced neuroinflammatory rat model. We have shown that unilateral striatal injection of 10µg LPS does not lead to dopaminergic neuron loss in the substantia nigra nor fibre loss in the striatum. Even though, we have shown no changes in the dopaminergic markers, we demonstrated an inverse correlation between AADC, TH, and VMAT2 and IBA1 gene expression. In addition, these dopaminergic markers were inversely associated wiht TSPO-$BP_{nd}$ and microglial density. These data strongly support the hypothesis that neuroinflammatory events underlie suffering of dopaminergic neurons.

## 5. Supplementary data by Dr. Gubinelli

**Similar to what is shown here, Dr. Gubinelli (2019) showed in his doctoral thesis a significant increase of IBA1 cells 7 days increase of IBA1 cells 7 days post-LPS injection as compared to PBS-injected or non-injected animals, and measured by %- and measured by %-occupied area of the total striatum after immunohistochemical staining (**

Figure 56). Additionally, Dr. Gubinelli (2019) showed a significant increase of GFAP (Figure 57) and vimentin positive cells after LPS injection (Figure 58).

Moreover, several inflammation markers were assessed using RT-qPCR, all of which displayed a significant increase in the LPS-injected animals (Figure 59); C1qa and C1 are components of the complement system, CCL2 is recruites cells on the insult-site, IBA1 is a marker for microglial activation, IL1b is a mediator of inflammatory response, ITGAM is a marker for activated macrophages and phagocytosis, and TNFα is a proinflammatory cytokine. Conversely, NeuN, specific neuronal marker expressed in all striatal neurons, showed a significant decrease.

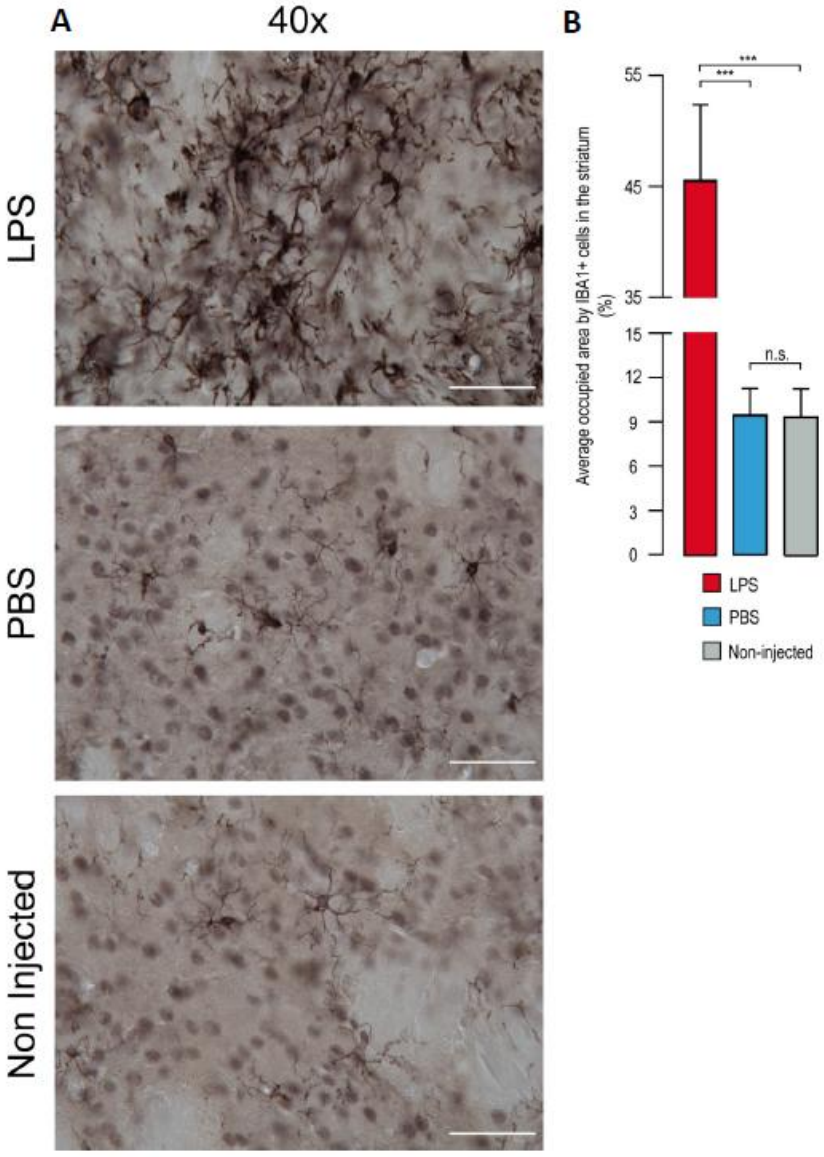

**Figure 56: Histological evaluation of IBA1 in LPS-injected, PBS-injected, or non-injected animals at 7dpi. A) Representative photomicrographs showing striatal IBA1 staining in the striatum of the animals of the three experimental groups. B) Striatal area occupied by IBA1+ cells were evaluated in relation to the striatal area and expressed as percentage. One-way ANOVA was used for between-group comparison and Bonferroni post hoc correction for multiple comparisons was applied. n=6/group. Scale bar: 50 µm. ***p<0.001. Figure by Dr. Gubinelli (2019).**

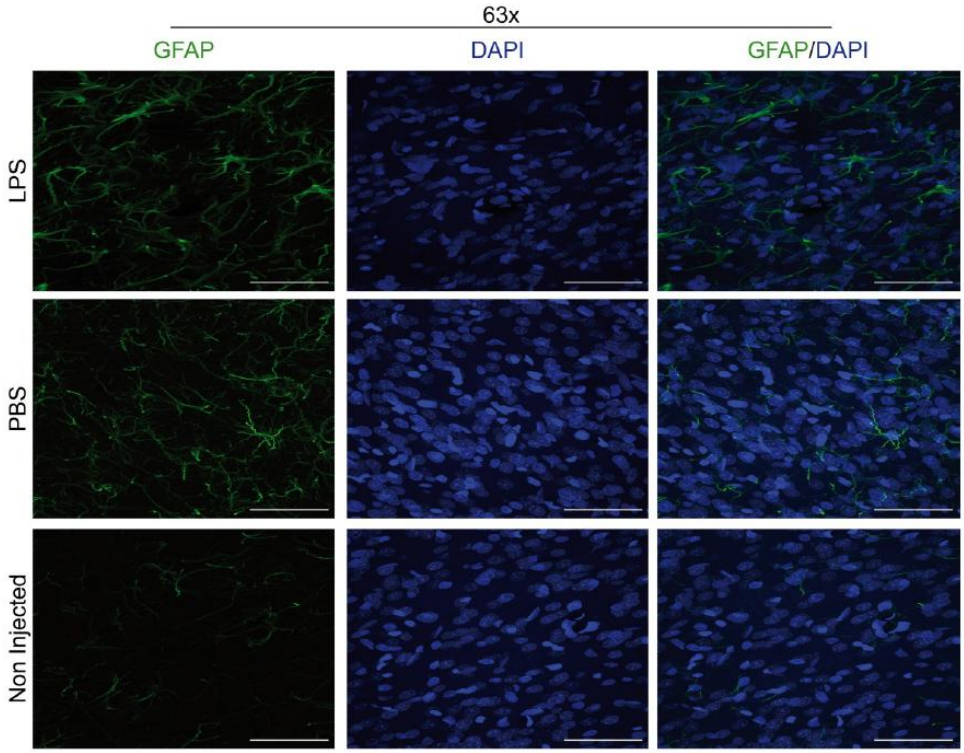


**Figure 57: Representative striatal GFAP expression in LPS, PBS, or non-injected rats at 7dpi. Confocal Z-stack pictures were taken in different points of the striatum close to the injection point. Scale bar: 50 µm. Figure by Dr. Gubinelli (2019).**

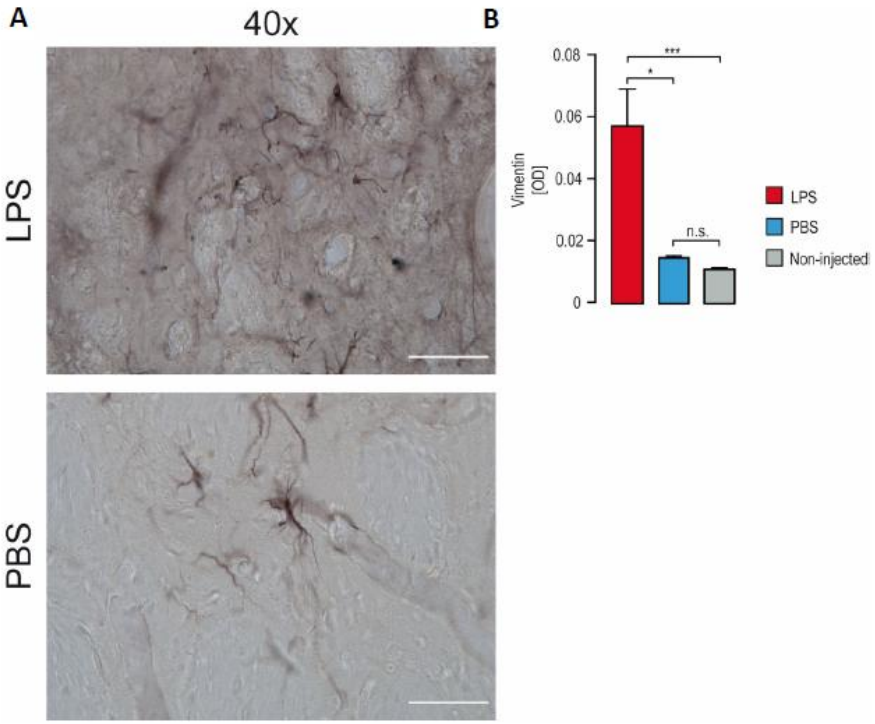

**Figure 58: Vimentin histological evaluation after striatal injection of LPS, PBS or non-injection at 7dpi. A) Representative striatal vimentin staining for LPS and PBS-injected groups. B) Striatal optical density for the evaluated groups. Kruskal-Wallis test was used for between-group comparison and Dunn's test of multiple comparisons was applied. n=6/group. Scale bar: 50 µm. *p<0.05, ***p<0.001. Figure by Dr. Gubinelli (2019).**

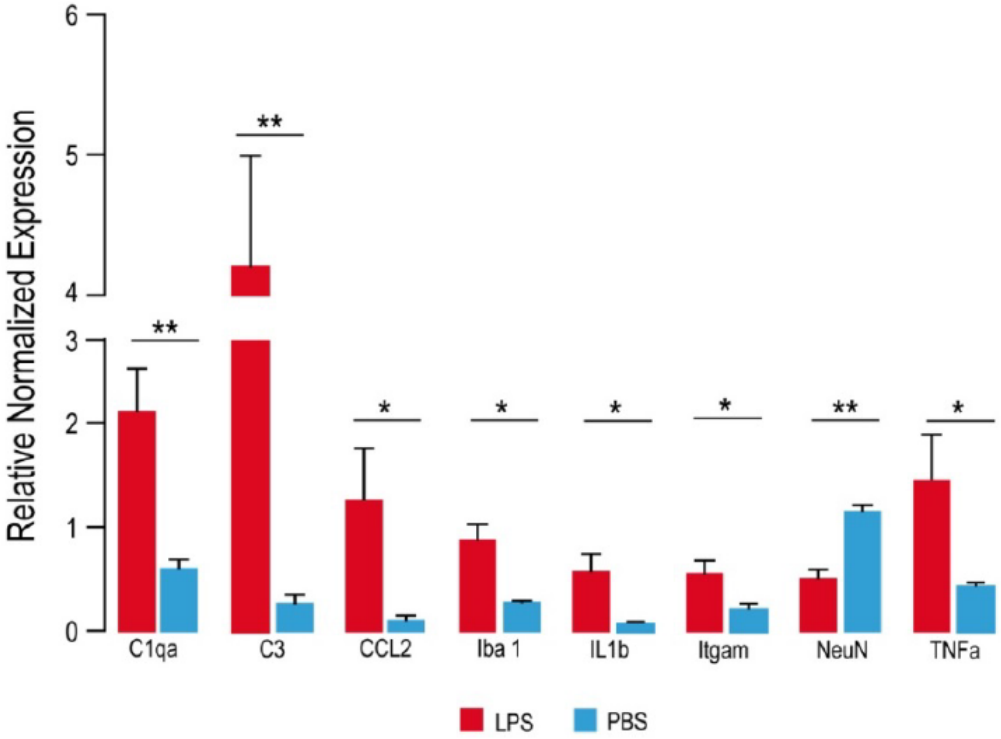


**Figure 59: Striatal mRNA expression of different genes related to the inflammatory response. Mann-Whitney U test was used for between-group comparison. n=6/group. *p<0.05, **p<0.01. Figure by Dr. Gubinelli (2019).**

# 7

# *General Discussion*

***EVALUATION OF THE DOPAMINERGIC SYSTEM USING IN VIVO PET IMAGING AND POST-MORTEM ANALYSES IN THE CONTEXT OF MILD NEURODEGENERATIVE AND NEUROINFLAMMATORY PD MODELS***

In this PhD thesis I aimed to evaluate the effects of α-synuclein overexpression and neuroinflammation on dopaminergic neuron loss and the dopaminergic system. To achieve this I have used both *in vivo* techniques, i.e. behavioural assessment and PET imaging, complimented with *post-mortem* techniques, i.e. immunohistochemistry and RT-qPCR, obtained from the same animals. By combinging these tools in the same animals, we also searched for a better comprehension of the underlying mechanisms of the *in vivo* biomarkers.

## 1. Interplay inflammation, α-synuclein, LRRK2, and neuronal loss

Using viral vector strategies, we have first overexpressed different forms of α-synuclein in the substantia nigra of rats, and later expressed α-synuclein in combination with different mutant forms of LRRK2. We have shown that overexpression of human WT-α-synclein in the substantia nigra through viral vectors (AAV2/6-PGK-WT-α-synuclein) does not generate detectable neuronal loss in the substantia nigra, nor does it generate *in vivo* motor deficits or changes in the dopaminergic system as seen by *in vivo* PET imaging. In contrast, overexpression of A53T-α-synuclein in the substantia nigra, using AAV2/6-PGK-A53T-α-synuclein viral vector approach, resulted in significant α-synuclein aggregation in the substantia nigra as soon as 8wpi, but not in the striatum. In our model, α-synuclein aggregation induced a mild but progressive degeneration of dopaminergic neurons in the substantia nigra but limited fibre loss in the striatum. This coincided with initially moderate, followed by a more pronounced, microglial response. These data suggest that, in this model, neuronal loss is induced by A53T-α-synuclein overexpression and that neuroinflammation might occur secondary to neuronal loss. Additionally, overexpression of AAV2/6-PGK-A53T-α-synuclein in combination with AAV2/6-PGK-G2019S-LRRK2 generated an added toxicity as demonstrated by unbiased stereology. LRRK2 interacts with α-synuclein via many direct and indirect pathways, which have recently been reviewed by Cresto and colleagues (2018). Our data show the potential of LRRK2 as a therapeutic target, but also underline the complexity of the use of *in vivo* biomarkers to accurately measure LRRK2-induced toxicity.

There are multiple putative mechanisms by which α-synuclein causes toxicity in the neurons, which ultimately leads to neurodegeneration. Amongst those, literature reports on genomic damage, mitochondrial dysfunction, lipid membrane interactions and disruption, lipid synthesis and metabolism, impaired vesicular trafficking, proteostasis disturbances, and nuclear dysfunction (Zhang *et al.*, 2018; Bernal-Conde *et al.*, 2020; Fanning, Selkoe and Dettmer, 2020; Han *et al.*, 2020; Vasquez *et al.*, 2020). Interestingly, α-synuclein can also cause neuroinflammatory events by activating microglia and inducing migration (Bliederhaeuser *et al.*, 2016; Zhang *et al.*, 2018).

Moreover, it has been demonstrated that aggravated neuroinflammatory responses eventually lead to specific loss of the dopaminergic neurons, and therefore may have potential as therapeutic targets (Wang, Liu and Zhou, 2015). To that end, LPS is the tool of choice to generate systemic and/or neuroinflammation and evaluate its impact on the survival of the dopaminergic neurons. Here we performed a single-site, unilateral injection of a low dose of LPS (10µg) in the striatum, to evaluate the impact of neuroinflammation on the expression of defined dopaminergic markers. We induced an acute neuroinflammatory reaction in the striatum, reaching maximum

intensity at 7dpi without any dopaminergic neuronal loss in the substantia nigra or synaptic loss in the striatum at 7dpi nor at 30dpi. Nevertheless, we observed a significant inverse correlation between inflammation markers and markers for dopamine production (TH, AADC) and storage (VMAT2) in this inflammatory-based model. These data support the hypothesis that neuroinflammation alters dopaminergic markers and eventually can induce dopaminergic neuron loss. Epidemiological studies that have associated the frequent use of non-steroidal anti-inflammatory drugs (e.g. aspirin, ibuprofen) with a lower risk for PD (Chen et al., 2003, 2005; Noyce et al., 2012), are in support of these results, supporting the hypothesis that neuroinflammation is a potential target in PD therapeutical strategies.

## 2. PET imaging to measure PD progression

In all the above-mentioned models PET imaging was applied. We imaged the most commonly used presynaptic dopaminergic targets, measuring AADC enzymatic activity and DAT binding. Ont he other hand, we imaged neuroinflammation using the gold standard neuroinflammation marker, 18kD TSPO. DAT-PET imaging, using [$^{18}$F]LBT999, and AADC-PET, using [$^{18}$F]FMT, was performed in viral vector models transducing AAV2/6-PGK-WT-α-synuclein or AAV2/6-PGK-A53T-α-synuclein. DAT-PET imaging, but not AADC-PET imaging, was able to measure mild neuronal loss in the A53T-α-synuclein model as soon as 8 weeks post-injection (wpi). We observed a larger asymmetry at 12wpi, which corresponded to an increased dopaminergic neuronal loss. Here, we showed that DAT-PET was more sensitive than robust behavioural testing. Surprisingly, DAT-PET imaging on models overexpressing A53T-α-synuclein in combination with G2019S- or dead kinase-ΔLRRK2 overexpression, showed asymmetrical DAT-PET binding per group, however, we were unable do demonstrate between-group differences. Statistical parametric mapping analyses on DAT $BP_{nd}$-ratios underlined regional heterogeneity of DAT $BP_{nd}$-ratios within the striatum. In addition, we showed that DAT $BP_{nd}$-ratios followed the same tendency as behavioural measurements. Surprisingly, in this study, *in vivo* data followed the opposite pattern of *post-mortem* data.

The combination of *in vivo* and *post-mortem* data in our studies suggests that DAT-PET does not merely reflect neuronal loss, but might be influenced by α-synuclein accumulation (Kobayashi *et al.*, 2019) and regulatory gene expression mechanisms (Shumay, Fowler and Volkow, 2010). Compensatory mechanisms are being reported in the literature to occur at molecular and synaptic levels, both pre- and postsynaptically of the dopaminergic neuron to counterbalance the loss of the dopaminergic neuron (Adams *et al.*, 2005; Blesa *et al.*, 2017; Fu *et al.*, 2019).

Postsynaptic compensation mechanisms are mainly reported at the level of the dopamine receptor; demonstrating increased binding to post-synaptic $D_2/D_3R$ as observed in asymptomatic 6-OHDA-lesioned rats in both the ipsilateral and contralateral hemisphere (Nikolaus *et al.*, 2003; Sahin *et al.*, 2014). Bezard and colleagues (2001) showed biphasic compensation mechanisms of $D_2R$-like biding using autoradiography in MPTP-treated non-human primates; an initial decrease in the presymptomatic period was followed by an upregulation of postsynaptic receptors commencing when striatal dopaminergic homeostasis is broken (Bezard *et al.*, 2001). PET imaging studies visualising $D_2/D_3R$ can benefit from these post-synaptic compensation mechanisms to measure the functional outcome of endogenous dopamine replenishment after gene therapy (Palfi *et al.*, 2014) or cell replacement therapies (Sahin *et al.*, 2014).

Presynaptic compensation mechanisms have been reported at the level of dopamine synthesis, but also at the level of DAT expression and availability. These compensatory mechanisms occur to counterbalance the dopaminergic loss (Blesa *et al.*, 2017; Herfert *et al.*, 2019).

Even though we were not able to demonstrate significantly increased expression of TH in the contralateral substantia nigra, the left-right asymmetry measured in the A53T-α-synuclein model at 12wpi might possibly be due to an upregulation in the contralateral side rather than an increased neuronal loss ipsilateral to AAV-induced A53T-α-synuclein overexpression.

Comparison of *in vivo* and *post-mortem* data at 8wpi revealed that the asymmetry observed with both behaviour (Δ76±23%) and DAT-PET (Δ33±7%) was larger than observed with *post-mortem* stereological counting (Δ17±5%). At this timepoint, no change was observed in DAT gene-, or protein expression. At the late timepoint (13wpi), the behavioural deficit remained stable (Δ79±22%) but the asymmetry observed in DAT-PET was more pronounced (Δ54±8%). Again, both *in vivo* measures revealed higher differences than *post-mortem* DAT gene- and protein expression data, which were both around similar levels (Δ30%). Interestingly, DAT *post-mortem* data were coherent with stereological counting in the SN (Δ33±10%) and TH optical density data in the striatum (Δ40±12%).

This phenomenon of exacerbated DAT decrease was also observed MPTP-treated non-human primates (Bezard *et al.*, 2001). Reduced DAT availability has been demonstrated to reduce pre-synaptic dopamine uptake, in order to increase dopamine availability in the synapse (Vezoli *et al.*, 2014; Blesa *et al.*, 2017). Recently, a DAT-SPECT study on 105 *de novo* PD patient demonstrated that lower dopamine transporter binding in early-onset PD predicts the later development of motor complications. In this study, DAT-binding was not related to severity of motor symptoms, suggesting age-related differences in striatal compensatory mechanisms in PD (Palermo *et al.*, 2020). Nevertheless, other studies report on adverse compensation effects. Del-Bel and colleagues (2014) observed a decrease of dopamine concentration in the ipsilateral striatum after a 6-OHDA lesioning in rats, accompanied by an increase of dopamine concentration in the contralateral striatum (Del-Bel et al., 2014). Similarly, Vezoli and colleagues (2014) show an unexpected increase of DAT-$BP_{nd}$ in the striatum using [$^{11}$C]PE2I before the onset of motor symptoms in MPTP treated non-human primates (Vezoli *et al.*, 2014). In our co-overexpression model of A53T-α-synuclein and DK- or G2019S-ΔLRRK2, DAT $BP_{nd}$-ratios also demonstrated an opposite tendency as observed by *post-mortem* data. Previously, Adams and colleagues (2005) demonstrated in a multitracer (AADC and DAT) PET study that the *in vivo* phenotype of LRRK2-patients is indistinguishable from that of sporadic PD patients, despite the pathological heterogeneity of the condition (Adams *et al.*, 2005).

Alltogether these data suggest that compensatory mechanisms of DAT availability occur very early in the pathology, and probably at the level of the synapse before the appearance of compensatory mechanism regulated by gene expression. It has been suggested that these compensatory changes, including downregulation of the DAT and upregulation of AADC activity, might delay the onset of parkinsonian symptoms (Adams *et al.*, 2005), and probably have a major impact on therepeutical approaches for PD (Navntoft and Dreyer, 2016).

In contrast to DAT, VMAT2 density is highly related to terminal degeneration and VMAT2-PET imaging might be less prone to presynaptic compensation events (Decressac, Mattsson and Björklund, 2012) In our studies, *post-mortem* data on VMAT2 protein-density did not demonstrate any left-right difference at either 8 or 13wpi. Similar to DAT gene-expression, VMAT2 gene-expression showed a significant left/right difference (Δ42%) at the late timepoint. Unfortunately, we did not have acces to VMAT2-PET radioligands. However, [$^{18}$F]DTBZ binding potential has been shown

to decrease in striatal regions of PD patients (Okamura et al., 2010; Lin et al., 2014), which was correlated with disease severity (Hsiao et al., 2014).

All together, this underlies the use of multitracer PET studies (e.g. Fu *et al.*, 2019) to contribute in imaging the patterns of different mechanisms underlying disease initiation or progression.

## 3. Future studies

In future studies I would recommend to investigate the nature of the small inflammatory response that was observed in the A53T-α-synuclein overexpression model, as was done for the LPS model. Vice versa, I would recommend to study the dopaminergic system more in depth in the LPS-induced inflammation model, especially using *in vivo* DAT versus VMAT-PET imaging. Additionally, I think studying the development of the LPS model, using a longitudinal design, would be beneficial, and could possibly provide answers about the cause and consequence of neuroinflammation and neurodegeneration.

In the context of the BrainMatTrain program I have focussed on the characterisation of rodent PD models and the understanding of *in vivo* biomarkers, with the overall aim to use these models for therapeutical assessement of multi-modal hydrogels containing cell grafts. The models described here all have their own strengths and weaknesses with regards to the evaluation of multi-model hydrogels.

The intanigral 6-OHDA model that was used here for methodological improvements generates near complete loss of the dopaminergic neurons in the substantian nigra and the synaptic terminals. This makes the 6-ODHA model very suitable to study graft survival, striatal re-innervation, and functional efficacy (Moriarty, Pandit and Dowd, 2017; Moriarty *et al.*, 2019). However, even though it is the gold-standard model for PD, it does not generate its extensive neuronal loss in a pathologically relevant way. Here, we have implementen several models based on hallmarks of PD; neuroinflammation and PD-related gene overexpression. As discussed above, the LPS-based neuroinflammation model allows the study of effects of neuroinflammation on dopaminergic cell and fibre loss. This model would be well suited to study the anti-inflammatory effects of a multi-modal hydrogel.

Lastly, we have used overexpression of PD-related genes through viral vectors. AAV2/6-PGK-WT-α-synuclein did not generate neuronal loss in our hands, making it less ideal to study multi-model hydrogels. AAV2/6-PGK-A53T-α-synuclein transduction, on the other hand, did generate significant progressive dopaminergic neuronal loss, changes in the dopaminergic system as seen by *in vivo* PET imaging, and a slight neuroinflammation. These qualities give the A53T-α-synuclein great potential to evaluate the efficacy neuroprotective and disease altering therapeutic strategies. The AAV2/6-PGK-A53T-α-synuclein model can also be used to study neurotoxic or neuroprotectice interactive effects, as we have aimed to for A53T-α-synuclein and G2019S-LRRK2 (Cresto *et al.*, 2020). Moreover, the relatively slow disease progression also means that it is possible to study the model in a prodromal-like phase, where less than 30% of the dopaminergic neurons have died. This could be especially useful in the study of early biomarkers for PD.

# Appendix 1

## *Animal Models of PD*

Even though, as described above, some important discoveries have been done on human samples, PD autopsy material is rare and precious. Animal models allow for study of different aspects of the disease, and explore both disease progression and evaluate possible treatment strategies. At the moment, there is still no perfect model available that mimics all pathological aspects of PD. The current available models can be broadly divided in four types; 1) pharmacological models, 2) toxin-based models, 3) PD hallmark-based models, and 4) genetic-based models.

## 1.1 Non-mammalian models of PD

Several non-mammalian model species have respective homologues for familial PD genes like LRRK2, Parkin, PINK1, and DJ-1 (Figure 60) (Pienaar, Götz and Feany, 2010; Jagmag *et al.*, 2016). These models could be considered for rapid testing of possible treatment targets and relative effects of genetic and environmental factors on PD pathology (Pienaar, Götz and Feany, 2010; Duty and Jenner, 2011; Konnova and Swanberg, 2018). Even though they are limited in the way they represent PD symptoms (Duty and Jenner, 2011), non-mammalian models have time and economic advantages over traditional rodent or non-human primate models (Pienaar, Götz and Feany, 2010; Konnova and Swanberg, 2018). The non-mammalian models are not thought to replace mammalian models, but precede or work alongside each other (Pienaar, Götz and Feany, 2010).

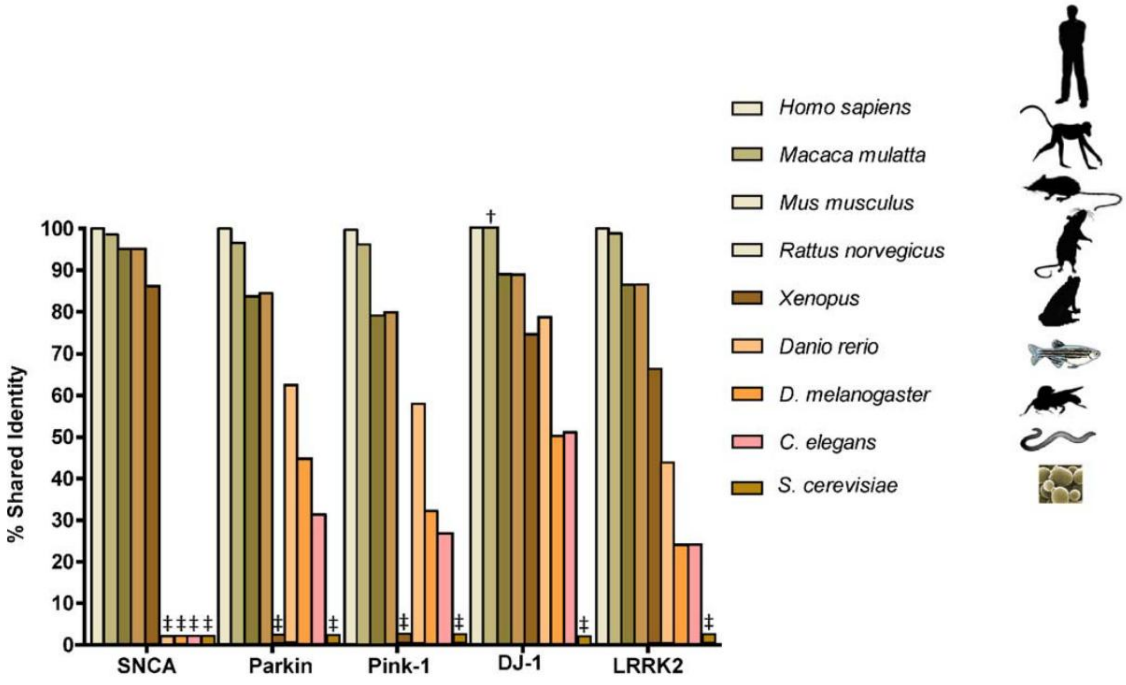


**Figure 60: Homologues for familial PD genes in model species. Figure from (Pienaar, Götz and Feany, 2010)**

### 1.1.1 Nematodes (Caenorhabditis elegans )

Nematodes (*Caenorhabditis elegans*) are small transparent roundworms that have a relatively short lifespan (2-3 weeks), fast reproduction, and high progeny number (~350), leading to easy and economic colony maintenance (Pienaar, Götz and Feany, 2010; Cooper and Van Raamsdonk, 2018). *C. elegans* can be self-fertilizing, thus creating genetically identical offspring (Cooper and Van Raamsdonk, 2018). Their basic cell biology and biochemistry is similar to mammals, including

neurotransmitters and receptors (Pienaar, Götz and Feany, 2010; Duty and Jenner, 2011). The connectome of *C. elegans* has been fully mapped; however it has a limited size of 302 neurons, of which only 8 are dopaminergic (White *et al.*, 1986; Pienaar, Götz and Feany, 2010; Duty and Jenner, 2011; Konnova and Swanberg, 2018). *C. elegans* has homologues for parkin, LRRK2, PINK1, and DJ-1, thus accounting for most of the major PD genes (Duty and Jenner, 2011; Jagmag *et al.*, 2016; Cooper and Van Raamsdonk, 2018).

Dopaminergic neurons of *C. elegans* exposed the neurotoxins 6-hydroxydopamine (6-OHDA) and rotenone underwent apoptosis (Nass *et al.*, 2002), while MPTP leads to decrease motility and degeneration of dopaminergic neurons (Braungart *et al.*, 2004). The discrepancy between motor symptoms and dopaminergic cells death shows that there is no clear-cut correlation between the two in *C. elegans. C. elegans* expressing wild-type or mutated human SNCA show behavioural deficits and reduced neuronal dopamine levels (Kuwahara *et al.*, 2006; Cooper and Van Raamsdonk, 2018). The later could be rescued by administration of dopamine (Kuwahara *et al.*, 2006).

RNA interference can easily be applied, since the nematodes can be fed on agar plates containing bacteria that express small interfering RNA (siRNA), to create knock-downs of targeted genes (Pienaar, Götz and Feany, 2010). RNA interference can be used on a large scale to screens for genes involved in specific pathways. For example, a RNA interference screen has identified a handful of genes that caused severe growth- and motor abnormalities SNCA transgenic *C. elegans* after knock-down (Kuwahara *et al.*, 2008).

Although *C. elegans* shows promising PD models, it must be noted that the anatomical and functional connectivity is much simpler than in mammals, and the relation of behavioural deficits might be limited (Pienaar, Götz and Feany, 2010; Duty and Jenner, 2011). However, *C. elegans* could be used to study the interaction between environment and genetic factors (Duty and Jenner, 2011). For example; DJ-1 and parkin mutations have been shown to increase the susceptibility to rotenone (Ved *et al.*, 2005). A more elaborate review of the use of *C. elegans* in PD research has been written by Cooper and Van Raamsdonk (2018).

### 1.1.2 Fruit fly (*Drosophila melanogaster*)

The fruit fly (*Drosophila melanogaster*) has a significantly bigger neuron pool than *C. elegans*, containing around 135.000 neurons, which is currently being mapped (Konnova and Swanberg, 2018), and includes dopaminergic neurons. As in vertebrates, dopamine modulates motor behaviour and circadian rhythms, amongst others (Riemensperger *et al.*, 2011). This motor ability can be affected by oral administration of paraquat, an herbicide and neurotoxin (see below); Drosophila exposed to paraquat developed parkinsonian symptoms including resting tremor, bradykenesia, and postural instability. This phenotype could be rescued by treatment with dopamine or levodopa. Interestingly, male Drosophila where earlier and more severely affected than their female counterparts (Chaudhuri *et al.*, 2007). Similarly, rotenone (another neurotoxin, see below) induced dopaminergic neurodegeneration and motor impairment, the latter could be rescued by levodopa (Coulom and Birman, 2004).

Drosophila has homologues for most PD-related genes, i.e. PINK1, Parkin, DJ-1, and LRRK2 (Whitworth, Wes and Pallanck, 2006), and models of PD are most commonly genetic models. Although no homologue for the SNCA gene is present in Drosophila, the human wild-type or mutant form can be over-expressed in transgenic flies. Feany and Bender (2000) have shown that this leads to adult onset dopaminergic neuron loss, motor dysfunction (reversible by levodopa (Pendleton *et*

*al.*, 2002)), and Lewy Body-like inclusions (Feany and Bender, 2000). The Drosophila genetic toolbox allows for tissue or neuron specific dominant mutations on one hand, and targeted point mutations or deletions for recessive mutations on the other hand (West *et al.*, 2015). See Pienaar *et al*. (2010) and West *et al*. (2015) for more detailed reviews on genetic PD research in Drosophila. In short, parkin, LRRK2, and PINK1 mutations all lead to a reduced amount dopaminergic neurons and behavioural phenotypes, which can be reversed by levodopa, while DJ-1 mutations have no effect on this (Duty and Jenner, 2011).

The short lifespan and easy husbandry of Drosophila make them great models for rapid screening of pharmacological therapeutics (Duty and Jenner, 2011). Although several pathways are conserved, the specific modifiers for PD still need to be verified in human PD. Another major downside of Drosophila is the lack of a α-synuclein homologue (Dawson, Ko and Dawson, 2010).

### 1.1.3 Zebrafish (*Danio rerio*)

The zebrafish (*Danio rerio*) is a vertebrate species with a high reproduction rate and small adult size (3-4cm), which allows for simple and economic husbandry. Additionally, the embryos are transparent and develop outside the mother (Pienaar, Götz and Feany, 2010). The zebrafish brain shows important similarity to the human brain; i.e. homologues for midbrain and ventral tegmental neurons, and a striatum-like region in the procencaphalon (Rink and Wullimann, 2001, 2002; Pienaar, Götz and Feany, 2010). Furthermore, zebrafish have homologues for several PD related genes, most notably parkin, PINK1, DJ-1, and LRRK2 (Jagmag *et al.*, 2016). Antisense morpholino oligonucleotides can be used, via microinjection in to single-cell embryos, to knockdown PD-related genes. This has been successfully shown for DJ-1 in combination with $H_2O_2$ and proteasome inhibitor MG132; leading to widespread neurodegeneration (Bretaud *et al.*, 2007), parkin; leading to dopaminergic neurodegeneration, which can be exacerbated by MPTP (Flinn *et al.*, 2009), and PINK1; leading to disrupted patterning of dopaminergic neurons and motor dysfunction (Xi *et al.*, 2010). Interestingly, LRRK2 seems the most promising gene to model PD in zebrafish (Duty and Jenner, 2011); deletion of the WD40 domain resulted in dopaminergic neuron loss and motor dysfunction (Xi, Noble and Ekker, 2011).

Due to the aquatic nature of zebrafish, hydrophilic substances can easily be added to the water and subsequently be absorbed through the skin and gills. This can be utilised to create models or perform drug screens and tests (Pienaar, Götz and Feany, 2010). For example, the neurotoxin MPTP reduces catecholaminergic innervations in larvae (Thirumalai and Cline, 2008), and induces dopaminergic neurodegeneration in zebrafish embryos, shown as a reduction of TH+ cells (Lam, Korzh and Strahle, 2005). Interestingly, exposure to exogenous dopamine reduced spontaneous swimming behaviour in zebrafish larvae, while pharmacologically blocking $D_2$-Receptors increased this swimming behaviour (Thirumalai and Cline, 2008). Alternatively, zebrafish can be injected with toxic substances; both 6-OHDA and MPTP significantly reduced the levels of dopamine and noradrenaline in adult brains, while also negatively affecting motor behaviour (Anichtchik *et al.*, 2003), while Rotenone and paraquat seemed to have no significant effects (Bretaud, Lee and Guo, 2004).

A major downside of the zebrafish as a model organism for PD is that many genetic mutation result in affected swimming behaviour, however, the neural mechanism for this behaviour is currently unknown, thus limiting the translatability to humans.

### 1.1.4 Frogs & toads (Anurans)

Although less used than the above described species, anurans (frogs and toads) have some valuable characteristics; they are easily raised, produce enormous single-celled eggs, have external development, have relatively large embryos which are easy to manipulate, and have transparent tadpoles (Pienaar, Götz and Feany, 2010). Additionally, the entire genome of *Xenopus laevis* has been sequenced (Session *et al.*, 2016). This includes a parkin homolog that might be subject to post-translational modifications like phosphorylation (Horowitz *et al.*, 2001). Anurans have a brain region homologues to the striatum (Endepols, Roden, *et al.*, 2004) and the substantia nigra pars compacta, containing dopaminergic neurons that innervate the striatum (Marin *et al.*, 1997). The substantia nigra is named for its darkly pigmented colour in humans, however most traditional model animals have very little to no neuromelanin. Since anurans do express neuromelanin they might be very suited to study the role of neuromelanin in PD (Pienaar, Götz and Feany, 2010).

Bilateral 6-OHDA injection, discussed in more detail below, causes a behavioural deficit as well as cognitive symptoms, and a decrease in TH-positive cells in *Hyla versicolor* (Endepols, Schul, *et al.*, 2004). Alternatively, consecutive intraperitoneal injections of MPTP, see below, caused numerous motor deficits, including rigidity, slowness, and freezing in *Rana Clamitans Clamitans* and *Rana Pipiens*. The dopamine concentration and melanin index were also affected by the MPTP injections (A Barbeau *et al.*, 1985; A. Barbeau *et al.*, 1985). Interestingly, paraquat causes similar symptoms in *Rana Pipiens*, but dopamine concentrations first rise before dropping (A Barbeau *et al.*, 1985).

## 1.2 Pharmacological models

Mammalian models have the benefit of resembling the human body and brain more closely. Many well-established experimental models exist for rodents. And while mice have the advantage of easier genomic manipulation, rats have a larger brain, which allows for better stereotactic accuracy (Cherry and Gambhir, 2001).

The first models to be used were pharmacological models. They generally cause dopamine depletion in the striatum, leading to PD-like motor symptoms. The downsides of pharmacological models are reversibility of the effects and relative short periods effect of time. Additionally, they do not cause neurodegeneration in the nigrostriatal pathway. Despite the limited applicability of the these model, they have led to some ground-breaking results.

### 1.2.1 Reserpine

The reserpine models was already used as early as 1957 (Carlsson, Lindqvist and Magnusson), and is thus the earliest model used in PD research (Duty and Jenner, 2011; Tieu, 2011). Reserpine's mode of action is through temporary blocking vesicular monoamine transporter (VMAT2) (Duty and Jenner, 2011) through magnesium and ATP-dependent mechanisms (Bezard, Imbert and Gross, 1998), which leads to global depletion of monoamines, e.g. noradrenaline, serotonin, and dopamine (Duty and Jenner, 2011). This temporary depletion of catecholamines has been shown to lead to PD-like motor deficits in many mammals, including mouse, rat, and monkey (Bezard, Imbert and Gross, 1998). In their ground-breaking research Carlsson and colleagues showed that these motor symptoms can be successfully reversed by levodopa (Carlsson, Lindqvist and Magnusson, 1957). The reserpine model has also greatly contributed to our knowledge of the link between monoamines and PD (Duty and Jenner, 2011).

The effects of reserpine are relatively transient, excluding the possibility to test repeated drug administration (Duty and Jenner, 2011; Tieu, 2011). However, the biggest drawback of the reserpine model is the lack of dopaminergic cell loss in the substantia nigra, which limits the therapeutic strategies to symptomatic treatments. Indeed, the reserpine model has led to many of the dopaminergic drugs currently used in clinics (e.g. pramipexole, ropinirole, and levodopa), thus showing the strong predictive value of this model (Duty and Jenner, 2011).

### 1.2.2 Haloperidol

Like reserpine model, the haloperidol model has already been used since a long time. Haloperidol's mode of action is through antagonizing dopamine $D_2$ (and $D_1$) receptor in medium spiny neurons, which results in a block of striatal dopamine transmission, leading to muscle rigidity and catalepsy (posture fixation) in rodents (Kobayashi *et al.*, 1997; Bezard, Imbert and Gross, 1998; Duty and Jenner, 2011). Additionally, acute administration of haloperidol leads to depletion of striatal dopamine, noradrenalin, and serotonin in rats (Kulkarni, Bishnoi and Chopra, 2009).

Again, like reserpine, the effects of haloperidol are transient, which limits their usefulness in long-term studies. Additionally, they only display limited symptomatic overlap with PD, limiting the use in neuroprotective and neuroreparative studies (Bezard, Imbert and Gross, 1998; Duty and Jenner, 2011). Despite the limited applicability, several drugs currently in use have shown efficacy in the haloperidol model (e.g. levodopa and carbidopa (Kobayashi *et al.*, 1997), and pramipexole (Maj *et al.*, 1997)).

### 1.2.3 Racemetirosine

Racemetirosine, also called α-methyl-ρ-tyrosine, inhibits tyrosine hydroxylase (TH), and thus dopamine and noradrenaline synthesis (Spector, Sjoerdsma and Udenfriend, 1965; Bezard, Imbert and Gross, 1998; Duty and Jenner, 2011; Tieu, 2011). Similar as described above, this leads to a transient dopamine depletion without any neuronal loss (Tieu, 2011). Racemetirosine can be used in combination with reserpine to potentiate its effects (Carlsson and Carlsson, 1989; Duty and Jenner, 2011).

## 1.3 Toxin-based mammalian models

Before the first genes involved in PD were identified, neurotoxin models were used to study the disease. Unlike pharmacological models, toxin-based models generally do cause neurodegeneration of the nigrostriatal pathway. While most of these models have the drawback to only portray PD in a limited, singular way, they have still taught us valuable lessons about PD. Of the neurotoxins, 6-hydroxydopamine (6-OHDA) was the first to be discovered and is the classic rodent model (Jackson-Lewis, Blesa and Przedborski, 2012), followed by 1-methyl-4-phenyl-1,2,3,6-tetrahydropyridine (MPTP), which alone is clearly linked to human parkinsonism (Dauer and Przedborski, 2003). Most of the other toxins used to model PD are pesticide based (Jackson-Lewis, Blesa and Przedborski, 2012) and are believed to act through reactive oxygen species (ROS) formation (Dauer and Przedborski, 2003).

### 1.3.1 6-hydroxydopamine

See Chapter 1: 2.1, page 24.

### 1.3.2 MPTP

See Chapter 1: 2.2, page 24.

### 1.3.3 Rotenone

Rotenone is a naturally occurring broad spectrum insecticide and pesticide (Dauer and Przedborski, 2003; Tieu, 2011; Jackson-Lewis, Blesa and Przedborski, 2012; Jagmag *et al.*, 2016; Konnova and Swanberg, 2018). Rotenone acts through inhibition of mitochondrial complex I, at the same site as MPP+, and thereby blocking the mitochondrial electron transport chain (Dauer and Przedborski, 2003; Duty and Jenner, 2011; Jagmag *et al.*, 2016). Rotenone is highly lipophilic and can thus easily cross the blood-brain barrier and enter cells, allowing for easy systemic injections (Betarbet *et al.*, 2000). Its short half-life (3-5 days) necessitates repeated injections (Jackson-Lewis, Blesa and Przedborski, 2012). Chronic systemic rotenone exposure has been shown to cause dopaminergic neuron degeneration as well as motor symptoms and formation of intracellular Lewy-body-like inclusions (Betarbet *et al.*, 2000).

However, there are several problems with the rotenone rat model which shake the validity of the model (Cicchetti, Drouin-Ouellet and Gross, 2009). Firstly, it is difficult to replicate studies due to the high mortality rate (Fleming *et al.*, 2004), due to systemic toxicity (Duty and Jenner, 2011). Secondly, it has been shown that chronic administration at low doses causes motor deficit, while failing to show dopaminergic cell dead (Fleming *et al.*, 2004). This could either point towards early stage PD modelling, or the involvement of other pathways and cell types. Thirdly, even though chronic rotenone treatment has been associated with sleep disturbances, an equally large effect has been shown after vehicle treatment (DMSO/PEG), meaning that these sleep disturbances cannot be attributed to dopaminergic cell loss (García-García *et al.*, 2005). Lastly, besides dopaminergic cell death, many other cell types and regions have been shown to be affected by chronic rotenone treatment, suggesting more general mitochondrial failure is involved than previously assumed (Höglinger *et al.*, 2003). A redeeming quality is the extensive microglial activation in both the substantia nigra and striatum (Sherer *et al.*, 2003). Despite the limitations, pesticide models like rotenone can be used to study the effect of environmental factors on PD, for example the interaction with other risk factors like age or genetic mutations (Konnova and Swanberg, 2018), or the relationship between aggregate formation and neuronal death (Dauer and Przedborski, 2003).

### 1.3.4 Paraquat

N,N'-dimethyl- 4–4–4'-bipiridinium (paraquat) is a widely used herbicide that shows structural resemblance to MPP+ (Snyder and D'Amato, 1985). But whereas MPP+ acts through blockage of mitochondrial complex I (Nicklas, Vyas and Heikkila, 1985), paraquat acts through redox mediated oxidative stress (Bonneh-Barkay *et al.*, 2005), generating reactive oxygen species, leading to damage of lipids, proteins, DNA, and RNA (Jackson-Lewis, Blesa and Przedborski, 2012). It is still unclear how paraquat crosses the blood-brain barrier (Konnova and Swanberg, 2018), but it appears to be mediated by the neutral amino acid transport system (Shimizu *et al.*, 2001). Unlike MPP+, paraquat is

not a substrate for Dopamine Transporter, raising the question how paraquat enters dopaminergic neurons (Tieu, 2011).

Chronic systemic injections of paraquat in mice (McCormack *et al.*, 2002) and rats (Cicchetti *et al.*, 2005) have been shown to lead to dopaminergic cell loss in the substantia nigra. Interestingly, in mice, this is not accompanied by dopamine depletion in the striatum or motor deficits, which the authors speculate might be due to compensatory mechanisms (McCormack *et al.*, 2002). However, higher α-synuclein levels have been observed, as well as aggregate formation (Manning-Bog *et al.*, 2002). In rats, again, there was no dopamine depletion observed, but some motor deficits were present. Additionally, microglial activation was observed, indicating that dopaminergic cell loss might be due to inflammation (Cicchetti *et al.*, 2005).

It has to be kept in mind that high doses of paraquat cause pulmonary fibrosis (Bismuth *et al.*, 1990), which could show PD-unrelated motor deficits (Konnova and Swanberg, 2018). Additionally, there is some controversy about the cell death and specificity or paraquat (Jackson-Lewis, Blesa and Przedborski, 2012; Jagmag *et al.*, 2016). Paraquat's strengths lie in the possibility to study Lewy body formation and the role of α-synuclein (Jackson-Lewis, Blesa and Przedborski, 2012).

### 1.3.5 Other toxin-based models

#### Maneb

2-(dithiocarboxy)aminoethylcarbamodithioato(2-)-kS, kS' manganese is a fungicide more commonly known as Maneb (Jagmag *et al.*, 2016). It preferentially inhibits complex III of the mitochondrial respiration chain (Zhang *et al.*, 2003). Maneb has been shown to evoke a motor deficit in mice, while no decrease in tyrosine hydroxylase (TH) or DAT immunoreactivity were observed (Thiruchelvam *et al.*, 2000). The same group has also shown that Maneb can exacerbate the effect of paraquat; only when both toxins were combined they observed a reduction in TH protein levels (Thiruchelvam *et al.*, 2000). In Sprague-Dawley rats the results were more variable, however, a reduction in striatal dopamine levels was observed (Tinakoua *et al.*, 2015).

#### DOPAL

3,4-dihydroxyphenylacetaldehyde (DOPAL) is an intermediate of the dopamine metabolism. DOPAL is created by oxidative deamination of dopamine by monoamine oxidase. DOPAL is normally cleaved by aldehyde dehydrogenase (ALDH1A1) into 3,4-dihydroxyphenylacetic acid (DOPAC) (Panneton *et al.*, 2010). Increased levels of DOPAL (Mattammal *et al.*, 1993) and decreased levels of ALDH1A1 (Galter *et al.*, 2003) have been reported in PD patients. Panneton and colleagues (2010) have shown a decrease of dopaminergic neurons in the substantia nigra of rats following DOPAL injections into the same region. Additionally, they show a motor deficit and reduced striatal dopamine levels (Panneton *et al.*, 2010), as well as α-synuclein accumulation (Burke *et al.*, 2008).

#### Amphetamines; Methamphetamine and MDMA

Methamphetamine can enter dopaminergic neurons via uptake by dopamine transporter, or via diffusion (Tieu, 2011). Inside the cells, methamphetamine interacts with VMAT2, which incapacitates the vesicular proton gradient, leading to dopamine oxidation in the cytosol, generating reactive oxygen species and leading to oxidative stress (Larsen *et al.*, 2002). Additionally, this dopamine release from the vesicles into the cytosol leads to an influx of dopamine into the synaptic cleft, via reverse transport through DAT (Sulzer, Maidment and Rayport, 1993), ultimately leading to

increase locomotor activity (Tieu, 2011). Interestingly, it is unclear if methamphetamine toxicity originates from oxidative stress or from hyperthermia (Tieu, 2011).

Repeated administration of methamphetamine has been shown to cause a continuing reduction of striatal dopamine levels in rats (and guinea pig) (Wagner, Seiden and Schuster, 1979), as well as TH levels in the substantia nigra (Trulson *et al.*, 1985). Methamphetamine acts more upon the dopaminergic nerve terminals than the cell bodies, unlike paraquat (cell bodies), and MPTP and 6-OHDA (both) (Tieu, 2011). Although, this model is not believed to be very reliable (Jackson-Lewis, Blesa and Przedborski, 2012), some believe it might hold value in combination with other neurotoxins likes MPTP or paraquat (Jagmag *et al.*, 2016)

3,4-methylenedioxymethamphetamine (MDMA or Ecstasy) is an amphetamine analogue that causes reduced levels of TH and DAT in the striatum (Granado, Escobedo, *et al.*, 2008) and substantia nigra of mice (Granado, O'Shea, *et al.*, 2008). Notably, while rats, non-human primates, and humans show severe effects of MDMA, the damage is localized to the serotonin system, with the dopaminergic system being spared (Green *et al.*, 2003).

#### Isoquinoline derivatives

Isoquinoline and its derivatives are naturally occurring in plants and animals, including in mammalian brains. Some derivatives can cross the blood-brain barrier, but they can also be synthesized from dopamine in the brain (Tieu, 2011). These compounds are structurally similar to MPTP, and their mechanism of toxicity has been shown to be very similar to MPP+, i.e. affinity for dopamine transporter and complex I inhibition (Tieu, 2011). However, derivatives can have different effects in different animal species, and, more importantly, they can easily be converted into other derivatives, some of which might even have neuroprotective properties (Tieu, 2011). It was also described that isoquinoline derivatives down-regulate tyrosine hydroxylase, thus confounding neuronal loss with TH down-regulation (Lorenc-Koci *et al.*, 2004).

## 1.4 PD hallmark-based models

While neurotoxin-based PD models are currently the most widely used models, they do not offer much information about disease progression and reversal of neuronal damage. While these models have taught us about the pathogenic mechanisms underlying neurodegeneration in PD, they have not shown us how to stop or slow its progression. Another way to constitute PD models is focussed on its hallmarks; formation of Lewy bodies and presence of activated microglia. These models have a high construct validity (Duty and Jenner, 2011).

### 1.4.1 Proteasomal inhibitors

The work on proteasomal inhibitors to model PD is fuelled by two key findings from last decade; a mutation in α-synuclein (A53T) responsible for a familial from of PD (Polymeropoulos *et al.*, 1997), and the presence of α-synuclein in Lewy bodies (Spillantini *et al.*, 1997). The discovery of two additional mutations of the ubiquitin-proteasome system (UCH-L1 (Leroy *et al.*, 1998), and parkin (Kitada *et al.*, 1998)) in familial forms is PD further propelled interest (Duty and Jenner, 2011).

*In vitro*, proteasomal inhibitors (lactacystin and ubiquitin aldehyde) caused concentration-dependent dopaminergic neurodegeneration. Lactacystin administration, affecting 26/20S proteasomes, was shown to lead to accumulation of α-synuclein and ubiquitin, as well as Lewy body-

like inclusions (Kevin St P. McNaught *et al.*, 2002). Subsequently, the same group was able to show that lactacystin injection into the substantia nigra of rats leads to PD-associated motor symptoms, reversible by apomorphine. Similarly as *in vitro, in vivo* they observed dose-dependent dopaminergic neurodegeneration and the aggregation of α-synuclein into Lewy body-like inclusions (Kevin St. P. McNaught *et al.*, 2002). Later work of the group showed similar effects using systemic injection of epoxomicin (naturally occurring proteasome inhibitor) or PSI (synthetic) in adult rats (McNaught *et al.*, 2004). Animals developed progressive motor-symptoms reversible by apomorphine, striatal dopamine depletion, dopaminergic cells loss, and Lewy body-like inclusion containing α-synuclein. Interestingly, this model also showed neuroinflammation in the substantia nigra (McNaught *et al.*, 2004).

Although proteasomal inhibition to model PD seemed very promising, other groups were unable to replicate McNaughts' findings using PSI (Kordower *et al.*, 2006; Manning-Boğ *et al.*, 2006). If the variability issue with proteasomal inhibitors can be addressed it could be a valuable model to test neuroprotective strategies due to its high construct validity (Duty and Jenner, 2011).

### 1.4.2 Lipopolysaccharide

See Chapter 1: 2.3, page 25.

## 1.5 Genetic-based models

The discovery of a mutation (A53T) in the α-synuclein gene (SNCA) that is responsible for a familial from of PD (Polymeropoulos *et al.*, 1997) led to the use of genetic based models. Even though genetic cases of PD are relatively rare and represent only a small group of patients (Dauer and Przedborski, 2003; Jackson-Lewis, Blesa and Przedborski, 2012), several autosomal dominant (SNCA and LRRK2) and autosomal recessive (PINK1, Parkin, DJ-1) mutations have been identified (Jackson-Lewis, Blesa and Przedborski, 2012). Studying genetic alterations of PD-related genes can reveal information about molecular pathways involved in PD (Cooper and Van Raamsdonk, 2018).

### 1.5.1 α-synuclein

See Chapter 1: 2.4, page 26.

### 1.5.2 LRRK2

See Chapter 1: 2.5, page 27.

### 1.5.3 Autosomal recessive genes

Apart from the aforementioned autosomal dominant genes, there are several autosomal recessive PD-related genes. Of these, Parkin is the most common, accounting for almost half of the early-onset cases of PD (Jackson-Lewis, Blesa and Przedborski, 2012); others are PINK1 and DJ-1.

#### Parkin

Mutations in the Parkin gene (PARK2) (Kitada *et al.*, 1998) account for almost half of the early-onset familial cases of PD (Lücking *et al.*, 2000; Jackson-Lewis, Blesa and Przedborski, 2012), and there are over 100 mutations known for the Parkin gene (Lücking *et al.*, 2000), most of which are

loss-of-function (Konnova and Swanberg, 2018). Parkin is involved in the ubiquitin proteasome system as an E3 ubiquitin ligase (Shimura *et al.*, 2000; Zhang *et al.*, 2000). In *Drosophila*, Parkin mutations lead to a reduced amount of dopaminergic neurons, as well behavioural phenotypes (Duty and Jenner, 2011), while Parkin knockout flies were shown to have decreased TH levels and dopaminergic neurodegeneration (Dawson, Ko and Dawson, 2010). However, most knockout models of Parkin in mice did not result in any nigrostriatal, dopaminergic, or behavioural pathology (Perez and Palmiter, 2005). Interestingly, overexpression of mutated (Q311X) Parkin in mice leads to dopaminergic neuronal loss in the substantia nigra, synaptic loss in the striatum, a reduction of striatal dopamine levels, Lewy body-like inclusions, and behavioural deficits (Lu *et al.*, 2009). Conversely, more recently, wild-type and mutant Parkin overexpression were shown to induce moderate neurodegeneration in rats (Van Rompuy *et al.*, 2014).

**PINK1**

The gene for Phosphatase and tensin (PTEN) homolog-induced novel kinase 1 (PINK1) is the second most commonly mutated in early-onset PD (Konnova and Swanberg, 2018). Similar to Parkin, PINK1 mutations are recessive, and lead to loss-of-function (Dawson, Ko and Dawson, 2010). PINK1 is normally localised in the mitochondria (Silvestri *et al.*, 2005), where it recruits Parkin and increases its ubiquination activity and induces Parkin-mediated mitophagy (Lazarou *et al.*, 2013). Again like Parkin, Pink1 mutations in *Drosophila* lead to a reduced amount of dopaminergic neurons, as well behavioural phenotypes (Duty and Jenner, 2011), with a small reduction of dopaminergic neurons (Dawson, Ko and Dawson, 2010). And again Pink1 knockout mice do not exhibit a major pathology (Kitada *et al.*, 2007). However, more recently it was shown Pink1 knockout in rats leads to progressive dopaminergic neurodegeneration, as well motor deficits (Dave *et al.*, 2014). Additionally, Pink1 knockout and knockdown mice were shown to be more sensitive to systemic MPTP treatment, resulting in greater neurodegeneration in the substantia nigra and reduced fibre density in the striatum (Haque *et al.*, 2012). This effect could be reversed by viral mediated overexpression of Parkin or DJ-1 (see below). This suggests a role for Pink1 in neuronal survival, and similar roles for Parkin and DJ-1, either acting parallel or downstream of Pink1 (Haque *et al.*, 2012).

**DJ-1**

DJ-1 is a redox sensitive molecular chaperone (Moore, Dawson and Dawson, 2006), whose mutations play a role in early-onset PD (Bonifati *et al.*, 2003); causing loss of function (Macedo *et al.*, 2003; Moore *et al.*, 2003). DJ-1 plays a role in the inhibition of α-synuclein aggregation (Shendelman *et al.*, 2004). It is expressed widely throughout the whole body, and localised in the cytosol, and mitochondria (Zhang *et al.*, 2005). In *Drosophila*, DJ-1 knockdown in dopaminergic neurons (through RNAi) led to age-dependent dopaminergic loss (Yang *et al.*, 2005). As seen in Parkin and Pink1, DJ-1 knockout mice did not display any major abnormalities in dopaminergic neuronal survival (Goldberg *et al.*, 2005). More recently it has been shown that DJ-1 knockout rats show progressive dopaminergic neurodegeneration and motor abnormalities (Dave *et al.*, 2014). Interestingly, knockdown of DJ-1 in mice increased sensitivity to MPTP (Kim *et al.*, 2005).

Even though the autosomal recessive models or Parkin, PINK1, and DJ-1 do not seem very promising or useful at first sight, they could shed light on the early stages of nigrostriatal dysfunction (Dawson, Ko and Dawson, 2010). The lack of neurodegeneration in rodent knockout models could point towards compensatory mechanisms which prevents manifestation of PD symptoms (Jackson-

Lewis, Blesa and Przedborski, 2012). In the future, studying mutations observed in PD patients could be of interest to better understand the mechanisms of Parkin, PINK1, and DJ-1 (Dawson, Ko and Dawson, 2010). Moreover, these genes are of particular interest to evaluate the interaction between genetic mutations and environmental factors.

# Appendix

## *THE C-TERMINAL FRAGMENT OF LRRK2 WITH THE G2019S SUBSTITUTION INCREASES THE NEUROTOXICITY OF MUTANT A53T A-SYNUCLEIN IN DOPAMINERGIC NEURONS IN VIVO (SUBMITTED)*

# 2

# Appendix 2 - The C-terminal fragment of LRRK2 with the G2019S substitution increases the neurotoxicity of mutant A53T α-synuclein in dopaminergic neurons in vivo

Noémie Cresto [1,2], Camille Gardier [1,2], Marie-Claude Gaillard [1,2], Francesco Gubinelli [1,2], **Pauline Roost** [1,2], Daniel Molina [1,2], Charlène Josephine [1,2], Gwenaëlle Auregan [1,2], Martine Guillermier [1,2], Suéva Bernier [1,2], Caroline Jan [1,2], Pauline Gipchtein [1,2], Philippe Hantraye [1,2], Marie-Christine Chartier-Harlin [3,4], Gilles Bonvento [1,2], Nadja Van Camp [1,2], Jean-Marc Taymans [3,4], Karine Cambon [1,2], Géraldine Liot [1,2], Alexis-Pierre Bemelmans [1,2], and Emmanuel Brouillet [1,2 §]

[1] CEA, DRF, Institut François Jacob, Molecular Imaging Research Center (MIRCen), F-92265 Fontenay-aux-Roses, France

[2] CNRS, CEA, Univ. Paris-Saclay, Neurodegenerative Diseases Laboratory (UMR9199), F-92265, Fontenay-aux-Roses, France

[3] University of Lille, Inserm, CHU Lille, UMR-S 1172 - JPArc - Centre de Recherche Jean-Pierre Aubert Neurosciences et Cancer, F-59000 Lille, France

[4] Inserm UMR-S 1172 Team "Early Stages of Parkinson´s Disease", Lille, France

## Abstract

**Background. Alpha-synuclein (α-syn) and leucine-rich repeat kinase 2 (LRRK2) likely play crucial roles both in sporadic and familial forms of Parkinson's disease (PD). The most prevalent mutation in LRRK2 is the G2019S substitution, which induces neurotoxicity through increased kinase activity. There is likely an interplay between LRRK2 and α-syn involved in the neurodegeneration of dopaminergic (DA) neurons in the substantia nigra (SNc) in PD. However, the mechanisms underlying this interplay are ill-defined. Here, we investigated whether LRRK2$^{G2019S}$ can increase the neurotoxicity induced by a mutant form of α-syn (A53T mutation) in DA neurons *in vivo*.**

**We used a co-transduction approach with AAV2/6 vectors encoding human a-syn$^{A53T}$ and the C-terminal portion of LRRK2 (ΔLRRK2), which contains the kinase domain, with either the G2019S mutation (ΔLRRK2$^{G2019S}$) alone or the D1994A mutation (ΔLRRK2$^{G2019S/D1994A}$), which inactivates the kinase activity of LRRK2. The AAVs were co-injected into the rat SNc and histological evaluation was performed at 6- and 15-weeks post-injection (PI).**

**Results: Most SNc neurons co-expressed ΔLRRK2 and human α-syn$^{A53T}$ after transduction. ΔLRRK2$^{G2019S}$ alone produced no cell loss at 15-weeks PI, whereas as expected, transduction with AAV-a-syn$^{A53T}$ mixed with a control AAV coding for GFP produced significant loss of DA neurons. Co-injection of AAV-ΔLRRK2$^{G2019S}$ and AAV-α-syn$^{A53T}$ induced a loss of DA neurons slightly but significantly greater than that produced by co-injection of AAV-α-syn$^{A53T}$ and AAVGFP. We also studied the inactive form, ΔLRRK2$^{G2019S/D1994A}$ at 6 weeks PI. Results showed that ΔLRRK2$^{G2019S/D1994A}$ did not alter the early toxicity of α-syn$^{A53T}$, in contrast to the active form ΔLRRK2$^{G2019S}$ that produced a moderate but significant increase in α-syn$^{A53T}$ toxicity.**

**Conclusion. Thus, these results show that mutant LRRK2 may selectively facilitate α-syn toxicity in DA neurons through a cell-autonomous mechanism involving its kinase activity.**

**However, considering that the effect of ΔLRRK2$^{G2019S}$ upon human α-syn$^{A53T}$ is moderate in our paradigm where pathological proteins are overexpressed, the study supports the hypothesis that the interplay between LRRK2 and α-syn also implicates non-cell-autonomous mechanisms such as those involved in neuroinflammation.**

**Keywords**
Parkinson's disease; Leucine-rich repeat kinase 2; α-synuclein; AAVs; cell-autonomous mechanisms

## Background

Parkinson's disease (PD) is a neurodegenerative disorder affecting approximately seven million people worldwide. Early in the course of the disease, the most obvious symptoms are movementrelated, including shaking (resting tremor), rigidity, and slowness of movement. The neuropathological hallmarks of PD are characterized by the progressive loss of dopaminergic (DA) neurons in the substantia nigra pars compacta (SNc) and the presence of neuronal aggregates (Lewy bodies) and dystrophic Lewy neurites containing the protein α-synuclein (α-syn) [1]. There is no treatment to delay neurodegeneration. The cause of α-syn aggregation and the preferential death of DA neurons is unknown. PD is mainly a sporadic neurodegenerative disorder but approximately 10% of the cases are of genetic origin. Several genes have been identified as causative factors.

Duplication, triplication, and rare mutations (A53T, A30P, E46K, H50Q, G51D, A53E) in the SNCA gene encoding the α-syn protein have been found in families with dominantly-inherited PD and are associated with early-onset forms of PD, with an amplification of α-syn aggregation [2–5]. The A53T [6], A30P [7] and E46K [8] substitutions have been the most studied so far. Compelling evidence shows that α-syn takes center stage in PD and plays a key role via various aggregated forms, including abnormally phosphorylated aggregates that produce multiple cellular alterations, eventually leading to the death of DA neurons [9].

Mutations in leucine-rich repeat kinase 2 (LRRK2) are the most common genetic cause of both familial and sporadic PD [10,11]. There are also variants in the LRRK2 locus that are considered to be risk factors for developing PD. The most prevalent mutation in LRRK2 is the G2019S substitution, accounting for 5 to 6% of AD familial PD and 1 to 2% of de novo generic PD cases [12,13]. The cases of patients harboring the G2019S and other mutations are clinically indistinguishable from idiopathic PD cases, including the presence of Lewy bodies (LBs) in most cases [14,15]. Although G2019S patients show similar clinical manifestations as those of sporadic patients [16], several studies have shown subtle differences [17,18]. Some have reported the presence of LBs in symptomatic LRRK2 mutation carriers and LRRK2 can be found in LBs [19], although this is still a subject of debate, as other neuropathological studies have instead reported the absence of detectable LBs in a sub-population of PD patients with LRRK2 mutations [20]. In general, although LRRK2 variants or mutations are considered to be risk factors for developing PD, the onset of symptoms in LRRK2 carriers has been found to be similar to that of idiopathic PD cases [21,22]. The mechanisms underlying LRRK2 neurotoxicity are still unknown. It is now generally accepted that the G2019S mutation increases LRRK2 kinase activity (both autophosphorylation and phosphorylation of exogenous kinase substrates) and that

neurotoxicity originates from such increased activity [23,24].

The central role of □-syn in PD pathogenesis has led to the hypothesis of a functional (and possibly physical) interaction between LRRK2 and □-syn [for a review[25]. Indeed, LRRK2 toxicity may require the presence of □-syn and, conversely, the presence of variant/mutant LRRK2 could increase the risk and/or impact of □-synucleopathy in PD. The level of kinase activity of LRRK2 could thus be a modifier of □-syn toxicity. If this is true, the therapeutic implication would be extremely important: the regulation of LRRK2 kinase activity could be theoretically beneficial in slowing disease progression not only in individuals harboring LRRK2 mutations, but also in idiopathic PD. Recent experiments in transgenic mouse models of LRRK2 and □-syn support these hypotheses. The results of experiments in genetic models of mutant or wildtype LRRK2, in particular the effect of the pharmacological blockade of the kinase activity of LRRK2G2019S in these models, suggest that LRRK2 may increase □-syn toxicity [26–28].

However, the mechanisms underlying the "protoxic" effect of LRRK2 (especially the G2019S mutation) on □-syn toxicity are not known and the exact role of the kinase domain has not been completely demonstrated. Pharmacological intervention suggests that the kinase activity of LRRK2 likely contributes to the synergy (for a review [16]). In addition, it is not known whether the potentiation of □-syn toxicity by the presence of LRRK2G2019S is related solely to a cell-autonomous mechanism. Alternatively, LRRK2-expressing cells that surround DA neurons, especially microglial cells, astrocytes, and cells of the immune system likely play a role. However, pharmacological intervention with LRRK2 inhibitors, pan-cellular knock out, or transgenic animals expressing wildtype LRRK2 or mutant LRRK2 cannot easily distinguish between cell-autonomous and non-cell-autonomous mechanisms *in vivo*.

Here, we attempted to precisely address these questions in a relevant cellular context by studying the effect of the C-terminal domain of human LRRK2 harboring the G2019S mutation (□LRRK2G2091S) or its inactive form, (mutations G2019S plus D1994A, called DK) □LRRK2DK, on the neurotoxicity of human □-syn with the A53T mutation (α-synA53T). We performed experiments using AAVs that lead to a moderate overexpression of the various forms of □LRRK2 and human □-synA53T alone or in combination in DA neurons of the SNc in adult rats. Quantitative histological evaluation showed that although □LRRK2G2091S alone induced no loss of DA neurons, it could significantly increase □-synA53Tinduced neurotoxicity likely through a mechanism involving the catalytic activity of the kinase domain.

## Materials and methods

### Viral construction and production

Adeno-associated viral vectors (AAVs). Plasmid constructs were packaged into AAV2/6 capsids as described previously [58]. Briefly, viral particles were produced by co-transfection of HEK-293T cells with (1) an adenovirus helper plasmid (pXX6-80), (2) an AAV packaging plasmid carrying the rep2 and cap8 genes, and (3) the AAV2 expression vector containing the transgene. Seventy-two hours following transfection, recombinant vectors were purified and concentrated from cell lysates and supernatants by ultracentrifugation on an iodixaniol density gradient followed by dialysis against PBSMK (0.5 mM MgCl2 and 1.25 mM KCl in PBS). The concentration of vector stocks was estimated by real-time-PCR following the method described by Aurnhammer et al. [59] and expressed as viral genomes per ml of concentrated stocks (Vg/ml). AAVs coding for human ΔLRRK2 (WT, G2019S, and "kinase dead), α-syn A53T, and GFP were produced.

### Stereotactic injection

Adult Sprague-Dawley rats (Charles River Laboratories), weighing ~250 g, were housed under a 12-h light/dark cycle with *ad libitum* access to food and water, in accordance with European Community (Directive 2010-63/EEC) and French (Code Rural R214/87-130) regulations. Experimental procedures were approved by the local ethics committee and registered with the French Research Ministry (committee #44, approval #12-100, and APAFIS#1372-2015080415269690v2). For stereotactic injections, the animals were deeply anaesthetized with 4% isoflurane, followed by a mixture of ketamine (75 mg/kg) and xylazine (5 mg/kg), and placed in a stereotactic frame. Recombinant adeno-associated viral vectors were injected unilaterally into the SNc, at the following stereotactic coordinates: +3.4 mm anterior to the interaural zero and ±2.0 mm lateral to bregma, at a depth of -7.8 mm relative to the skull, with the tooth bar set at -3.3 mm. We injected 4 µl of virus at a concentration of $2.5x10^{10}$ viral particles per site for single injections and $2.5x10^{10}$ viral particles of each vector for co-injections for a total of $5x10^{10}$ viral particles per site, with a 34-gauge blunt-tipped needle linked to a 10-µl Hamilton syringe by a polyethylene catheter at a rate of 0.25 µl/min using an automatic pump (CMA-4004). The needle was left in place for five minutes and then slowly withdrawn.

### Tissue processing

For all procedures, rats were first deeply anesthetized by isoflurane inhalation, followed by the intraperitoneal injection of a lethal dose of sodium pentobarbital.

For immunohistochemistry, rats were transcardially perfused with 300 ml 4% paraformaldehyde in phosphate buffer at a rate of 30 ml/min. After perfusion, the brain of each rat was quickly removed and immersed in ice-cold 4% paraformaldehyde/0.1X PBS for at least 24 h, before transfer to 15% sucrose for 24 h and then 30% sucrose the next day, for cryoprotection. The brains were then cut into 40-µm sections on a freezing microtome (CM1900, Leica, Germany). Serial sections of the striatum and midbrain were stored in antifreeze solution (30% sucrose/30% ethylene glycol in PBS) until use.

### Immunohistological analysis and quantification

*Immunohistochemistry*

Sections were removed from the antifreeze solution and washed in PBS. Endogenous peroxidase activity was quenched by transferring them to 1% $H_2O_2$ and incubation for 30 min at room temperature (RT) and washing them three times with PBS for 10 min each. The sections were then blocked by incubation with 4.5% normal goat serum for 30 min in PBS-T (0.2% Triton X-100 in PBS) and then incubated overnight with primary antibody in 3% normal goat serum in PBS-T at 4°C with gentle shaking. The following primary antibodies were used for the present study: anti-tyrosine hydroxylase (TH) antibody: MAB318 clone LNC1, Merk-Millipore, 1:3000; anti-hemagglutinin tag (HA), Covance clone 11, 1:1000; anti-human α-synuclein, syn 211, 1:1000; anti-phospho-α-synS129, ab51253, Abcam, 1:5000]. The next day, the sections were removed from the primary antibody solution, washed three times, and incubated for 1 h at RT with the appropriate biotinylated secondary antibody in PBS-T (Vector Laboratories, Burlingame, CA, USA, 1:1000). The sections were then washed and incubated with ABC complex solution in PBS-T (1:250, reagents A and B combined in a 1:1 ratio, Vector Laboratories) for 1 h. The sections were then incubated with DAB for 30 s to 1 min and mounted on slides in Eukitt mounting medium.

*Cell counting*

Optical fractionator sampling was carried out on a Zeiss microscope AxioPlan. Midbrain dopaminergic neurons were outlined on the basis of TH immunolabelling with reference to a coronal atlas of the rat brain (Paxinos and Watson, 6th

edition). TH-positive cells were counted by unbiased stereology in the entire SNc and the number of positive neurons per section was calculated using Mercator Software (Explora Nova, France). We placed 100 × 100 µm grids in a systematically random manner, 80 × 80 µm apart, with a 3-µm offset from the surface of the section. Quantification was performed on 12 serial sections spaced by 200 µm, corresponding to the entire SNc.

The phosphorylation of α-syn on S129 (P-α-syn$^{S129}$) was evaluated by counting the number of P-α-syn$^{S129}$-positive neurons in the SNc using stereology methods. The SNc was delimited by Nissl staining and the grids (250 x 250 µm) placed, with a space of 100 x 100 µm. Quantification was performed on six serial sections spaced by 400 µm, corresponding to the entire SNc. In the striatum, a threshold was applied to select only the P-α-syn$^{S129}$-positive neurons by immunostaining and quantification performed on three slices, corresponding to the beginning, middle, and end of the striatum.

*Immunofluorescence*

The procedure used was similar to that for immunohistochemistry, but without the incubation in 1% $H_2O_2$. The primary antibodies used for the immunofluorescence procedure were the same as previously described (IBA1, Dako, 1:1000). Sections were first incubated with the primary antibody overnight at 4°C. The next day, they were incubated with a fluorescent secondary antibody (Alexa Fluor 594-labeled goat anti-rabbit IgG or Alexa Fluor 488-labeled goat anti-rabbit IgG (1:1000, Life Technologies)) for 1h at RT. Sections were then washed and incubated overnight at 4°C with another primary antibody. Finally, they were incubated with a second fluorescent secondary antibody (Alexa Fluor 488-labeled goat anti-mouse IgG or 594-labeled goat anti-mouse IgG (1:1000, Life Technologies)) for 1h at RT. The sections were stained with DAPI, washed, and mounted in a fluorescence mounting medium. Images were acquired with a laser confocal microscope (SP8, Leica, Germany) or an epifluorescence microscope (DM8000, Leica, Germany).

*Colocalization*

The percentage of co-localization between ΔLRRK2 and α-syn was determined by counting the number of cells co-expressing both ΔLRRK2 and α-syn proteins divided by the number of cells expressing α-syn alone. Images were acquired with a laser confocal microscope (SP8, Leica, Germany). On the same acquisitions, the levels of ΔLRRK2 and α-syn proteins were evaluated on three coronal sections in the SNc. Twenty cells co-expressing both ΔLRRK2 and α-syn proteins were delineated per animal using image J software and the mean fluorescence intensity in the red and in green channels (corresponding to ΔLRRK2 and α-syn proteins, respectively) was measured in each cell.

*Fluorescence intensity measurement*

Striatal dopaminergic innervation at 15 weeks was quantified by measuring the fluorescence intensity of TH-immunoreactive terminals on three coronal striatal sections. The sections were observed by epifluorescence microscopy at a magnification of 63X and the fluorescence intensity determined using MorphoStrider software (Explora Nova, France).

*Microglia area measurement*

The area occupied by microglia was evaluated by confocal microscopy at a magnification of 20X in the dorso-medial part of the striatum and in the SN *pars reticulata*. A threshold was applied and the area of 20 microglia cells measured per acquisition. Three acquisitions per animal were used.

### Statistical analysis

Normal distribution of data was checked by Shapiro test. Data were analyzed by two-tailed, one-way analysis of variance (ANOVA) performed with Statistica software (Statsoft Inc., Tulsa, Oklahoma, USA) and, when appropriate, LSD post-

hoc correction for multiple comparisons was applied. Unpaired Student's t-tests were performed for pairwise comparisons. The annotations used to indicate the level of significance are as follows: *$p < 0.05$, **$p < 0.01$, ***$p < 0.001$.

## Results

### Determination of the experimental conditions to detect potential synergy between AAV-a-syn$^{A53T}$ and AAV-ΔLRRK2$^{G2019S}$ toxicity

We investigated whether human LRRK2 can increase the toxicity of human α-syn in DA neurons through cell-autonomous mechanisms. We used AAVs, which allow selective expression in neuronal cells and efficiently transduce a large volume of brain tissue due to their good diffusion properties. In a previous study [29], we showed that the C-terminal portion of human LRRK2$^{G2019S}$ (ΔLRRK2$^{G2019S}$, 1330-2527 aa) retains, at least in part, the biochemical properties of full-length LRRK2$^{G2019S}$, including higher kinase activity than the wildtype fragment. In addition, we found that overexpression of the C-terminal portion of human ΔLRRK2$^{G2019S}$ in the adult rat SNc, using AAVs, produced partial (~30%) but significant loss of DA neurons at 25 weeks post-transduction, whereas overexpression of the wildtype form of LRRK2 (ΔLRRK2$^{WT}$) was not toxic. Here, we used a similar approach using a slightly larger fragment (aa 1283-2527) (Fig. 1A).

We studied the effects of AAV-ΔLRRK2$^{G2019S}$, AAV-ΔLRRK2$^{WT}$, and AAV-ΔLRRK2$^{G2019S/D1994A}$ alone at 15 weeks PI. We injected 4 µl of viral vector solution in all cases. A final amount of $2.5x10^{10}$ viral particles per site and per vector was used. Each AAV was injected unilaterally into the SNc ($2.5\ 10^{10}$ vg). In addition to the three experimental groups, a control group received injections of vehicle (PBS/pluronic acid). The integrity of the nigrostriatal pathway was assessed using unbiased stereology to count the number of DA neurons displaying tyrosine hydroxylase (TH) staining in the injected part of the SNc (Fig. 1). Observation at low-magnification revealed no major loss of TH-positive cells in any of the groups injected with AAVs encoding the LRRK2 fragments (Fig. 1B). The total number of TH-positive cells in the SNc did not differ significantly between the control group (PBS) and AAV-ΔLRRK2$^{WT}$, AAV-ΔLRRK2$^{G2019S}$, or AAV-ΔLRRK2$^{G2019S/D1994A}$ groups (Fig. 1C). Thus, these results suggest that the ΔLRRK2 fragments alone did not trigger significant neurodegeneration of DA neurons at 15 weeks PI.

We sought an injection protocol that leads to mild degeneration, in such a way that potential "pro-toxic" effect of LRRK2 constructs could be easily detected, as we wanted to investigate whether AAVs encoding the different ΔLRRK2 constructs could increase the toxicity of AAV-α-syn$^{A53T}$. We conducted pilot experiments to determine the appropriate dose (titers) of AAV-α-syn alone that would lead to progressive and partial loss of DA neurons. Quantification of TH-positive cells in the SNc showed a moderate loss of DA neurons (~30%) at 12 and 15 weeks after transduction with AAV-α- syn$^{A53T}$ (2.5x10$^{10}$ particles post-injection (PI)) (Supplementary Fig. S1A-B). After transduction, DA neurons often displayed accumulation of α-syn phosphorylated at its serine 129 (p-synS129). The cells positive for p-synS19 were also positive for ThioS suggesting that these accumulations were aggregates (Supplementary Fig. S1C).

Thus, a co-injection protocol with AAV- α-syn$^{A53T}$ and AAV-ΔLRRK2$^{G2019S}$ and the evaluation of DA cell loss at 15 weeks PI appeared to be suitable for the detection of the potential synergy of toxicity between the two pathological transgenes.

### Effects of co-transduction with AAV- α-syn$^{A53T}$ and AAV-ΔLRRK2$^{G2019S}$

We next investigated whether the presence of the various ΔLRRK2 fragments (wildtype, G2019S, or G2019S/D1994A) in DA neurons could modify the toxicity of human α-syn$^{A53T}$ using this co-transduction paradigm (with 2.5x10$^{10}$ particles for each vector).

We first studied the neurotoxic effects produced by AAV- α-syn$^{A53T}$ in the presence or absence of AAV-ΔLRRK2$^{G2019S}$ at 15 weeks PI. We assessed the co-localization of human α-syn$^{A53T}$

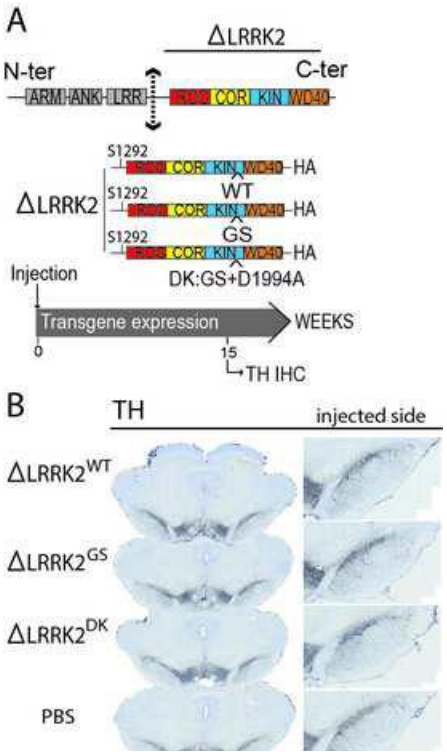


**Fig. 1 Immunohistochemistry for tyrosine hydroxylase (TH). A The C-terminal fragment of LRRK2, called ΔLRRK2, was generated in different forms, WT: G2019S, or dead kinase (DK). B-C, The three fragments were cloned into an AAV and unilaterally injected into the rat SNc. Fifteen weeks PI, TH immunohistochemistry was performed (B). The number of TH-positive neurons was evaluated by stereology (C), with no obvious toxicity due to the LRRK2 fragments at 15 weeks PI. Results are expressed as means ± the standard error of the mean (SEM). N = 10 animals/group. ANOVA and PLSD post hoc test. n.s.: not significant. Scale bars: 750 µm and 400 µm.**

and LRRK2 fragments in the SNc after co-transduction, as we wanted to investigate the combined effects of α-syn$^{A53T}$ and the various LRRK2 fragments in DA neurons. Analysis by confocal microscopy showed that human α-syn expression in the SNc was high in TH-positive neurons (Fig. 2A). On average, 70% of neurons co-expressed both human α-syn$^{A53T}$ and the LRRK2 fragments (Fig. 2B).

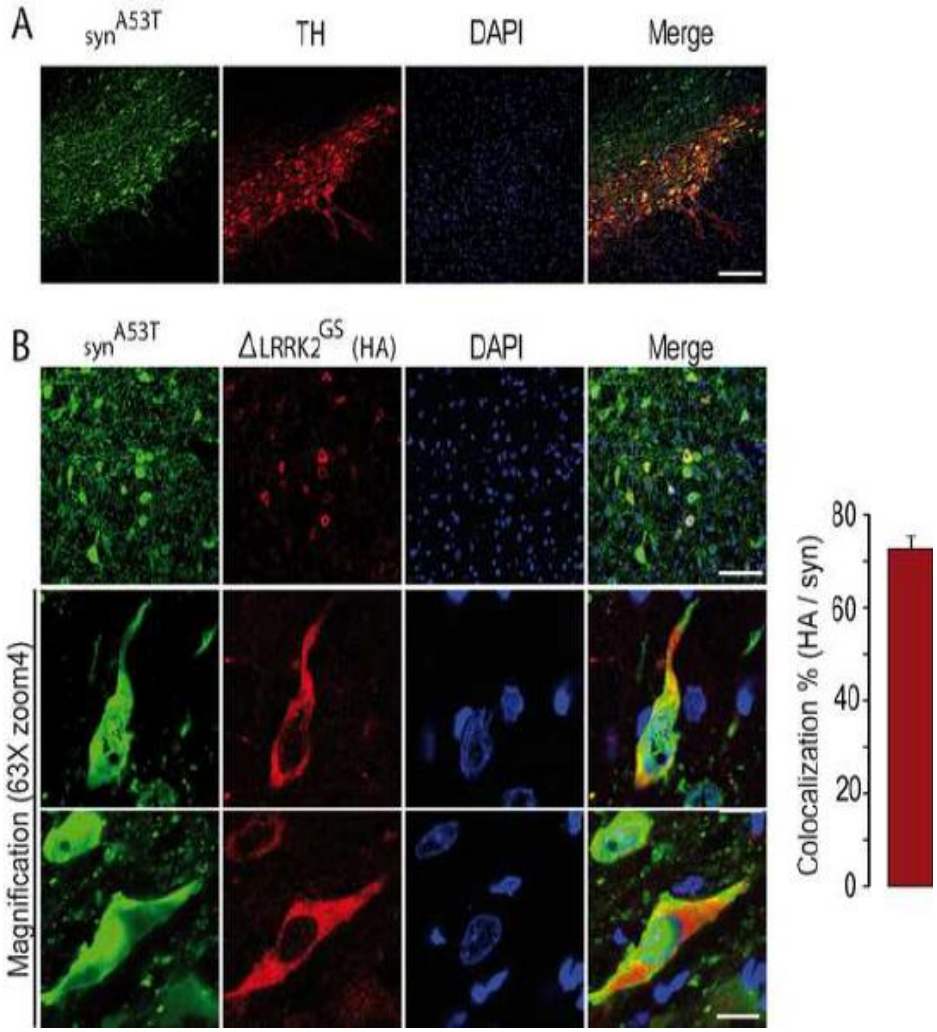


**Fig. 2 Histological evaluation of transgene expression in the SNpc at 15 weeks post-injection. (A) Evaluation of α-syn (in green) transduction in the SNpc. TH staining, in red. Scale bar: 500 µm. (B) Measurement of the number of neurons expressing both α-syn and ΔLRRK2GS. The higher magnification shows cytoplasm localization of ΔLRRK2GS. Results are expressed as means ± the standard error of the mean (SEM). Scale bars: 40X = 60 µm, 63X zoom 4 = 10 µm.**

We next evaluated the toxic effects of human α-syn$^{A53T}$ in the presence or absence of AAV-ΔLRRK2$^{G2019S}$. AAV-α-syn$^{A53T}$ alone produced a significant 38% loss of TH-positive cells, as measured by unbiased stereology in the SNc at 15 weeks PI (mean count ± SEM: Control, 12,344 ± 734; AAV-α-syn$^{A53T}$, 7,555 ± 527). The co-injection of AAV-α-syn$^{A53T}$ with AAV-GFP (as a control of viral load) induced a 46% loss of DA neurons, which was not statistically different from that obtained with AAV-α-syn$^{A53T}$ alone (6,601 ± 360). The co-injection of AAV-a-syn$^{A53T}$ and AAV-ΔLRRK2$^{G2019S}$ induced a loss (-55%) of DA neurons (mean count ± SEM: 5,585 ± 355) that was significantly greater than that measured in the two other groups injected with AAV-α-syn$^{A53T}$ (Fig. 3A). We evaluated the impact of SNc cell loss on the level of dopaminergic terminals in the dorso-medial striatum using TH-immunofluorescence in both the α-syn$^{A53T}$/GFP and α-syn$^{A53T}$/ΔLRRK2$^{G2019S}$ groups (Fig. 4A). These measurements were performed in the dorsal striatum, which receives projections from the injected SNc region. TH immunoreactivity in the striatum in both the α-syn$^{A53T}$/GFP and α-syn$^{A53T}$/ΔLRRK2$^{G2019S}$ groups was 15% lower than in the control group (PBS). This small α-syn$^{A53T}$-induced loss of TH-positive fibers was similar in the GFP and ΔLRRK2$^{G2019S}$ groups (Fig. 4C).

We also counted the number of SNc cells showing P-α-synS129 immunoreactivity, a marker of α-syn aggregation, in the different groups (Fig. 3C). The number of P-α-synS129-positive cells was

significantly lower in the group co-infected with AAV-α-syn$^{A53T}$ and AAV-ΔLRRK2$^{G2019S}$ than that of the groups infected with AAV-α-syn$^{A53T}$ alone or in combination with AAV-GFP (Fig. 3D). We also evaluated P-α-synS129 immunoreactivity in the striatum. Small P-α-synS129 immuno-positive objects with an elongated form or with a pearl necklace-like shape, reminiscent of neurite-like aggregates were seen in the striatum (Fig. 3E). Consistent with the results obtained in the SNc, we found lower levels of aggregated α-syn in the striatum of rats co-infected with AAV-α-syn$^{A53T}$ and AAV-ΔLRRK2$^{G2019S}$ than in those infected with AAV-α-syn$^{A53T}$ / GFP (Fig. 3E-F).

### Differential effects of AAV-ΔLRRK2$^{G2019S}$ and AAV-ΔLRRK2$^{G2019S/D1994A}$ on AAV-α-syn$^{A53T}$ toxicity

We next investigated whether the effect of AAV-ΔLRRK2$^{GS}$ on AAV-α-syn$^{A53T}$-induced toxicity was dependent on the kinase activity of the LRRK2 construct. We thus compared the effect of ΔLRRK2$^{G2019S}$ with that of the dead kinase form ΔLRRK2$^{DK}$. We examined an earlier time point PI (6 weeks) for these experiments. We reasoned that, although the kinase activity of ΔLRRK2$^{DK}$ is "dead", it may lead to cellular disturbances in long-term experiments because of its potential dominant-negative effect on endogenous LRRK2.

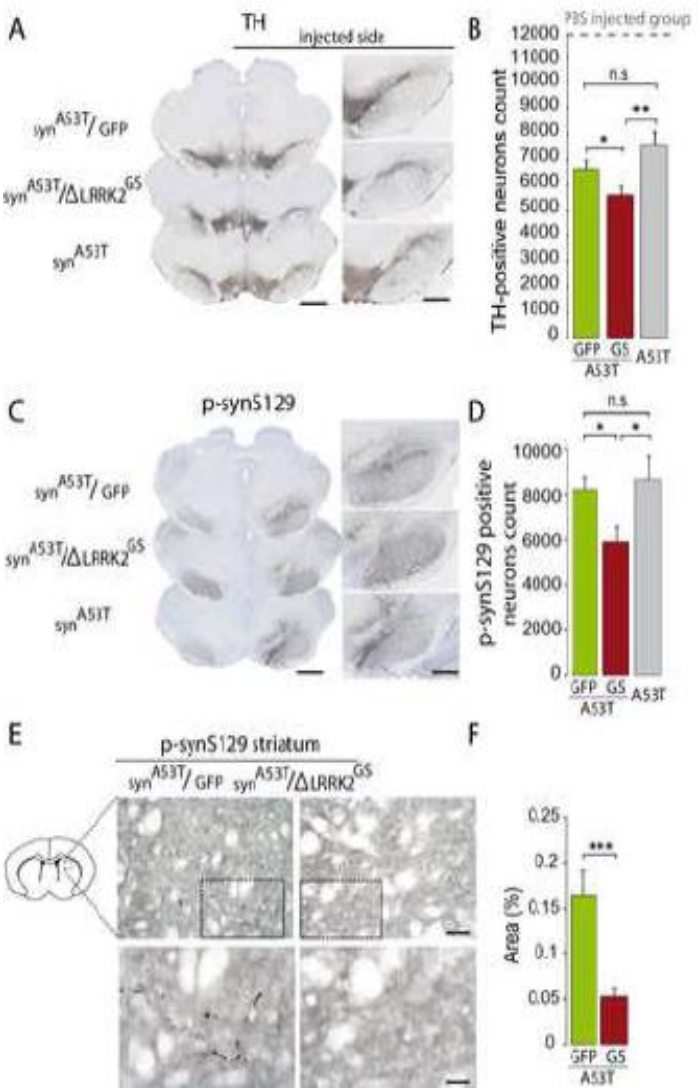


**Fig. 3 Immunohistochemistry for tyrosine hydroxylase (TH) and phospho-α-synS129 aggregates at 15 weeks post-injection. (A-D) Evaluation of the number of TH-positive and P-α-synS129-positive neurons by stereology in the SNpc. Scale bars: 750 µm, 400 µm. (E-F) Determination of the percentage of the area occupied by P-α-synS129-positive staining in the striatum at 15 weeks PI. Results are expressed as means ± the standard error of the mean (SEM). N = 10 animals/group. ANOVA and PLSD post hoc test. *P < 0.05, ***P < 0.001. Scale bars: 200 µm,50 µm.**

We first compared the levels of transgene expression after transduction with α-syn$^{A53T}$ and AAV-ΔLRRK2$^{G2019S}$ or AAV-ΔLRRK2$^{DK}$. Quantitative immunofluorescence analysis showed that almost the entire SNc was infected by AAV-α-syn$^{A53T}$ when co-infected with either AAV-ΔLRRK2$^{GS}$ or AAV-ΔLRRK2$^{DK}$ (Fig. 5). We also re-evaluated the co-localization of the LRRK2-related transgenes and α-syn$^{A53T}$ (Fig. 6). In total, 76% of neurons expressed both α-syn$^{A53T}$ and ΔLRRK2 (Fig. 6C), consistent with our observations in the experiments described above (see Fig. 1). We evaluated the level of fluorescence intensity corresponding to ΔLRRK2-HA staining at higher magnification. ΔLRRK2$^{GS}$ and ΔLRRK2$^{DK}$ were expressed at the same level in SNc neurons (Fig. 6C). In addition, human α-syn$^{A53T}$ protein was expressed at the same levels in neurons co-expressing ΔLRRK2$^{GS}$ and ΔLRRK2$^{DK}$ (Fig. 6C).

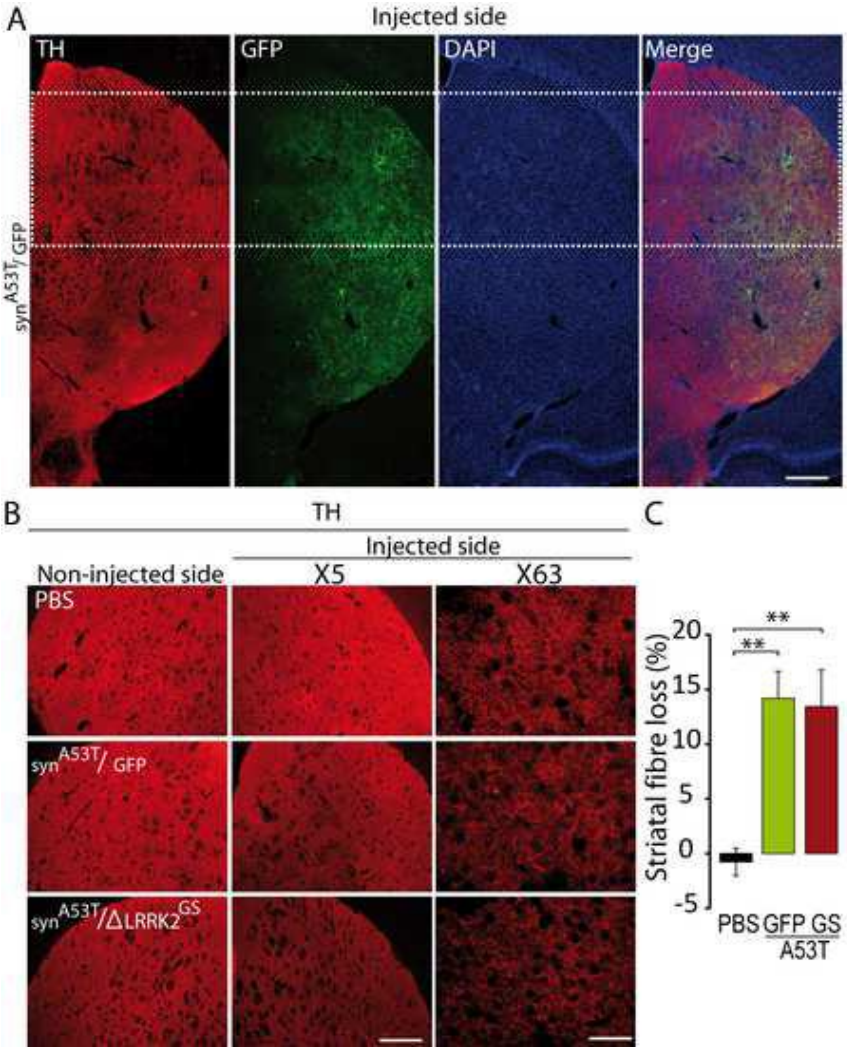


**Fig. 4 Immunohistochemistry for tyrosine hydroxylase (TH). (A) Evaluation of striatal fiber loss in the dorso-medial striatum by TH-immunofluorescence. Scale bar: 1000 µm. (B-C) Quantification of the mean grey value at a magnification of 5X. Results are expressed as means ± the standard error of the mean (SEM). N = 10 animals/group. ANOVA and PLSD post hoc test. **P < 0.01 (A-B) scale bar: 1000 µm. (B-C) scale bar: 100 µm.**

We then assessed the loss of DA neurons produced by AAV-α-syn$^{A53T}$ when co-injected with either AAV-ΔLRRK2$^{G2019S}$ or AAV-ΔLRRK2$^{DK}$. The loss of DA neurons induced by human α-syn$^{A53T}$ was significantly lower in the presence of ΔLRRK2$^{DK}$ than that in the presence of ΔLRRK2$^{GS}$ (Fig. 7A-B). The number of cells with P-α-synS129 immunoreactivity was similar in the ΔLRRK2$^{DK}$ and ΔLRRK2$^{G2019S}$ groups.

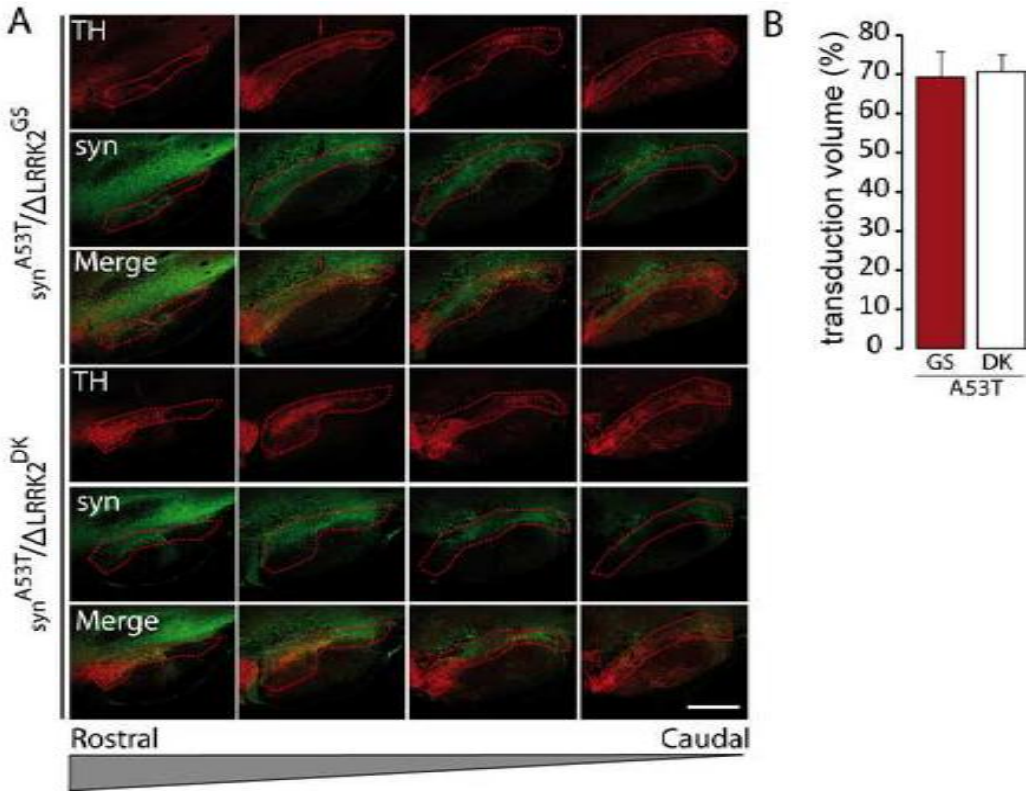


**Fig. 5 Measurement of transduction volume. A, confocal images to delineate the SNpc based on TH staining (in red), reported in the green channel, corresponding to the human α-syn protein when co-expressed with LRRK2G2019S (GS) and the dead kinase form of LRRK2. Scale bar: 1000 µm. B, Quantification of the fraction (%) of the SNpc expressing human α-syn protein after cotransduction with LRRK2G2019S or LRRK2DK. Note that the level of overexpression of human α-syn protein is similar between the two conditions. Results are expressed as means ± the standard error of the mean (SEM). N = 8 animals/group. No statistical difference, Student t test.**

Finally, we carried out a preliminary characterization of the status of microglial cells at this early time point (6 weeks PI), by immunohistochemistry using a validated marker (Iba1), because of the role of neuroinflammation in neurodegeneration observed in human α-syn$^{A53T}$ models. As expected, microglial cells in rats overexpressing human α-syn$^{A53T}$ appeared more reactive as compared to rats injected with vehicle. The quantification of immunofluorescence levels in the SN and striatum showed that human α-syn$^{A53T}$ significantly activated microglia. However, overexpression of ΔLRRK2$^{G2019S}$ and ΔLRRK2$^{DK}$ did not have any impact on the microglial activation induced by the mutant human α-syn (Supplementary Fig. S2).

Finally, we investigated whether the "pro-toxic" effect of ΔLRRK2$^{G2019S}$ on α-syn$^{A53T}$ could also be detected for other aggregating proteins. Using a different approach with lentiviral vectors in mice, we tested whether the different forms of ΔLRRK2 could modify the neurotoxicity produced by the N-terminal domain of human huntingtin (Htt) with a pathological expansion of its poly-glutamine (Q) region (Htt-N171-82Q) [30]. Lentiviral vectors were injected into the striatum of wildtype mice to produce local cell loss within the six weeks following transduction, as previously described [31,32]. The striatal lesions were characterized by the loss of neuronal markers DARPP32 and COX (not shown) as well as NeuN (Fig. 8A-B). Localization of the lesions in the striatum coincided with that of the expression of LRRK2 fragments detected using the HA-tag (Fig. 8C). Quantitative analysis of these histological markers showed that none of the ΔLRRK2 forms significantly modified the volume of the striatal

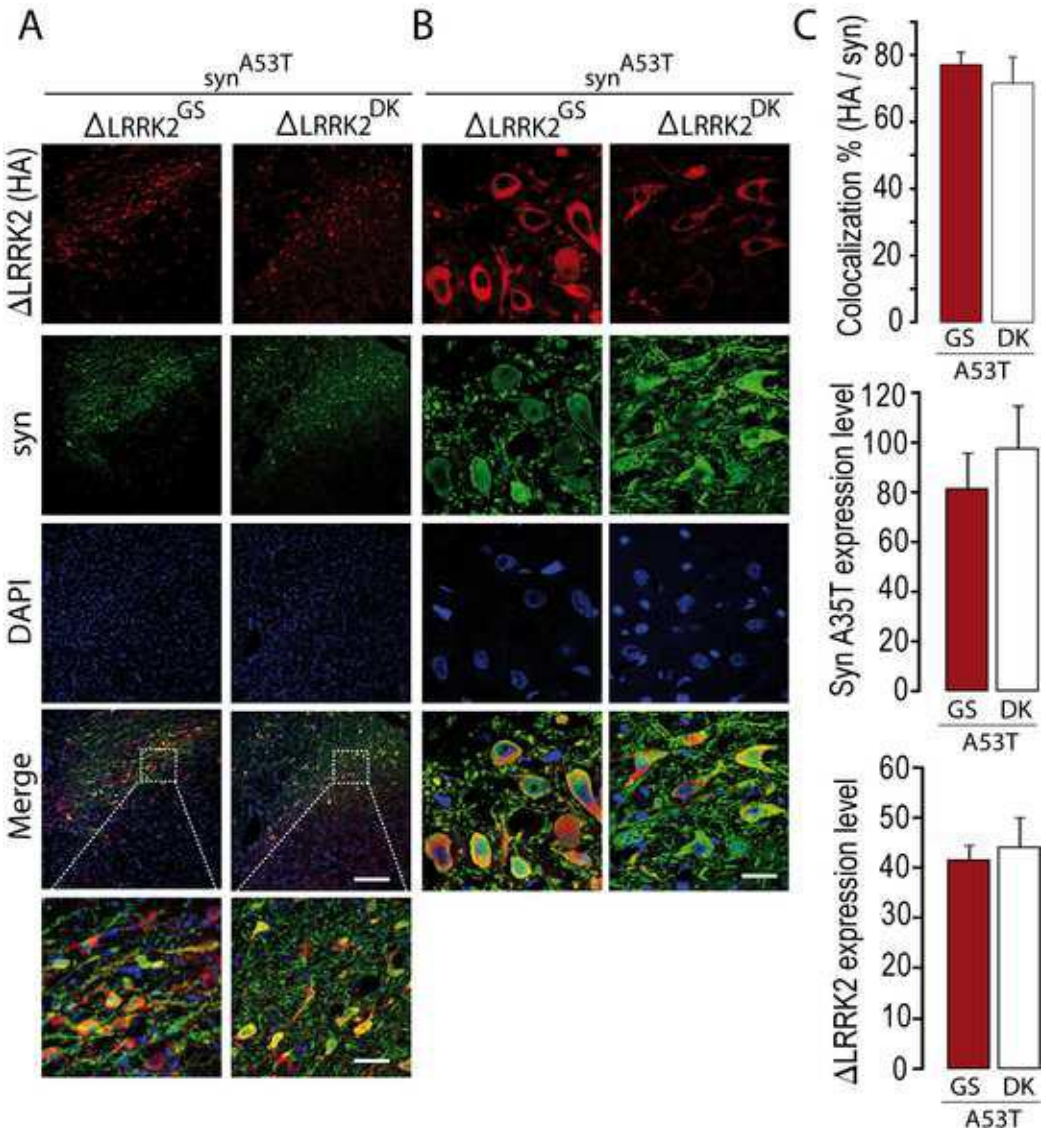


**Fig. 6 Co-localization and expression of ΔLRRK2 and α-syn. A-B, Double immuno-fluorescence of ΔLRRK2 and α-syn at low and high-magnification, showing co-expression of both transgenes at similar levels by most cells. Scale bars: 200 µm, magnifications = 50 µm and 10 µm. C, Quantification of the percentage of co-localization and protein levels (mean fluorescence) for two different groups. Results are expressed as means ± the standard error of the mean (SEM). N = 8 animals/group. No statistical difference, Student t test.**

lesions produced by mutant Htt (Fig. 8B). In addition, overexpression of the mutant Htt-fragment led to the accumulation of inclusions containing ubiquitin (mostly nuclear) (data not shown). Quantification of the presence of ubiquitin positive inclusions did not indicated differences within groups (Fig.8 D). We also selectively detected mutant Htt aggregates using the EM48 antibody which specifically recognizes the aggregated form of the N-terminal domain of mutant Htt [33–35]. ΔLRRK2$^{G2019S}$ significantly increased by 44% the number of EM48-positive aggregates when compared to the control group (LV-LacZ), an effect not seen with the WT or DK forms (Fig. 8D-E).

Our results show that the synergistic effect of ΔLRRK2$^{G2019S}$ on the toxicity of human α-syn$^{A53T}$ towards DA neurons depends on its kinase activity. Importantly, ΔLRRK2$^{G2019S}$ overexpression did not significantly increase the neurotoxic effects produced by a different aggregating protein, mutant Htt, suggesting that the effect of ΔLRRK2$^{G2019S}$ on α-syn$^{A53T}$-induced neurotoxicity is

not due to a general increase in the vulnerability of the neurons.

## Discussion

The mechanisms leading to the degeneration of DA neurons in LRRK2 mutation gene carriers with PD are unknown. It is generally accepted that the LRRK2$^{G2019S}$ mutation leads to increased kinase activity and that such abnormally increased kinase activity could lead to cell death [23,36–38].

In addition, a role for LRRK2 in α-syn toxicity has been suggested [26–28]. Indeed, neuropathological evaluation of the brain of PD patients with LRRK2 mutations shows in many cases the presence of *bona fide* LBs and Lewy neurites [39]. However, the role of the kinase in the crosstalk between LRRK2 and α-syn, especially how the kinase activity of LRRK2$^{G2019S}$ modulates α-syn neurotoxicity in the SNc is unknown. In addition, the respective roles of cell-autonomous and non-cell-autonomous mechanisms are largely unknown in this crosstalk.

Here, we used an AAV-based approach to selectively target SNc DA neurons and investigated how the C-terminal domain of LRRK2, harboring the G2019S mutation, with increased kinase activity, could modify the loss of DA neurons induced by the overexpression of α-syn$^{A53T}$ in the rat SNc. Under our experimental conditions, AAV-ΔLRRK2$^{G2019S}$ alone did not induce the loss of DA neurons and AAV-α-syn$^{A53T}$ alone induced a partial

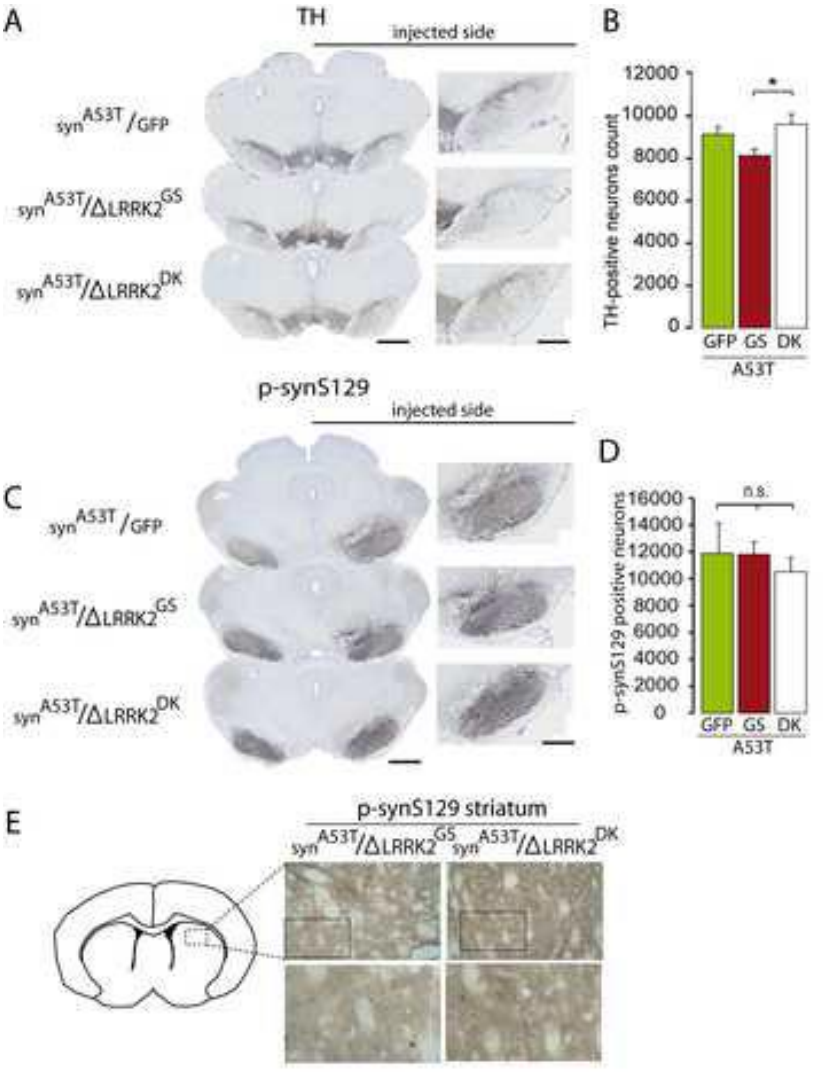


**Fig. 7 Immunohistochemistry for tyrosine hydroxylase (TH) and phospho-α-synS129 aggregates at six weeks post-injection. (A-D) Evaluation of the number of TH-positive and P-α- synS129-positive neurons in the SNc by stereology. Results are expressed as means ± the standard error of the mean (SEM). N = 10 animals/group. ANOVA and Fisher PLSD post hoc test. *, P < 0.05. Scale bar: 750 µm, 400 µm.**

loss. The loss of DA cells produced by co-expression of ΔLRRK2$^{G2019S}$ and α-syn$^{A53T}$ was significantly higher than that measured in rats injected with AAV-α-syn$^{A53T}$ alone or co-injected with a control vector (AAV-GFP). Conversely, overexpression of the inactive "kinase dead" form ΔLRRK2$^{DK}$, at levels similar to those of ΔLRRK2$^{G2019S}$, did not alter the toxicity of α-synA53T. Although preliminary, quantitative characterization of microglial reactivity induced by human -α-syn$^{A53T}$ in SNc and striatum did not show obvious changes attributable to LRRK2 fragments. These novel findings further support the hypothesis that the C-terminal domain of LRRK2$^{G2019S}$ is sufficient to augment the toxic effects of α-syn$^{A53T}$ through a cell-autonomous mechanism involving the catalytic activity of its kinase domain.

The histological evaluation we performed after transduction of the SNc with AAV and AAV-ΔLRRK2$^{G2019S}$ show that both transgenes were overexpressed in DA neurons. In both cases, approximately 70% of the SNc was infected. After co-injection, co-localization of both transgenes was found in most neurons in the SNc. Neuropathological evaluation at 15 weeks PI after transduction with AAV-α-syn$^{A53T}$ showed the partial loss of DA neurons, based on the detection of TH-positive cells. This

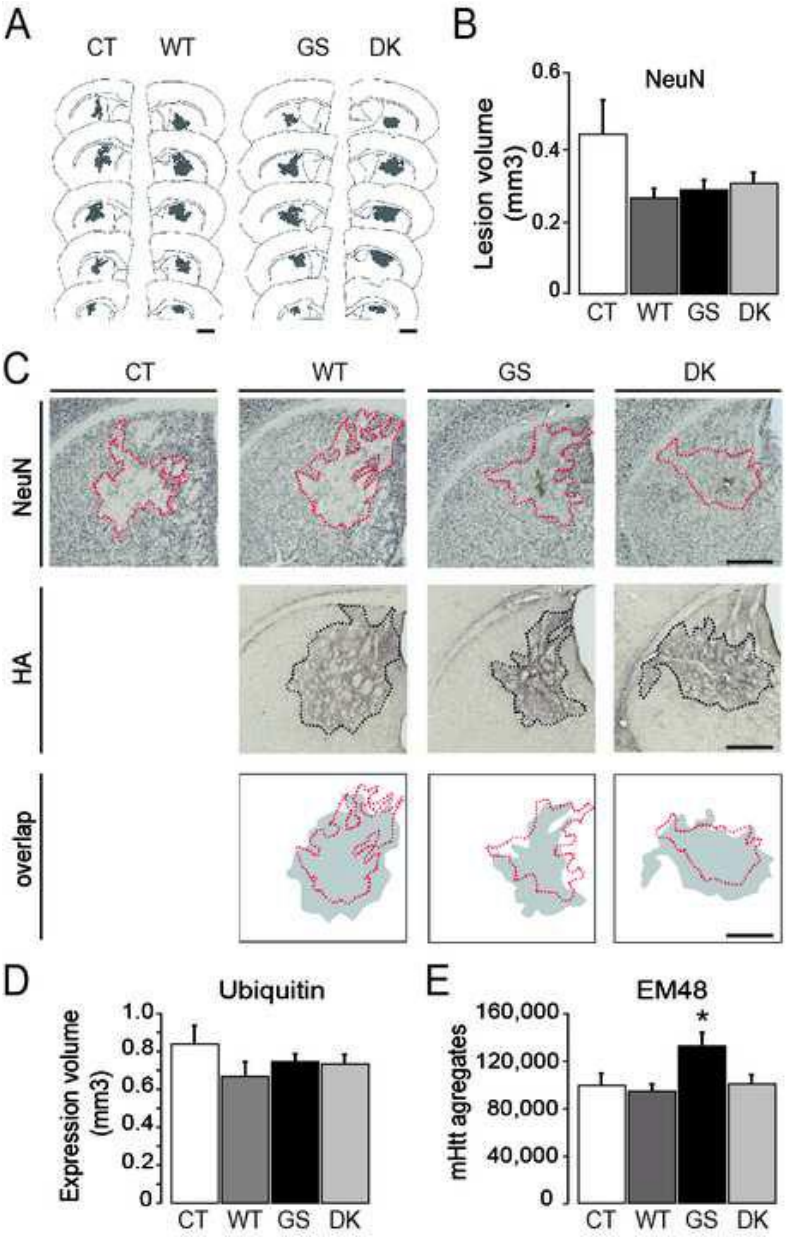


**Fig. 8 Effect of the various forms of ΔLRRK2 on the toxicity of mutant Htt Mice received a bilateral intrastriatal injection of a mixture of two lentiviral vectors (LV): LV-Htt171- 82Q with LV-LacZ (CT, control), LV-ΔLRRK2WT (WT), LV-LRRK2G2019S (GS) or LV-ΔLRRK2G2019S/A1994E (DK). Six weeks after injection, brains were processed for histological evaluation by immunohistochemistry (ICH) for the HA-tag, NeuN, ubiquitin and mutant Htt aggregates using the EM48 antibody to evaluate Htt171-82Q-dependent neurotoxicity. (A) Camera Lucida representation of the rostro-caudal extension of striatal lesions produced by the mutant Htt fragment as seen using NeuN ICH. Dark gray spots in the striatum represent area with loss of NeuN staining (lesions). (B) Histograms of the volumes of the striatal lesions for the four groups. (C) Photomicrographs of the mouse striatum showing that lesions superimposed with HA tag-positive areas in the 3 ΔLLRK2 groups. (D, E) Histograms showing quantification of mutant Htt inclusions (ubiquitin) and aggregates (EM48). Note the absence of major effects of ΔLLRK2 constructs on mutant Htt toxicity, except for a mild increase of the number of EM48 aggregates in the ΔLLRK2G2019S group. Results are expressed as the mean ± the standard error of the mean (SEM). N = 10-12/group. One-way ANOVA and post hoc Fisher's PLSD test. *, p<0.05,**

likely reflects neuronal loss, as suggested in our previous work [29].

The relevance of overexpressing the C-terminal domain of LRRK2 *versus* the full-length protein is potentially debatable. Indeed, ΔLRRK2$^{G2019S}$ lacks N-terminal domains that are known to play crucial roles in LRRK2 function. we previously showed that overexpression of the ΔLRRK2$^{G2019S}$ fragment using AAVs triggers neurodegeneration of DA neurons six months post-transduction, whereas the ΔLRRK2$^{WT}$ fragment, expressed at similar high levels, was devoid of obvious neurotoxicity [29]. Cell death produced by this fragment which has a detectable kinase activity is likely independent of the interaction with RAB10, since the ΔLRRK2 fragment was found unable to interact with RAB10, in contrary to full-length LRRK2 fragment [29]. Thus, it is conceivable that the overexpression of ΔLRRK2$^{G2019S}$ leads to abnormal/higher phosphorylation of substrates, relative to that by the overexpression of ΔLRRK2$^{WT}$, that is at least partially in common with that of full-length LRRK2 [40–43].

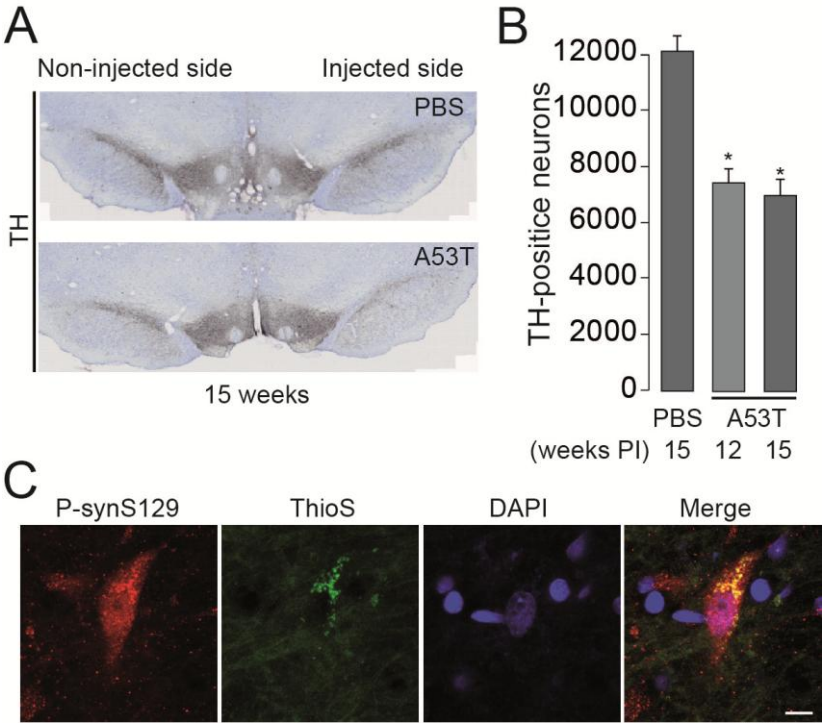


**Supp Fig 1 Results of the pilot experiments carried out to set up the AAV-α-synA53T model, characterized by partial degeneration of DA neurons in the SNc of adult rats. (A, B) AAV-α- synA53T produced partial loss of TH-positive neurons in the SNc at 12 and 15 weeks post injection. Stereological cell count in B shows significant loss compared to control rats of the same age (injected with PBS). Neurons in the SNc after infection were found to be immune-positive for the phosphorylated form of α-syn at serine 129 (P-synS129) and thioflavin S (ThioS) fluorescence suggesting aggregation of α-synS129. Results are expressed as the mean ± the standard error of the mean (SEM). One-way ANOVA and post hoc Fisher's PLSD test. *, p<0.01. Scale bar in C, 10 µm.**

We investigated whether ΔLRRK2$^{G2019S}$ effect on α-syn$^{A53T}$ was specific of these two pathological proteins, or only resulted from a non-specific vulnerability of neurons expression the LRRK2 fragment. We tested in a different cellular context the effect of ΔLRRK2$^{G2019S}$ against mutant Htt in the striatum using a simple approach with lentiviral vectors. In this case, the degeneration of striatal neurons induced by mutant Htt within the 6 weeks PI was not significantly changed by the overexpression of ΔLRRK2$^{G2019S}$. Thus the effect of ΔLRRK2$^{G2019S}$ upon α-syn$^{A53T}$ toxicity is likely specific of a particular interplay between these two proteins.

The present experimental paradigm using AAVs allowed addressing the question of the potential cell-autonomous exacerbation of α-syn$^{A53T}$ toxicity by the kinase activity of LRRK2 directly in the SNc and only in neurons. In contrast, other viral vector models (HSV or adeno) also transduce different cell types in the striatum [44,45]. Here, we directly investigated whether there is a functional interaction between AAV-α-syn$^{A53T}$ and-ΔLRRK2$^{G2019S}$ in DA neurons. Our results show the existence of such an interaction, as overexpression of ΔLRRK2$^{G2019S}$ significantly enhanced the neurotoxic effects of α-syn$^{A53T}$ in rat SNc. Lin *et al.* showed that the overexpression of

LRRK2 (wildtype or with the G2019S mutation) in forebrain neurons (striatum and cerebral cortex) increased the toxicity of α-syn$^{A53T}$ in transgenic animals [28]. In these double-transgenic mice, the authors found significant degeneration of the striatum and cortex and enhanced accumulation of α-syn aggregates. This proved the existence of a functional cross talk between α-syn and LRRK2 in neurons *in vivo* when the proteins are expressed at relatively high levels. Pathological transgenes were not expressed in the SNc and no DA degeneration was detected in these models. The CamKIIα promoter used to drive the expression of the tetracycline transactivator (tTA), which activates the TetO promoter of the LRRK2 and α-syn$^{A53T}$ transgenes in these mice, is likely not active in SNc DA neurons, as endogenous expression of CamKIIα in neurons of the SNc is lower than that observed in forebrain neurons. In LRRK2 knockout rats, the toxicity induced by AAV coding for α-syn is lower than that in wildtype rats [27]. Daher *et al.* found no synergy between the transgenes following the crossbreeding of other transgenic models in which the promoters driving LRRK2$^{G2019S}$ and α-syn$^{A53T}$ expression were different (Prion and CMV respectively) [46]. These observations and our results suggest that the crosstalk between LRRK2 and α-syn can occur in the same neurons. Thus, our results show that synergy between LRRK2 and α-syn depends, at least in part, on cell-autonomous mechanisms. However, our results also indicate that even in an experimental condition where the two proteins are expressed in high levels (approximately 5-50 fold the level of endogenous α-syn and LRRK2 respectively), the effect of ΔLRRK2$^{G2019S}$ on α-synA53T is moderate. Thus, it is reasonable to speculate that in a condition where physiological levels of expression of LRRK2 and α-syn, the cell-autonomous crosstalk between the two proteins might be of moderate importance in DA neurons. Non-cell autonomous mechanisms involving interaction of DA neurons with neighboring glial cells and immune cells may have more important roles in patients and transgenic animal models. For example, it has been recently shown that the seeding of α-syn

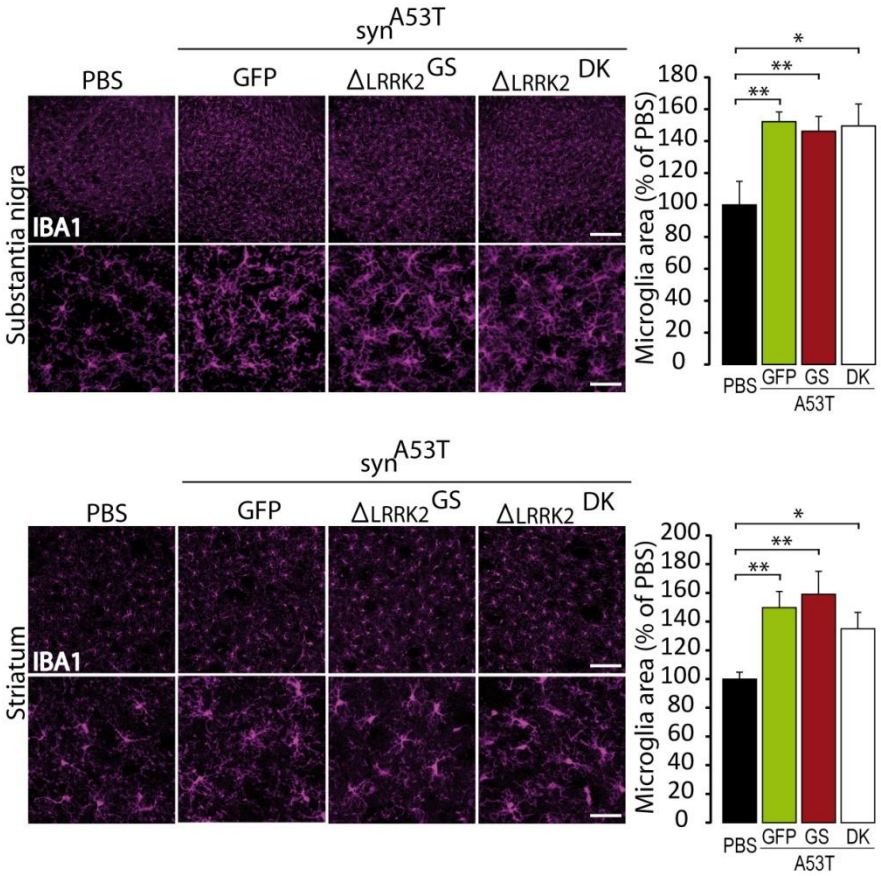


**Supp Fig 2 Evaluation of microglial activation (microglia fluorescent area) based on IBA1 immunofluorescence in the SNc (A-B) and striatum (C-D). Results are expressed as the percentage of staining of the control group (PBS). Results are expressed as the mean ± the standard error of the mean (SEM). N = 8 animals/group. ANOVA and PLSD post hoc test (SNc) and Kruskal-Wallis and Mann-Whitney test (striatum). *, p < 0.05; **, p<0.01. Scale bar: low magnification, 200 µm; high magnifications, 50 µm.**

aggregates by the exposure of neurons to α-syn fibrils is higher in neurons expressing mutant LRRK2 [47]. The level of LRRK2 activity in microglial cells may also regulate protoxic phenomena associated with α-syn-induced neuroinflammation [26,48,49]. LRRK2 plays a key role in the immune system [50]. A single nucleotide polymorphism (N2081D) in the region coding for kinase domain of LRRK2 is a major risk factors for Crohn disease, a form of inflammatory bowel disease [51].

We investigated whether ΔLRRK2$^{G2019S}$ effect on α-syn$^{A53T}$ was specific of these two pathological proteins, or only resulted from a non-specific vulnerability of neurons expression the LRRK2 fragment. We tested in a different cellular context the effect of ΔLRRK2$^{G2019S}$ against mutant Htt in the striatum using a simple approach with lentiviral vectors. In this case, the degeneration of striatal neurons induced by mutant Htt within the 6 weeks PI was not significantly changed by the overexpression of ΔLRRK2$^{G2019S}$. Thus the effect of ΔLRRK2$^{G2019S}$ upon α-syn$^{A53T}$ toxicity is likely specific of functional interplay between these two proteins.

The neuronal mechanisms underlying the synergy between LRRK2 and α-syn are ill defined. It is possible that LRRK2 - α-syn$^{A53T}$ interplay involves a direct physical interaction between the two proteins [52], although, indirect effects leading to a functional interplay is more often discussed. In addition, the role of the kinase domain of LRRK2 is unclear. It is generally accepted that the higher kinase activity of LRRK2$^{G2019S}$, relative to that of wild-type LRRK2, leads to neurodegeneration through increased phosphorylation of substrates, possibly through multifactorial cellular changes, including the disruption of microtubule assembly, mitochondrial defects, and alterations in protein translation [53]. However, whether the increased kinase activity of LRRK2 mutations plays a key role is still a subject of debate. As already mentioned, various transgenic rodent models expressing LRRK2$^{G2019S}$ have been developed and extensively characterized. These models display no (or very limited) degeneration of DA cells in the SNc. Various experimental approaches clearly demonstrate that the severity of the resulting toxicity is dependent on the level of expression of LRRK2$^{G2019S}$ [54]. There is limited evidence obtained *in vivo* that shows a relationship between the higher kinase activity of LRRK2$^{G2019S}$ and neurotoxicity to dopaminergic cells of the SNc. The overexpression of LRRK2$^{G2019S}$ (or ΔLRRK2$^{G2019S}$) in the SNc was found to induce the loss of DA neurons using HSV and adenovirus models injected into the striatum [23,55], as well as in our previous study with AAV-ΔLRRK2$^{G2019S}$ injected into the SNc [56].

Only a few studies have directly addressed the role of the kinase in the interaction between α-syn and LRRK2 toxicity. It was shown that neuroinflammation and neurodegeneration produced by the transduction of the SNc with AAV-α-syn is significantly attenuated in LRRK2 KO rats relative to that in wildtype littermates. In these experiments, the role of the kinase activity was not assessed [26]. More recently, Daher *et al.* showed that the toxicity of AAV-α-synuclein in the SNc was higher in transgenic LRRK2$^{G2019S}$ than wildtype rats. Interestingly, treatment of both genotypes with the LRRK2 inhibitor PF-06447475 (PF) reduced the toxicity of α-syn [27]. This suggests that the exacerbation of α-syn toxicity by LRRK2$^{G2019S}$ could result from elevated catalytic activity of the kinase. However, LRRK2 inhibitors, including PF, destabilize LRRK2, leading to reduced cellular levels of the protein [57]. Thus, protection by PF against combined α-syn/LRRK2$^{G2019S}$ toxicity may result from the reduction of LRRK2 levels rather than actual inhibition of the catalytic activity of the kinase. Here, we found that overexpression of the inactive protein ΔLRRK2$^{G2019S/D1994S}$ did not alter the toxicity AAV-α-syn$^{A53T}$, whereas expression of ΔLRRK2$^{G2019S}$ increased the toxicity of AAV-α-syn$^{A53T}$ towards DA neurons. In our experimental system where both proteins have high expression levels, we were able to verify that the difference between the toxicity

of ΔLRRK2$^{G2019S}$ and ΔLRRK2$^{DK}$ was not related to a difference in protein levels. Quantitative confocal analysis showed that the levels of the two proteins were similar in DA neurons *in vivo*. Thus, it is likely that the difference between the effects of ΔLRRK2$^{WT}$ and ΔLRRK2$^{G2019S}$ is mainly due to their different kinase activities.

## Conclusion

Our results suggest that the C-terminal domain of LRRK2$^{G2019S}$ containing the ROC-COR, Kinase and WD40 domains is sufficient to potentiate the toxicity of human α-syn$^{A53T}$ in DA neurons *in vivo* and that this effect is kinase-dependent. This cell-autonomous mechanism may additively or synergistically acts with other non-cell-autonomous mechanisms, especially those involving neuro-inflammation to trigger the death of DA neurons in PD. Our findings further support the view that inhibition of the kinase activity of LRRK2 might be beneficial to slow α-syn-dependent mechanisms in PD.


## Acknowledgements/Funding

This work was funded by rolling grants from the CEA and the CNRS. The research leading to these results received funding from la Fondation de France (Parkinson Committee, AAP 2010, Engt 00016819 and AAP 2014, Engt 2014-0052580). Noemie Cresto and Pauline Roost are recipients of PhD fellowships from the Association France Parkinson (2016 and 2019 respectively). This work benefited from support from the national "Translational Research Infrastructure for Biotherapies in Neurosciences" (NeurATRIS, "Investissement d'Avenir", ANR-11-INBS-0011).

## References


1. Braak H, Braak E. Pathoanatomy of Parkinson's disease. J Neurol. 2000;247:II3–10.

2. Chartier-Harlin MC, Kachergus J, Roumier C, Mouroux V, Douay X, Lincoln S, et al. alpha-Synuclein locus duplication as a cause of familial Parkinson's disease. Lancet. 2004;364:1167–1169.

3. Cobb MM, Ravisankar A, Skibinski G, Finkbeiner S. iPS cells in the study of PD molecular pathogenesis. Cell Tissue Res. 2018;373:61–77.

4. Lesage S, Brice A. Parkinson's disease: from monogenic forms to genetic susceptibility factors. Hum Mol Genet. 2009;18:R48–59.

5. Singleton AB, Farrer M, Johnson J, Singleton A, Hague S, Kachergus J, et al. alpha-Synuclein locus triplication causes Parkinson's disease. Science. 2003;302:841.

6. Polymeropoulos MH, Lavedan C, Leroy E, Ide SE, Dehejia A, Dutra A, et al. Mutation in the α-Synuclein Gene Identified in Families with Parkinson's Disease. Science. 1997;276:2045–7.

7. Krüger R, Kuhn W, Müller T, Woitalla D, Graeber M, Kösel S, et al. AlaSOPro mutation in the gene encoding α-synuclein in Parkinson's disease. Nat Genet. 1998;18:106–8.

8. Zarranz JJ, Alegre J, Gómez-Esteban JC, Lezcano E, Ros R, Ampuero I, et al. The new mutation, E46K, of α-synuclein causes parkinson and Lewy body dementia. Ann Neurol. 2004;55:164–73.

9. Saito Y, Kawashima A, Ruberu NN, Fujiwara H, Koyama S, Sawabe M, et al. Accumulation of Phosphorylated α-Synuclein in Aging Human Brain. J Neuropathol Exp Neurol. 2003;62:644–54.

10. Paisán-Ruíz C, Jain S, Evans EW, Gilks WP, Simón J, van der Brug M, et al. Cloning of the Gene Containing Mutations that Cause PARK8-Linked Parkinson's Disease. Neuron. 2004;44:595–600.

11. Zimprich A, Biskup S, Leitner P, Lichtner P, Farrer M, Lincoln S, et al. Mutations in LRRK2 Cause Autosomal-Dominant Parkinsonism with Pleomorphic Pathology. Neuron. 2004;44:601–7.

12. Gilks WP, Abou-Sleiman PM, Gandhi S, Jain S, Singleton A, Lees AJ, et al. A common LRRK2 mutation in idiopathic Parkinson's disease. The Lancet. 2005;365:415–6.

13. Healy DG, Falchi M, O'Sullivan SS, Bonifati V, Durr A, Bressman S, et al. Phenotype, genotype, and worldwide genetic penetrance of LRRK2-associated Parkinson's disease: a case-control study. Lancet Neurol. 2008;7:583–90.

14. Biskup S, West AB. Zeroing in on LRRK2-linked pathogenic mechanisms in Parkinson's disease. Biochim Biophys Acta BBA - Mol Basis Dis. 2009;1792:625–33.

15. Yahalom G, Orlev Y, Cohen OS, Kozlova E, Friedman E, Inzelberg R, et al. Motor progression of Parkinson's disease with the leucine-rich repeat kinase 2 G2019S mutation: Disease progression in PD with G2019S mutation. Mov Disord. 2014;29:1057–60.

16. Cresto N, Gardier C, Gubinelli F, Gaillard M-C, Liot G, West AB, et al. The Unlikely Partnership Between LRRK2 and α-Synuclein in Parkinson's Disease. Eur J Neurosci. 2018;0–1.

17. Ben Romdhan S, Farhat N, Nasri A, Lesage S, Hdiji O, Ben Djebara M, et al. LRRK2 G2019S Parkinson's disease with more benign phenotype than idiopathic. Acta Neurol Scand. 2018;138:425–31.

18. Sayad M, Zouambia M, Chaouch M, Ferrat F, Nebbal M, Bendini M, et al. Greater improvement in LRRK2 G2019S patients undergoing Subthalamic Nucleus Deep Brain Stimulation compared to non-mutation carriers. BMC Neurosci. 2016;17:6.

19. Zimprich A, Biskup S, Leitner P, Lichtner P, Farrer M, Lincoln S, et al. Mutations in LRRK2 cause autosomal-dominant parkinsonism with pleomorphic pathology. Neuron. 2004;44:601–607.

20. Kalia LV, Lang AE, Hazrati L-N, Fujioka S, Wszolek ZK, Dickson DW, et al. Clinical Correlations With Lewy Body Pathology in LRRK2-Related Parkinson Disease. JAMA Neurol. 2015;72:100–5.

21. Brockmann K, Gröger A, Di Santo A, Liepelt I, Schulte C, Klose U, et al. Clinical and brain imaging characteristics in leucine-rich repeat kinase 2-associated PD and asymptomatic mutation carriers. Mov Disord Off J Mov Disord Soc. 2011;26:2335–42.

22. Oosterveld LP, Allen JC, Ng EYL, Seah S-H, Tay K-Y, Au W-L, et al. Greater motor progression in patients with Parkinson disease who carry LRRK2 risk variants. Neurology. 2015;85:1039–42.

23. Lee BD, Shin J-H, VanKampen J, Petrucelli L, West AB, Ko HS, et al. Inhibitors of Leucine Rich Repeat Kinase 2 (LRRK2) Protect Against LRRK2-Models of Parkinson's Disease. Nat Med. 2010;16:998–1000.

24. West AB, Moore DJ, Choi C, Andrabi SA, Li X, Dikeman D, et al. Parkinson's disease-associated mutations in LRRK2 link enhanced GTP-binding and kinase activities to neuronal toxicity. Hum Mol Genet. 2007;16:223–32.

25. Cresto N, Gardier C, Gubinelli F, Gaillard M-C, Liot G, West AB, et al. The unlikely partnership between LRRK2 and α-synuclein in Parkinson's disease. Eur J Neurosci. 2019;49:339–63.

26. Daher JPL, Volpicelli-Daley LA, Blackburn JP, Moehle MS, West AB. Abrogation of α-synuclein–mediated dopaminergic neurodegeneration in LRRK2-deficient rats. Proc Natl Acad Sci U S A. 2014;111:9289–94.

27. Daher JPL, Abdelmotilib HA, Hu X, Volpicelli-Daley LA, Moehle MS, Fraser KB, et al. Leucine-rich Repeat Kinase 2 (LRRK2) Pharmacological Inhibition Abates α-Synuclein Gene-induced Neurodegeneration. J Biol Chem. 2015;290:19433–44.

28. Lin X, Parisiadou L, Gu X-L, Wang L, Shim H, Sun L, et al. Leucine-rich repeat kinase 2 regulates the progression of neuropathology induced by Parkinson's-disease-related mutant alpha-synuclein. Neuron. 2009;64:807–27.

29. Cresto N, Gaillard M-C, Gardier C, Gubinelli F, Diguet E, Bellet D, et al. The C-terminal domain of LRRK2 with the G2019S mutation is sufficient to produce neurodegeneration of dopaminergic neurons in vivo. Neurobiol Dis. 2020;134:104614.

30. Ruiz M, Déglon N. Viral-mediated overexpression of mutant huntingtin to model HD in various species. Neurobiol Dis. 2012;48:202–11.

31. Francelle L, Galvan L, Gaillard M-C, Guillermier M, Houitte D, Bonvento G, et al. Loss of the thyroid hormone-binding protein Crym renders striatal neurons more vulnerable to mutant huntingtin in Huntington's disease. Hum Mol Genet. 2015;24:1563–73.

32. Galvan L, Francelle L, Gaillard M-C, de Longprez L, Carrillo-de Sauvage M-A, Liot G, et al. The striatal kinase DCLK3 produces neuroprotection against mutant huntingtin. Brain. 2018;141:1434–54.

33. Damiano M, Diguet E, Malgorn C, D'Aurelio M, Galvan L, Petit F, et al. A role of mitochondrial complex II defects in genetic models of Huntington's disease expressing N-terminal fragments of mutant huntingtin. Hum Mol Genet. 2013;22:3869–82.

34. Diguet E, Petit F, Escartin C, Cambon K, Bizat N, Dufour N, et al. Normal aging modulates the neurotoxicity of mutant huntingtin. PloS One. 2009;4:e4637.

35. Gutekunst CA, Li SH, Yi H, Mulroy JS, Kuemmerle S, Jones R, et al. Nuclear and neuropil aggregates in Huntington's disease: relationship to neuropathology. J Neurosci Off J Soc Neurosci. 1999;19:2522–34.

36. Greggio E, Jain S, Kingsbury A, Bandopadhyay R, Lewis P, Kaganovich A, et al. Kinase activity is required for the toxic effects of mutant LRRK2/dardarin. Neurobiol Dis. 2006;23:329–341.

37. Smith WW, Pei Z, Jiang H, Dawson VL, Dawson TM, Ross CA. Kinase activity of mutant LRRK2 mediates neuronal toxicity. Nat Neurosci. 2006;9:1231–3.

38. West AB, Moore DJ, Choi C, Andrabi SA, Li X, Dikeman D, et al. Parkinson's disease-associated mutations in LRRK2 link enhanced GTP-binding and kinase activities to neuronal toxicity. Hum Mol Genet. 2007;16:223–32.

39. Giasson BI, Covy JP, Bonini NM, Hurtig HI, Farrer MJ, Trojanowski JQ, et al. Biochemical and pathological characterization of Lrrk2. Ann Neurol. 2006;59:315–22.

40. Deng J, Lewis PA, Greggio E, Sluch E, Beilina A, Cookson MR. Structure of the ROC domain from the Parkinson's disease-associated leucine-rich repeat kinase 2 reveals a dimeric GTPase. Proc Natl Acad Sci U S A. 2008;105:1499–504.

41. Gloeckner CJ, Kinkl N, Schumacher A, Braun RJ, O'Neill E, Meitinger T, et al. The Parkinson disease causing LRRK2 mutation I2020T is associated with increased kinase activity. Hum Mol Genet. 2006;15:223–32.

42. Greggio E, Zambrano I, Kaganovich A, Beilina A, Taymans J-M, Daniëls V, et al. The Parkinson Disease-associated Leucine-rich Repeat Kinase 2 (LRRK2) Is a Dimer That Undergoes Intramolecular Autophosphorylation. J Biol Chem. 2008;283:16906–14.

43. Ito G, Iwatsubo T. Re-examination of the dimerization state of leucine-rich repeat kinase 2: predominance of the monomeric form. Biochem J. 2012;441:987–98.

44. Melrose HL, Dächsel JC, Behrouz B, Lincoln SJ, Yue M, Hinkle KM, et al. Impaired dopaminergic neurotransmission and microtubule-associated protein tau alterations in human LRRK2 transgenic mice. Neurobiol Dis. 2010;40:503–17.

45. Ramonet D, Daher JPL, Lin BM, Stafa K, Kim J, Banerjee R, et al. Dopaminergic Neuronal Loss, Reduced Neurite Complexity and Autophagic Abnormalities in Transgenic Mice Expressing G2019S Mutant LRRK2. PLoS ONE [Internet]. 2011 [cited 2016 Jan 12];6. Available from: http://www.ncbi.nlm.nih.gov/pmc/articles/PMC3071839/

46. Daher JPL, Pletnikova O, Biskup S, Musso A, Gellhaar S, Galter D, et al. Neurodegenerative phenotypes in an A53T α-synuclein transgenic mouse model are independent of LRRK2. Hum Mol Genet. 2012;21:2420–31.

47. Volpicelli-Daley LA, Abdelmotilib H, Liu Z, Stoyka L, Daher JPL, Milnerwood AJ, et al. G2019S-LRRK2 Expression Augments α-Synuclein Sequestration into Inclusions in Neurons. J Neurosci. 2016;36:7415–27.

48. Maekawa T, Sasaoka T, Azuma S, Ichikawa T, Melrose HL, Farrer MJ, et al. Leucine-rich repeat kinase 2 (LRRK2) regulates α-synuclein clearance in microglia. BMC Neurosci. 2016;17:77.

49. Russo I, Bubacco L, Greggio E. LRRK2 and neuroinflammation: partners in crime in Parkinson's disease? J Neuroinflammation. 2014;11:52.

50. Dzamko NL. LRRK2 and the Immune System. Adv Neurobiol. 2017;14:123–43.

51. Hui KY, Fernandez-Hernandez H, Hu J, Schaffner A, Pankratz N, Hsu N-Y, et al. Functional variants in the LRRK2 gene confer shared effects on risk for Crohn's disease and Parkinson's disease. Sci Transl Med. 2018;10.

52. Guerreiro PS, Huang Y, Gysbers A, Cheng D, Gai WP, Outeiro TF, et al. LRRK2 interactions with α-synuclein in Parkinson's disease brains and in cell models. J Mol Med. 2013;91:513–522.

53. Rosenbusch KE, Kortholt A. Activation Mechanism of LRRK2 and Its Cellular Functions in Parkinson's Disease. Park Dis. 2016;2016:7351985.

54. Skibinski G, Nakamura K, Cookson MR, Finkbeiner S. Mutant LRRK2 Toxicity in Neurons Depends on LRRK2 Levels and Synuclein But Not Kinase Activity or Inclusion Bodies. J Neurosci. 2014;34:418–33.

55. Dusonchet J, Kochubey O, Stafa K, Young SM, Zufferey R, Moore DJ, et al. A Rat Model of Progressive Nigral Neurodegeneration Induced by the Parkinson's Disease-Associated G2019S Mutation in LRRK2. J Neurosci. 2011;31:907–12.

56. Cresto N, Gaillard M-C, Gardier C, Gubinelli F, Diguet E, Bellet D, et al. The C-terminal domain of LRRK2 with the G2019S mutation is sufficient to produce neurodegeneration of dopaminergic neurons in vivo. Neurobiol Dis. 2019;134:104614.

57. Lobbestael E, Civiero L, Wit TD, Taymans J-M, Greggio E, Baekelandt V. Pharmacological LRRK2 kinase inhibition induces LRRK2 protein destabilization and proteasomal degradation. Sci Rep. 2016;6:33897.

58. Berger A, Lorain S, Joséphine C, Desrosiers M, Peccate C, Voit T, et al. Repair of Rhodopsin mRNA by Spliceosome-Mediated RNA Trans-Splicing: A New Approach for Autosomal Dominant Retinitis Pigmentosa. Mol Ther. 2015;23:918–30.

59. Aurnhammer C, Haase M, Muether N, Hausl M, Rauschhuber C, Huber I, et al. Universal real-time PCR for the detection and quantification of adeno-associated virus serotype 2-derived inverted terminal repeat sequences. Hum Gene Ther Methods. 2012;23:18–28.

# Appendix 3 – Lists of figures and tables

# Appendix 4 – French summary – long

***ÉVALUATION DU SYSTEME DOPAMINERGIQUE EN UTILISANT L'IMAGERIE TEP IN VIVO ET DES ANALYSES POST MORTEM DANS LE CONTEXTE D'UN MOD PD NEURODEGENERATIF ET NEUROINFLAMMATOIRE LEGER***

La maladie de Parkinson (MP) est le deuxième trouble neurodégénératif le plus commenté, affectant plus de 10 millions de patients dans le monde. La pathologie cérébrale de la maladie de Parkinson est caractérisée par une perte progressive des neurones dopaminergiques de la substantia nigra et une accumulation d'agrégats d'a-synucléine. Une autre caractéristique de la MP est la présence de neuroinflammation. Le plus grand facteur de risque de MP est l'âge, mais les facteurs génétiques et environnementaux jouent également un rôle. Dans cette thèse de doctorat, je visais à évaluer, in vivo et post mortem, les effets de trois facteurs sur le système dopaminergique: 1) la surexpression α-synucléine, 2) la co-expression α-synucléine et LRRK2, et 3) la neuroinflammation légère , sur le système dopaminergique et la perte de cellules neuronales dopaminergiques.

À cette fin, l'imagerie par tomographie par émission de positons (TEP) et les études comportementales ont été sélectionnées comme principaux outils in vivo. J'ai utilisé l'imagerie TEP [18F] LBT999 et [18F] FMT pour évaluer les niveaux striataux de transporteur de dopamine (DAT) et l'enzyme AADC synthétisant la dopamine, respectivement. Pour évaluer la neuroinflammation, j'ai utilisé le [18F] DPA714 pour évaluer la liaison du TSPO à 18 kDa. Les données in vivo ont été validées par des techniques post mortem évaluant l'expression des gènes (RT-qPCR) et des protéines (immunohistochimie).

Tout d'abord, j'ai mis en place, évalué et amélioré plusieurs techniques existantes dans notre laboratoire en utilisant le modèle 6-OHDA standard. Ensuite, les résultats de mon travail montrent que la surexpression de la WT-α-synucléine humaine dans la substantia nigra par le biais de vecteurs viraux (AAV2 / 6-PGK-WT-α-synucléine) ne génère pas de perte neuronale détectable dans la substantia nigra, pas plus que la il génère des déficits moteurs in vivo ou des modifications du système dopaminergique comme le montre l'imagerie TEP in vivo 10 à 12 semaines après l'injection (wpi).

D'autre part, j'ai démontré ici que la surexpression de A53T-α-synucléine dans la substantia nigra, en utilisant une approche de vecteur viral AAV2 / 6-PGK-A53T-α-synucléine, a entraîné une agrégation significative de la α-synucléine dans la substantia nigra dès 8wpi, mais pas dans le striatum. Des analyses microscopiques quantitatives montrent que l'agrégation A53T-α-synucléine induit une dégénérescence légère mais progressive des neurones dopaminergiques dans la substantia nigra. La perte de fibres dopaminergiques dans le striatum détectée par l'immunohistochimie de la tyrosine hydroxylase (TH) reste cependant modérée. L'imagerie DAT-PET, mais pas l'imagerie AADC-PET, a pu mesurer la perte neuronale progressive. À 12 ppp, nous avons observé des réductions significatives de l'ARNm de DAT dans la substantia nigra et de la protéine DAT dans le striatum. Ensemble, nos données in vivo et post mortem suggèrent que les mécanismes compensatoires de la disponibilité du DAT se produisent très tôt dans la pathologie, et probablement au niveau de la synapse avant l'apparition d'un mécanisme compensatoire régulé par l'expression des gènes. Une réduction des niveaux de DAT, combinée à des niveaux normaux de TH et d'AADC, pourrait normaliser les concentrations de dopamine synaptique dans le striatum. En outre, cette

perte neuronale dopaminergique a coïncidé avec une réponse initialement modérée, suivie d'une réponse microgliale plus prononcée.

Dans un modèle de vecteur viral de co-surexpression de AAV2 / 6-PGK-A53T-α-synucléine et AAV2 / 6-PGK-G2019S-LRRK2, nous n'avons pas observé de neurotoxicité supplémentaire de LRRK2 muté G2019S en toxicité A53T-α-synucléine en utilisant évaluation comportementale in vivo et imagerie TEP. Cependant, la stéréologie TH a démontré que la co-surexpression de G2019S-ΔLRRK2 et A53T-α-synucléine a légèrement augmenté la neurodégénérescence par rapport à la co-surexpression de A53T-α-synucléine et GFP, ce qui pourrait suggérer que même si G2019S-ΔLRRK2 augmente la mort cellulaire , il déclenche également un mécanisme compensatoire qui est visible avec DAT-PET et l'analyse comportementale.

Dans un modèle aigu suivant l'injection de LPS dans le striatum, l'imagerie TSPO-PET in vivo et les analyses post mortem, nous avons observé une réponse neuroinflammatoire dans le striatum, indiquant l'implication de microglies, d'astrocytes et, éventuellement, d'infiltration de macrophages. De plus, l'analyse post mortem a révélé l'absence de perte neuronale dopaminergique dans la substantia nigra et de perte synaptique dans le striatum. Néanmoins, j'ai observé une corrélation inverse significative entre les marqueurs de l'inflammation (expression TSPO-PET et IBA1) et les marqueurs pour la production de dopamine (TH) et le stockage (VMAT2). Ces données soutiennent l'hypothèse selon laquelle la neuroinflammation peut altérer la fonctionnalité du système dopaminergique, quelle que soit la présence de perte de neurones dopaminergiques. De plus, dans la littérature, il a été démontré que les réponses neuro-inflammatoires aggravées conduisent finalement à une perte spécifique des neurones dopaminergiques et peuvent donc avoir un potentiel en tant que cibles thérapeutiques.

En conclusion, les résultats de ma thèse confirment l'intérêt du PET pour démontrer les dommages fonctionnels in vivo, qui ne peuvent pas être démontrés post mortem dans des modèles animaux de PD. Dans l'ensemble, cela sous-tend l'utilisation d'études de TEP multi-racers pour contribuer à l'imagerie des modèles de différents mécanismes sous-jacents à l'initiation ou à la progression de la maladie.

Dans le cadre du programme BrainMatTrain, je me suis concentré sur l'amélioration et la caractérisation des modèles PD de rongeurs dans le but général d'utiliser ces modèles pour l'évaluation thérapeutique d'hydrogels multimodaux contenant des greffes cellulaires. Les modèles décrits ici ont tous leurs propres forces et faiblesses en ce qui concerne l'évaluation des hydrogels multimodèles. Le modèle 6-OHDA intanigral qui a été utilisé ici génère une perte presque complète des neurones dopaminergiques dans le substantif nigra et les terminaisons synaptiques, mais pas de manière pathologiquement pertinente. Ici, nous avons également utilisé deux modèles basés sur les caractéristiques de PD; neuroinflammation et surexpression des gènes liés à la PD. Comme discuté ci-dessus, le modèle de neuroinflammation basé sur le LPS permet l'étude des effets de la neuroinflammation sur la perte de cellules et de fibres dopaminergiques. Enfin, le modèle A53T-α-synucléine a un grand potentiel pour évaluer l'efficacité des stratégies thérapeutiques neuroprotectrices et modifiant la maladie. De plus, la progression relativement lente de la maladie signifie également qu'il est possible d'étudier le modèle dans une phase de type prodromique, où moins de 30% des neurones dopaminergiques sont morts. Cela pourrait être particulièrement utile dans l'étude des premiers biomarqueurs de la MP.

# References

## References


Abbasi Gharibkandi, N. and Hosseinimehr, S. J. (2019) 'Radiotracers for imaging of Parkinson's disease', *European Journal of Medicinal Chemistry*. Elsevier Masson SAS, 166, pp. 75–89. doi: 10.1016/j.ejmech.2019.01.029.

Abbott, R. D. *et al.* (2001) 'Frequency of bowel movements and the future risk of Parkinson's disease.', *Neurology*, 57(3), pp. 456–62. doi: 10.1212/wnl.57.3.456.

Abdelmotilib, H. *et al.* (2017) 'α-Synuclein fibril-induced inclusion spread in rats and mice correlates with dopaminergic Neurodegeneration.', *Neurobiology of disease*, 105, pp. 84–98. doi: 10.1016/j.nbd.2017.05.014.

Abeliovich, A. *et al.* (2000) 'Mice Lacking α-Synuclein Display Functional Deficits in the Nigrostriatal Dopamine System', *Neuron*, 25(1), pp. 239–252. doi: 10.1016/S0896-6273(00)80886-7.

Adams, J. R. *et al.* (2005) 'PET in LRRK2 mutations: comparison to sporadic Parkinson's disease and evidence for presymptomatic compensation.', *Brain : a journal of neurology*, 128(Pt 12), pp. 2777–85. doi: 10.1093/brain/awh607.

Akamatsu, G. *et al.* (2017) 'A revisit to quantitative PET with 18F-FDOPA of high specific activity using a high-resolution condition in view of application to regenerative therapy.', *Annals of nuclear medicine*, 31(2), pp. 163–171. doi: 10.1007/s12149-016-1143-2.

Alessi, D. R. and Sammler, E. (2018) 'LRRK2 kinase in Parkinson's disease.', *Science (New York, N.Y.)*, 360(6384), pp. 36–37. doi: 10.1126/science.aar5683.

Alves, I. L. *et al.* (2017) 'Dual time point method for the quantification of irreversible tracer kinetics: A reference tissue approach applied to [18F]-FDOPA brain PET', *Journal of Cerebral Blood Flow and Metabolism*, 37(9), pp. 3124–3134. doi: 10.1177/0271678X16684137.

Anichtchik, O. V. *et al.* (2003) 'Neurochemical and behavioural changes in zebrafish Danio rerio after systemic administration of 6-hydroxydopamine and 1-methyl-4-phenyl-1,2,3,6-tetrahydropyridine', *Journal of Neurochemistry*. John Wiley & Sons, Ltd (10.1111), 88(2), pp. 443–453. doi: 10.1111/j.1471-4159.2004.02190.x.

Appel-Cresswell, S. *et al.* (2013) 'Alpha-synuclein p.H50Q, a novel pathogenic mutation for Parkinson's disease', *Movement Disorders*, 28(6), pp. 811–813. doi: 10.1002/mds.25421.

Arena, J. E. and Stoessl, A. J. (2016) 'Optimizing diagnosis in Parkinson's disease: Radionuclide imaging', *Parkinsonism & Related Disorders*, 22, pp. S47–S51. doi: 10.1016/j.parkreldis.2015.09.029.

Arlicot, N. *et al.* (2012) 'Initial evaluation in healthy humans of [ 18F]DPA-714, a potential PET biomarker for neuroinflammation', *Nuclear Medicine and Biology*. Elsevier Inc., 39(4), pp. 570–578. doi: 10.1016/j.nucmedbio.2011.10.012.

Arlicot, N. *et al.* (2017) 'PET imaging of Dopamine Transporter with 18F-LBT999: first human exploration', *Journal of Nuclear Medicine*. Society of Nuclear Medicine, 58(supplement 1), pp. 276–276. Available at: http://jnm.snmjournals.org/cgi/content/short/58/supplement_1/276 (Accessed: 19 March 2020).

Aron Badin, R. *et al.* (2013) 'IRC-082451, a Novel Multitargeting Molecule, Reduces L-DOPA-Induced Dyskinesias in MPTP Parkinsonian Primates', *PLoS ONE*, 8(1). doi: 10.1371/journal.pone.0052680.

Aron Badin, R. *et al.* (2019) 'Gene Therapy for Parkinson's Disease: Preclinical Evaluation of Optimally Configured TH:CH1 Fusion for Maximal Dopamine Synthesis', *Molecular Therapy - Methods & Clinical Development*, 14(September), pp. 206–216. doi: 10.1016/j.omtm.2019.07.002.

Ascherio, A. *et al.* (2001) 'Prospective study of caffeine consumption and risk of Parkinson's disease in men and women', *Annals of Neurology*, 50(1), pp. 56–63. doi: 10.1002/ana.1052.

Ascherio, A. *et al.* (2004) 'Coffee consumption, gender, and Parkinson's disease mortality in the Cancer Prevention Study II cohort: The modifying effects of estrogen', *American Journal of Epidemiology*, 160(10), pp. 977–984. doi: 10.1093/aje/kwh312.

Aschrafi, A. *et al.* (2017) 'Disruption of the axonal trafficking of tyrosine hydroxylase mRNA impairs catecholamine biosynthesis in the axons of sympathetic neurons', *eNeuro*, 4(3), pp. 1–13. doi: 10.1523/ENEURO.0385-16.2017.

Aurnhammer, C. *et al.* (2012) 'Universal Real-Time PCR for the Detection and Quantification of Adeno-Associated Virus Serotype 2-Derived Inverted Terminal Repeat Sequences', *Human Gene Therapy Methods*, 23(1), pp. 18–28. doi: 10.1089/hgtb.2011.034.

Azzouz, M. *et al.* (2002) 'Multicistronic lentiviral vector-mediated striatal gene transfer of aromatic L-amino acid decarboxylase, tyrosine hydroxylase, and GTP cyclohydrolase I induces sustained transgene expression, dopamine production, and functional improvement in a rat model ', *Journal of Neuroscience*, 22(23), pp. 10302–10312. doi: 10.1523/jneurosci.22-23-10302.2002.

Ball, N. *et al.* (2019) 'Parkinson's Disease and the Environment', *Frontiers in Neurology*, 10(March). doi: 10.3389/fneur.2019.00218.

Banati, R. B. (2002) 'Visualising microglial activation in vivo', *Glia*, 40(2), pp. 206–217. doi: 10.1002/glia.10144.

Bandres-Ciga, S. *et al.* (2020) 'Genetics of Parkinson's disease: An introspection of its journey towards precision medicine', *Neurobiology of Disease*. Elsevier, 137(January), p. 104782. doi: 10.1016/j.nbd.2020.104782.

Bankiewicz, K. S. *et al.* (2006) 'Long-Term Clinical Improvement in MPTP-Lesioned Primates after Gene Therapy with AAV-hAADC', *Molecular Therapy*. The American Society of Gene Therapy, 14(4), pp. 564–570. doi: 10.1016/j.ymthe.2006.05.005.

Barbeau, A *et al.* (1985) 'Comparative behavioral, biochemical and pigmentary effects of MPTP, MPP+ and paraquat in rana pipiens', *Life Sciences*, 37(16), pp. 1529–1538. doi: 10.1016/0024-3205(85)90185-7.

Barbeau, A. *et al.* (1985) 'New amphibian models for the study of 1-methyl-4-phenyl-1,2,3,6-tetrahydropyridine (MPTP)', *Life Sciences*, 36(11), pp. 1125–1134. doi: 10.1016/0024-3205(85)90498-9.

Barker, R. A. *et al.* (2017) 'Human Trials of Stem Cell-Derived Dopamine Neurons for Parkinson's Disease: Dawn of a New Era.', *Cell stem cell*, 21(5), pp. 569–573. doi: 10.1016/j.stem.2017.09.014.

Barker, R. A. and de Beaufort, I. (2013) 'Scientific and ethical issues related to stem cell research and interventions in neurodegenerative disorders of the brain', *Progress in Neurobiology*. Elsevier Ltd, 110, pp. 63–73. doi: 10.1016/j.pneurobio.2013.04.003.

Barker, R. A., Drouin-Ouellet, J. and Parmar, M. (2015) 'Cell-based therapies for Parkinson disease—past insights and future potential.', *Nature reviews. Neurology*, 11(9), pp. 492–503. doi: 10.1038/nrneurol.2015.123.

Barrio, J. R. *et al.* (1996) 'Radiofluorinated L-m-tyrosines: New in-vivo probes for central dopamine biochemistry', *Journal of Cerebral Blood Flow and Metabolism*, 16(4), pp. 667–678. doi: 10.1097/00004647-199607000-00018.

Bartels, A. L. and Leenders, K. L. (2007) 'Neuroinflammation in the pathophysiology of Parkinson's disease: Evidence from animal models to human in vivo studies with [11C]-PK11195 PET', *Movement Disorders*, 22(13), pp. 1852–1856. doi: 10.1002/mds.21552.

Bartels, A. L. and Leenders, K. L. (2009) 'Parkinson's disease: the syndrome, the pathogenesis and pathophysiology.', *Cortex; a journal devoted to the study of the nervous system and behavior*, 45(8), pp. 915–21. doi: 10.1016/j.cortex.2008.11.010.

*Basal ganglia diagram* (2013). Available at: https://commons.wikimedia.org/wiki/File:Basal-ganglia-classic.png#/media/File:Basal_ganglia_diagram.svg (Accessed: 1 April 2020).

Batista, C. R. A. *et al.* (2019) 'Lipopolysaccharide-induced neuroinflammation as a bridge to understand neurodegeneration', *International Journal of Molecular Sciences*, 20(9). doi: 10.3390/ijms20092293.

Beach, T. G. *et al.* (2010) 'Multi-organ distribution of phosphorylated alpha-synuclein histopathology in subjects with Lewy body disorders.', *Acta neuropathologica*, 119(6), pp. 689–702. doi: 10.1007/s00401-010-0664-3.

Becker, G. *et al.* (2017) 'Comparative assessment of 6-[18F]fluoro-L-m-tyrosine and 6-[18F]fluoro-L-dopa to evaluate dopaminergic presynaptic integrity in a Parkinson's disease rat model', *Journal of Neurochemistry*. doi: 10.1111/jnc.14016.

Belloli, S. *et al.* (2017) 'Early upregulation of 18-kDa translocator protein in response to acute neurodegenerative damage in TREM2-deficient mice', *Neurobiology of Aging*, 53, pp. 159–168. doi: 10.1016/j.neurobiolaging.2017.01.010.

Benabid, A. L. *et al.* (1987) 'Combined (thalamotomy and stimulation) stereotactic surgery of the VIM thalamic nucleus for bilateral Parkinson disease.', *Applied neurophysiology*, 50(1–6), pp. 344–6. doi: 10.1159/000100803.

Berdyyeva, T. *et al.* (2019) 'PET Imaging of the P2X7 Ion Channel with a Novel Tracer [18F]JNJ-64413739 in a Rat Model of Neuroinflammation', *Molecular Imaging and Biology*. Molecular Imaging and Biology, 21(5), pp. 871–878. doi: 10.1007/s11307-018-01313-2.

Berg, D. *et al.* (2011) 'AFQ056 treatment of levodopa-induced dyskinesias: results of 2 randomized controlled trials.', *Movement disorders : official journal of the Movement Disorder Society*, 26(7), pp. 1243–50. doi: 10.1002/mds.23616.

Berger, A. *et al.* (2015) 'Repair of Rhodopsin mRNA by Spliceosome-Mediated RNA Trans -Splicing: A New Approach for Autosomal Dominant Retinitis Pigmentosa', *Molecular Therapy*, 23(5), pp. 918–930. doi: 10.1038/mt.2015.11.

Berger, K., Przedborski, S. and Cadet, J. L. (1991) 'Retrograde degeneration of nigrostriatal neurons induced by intrastriatal 6-hydroxydopamine injection in rats', *Brain Research Bulletin*, 26(2), pp. 301–307. doi: 10.1016/0361-9230(91)90242-C.

Bernal-Conde, L. D. *et al.* (2020) 'Alpha-Synuclein Physiology and Pathology: A Perspective on Cellular Structures and Organelles', *Frontiers in Neuroscience*, 13(January), pp. 1–22. doi: 10.3389/fnins.2019.01399.

Berwick, D. C. *et al.* (2019) 'LRRK2 Biology from structure to dysfunction: research progresses, but the themes remain the same.', *Molecular neurodegeneration*, 14(1), p. 49. doi: 10.1186/s13024-019-0344-2.

Best, L. *et al.* (2019) 'New and Old TSPO PET Radioligands for Imaging Brain Microglial Activation in Neurodegenerative Disease', *Current Neurology and Neuroscience Reports*. Current Neurology and Neuroscience Reports, 19(5). doi: 10.1007/s11910-019-0934-y.

Betarbet, R. *et al.* (2000) 'Chronic systemic pesticide exposure reproduces features of Parkinson's disease', *Nature Neuroscience*, 3(12), pp. 1301–1306. doi: 10.1038/81834.

Beutler, E. (1992) 'Gaucher disease: new molecular approaches to diagnosis and treatment.', *Science (New York, N.Y.)*, 256(5058), pp. 794–9. doi: 10.1126/science.1589760.

Bezard, E. *et al.* (2000) 'Adaptive changes in the nigrostriatal pathway in response to increased 1-methyl-4-phenyl-1,2,3,6-tetrahydropyridine-induced neurodegeneration in the mouse.', *The European journal of neuroscience*, 12(8), pp. 2892–900. doi: 10.1046/j.1460-9568.2000.00180.x.

Bezard, E. *et al.* (2001) 'Relationship between the appearance of symptoms and the level of nigrostriatal degeneration in a progressive 1-methyl-4-phenyl-1,2,3,6-tetrahydropyridine-lesioned macaque model of Parkinson's disease', *Journal of Neuroscience*, 21(17), pp. 6853–6861. doi: 10.1523/jneurosci.21-17-06853.2001.

Bezard, E., Imbert, C. and Gross, C. E. (1998) 'Experimental models of Parkinson's disease: From the static to the dynamic', *Reviews in the Neurosciences*, 9(2), pp. 71–90. doi: 10.1515/REVNEURO.1998.9.2.71.

Lo Bianco, C. *et al.* (2002) 'alpha -Synucleinopathy and selective dopaminergic neuron loss in a rat lentiviral-based model of Parkinson's disease.', *Proceedings of the National Academy of Sciences of the United States of America*, 99(16), pp. 10813–8. doi: 10.1073/pnas.152339799.

Billingsley, K. J. *et al.* (2018) 'Genetic risk factors in Parkinson's disease.', *Cell and tissue research*, 373(1), pp. 9–20. doi: 10.1007/s00441-018-2817-y.

Bismuth, C. *et al.* (1990) 'Paraquat Poisoning', *Drug Safety*, 5(4), pp. 243–251. doi: 10.2165/00002018-199005040-00002.

Björklund, A. *et al.* (1981) 'Functional reactivation of the deafferented neostriatum by nigral transplants', *Nature*, 289(5797), pp. 497–499. doi: 10.1038/289497a0.

Bjorklund, T. (2018) 'Repairing the brain: Gene therapy', *Journal of Parkinson's Disease*, 8(s1), pp. S123–S130. doi: 10.3233/JPD-181485.

Blesa, J. *et al.* (2017) 'Compensatory mechanisms in Parkinson's disease: Circuits adaptations and role in disease modification', *Experimental Neurology*, 298(October), pp. 148–161. doi: 10.1016/j.expneurol.2017.10.002.

Bliederhaeuser, C. *et al.* (2016) 'Age-dependent defects of alpha-synuclein oligomer uptake in microglia and monocytes.', *Acta neuropathologica*, 131(3), pp. 379–91. doi: 10.1007/s00401-015-1504-2.

Blumenstock, S. *et al.* (2017) 'Seeding and transgenic overexpression of alpha-synuclein triggers dendritic spine pathology in the neocortex', *EMBO Molecular Medicine*, 9(5), pp. 716–731. doi: 10.15252/emmm.201607305.

Bobela, W., Aebischer, P. and Schneider, B. L. (2015) 'Alpha-synuclein as a mediator in the interplay between aging and Parkinson's disease', *Biomolecules*, 5(4), pp. 2675–2700. doi: 10.3390/biom5042675.

Bohnen, N. I. *et al.* (2006) 'Positron emission tomography of monoaminergic vesicular binding in aging and Parkinson disease', *Journal of Cerebral Blood Flow and Metabolism*, 26(9), pp. 1198–1212. doi: 10.1038/sj.jcbfm.9600276.

Bonifati, V. *et al.* (2003) 'Mutations in the DJ-1 gene associated with autosomal recessive early-onset parkinsonism.', *Science (New York, N.Y.)*, 299(5604), pp. 256–9. doi: 10.1126/science.1077209.

Bonneh-Barkay, D. *et al.* (2005) 'Redox cycling of the herbicide paraquat in microglial cultures', *Molecular Brain Research*, 134(1), pp. 52–56. doi: 10.1016/j.molbrainres.2004.11.005.

Bonsack, F. and Sukumari-Ramesh, S. (2018) 'TSPO: An evolutionarily conserved protein with elusive functions', *International Journal of Molecular Sciences*, 19(6). doi: 10.3390/ijms19061694.

Bordia, T. *et al.* (2015) 'The α7 nicotinic receptor agonist ABT-107 protects against nigrostriatal damage in rats with unilateral 6-hydroxydopamine lesions', *Experimental Neurology*. Elsevier Inc., 263, pp. 277–284. doi: 10.1016/j.expneurol.2014.09.015.

Borowski, T. *et al.* (1998) 'Lipopolysaccharide, central in vivo biogenic amine variations, and anhedonia.', *Neuroreport*, 9(17), pp. 3797–802. doi: 10.1097/00001756-199812010-00006.

Braak, H., Rüb, U., *et al.* (2003) 'Idiopathic Parkinson's disease: Possible routes by which vulnerable neuronal types may be subject to neuroinvasion by an unknown pathogen', *Journal of Neural Transmission*, 110(5), pp. 517–536. doi: 10.1007/s00702-002-0808-2.

Braak, H., Del Tredici, K., *et al.* (2003) 'Staging of brain pathology related to sporadic Parkinson's disease', *Neurobiology of Aging*, 24(2), pp. 197–211. doi: 10.1016/S0197-4580(02)00065-9.

Braak, H., Sastre, M. and Del Tredici, K. (2007) 'Development of alpha-synuclein immunoreactive astrocytes in the forebrain parallels stages of intraneuronal pathology in sporadic Parkinson's disease.', *Acta neuropathologica*, 114(3), pp. 231–41. doi: 10.1007/s00401-007-0244-3.

Braungart, E. *et al.* (2004) 'Caenorhabditis elegans MPP+ Model of Parkinson's Disease for High-Throughput Drug Screenings', *Neurodegenerative Diseases*, 1(4–5), pp. 175–183. doi: 10.1159/000080983.

Breckenridge, C. B. *et al.* (2016) 'Association between Parkinson's disease and cigarette smoking, rural living, well-water consumption, farming and pesticide use: Systematic review and meta-analysis', *PLoS ONE*, 11(4), pp. 1–42. doi: 10.1371/journal.pone.0151841.

Bretaud, S. *et al.* (2007) 'p53-dependent neuronal cell death in a DJ-1-deficient zebrafish model of Parkinson's disease.', *Journal of neurochemistry*, 100(6), pp. 1626–35. doi: 10.1111/j.1471-4159.2006.04291.x.

Bretaud, S., Lee, S. and Guo, S. (2004) 'Sensitivity of zebrafish to environmental toxins implicated in Parkinson's disease', *Neurotoxicology and Teratology*, 26(6 SPEC. ISS.), pp. 857–864. doi: 10.1016/j.ntt.2004.06.014.

Broadfoot, C. K. *et al.* (2019) 'Research-based Updates in Swallowing and Communication Dysfunction in Parkinson Disease: Implications for Evaluation and Management.', *Perspectives of the ASHA special interest groups*, 4(5), pp. 825–841. doi: 10.1044/2019_pers-sig3-2019-0001.

Brocks, D. R. (1999) 'Anticholinergic drugs used in Parkinson's disease: An overlooked class of drugs from a pharmacokinetic perspective.', *Journal of pharmacy & pharmaceutical sciences : a publication of the Canadian Society for Pharmaceutical Sciences, Societe canadienne des sciences pharmaceutiques*, 2(2), pp. 39–46. Available at: http://www.ncbi.nlm.nih.gov/pubmed/10952768.

Brooks, D. J. (2016) 'Molecular imaging of dopamine transporters.', *Ageing research reviews*, 30, pp. 114–21. doi: 10.1016/j.arr.2015.12.009.

Brown, G. C. (2019) 'The endotoxin hypothesis of neurodegeneration', *Journal of neuroinflammation*. Journal of Neuroinflammation, 16(1), p. 180. doi: 10.1186/s12974-019-1564-7.

Bruggeman, K. F. *et al.* (2019) 'Harnessing stem cells and biomaterials to promote neural repair', *British Journal of Pharmacology*, 176(3), pp. 355–368. doi: 10.1111/bph.14545.

Brundin, P., Melki, R. and Kopito, R. (2010) 'Prion-like transmission of protein aggregates in neurodegenerative diseases.', *Nature reviews. Molecular cell biology*, 11(4), pp. 301–7. doi: 10.1038/nrm2873.

Burke, W. J. *et al.* (2008) 'Aggregation of α-synuclein by DOPAL, the monoamine oxidase metabolite of dopamine', *Acta Neuropathologica*, 115(2), pp. 193–203. doi: 10.1007/s00401-007-0303-9.

Burns, R. S. *et al.* (1984) 'The neurotoxicity of 1-methyl-4-phenyl-1,2,3,6-tetrahydropyridine in the monkey and man.', *The Canadian journal of neurological sciences. Le journal canadien des sciences neurologiques*, 11(1 Suppl), pp. 166–8. doi: 10.1017/s0317167100046345.

Cabezudo, D., Baekelandt, V. and Lobbestael, E. (2020) 'Multiple-Hit Hypothesis in Parkinson's Disease: LRRK2 and Inflammation', *Frontiers in Neuroscience*, 14(April). doi: 10.3389/fnins.2020.00376.

Cadet, J. L. and Brannock, C. (1998) 'Free radicals and the pathobiology of brain dopamine systems', *Neurochemistry International*. Pergamon, 32(2), pp. 117–131. doi: 10.1016/S0197-0186(97)00031-4.

Calne, D. B. *et al.* (1985) 'Positron emission tomography after MPTP: observations relating to the cause of Parkinson's disease', *Nature*, 317(6034), pp. 246–248. doi: 10.1038/317246a0.

Van Camp, N. *et al.* (2019) 'Assessment of simplified methods for quantification of [ 18 F]-DPA-714 using 3D whole-brain TSPO immunohistochemistry in a non-human primate', *Journal of Cerebral Blood Flow & Metabolism*, p. 0271678X1985903. doi: 10.1177/0271678X19859034.

Van Camp, N., Bramoullé, Y. and Hantraye, P. (2011) 'Quantification of Brain Function and Neurotransmission System In Vivo by Positron Emission Tomography: A Review of Technical Aspects and Practical Considerations in Preclinical Research', in *Neuromethods*, pp. 151–190. doi: 10.1007/978-1-61779-298-4_9.

Carlsson, A., Lindqvist, M. and Magnusson, T. (1957) '3,4-Dihydroxyphenylalanine and 5-Hydroxytryptophan as Reserpine Antagonists', *Nature*, 180(4596), pp. 1200–1200. doi: 10.1038/1801200a0.

Carlsson, M. and Carlsson, A. (1989) 'Dramatic synergism between MK-801 and clonidine with respect to locomotor stimulatory effect in monoamine-depleted mice', *Journal of Neural Transmission*, 77(1), pp. 65–71. doi: 10.1007/BF01255820.

Casteels, C. *et al.* (2006) 'Construction and evaluation of multitracer small-animal PET probabilistic atlases for voxel-based functional mapping of the rat brain.', *Journal of nuclear medicine : official publication, Society of Nuclear Medicine*, 47(11), pp. 1858–66. doi: 10.1371/journal.pone.0065286.

Casteels, C. *et al.* (2008) 'Metabolic-dopaminergic mapping of the 6-hydroxydopamine rat model for Parkinson's disease.', *European journal of nuclear medicine and molecular imaging*, 35(1), pp. 124–34. doi: 10.1007/s00259-007-0558-3.

Castilho, R. F., Hansson, O. and Brundin, P. (2000) 'Improving the survival of grafted embryonic dopamine neurons in rodent models of Parkinson's disease.', *Progress in brain research*, 127, pp. 203–31. doi: 10.1016/s0079-6123(00)27011-8.

Caudle, W. M. *et al.* (2012) 'Industrial toxicants and Parkinson's disease', *NeuroToxicology*. Elsevier B.V., 33(2), pp. 178–188. doi: 10.1016/j.neuro.2012.01.010.

Chalon, S. *et al.* (2006) 'Pharmacological characterization of (E)-N-(4-fluorobut-2-enyl)-2beta-carbomethoxy-3beta-(4'-tolyl)nortropane (LBT-999) as a highly promising fluorinated ligand for the dopamine transporter.', *The Journal of pharmacology and experimental therapeutics*, 317(1), pp. 147–52. doi: 10.1124/jpet.105.096792.

Chalon, S. *et al.* (2019) 'The story of the dopamine transporter PET tracer [18F]LBT-999: From conception to clinical use', *Frontiers in Medicine*, 6(APR), pp. 1–5. doi: 10.3389/fmed.2019.00090.

Chang, J. W. *et al.* (1999) 'Biochemical and anatomical characterization of forepaw adjusting steps in rat models of Parkinson's disease: studies on medial forebrain bundle and striatal lesions.', *Neuroscience*, 88(2), pp. 617–28. doi: 10.1016/s0306-4522(98)00217-6.

Chang, Y. T., Mues, G. and Hyland, K. (1996) 'Alternative splicing in the coding region of human aromatic L-amino acid decarboxylase mRNA.', *Neuroscience letters*, 202(3), pp. 157–60. doi: 10.1016/0304-3940(95)12234-6.

Chartier-Harlin, M.-C. *et al.* (2004) 'Alpha-synuclein locus duplication as a cause of familial Parkinson's disease.', *Lancet (London, England)*, 364(9440), pp. 1167–9. doi: 10.1016/S0140-6736(04)17103-1.

Chaudhuri, A. *et al.* (2007) 'Interaction of genetic and environmental factors in a Drosophila parkinsonism model.', *The Journal of neuroscience : the official journal of the Society for Neuroscience*. Society for Neuroscience, 27(10), pp. 2457–67. doi: 10.1523/JNEUROSCI.4239-06.2007.

Chauveau, F. *et al.* (2009) 'Comparative evaluation of the translocator protein radioligands 11C-DPA-713, 18F-DPA-714, and 11C-PK11195 in a rat model of acute neuroinflammation.', *Journal of nuclear medicine : official publication, Society of Nuclear Medicine*, 50(3), pp. 468–76. doi: 10.2967/jnumed.108.058669.

Chen, H. *et al.* (2003) 'Nonsteroidal anti-inflammatory drugs and the risk of Parkinson disease.', *Archives of neurology*, 60(8), pp. 1059–64. doi: 10.1001/archneur.60.8.1059.

Chen, H. *et al.* (2005) 'Nonsteroidal antiinflammatory drug use and the risk for Parkinson's disease.', *Annals of neurology*, 58(6), pp. 963–7. doi: 10.1002/ana.20682.

Chen, M. K. *et al.* (2008) 'VMAT2 and dopamine neuron loss in a primate model of Parkinson's disease', *Journal of Neurochemistry*, 105(1), pp. 78–90. doi: 10.1111/j.1471-4159.2007.05108.x.

Chen, Y. *et al.* (2018) 'Prion-like propagation of α-synuclein in the gut-brain axis', *Brain Research*

*Bulletin*, 140, pp. 341–346. doi: 10.1016/j.brainresbull.2018.06.002.

Cheng, P. *et al.* (2015) 'Dietary intake of iron, zinc, copper, and risk of Parkinson's disease: a meta-analysis', *Neurological Sciences*, 36(12), pp. 2269–2275. doi: 10.1007/s10072-015-2349-0.

Cherry, S. R. and Gambhir, S. S. (2001) 'Use of positron emission tomography in animal research', *ILAR Journal*, 42(3), pp. 219–232. doi: 10.1093/ilar.42.3.219.

Cho, B. P. *et al.* (2006) 'Pathological dynamics of activated microglia following medial forebrain bundle transection', *Glia*, 53(1), pp. 92–102. doi: 10.1002/glia.20265.

Choi, D. Y. *et al.* (2009) 'Striatal neuroinflammation promotes parkinsonism in rats', *PLoS ONE*, 4(5). doi: 10.1371/journal.pone.0005482.

Choi, J. Y. *et al.* (2012) 'Evaluation of dopamine transporters and D2 receptors in hemiparkinsonian rat brains in vivo using consecutive PET scans of [18F]FPCIT and [18F]fallypride.', *Applied radiation and isotopes : including data, instrumentation and methods for use in agriculture, industry and medicine*. Elsevier, 70(12), pp. 2689–94. doi: 10.1016/j.apradiso.2012.08.005.

Chow, P. L., Rannou, F. R. and Chatziioannou, A. F. (2005) 'Attenuation correction for small animal PET tomographs', *Physics in Medicine and Biology*, 50(8), pp. 1837–1850. doi: 10.1088/0031-9155/50/8/014.

Christensen, A. B. *et al.* (2018) 'Pirouetting pigs: A large non-primate animal model based on unilateral 6-hydroxydopamine lesioning of the nigrostriatal pathway', *Brain Research Bulletin*. Elsevier, 139, pp. 167–173. doi: 10.1016/J.BRAINRESBULL.2018.02.010.

Christine, C. W. *et al.* (2009) 'Safety and tolerability of putaminal AADC gene therapy for Parkinson disease.', *Neurology*, 73(20), pp. 1662–9. doi: 10.1212/WNL.0b013e3181c29356.

Chung, C. Y. *et al.* (2009) 'Dynamic Changes in Presynaptic and Axonal Transport Proteins Combined with Striatal Neuroinflammation Precede Dopaminergic Neuronal Loss in a Rat Model of AAV - Synucleinopathy', *Journal of Neuroscience*, 29(11), pp. 3365–3373. doi: 10.1523/JNEUROSCI.5427-08.2009.

Cicchetti, F. *et al.* (2005) 'Systemic exposure to paraquat and maneb models early Parkinson's disease in young adult rats', *Neurobiology of Disease*, 20(2), pp. 360–371. doi: 10.1016/j.nbd.2005.03.018.

Cicchetti, F., Drouin-Ouellet, J. and Gross, R. E. (2009) 'Environmental toxins and Parkinson's disease: what have we learned from pesticide-induced animal models?', *Trends in Pharmacological Sciences*, 30(9), pp. 475–483. doi: 10.1016/j.tips.2009.06.005.

Coon, S. *et al.* (2006) 'Whole-Body Lifetime Occupational Lead Exposure and Risk of Parkinson's Disease', *Environmental Health Perspectives*, 114(12), pp. 1872–1876. doi: 10.1289/ehp.9102.

Cooper, J. F. and Van Raamsdonk, J. M. (2018) 'Modeling Parkinson's disease in C. elegans', *Journal of Parkinson's Disease*, 8(1), pp. 17–32. doi: 10.3233/JPD-171258.

Cotzias, G. C., Papavasiliou, P. S. and Gellene, R. (1969) 'Modification of Parkinsonism — Chronic Treatment with L-Dopa', *New England Journal of Medicine*, 280(7), pp. 337–345. doi: 10.1056/NEJM196902132800701.

Coulom, H. and Birman, S. (2004) 'Chronic exposure to rotenone models sporadic Parkinson's disease in Drosophila melanogaster.', *The Journal of neuroscience : the official journal of the Society for Neuroscience*, 24(48), pp. 10993–8. doi: 10.1523/JNEUROSCI.2993-04.2004.

Crabbé, M. *et al.* (2019) 'Temporal changes in neuroinflammation and brain glucose metabolism in a rat model of viral vector-induced α-synucleinopathy', *Experimental Neurology*. Elsevier, 320(March), p. 112964. doi: 10.1016/j.expneurol.2019.112964.

Cresto, N. *et al.* (2018) 'The unlikely partnership between LRRK2 and α-synuclein in Parkinson's disease', *European Journal of Neuroscience*. doi: 10.1111/ejn.14182.

Cresto, N. *et al.* (2020) 'The C-terminal domain of LRRK2 with the G2019S mutation is sufficient to produce neurodegeneration of dopaminergic neurons in vivo.', *Neurobiology of disease*, 134, p. 104614. doi: 10.1016/j.nbd.2019.104614.

Cui, M. *et al.* (2009) 'The organic cation transporter-3 is a pivotal modulator of neurodegeneration in the nigrostriatal dopaminergic pathway.', *Proceedings of the National Academy of Sciences of the United States of America*, 106(19), pp. 8043–8. doi: 10.1073/pnas.0900358106.

Currie, G. M. (2019) 'Biodistribution of 18F-FDG after oral administration to a honeybee: PET/CT proof of concept', *Journal of Nuclear Medicine*, 60(10), p. 1493. doi: 10.2967/jnumed.119.231381.

Daher, J. P. L. *et al.* (2014) 'Abrogation of -synuclein-mediated dopaminergic neurodegeneration in LRRK2-deficient rats', *Proceedings of the National Academy of Sciences*, 111(25), pp. 9289–9294. doi: 10.1073/pnas.1403215111.

Daher, J. P. L. *et al.* (2015) 'Leucine-rich repeat kinase 2 (LRRK2) pharmacological inhibition abates α-synuclein gene-induced neurodegeneration', *Journal of Biological Chemistry*, 290(32), pp. 19433–19444. doi: 10.1074/jbc.M115.660001.

Dallapiazza, R. F. *et al.* (2018) *Considerations for Patient and Target Selection in Deep Brain Stimulation Surgery for Parkinson's Disease*, *Parkinson's Disease: Pathogenesis and Clinical Aspects*. Available at: http://www.ncbi.nlm.nih.gov/pubmed/30702838.

Damier, P. *et al.* (1993) 'Glutathione peroxidase, glial cells and Parkinson's disease.', *Neuroscience*, 52(1), pp. 1–6. doi: 10.1016/0306-4522(93)90175-f.

Damont, A. *et al.* (2008) 'Radiosynthesis of [18F]DPA-714, a selective radioligand for imaging the translocator protein (18 kDa) with PET', *Journal of Labelled Compounds and Radiopharmaceuticals*, 51(7), pp. 286–292. doi: 10.1002/jlcr.1523.

Daniel, S. E. and Hawkes, C. H. (1992) 'Preliminary diagnosis of Parkinson's disease by olfactory bulb pathology.', *Lancet (London, England)*, 340(8812), p. 186. doi: 10.1016/0140-6736(92)93275-r.

Dauer, W. *et al.* (2002) 'Resistance of alpha -synuclein null mice to the parkinsonian neurotoxin MPTP.', *Proceedings of the National Academy of Sciences of the United States of America*, 99(22), pp. 14524–9. doi: 10.1073/pnas.172514599.

Dauer, W. and Przedborski, S. (2003) 'Parkinson's Disease: Mechanisms and Models', *Neuron*, 39(6), pp. 889–909. doi: 10.1016/S0896-6273(03)00568-3.

Dave, K. D. *et al.* (2014) 'Phenotypic characterization of recessive gene knockout rat models of Parkinson's disease.', *Neurobiology of disease*, 70, pp. 190–203. doi: 10.1016/j.nbd.2014.06.009.

Davis, G. C. *et al.* (1979) 'Chronic parkinsonism secondary to intravenous injection of meperidine analogues', *Psychiatry Research*, 1(3), pp. 249–254. doi: 10.1016/0165-1781(79)90006-4.

Dawson, T. M., Ko, H. S. and Dawson, V. L. (2010) 'Genetic Animal Models of Parkinson's Disease', *Neuron*, 66(5), pp. 646–661. doi: 10.1016/j.neuron.2010.04.034.

Decressac, M. *et al.* (2012) 'Progressive neurodegenerative and behavioural changes induced by AAV-mediated overexpression of α-synuclein in midbrain dopamine neurons', *Neurobiology of Disease*. Elsevier Inc., 45(3), pp. 939–953. doi: 10.1016/j.nbd.2011.12.013.

Decressac, M., Mattsson, B. and Björklund, A. (2012) 'Comparison of the behavioural and histological characteristics of the 6-OHDA and α-synuclein rat models of Parkinson's disease', *Experimental Neurology*. Elsevier Inc., 235(1), pp. 306–315. doi: 10.1016/j.expneurol.2012.02.012.

Dejesus, O. T. *et al.* (2001) 'Noninvasive assessment of aromatic L-amino acid decarboxylase activity in aging rhesus monkey brain in vivo.', *Synapse (New York, N.Y.)*, 39(1), pp. 58–63. doi: 10.1002/1098-2396(20010101)39:1<58::AID-SYN8>3.0.CO;2-B.

DeJesus, O. T. *et al.* (1997) 'Evaluation of fluorinated m-tyrosine analogs as PET imaging agents of dopamine nerve terminals: comparison with 6-fluoroDOPA.', *Journal of nuclear medicine : official publication, Society of Nuclear Medicine*, 38(4), pp. 630–6. Available at: http://www.ncbi.nlm.nih.gov/pubmed/9098215.

DeJesus, O. T. *et al.* (2005) 'Aromatic L-amino acid decarboxylase turnover in vivo in rhesus macaque striatum: a microPET study.', *Brain research*, 1054(1), pp. 55–60. doi: 10.1016/j.brainres.2005.06.086.

Del-Bel, E. *et al.* (2014) 'Counteraction by nitric oxide synthase inhibitor of neurochemical alterations of dopaminergic system in 6-OHDA-lesioned rats under L-DOPA treatment.', *Neurotoxicity research*, 25(1), pp. 33–44. doi: 10.1007/s12640-013-9406-3.

DeLong, M. and Wichmann, T. (2010) 'Changing views of basal ganglia circuits and circuit disorders.', *Clinical EEG and neuroscience*, 41(2), pp. 61–7. doi: 10.1177/155005941004100204.

DeMaagd, G. and Philip, A. (2015) 'Parkinson's Disease and Its Management: Part 1: Disease Entity, Risk Factors, Pathophysiology, Clinical Presentation, and Diagnosis.', *P & T : a peer-reviewed journal for formulary management*, 40(8), pp. 504–32. Available at: http://www.ncbi.nlm.nih.gov/pubmed/26236139.

Deng, H., Wang, P. and Jankovic, J. (2018) 'The genetics of Parkinson disease.', *Ageing research reviews*, 42, pp. 72–85. doi: 10.1016/j.arr.2017.12.007.

Deng, I. *et al.* (2020) 'Lipopolysaccharide Animal Models of Parkinson's Disease: Recent Progress and Relevance to Clinical Disease', *Brain, Behavior, & Immunity - Health*. Elsevier Inc., p. 100060. doi: 10.1016/j.bbih.2020.100060.

Dentresangle, C. *et al.* (2001) 'Increased extracellular DA and normal evoked DA release in the rat striatum after a partial lesion of the substantia nigra.', *Brain research*, 893(1–2), pp. 178–85. doi: 10.1016/s0006-8993(00)03311-4.

Devrome, M. *et al.* (2019) 'Identifying a glucose metabolic brain pattern in an adeno-associated viral vector based rat model for Parkinson's disease using 18F-FDG PET imaging', *Scientific Reports*. Springer US, 9(1), pp. 1–8. doi: 10.1038/s41598-019-48713-0.

Dickson, D. W. (2012) 'Parkinson's disease and parkinsonism: neuropathology.', *Cold Spring Harbor perspectives in medicine*, 2(8), pp. 1–15. doi: 10.1101/cshperspect.a009258.

Dollé, F. *et al.* (2006) 'Synthesis, radiosynthesis and in vivo preliminary evaluation of [11C]LBT-999, a selective radioligand for the visualisation of the dopamine transporter with PET.', *Bioorganic & medicinal chemistry*, 14(4), pp. 1115–25. doi: 10.1016/j.bmc.2005.09.035.

Dollé, F. *et al.* (2007) 'One-step radiosynthesis of [18F]LBT-999: A selective radioligand for the

visualization of the dopamine transporter with PET', *Journal of Labelled Compounds and Radiopharmaceuticals*, 50(8), pp. 716–723. doi: 10.1002/jlcr.1412.

Doty, R. L. (2012) 'Olfactory dysfunction in Parkinson disease.', *Nature reviews. Neurology*, 8(6), pp. 329–39. doi: 10.1038/nrneurol.2012.80.

Dowd, E. *et al.* (2005) 'The Corridor Task: a simple test of lateralised response selection sensitive to unilateral dopamine deafferentation and graft-derived dopamine replacement in the striatum.', *Brain research bulletin*, 68(1–2), pp. 24–30. doi: 10.1016/j.brainresbull.2005.08.009.

Duchemin, A. M. *et al.* (2000) 'Phosphorylation and activation of brain aromatic L-amino acid decarboxylase by cyclic AMP-dependent protein kinase.', *Journal of neurochemistry*, 75(2), pp. 725–31. doi: 10.1046/j.1471-4159.2000.0750725.x.

Dujardin, K. and Sgambato, V. (2020) 'Neuropsychiatric Disorders in Parkinson's Disease: What Do We Know About the Role of Dopaminergic and Non-dopaminergic Systems?', *Frontiers in neuroscience*, 14, p. 25. doi: 10.3389/fnins.2020.00025.

Dunn, A. J. (1992) 'Endotoxin-induced activation of cerebral catecholamine and serotonin metabolism: comparison with interleukin-1.', *The Journal of pharmacology and experimental therapeutics*, 261(3), pp. 964–9. Available at: http://www.ncbi.nlm.nih.gov/pubmed/1602402.

Dusonchet, J. *et al.* (2011) 'A Rat Model of Progressive Nigral Neurodegeneration Induced by the Parkinson's Disease-Associated G2019S Mutation in LRRK2', *Journal of Neuroscience*, 31(3), pp. 907–912. doi: 10.1523/JNEUROSCI.5092-10.2011.

Dutta, S. K. *et al.* (2019) 'Parkinson's disease: The emerging role of gut dysbiosis, antibiotics, probiotics, and fecal microbiota transplantation', *Journal of Neurogastroenterology and Motility*, 25(3), pp. 363–376. doi: 10.5056/jnm19044.

Duty, S. and Jenner, P. (2011) 'Animal models of Parkinson's disease: A source of novel treatments and clues to the cause of the disease', *British Journal of Pharmacology*, 164(4), pp. 1357–1391. doi: 10.1111/j.1476-5381.2011.01426.x.

Dzamko, N. and Halliday, G. M. (2012) 'An emerging role for LRRK2 in the immune system', *Biochemical Society Transactions*, 40(5), pp. 1134–1139. doi: 10.1042/BST20120119.

Eberling, J. L. *et al.* (2007) 'PET 6-[F]fluoro-L-m-tyrosine Studies of Dopaminergic Function in Human and Nonhuman Primates.', *Frontiers in human neuroscience*, 1(MAR), p. 9. doi: 10.3389/neuro.09.009.2007.

Edison, P. *et al.* (2013) 'Microglia, amyloid, and glucose metabolism in Parkinson's disease with and without dementia.', *Neuropsychopharmacology : official publication of the American College of Neuropsychopharmacology*, 38(6), pp. 938–49. doi: 10.1038/npp.2012.255.

Van Den Eeden, S. K. *et al.* (2003) 'Incidence of Parkinson's disease: variation by age, gender, and race/ethnicity.', *American journal of epidemiology*, 157(11), pp. 1015–22. doi: 10.1093/aje/kwg068.

Ehringer, H. and Hornykiewicz, O. (1998) 'Distribution of noradrenaline and dopamine (3-hydroxytyramine) in the human brain and their behavior in diseases of the extrapyramidal system', *Parkinsonism & Related Disorders*, 4(2), pp. 53–57. doi: 10.1016/S1353-8020(98)00012-1.

Eidelberg, D. *et al.* (1994) 'The metabolic topography of parkinsonism.', *Journal of cerebral blood flow and metabolism : official journal of the International Society of Cerebral Blood Flow and Metabolism*, 14(5), pp. 783–801. doi: 10.1038/jcbfm.1994.99.

Eisenhofer, G., Kopin, I. J. and Goldstein, D. S. (2004) 'Catecholamine metabolism: a contemporary view with implications for physiology and medicine.', *Pharmacological reviews*, 56(3), pp. 331–49. doi: 10.1124/pr.56.3.1.

Elbaz, A. *et al.* (2009) 'Professional exposure to pesticides and Parkinson disease', *Annals of Neurology*, 66(4), pp. 494–504. doi: 10.1002/ana.21717.

Elsinga, P. H., Hatano, K. and Ishiwata, K. (2006) 'PET tracers for imaging of the dopaminergic system.', *Current medicinal chemistry*, 13(18), pp. 2139–53. doi: 10.2174/092986706777935258.

Endepols, H., Schul, J., *et al.* (2004) '6-hydroxydopamine lesions in anuran amphibians: A new model system for Parkinson's disease?', *Journal of Neurobiology*, 60(4), pp. 395–410. doi: 10.1002/neu.20047.

Endepols, H., Roden, K., *et al.* (2004) 'Dorsal striatopallidal system in anurans', *The Journal of Comparative Neurology*, 468(2), pp. 299–310. doi: 10.1002/cne.11006.

Endres, C. J. *et al.* (1997) 'Affinities of dopamine analogs for monoamine granular and plasma membrane transporters: implications for PET dopamine studies.', *Life sciences*, 60(26), pp. 2399–406. doi: 10.1016/s0024-3205(97)00300-7.

Engelender, S. and Isacson, O. (2017) 'The Threshold Theory for Parkinson's Disease', *Trends in Neurosciences*. Elsevier Ltd, 40(1), pp. 4–14. doi: 10.1016/j.tins.2016.10.008.

Espa, E. *et al.* (2019) 'Seeding of protein aggregation causes cognitive impairment in rat model of cortical synucleinopathy', *Movement Disorders*, 34(11), pp. 1699–1710. doi: 10.1002/mds.27810.

Fahn, S. (2018) 'The 200-year journey of Parkinson disease: Reflecting on the past and looking towards the future', *Parkinsonism & Related Disorders*, 46, pp. S1–S5. doi: 10.1016/j.parkreldis.2017.07.020.

Fan, Y. *et al.* (2018) 'Differential Regulation of Adhesion and Phagocytosis of Resting and Activated Microglia by Dopamine.', *Frontiers in cellular neuroscience*, 12(September), p. 309. doi: 10.3389/fncel.2018.00309.

Fanning, S., Selkoe, D. and Dettmer, U. (2020) 'Parkinson's disease: proteinopathy or lipidopathy?', *NPJ Parkinson's disease*. Springer US, 6, p. 3. doi: 10.1038/s41531-019-0103-7.

Feany, M. B. and Bender, W. W. (2000) 'A Drosophila model of Parkinson's disease', *Nature*. Nature Publishing Group, 404(6776), pp. 394–398. doi: 10.1038/35006074.

Fearnley, J. M. and Lees, A. J. (1991) 'Ageing and Parkinson's disease: substantia nigra regional selectivity.', *Brain : a journal of neurology*, 114 ( Pt 5(5), pp. 2283–301. doi: 10.1093/brain/114.5.2283.

Fischer, H., Gottschlich, R. and Seelig, A. (1998) 'Blood-brain barrier permeation: Molecular parameters governing passive diffusion', *Journal of Membrane Biology*, 165(3), pp. 201–211. doi: 10.1007/s002329900434.

Fisher, B. E. *et al.* (2013) 'Treadmill exercise elevates striatal dopamine D2 receptor binding potential in patients with early Parkinson's disease.', *Neuroreport*, 24(10), pp. 509–14. doi: 10.1097/WNR.0b013e328361dc13.

Fitzsimmons, D. F., Moloney, T. C. and Dowd, E. (2006) 'Further validation of the corridor task for assessing deficit and recovery in the hemi-Parkinsonian rat: restoration of bilateral food retrieval by

dopamine receptor agonism.', *Behavioural brain research*, 169(2), pp. 352–5. doi: 10.1016/j.bbr.2006.01.013.

Fleming, S. M. *et al.* (2004) 'Behavioral and immunohistochemical effects of chronic intravenous and subcutaneous infusions of varying doses of rotenone', *Experimental Neurology*, 187(2), pp. 418–429. doi: 10.1016/j.expneurol.2004.01.023.

Fleming, S. M., Fernagut, P. O. and Chesselet, M. F. (2005) 'Genetic mouse models of Parkinsonism: Strengths and limitations', *NeuroRx*, 2(3), pp. 495–503. doi: 10.1602/neurorx.2.3.495.

Flinn, L. *et al.* (2009) 'Complex I deficiency and dopaminergic neuronal cell loss in parkin-deficient zebrafish (Danio rerio)', *Brain*, 132(6), pp. 1613–1623. doi: 10.1093/brain/awp108.

Flores-Martinez, Y. M. *et al.* (2018) 'Acute neuroinflammatory response in the substantia nigra pars compacta of rats after a local injection of lipopolysaccharide', *Journal of Immunology Research*, 2018. doi: 10.1155/2018/1838921.

Forno, L. S. *et al.* (1986) 'Locus ceruleus lesions and eosinophilic inclusions in MPTP-treated monkeys', *Annals of Neurology*, 20(4), pp. 449–455. doi: 10.1002/ana.410200403.

Frantz, C., Stewart, K. M. and Weaver, V. M. (2010) 'The extracellular matrix at a glance', *Journal of Cell Science*, 123(24), pp. 4195–4200. doi: 10.1242/jcs.023820.

Franzmeier, N. *et al.* (2020) 'Functional brain architecture is associated with the rate of tau accumulation in Alzheimer's disease', *Nature Communications*, 11(1), pp. 1–17. doi: 10.1038/s41467-019-14159-1.

Fu, J. F. *et al.* (2019) 'Joint pattern analysis applied to PET DAT and VMAT2 imaging reveals new insights into Parkinson's disease induced presynaptic alterations', *NeuroImage: Clinical*. Elsevier, 23(April), p. 101856. doi: 10.1016/j.nicl.2019.101856.

Fukai, M. *et al.* (2019) 'Endogenous dopamine release under transcranial direct-current stimulation governs enhanced attention: a study with positron emission tomography', *Translational Psychiatry*. Springer US, 9(1). doi: 10.1038/s41398-019-0443-4.

Furube, E. *et al.* (2018) 'Brain Region-dependent Heterogeneity and Dose-dependent Difference in Transient Microglia Population Increase during Lipopolysaccharide-induced Inflammation.', *Scientific reports*, 8(1), p. 2203. doi: 10.1038/s41598-018-20643-3.

Gallagher, C. L. *et al.* (2011) 'A within-subject comparison of 6-[18F]fluoro-m-tyrosine and 6-[18F]fluoro-L-dopa in Parkinson's disease.', *Movement disorders : official journal of the Movement Disorder Society*, 26(11), pp. 2032–8. doi: 10.1002/mds.23778.

Galter, D. *et al.* (2003) 'ALDH1 mRNA: Presence in human dopamine neurons and decreases in substantia nigra in Parkinson's disease and in the ventral tegmental area in schizophrenia', *Neurobiology of Disease*, 14(3), pp. 637–647. doi: 10.1016/j.nbd.2003.09.001.

García-García, F. *et al.* (2005) 'Sleep disturbances in the rotenone animal model of Parkinson disease', *Brain Research*, 1042(2), pp. 160–168. doi: 10.1016/j.brainres.2005.02.036.

García-Lorenzo, D. *et al.* (2018) 'Validation of an automatic reference region extraction for the quantification of [ 18 F]DPA-714 in dynamic brain PET studies', *Journal of Cerebral Blood Flow and Metabolism*, 38(2), pp. 333–346. doi: 10.1177/0271678X17692599.

Garcia, D. V. *et al.* (2015) 'A standardized method for the construction of tracer specific PET and

SPECT rat brain templates: Validation and implementation of a toolbox', *PLoS ONE*. doi: 10.1371/journal.pone.0122363.

Garnett, E. S., Firnau, G. and Nahmias, C. (1983) 'Dopamine visualized in the basal ganglia of living man.', *Nature*, 305(5930), pp. 137–8. doi: 10.1038/305137a0.

Gaskill, P. J. *et al.* (2012) 'Characterization and function of the human macrophage dopaminergic system: Implications for CNS disease and drug abuse', *Journal of Neuroinflammation*, 9, pp. 1–14. doi: 10.1186/1742-2094-9-203.

Gerfen, C. R. and Bolam, J. P. (2010) 'The Neuroanatomical Organization of the Basal Ganglia', *Handbook of Behavioral Neuroscience*. Elsevier, 20, pp. 3–28. doi: 10.1016/B978-0-12-374767-9.00001-9.

Gerhard, A. *et al.* (2006) 'In vivo imaging of microglial activation with [11C](R)-PK11195 PET in idiopathic Parkinson's disease', *Neurobiology of Disease*, 21(2), pp. 404–412. doi: 10.1016/j.nbd.2005.08.002.

Gerlach, M. *et al.* (2011) 'Role of dopamine D 3 and serotonin 5-HT 1A receptors in l-DOPA-induced dyskinesias and effects of sarizotan in the 6-hydroxydopamine- lesioned rat model of Parkinson's disease', *Journal of Neural Transmission*, 118(12), pp. 1733–1742. doi: 10.1007/s00702-010-0571-8.

Giovanni, A. *et al.* (1994) 'Studies on species sensitivity to the dopaminergic neurotoxin 1-methyl-4-phenyl-1,2,3,6-tetrahydropyridine. Part 1: Systemic administration.', *The Journal of pharmacology and experimental therapeutics*, 270(3), pp. 1000–7. Available at: http://www.ncbi.nlm.nih.gov/pubmed/7932147.

Glaab, E. *et al.* (2019) 'Integrative analysis of blood metabolomics and PET brain neuroimaging data for Parkinson's disease', *Neurobiology of Disease*. Elsevier, 124(October 2018), pp. 555–562. doi: 10.1016/j.nbd.2019.01.003.

Glass, C. K. *et al.* (2010) 'Mechanisms Underlying Inflammation in Neurodegeneration', *Cell*, 140(6), pp. 918–934. doi: 10.1016/j.cell.2010.02.016.

Goldberg, M. S. *et al.* (2005) 'Nigrostriatal dopaminergic deficits and hypokinesia caused by inactivation of the familial Parkinsonism-linked gene DJ-1.', *Neuron*, 45(4), pp. 489–96. doi: 10.1016/j.neuron.2005.01.041.

Goldenberg, M. M. (2008) 'Medical management of Parkinson's disease', *P and T*, 33(10).

Gombash, S. E. *et al.* (2013) 'Morphological and behavioral impact of AAV2/5-mediated overexpression of human wildtype alpha-synuclein in the rat nigrostriatal system.', *PloS one*. Edited by M. G. Tansey, 8(11), p. e81426. doi: 10.1371/journal.pone.0081426.

Gorbatyuk, O. S. *et al.* (2008) 'The phosphorylation state of Ser-129 in human alpha-synuclein determines neurodegeneration in a rat model of Parkinson disease.', *Proceedings of the National Academy of Sciences of the United States of America*. National Academy of Sciences, 105(2), pp. 763–8. doi: 10.1073/pnas.0711053105.

Gorell, J. M. *et al.* (1997) 'Occupational exposures to metals as risk factors for Parkinson's disease', *Neurology*, 48(3), pp. 650–658. doi: 10.1212/WNL.48.3.650.

Granado, N., Escobedo, I., *et al.* (2008) 'Early loss of dopaminergic terminals in striosomes after MDMA administration to mice', *Synapse*, 62(1), pp. 80–84. doi: 10.1002/syn.20466.

Granado, N., O'Shea, E., *et al.* (2008) 'Persistent MDMA-induced dopaminergic neurotoxicity in the striatum and substantia nigra of mice', *Journal of Neurochemistry*. doi: 10.1111/j.1471-4159.2008.05705.x.

Grealish, S. *et al.* (2014) 'Human ESC-derived dopamine neurons show similar preclinical efficacy and potency to fetal neurons when grafted in a rat model of Parkinson's disease', *Cell Stem Cell*. doi: 10.1016/j.stem.2014.09.017.

Green, A. R. *et al.* (2003) 'The Pharmacology and Clinical Pharmacology of 3,4-Methylenedioxymethamphetamine (MDMA, "Ecstasy")', *Pharmacological Reviews*, 55(3), pp. 463–508. doi: 10.1124/pr.55.3.3.

Greenwood, C. E. *et al.* (1991) 'Increased dopamine synthesis in aging substantia nigra neurons.', *Neurobiology of aging*, 12(5), pp. 557–65. doi: 10.1016/0197-4580(91)90087-z.

Greggio, E. *et al.* (2006) 'Kinase activity is required for the toxic effects of mutant LRRK2/dardarin.', *Neurobiology of disease*, 23(2), pp. 329–41. doi: 10.1016/j.nbd.2006.04.001.

Groiss, S. J. *et al.* (2009) 'Deep brain stimulation in Parkinson-s disease', *Therapeutic Advances in Neurological Disorders*, 2(6), pp. 379–391. doi: 10.1177/1756285609339382.

Gubinelli, F. (2019) *Evaluation of an in situ polymerizing hydrogel scaffold as a brain delivery system for Parkinson's disease therapeutics*. Université Paris-Saclay. Available at: http://www.theses.fr/s181084.

Guo, J. D. *et al.* (2018) 'Damage to dopaminergic neurons by oxidative stress in Parkinson's disease (Review)', *International Journal of Molecular Medicine*, 41(4), pp. 1817–1825. doi: 10.3892/ijmm.2018.3406.

Haber, S. N. (2014) 'The place of dopamine in the cortico-basal ganglia circuit.', *Neuroscience*, 282(1), pp. 248–57. doi: 10.1016/j.neuroscience.2014.10.008.

Hamilton, B. A. (2004) 'alpha-Synuclein A53T substitution associated with Parkinson disease also marks the divergence of Old World and New World primates.', *Genomics*, 83(4), pp. 739–42. doi: 10.1016/j.ygeno.2003.09.016.

Han, D. *et al.* (2020) 'Proteostasis of α-Synuclein and Its Role in the Pathogenesis of Parkinson's Disease', *Frontiers in Cellular Neuroscience*, 14(March), pp. 1–10. doi: 10.3389/fncel.2020.00045.

Haque, M. E. *et al.* (2012) 'Inactivation of Pink1 Gene in Vivo Sensitizes Dopamine-producing Neurons to 1-Methyl-4-phenyl-1,2,3,6-tetrahydropyridine (MPTP) and Can Be Rescued by Autosomal Recessive Parkinson Disease Genes, Parkin or DJ-1', *Journal of Biological Chemistry*, 287(27), pp. 23162–23170. doi: 10.1074/jbc.M112.346437.

Hawkes, C. H., Del Tredici, K. and Braak, H. (2009) 'Parkinson's disease: The dual hit theory revisited', *Annals of the New York Academy of Sciences*, 1170, pp. 615–622. doi: 10.1111/j.1749-6632.2009.04365.x.

Healy, D. G. *et al.* (2008) 'Phenotype, genotype, and worldwide genetic penetrance of LRRK2-associated Parkinson's disease: a case-control study.', *The Lancet. Neurology*, 7(7), pp. 583–90. doi: 10.1016/S1474-4422(08)70117-0.

van Heesch, F. *et al.* (2014) 'Lipopolysaccharide increases degradation of central monoamines: an in vivo microdialysis study in the nucleus accumbens and medial prefrontal cortex of mice.', *European journal of pharmacology*. Elsevier, 725(1), pp. 55–63. doi: 10.1016/j.ejphar.2014.01.014.

Heikkila, R. E. *et al.* (1984) 'Protection against the dopaminergic neurotoxicity of 1-methyl-4-phenyl-1,2,5,6-tetrahydropyridine by monoamine oxidase inhibitors.', *Nature*, 311(5985), pp. 467–9. Available at: http://www.ncbi.nlm.nih.gov/pubmed/6332989 (Accessed: 28 March 2019).

Herfert, K. *et al.* (2019) 'Quantitative Rodent Brain Receptor Imaging', *Molecular Imaging and Biology*. Molecular Imaging and Biology. doi: 10.1007/s11307-019-01368-9.

Hernán, M. A. *et al.* (2002) 'A meta-analysis of coffee drinking, cigarette smoking, and the risk of Parkinson's disease', *Annals of Neurology*, 52(3), pp. 276–284. doi: 10.1002/ana.10277.

Herrera, A. J. *et al.* (2000) 'The single intranigral injection of LPS as a new model for studying the selective effects of inflammatory reactions on dopaminergic system', *Neurobiology of Disease*, 7(4), pp. 429–447. doi: 10.1006/nbdi.2000.0289.

Hitti, F. L. *et al.* (2019) 'Human gene therapy approaches for the treatment of Parkinson's disease: An overview of current and completed clinical trials.', *Parkinsonism & related disorders*, 66, pp. 16–24. doi: 10.1016/j.parkreldis.2019.07.018.

Hoban, D. B. *et al.* (2013) 'Further characterisation of the LPS model of Parkinson's disease: A comparison of intra-nigral and intra-striatal lipopolysaccharide administration on motor function, microgliosis and nigrostriatal neurodegeneration in the rat', *Brain, Behavior, and Immunity*. Elsevier Inc., 27(1), pp. 91–100. doi: 10.1016/j.bbi.2012.10.001.

Höglinger, G. U. *et al.* (2003) 'Chronic systemic complex I inhibition induces a hypokinetic multisystem degeneration in rats', *Journal of Neurochemistry*, 84(3), pp. 491–502. doi: 10.1046/j.1471-4159.2003.01533.x.

Holness, C. L. and Simmons, D. L. (1993) 'Molecular cloning of CD68, a human macrophage marker related to lysosomal glycoproteins.', *Blood*, 81(6), pp. 1607–13. Available at: http://www.ncbi.nlm.nih.gov/pubmed/7680921.

Holtbernd, F. *et al.* (2015) 'Dopaminergic correlates of metabolic network activity in Parkinson's disease.', *Human brain mapping*, 36(9), pp. 3575–85. doi: 10.1002/hbm.22863.

Honer, M. *et al.* (2006) 'Comparison of [18F]FDOPA, [18F]FMT and [18F]FECNT for imaging dopaminergic neurotransmission in mice', *Nuclear Medicine and Biology*, 33(5), pp. 607–614. doi: 10.1016/j.nucmedbio.2006.04.005.

Horowitz, J. M. *et al.* (2001) *Immunodetection of Parkin protein in vertebrate and invertebrate brains: a comparative study using specific antibodies*, *Journal of Chemical Neuroanatomy*. Available at: www.elsevier.com/locate/jchemneu.

Hruska, K. S. *et al.* (2008) 'Gaucher disease: Mutation and polymorphism spectrum in the glucocerebrosidase gene (GBA)', *Human Mutation*, 29(5), pp. 567–583. doi: 10.1002/humu.20676.

Hsiao, I.-T. *et al.* (2014) 'Correlation of Parkinson disease severity and 18F-DTBZ positron emission tomography.', *JAMA neurology*, 71(6), pp. 758–66. doi: 10.1001/jamaneurol.2014.290.

Huang, L. Z. *et al.* (2009) 'Nicotine is neuroprotective when administered before but not after nigrostriatal damage in rats and monkeys.', *Journal of neurochemistry*, 109(3), pp. 826–37. doi: 10.1111/j.1471-4159.2009.06011.x.

Huang, L. Z. *et al.* (2011) 'Nicotinic receptor agonists decrease L-dopa-induced dyskinesias most effectively in partially lesioned parkinsonian rats.', *Neuropharmacology*, 60(6), pp. 861–8. doi: 10.1016/j.neuropharm.2010.12.032.

Hudson, J. L. *et al.* (1993) 'Correlation of apomorphine- and amphetamine-induced turning with nigrostriatal dopamine content in unilateral 6-hydroxydopamine lesioned rats', *Brain Research*, 626(1–2), pp. 167–174. doi: 10.1016/0006-8993(93)90576-9.

Iannaccone, S. *et al.* (2013) 'In vivo microglia activation in very early dementia with Lewy bodies, comparison with Parkinson's disease.', *Parkinsonism & related disorders*, 19(1), pp. 47–52. doi: 10.1016/j.parkreldis.2012.07.002.

Ichise, M. *et al.* (1996) 'Noninvasive quantification of dopamine D2 receptors with iodine-123-IBF SPECT', *Journal of Nuclear Medicine*, 37(3), pp. 513–520.

Ikeda, K. *et al.* (1978) 'Idiopathic parkinsonism with lewy-type inclusions in cerebral cortex. A case report', *Acta Neuropathologica*, 41(2), pp. 165–168. doi: 10.1007/BF00689769.

Ikeda, K. *et al.* (2019) 'Dopamine Transporter Imaging in Parkinson Disease: Progressive Changes and Therapeutic Modification after Anti-parkinsonian Medications.', *Internal medicine (Tokyo, Japan)*, 58(12), pp. 1665–1672. doi: 10.2169/internalmedicine.2489-18.

Ishida, Y. *et al.* (2005) 'Alteration of striatal [11C]raclopride and 6-[18F]fluoro-L-3,4-dihydroxyphenylalanine uptake precedes development of methamphetamine-induced rotation following unilateral 6-hydroxydopamine lesions of medial forebrain bundle in rats.', *Neuroscience letters*, 389(1), pp. 30–4. doi: 10.1016/j.neulet.2005.06.060.

Jackson-Lewis, V., Blesa, J. and Przedborski, S. (2012) 'Animal models of Parkinson's disease', *Parkinsonism & Related Disorders*. Elsevier, 18, pp. S183–S185. doi: 10.1016/S1353-8020(11)70057-8.

Jackson, A. *et al.* (2019) 'Diet in Parkinson's Disease: Critical Role for the Microbiome', *Frontiers in Neurology*, 10(December), pp. 1–21. doi: 10.3389/fneur.2019.01245.

Jacobowitz, D. M. *et al.* (1984) 'N-methyl-4-phenyl-1,2,3,6-tetra-hydropyridine (MPTP) causes destruction of the nigrostriatal but not the mesolimbic dopamine system in the monkey.', *Psychopharmacology bulletin*, 20(3), pp. 416–22. Available at: http://www.ncbi.nlm.nih.gov/pubmed/6332329 (Accessed: 28 March 2019).

Jagmag, S. A. *et al.* (2016) 'Evaluation of Models of Parkinson's Disease', *Frontiers in Neuroscience*, 9(JAN). doi: 10.3389/fnins.2015.00503.

Jakobson Mo, S. *et al.* (2018) 'Dopamine transporter imaging with [18F]FE-PE2I PET and [123I]FP-CIT SPECT—a clinical comparison', *EJNMMI Research*. EJNMMI Research, 8. doi: 10.1186/s13550-018-0450-0.

James, M. L. *et al.* (2008) 'DPA-714, a new translocator protein-specific ligand: Synthesis, radiofluorination, and pharmacologic characterization', *Journal of Nuclear Medicine*, 49(5), pp. 814–822. doi: 10.2967/jnumed.107.046151.

Jarraya, B. *et al.* (2009) 'Dopamine gene therapy for Parkinson's disease in a nonhuman primate without associated dyskinesia.', *Science translational medicine*, 1(2), p. 2ra4. doi: 10.1126/scitranslmed.3000130.

Jaunmuktane, Z. and Brandner, S. (2019) 'Invited Review: The role of prion-like mechanisms in neurodegenerative diseases', *Neuropathology and Applied Neurobiology*, pp. 1–24. doi: 10.1111/nan.12592.

Javitch, J. A. *et al.* (1985) 'Parkinsonism-inducing neurotoxin, N-methyl-4-phenyl-1,2,3,6 - tetrahydropyridine: uptake of the metabolite N-methyl-4-phenylpyridine by dopamine neurons

explains selective toxicity.', *Proceedings of the National Academy of Sciences of the United States of America*. National Academy of Sciences, 82(7), pp. 2173–7. doi: 10.1073/pnas.82.7.2173.

Javoy, F. *et al.* (1976) 'Specificity of dopaminergic neuronal degeneration induced by intracerebral injection of 6-hydroxydopamine in the nigrostriatal dopamine system', *Brain Research*. Elsevier, 102(2), pp. 201–215. doi: 10.1016/0006-8993(76)90877-5.

Jeon, B. S., Jackson-Lewis, V. and Burke, R. E. (1995) '6-Hydroxydopamine Lesion of the Rat Substantia Nigra: Time Course and Morphology of Cell Death', *Neurodegeneration*. Academic Press, 4(2), pp. 131–137. doi: 10.1006/neur.1995.0016.

Jiménez-Jiménez, F. J. *et al.* (1992) 'Serum levels of zinc and copper in patients with Parkinson's disease.', *Journal of the neurological sciences*, 112(1–2), pp. 30–3. doi: 10.1016/0022-510x(92)90127-7.

Jonsson, G. (1980) 'Chemical Neurotoxins as Denervation Tools in Neurobiology', *Annual Review of Neuroscience*. Annual Reviews 4139 El Camino Way, P.O. Box 10139, Palo Alto, CA 94303-0139, USA , 3(1), pp. 169–187. doi: 10.1146/annurev.ne.03.030180.001125.

Jordan, S. *et al.* (1997) '6-[18F]fluoro-L-m-tyrosine: metabolism, positron emission tomography kinetics, and 1-methyl-4-phenyl-1,2,3,6-tetrahydropyridine lesions in primates.', *Brain research*, 750(1–2), pp. 264–76. doi: 10.1016/s0006-8993(96)01366-2.

Joyce, J. N. *et al.* (1997) 'Differential modification of dopamine transporter and tyrosine hydroxylase mRNAs in midbrain of subjects with Parkinson's, Alzheimer's with parkinsonism, and Alzheimer's disease.', *Movement disorders : official journal of the Movement Disorder Society*, 12(6), pp. 885–97. doi: 10.1002/mds.870120609.

Kaasinen, V. and Vahlberg, T. (2017) 'Striatal dopamine in Parkinson disease: A meta-analysis of imaging studies', *Annals of Neurology*. doi: 10.1002/ana.25103.

Kachergus, J. *et al.* (2005) 'Identification of a novel LRRK2 mutation linked to autosomal dominant parkinsonism: evidence of a common founder across European populations.', *American journal of human genetics*, 76(4), pp. 672–80. doi: 10.1086/429256.

Kahle, P. J. *et al.* (2002) 'Structure/function of alpha-synuclein in health and disease: rational development of animal models for Parkinson's and related diseases.', *Journal of neurochemistry*, 82(3), pp. 449–57. doi: 10.1046/j.1471-4159.2002.01020.x.

Kalia, L. V. and Lang, A. E. (2015) 'Parkinson's disease', *The Lancet*, 386(9996), pp. 896–912. doi: 10.1016/S0140-6736(14)61393-3.

Kang, Y. *et al.* (2018) 'Noninvasive PK11195-PET Image Analysis Techniques Can Detect Abnormal Cerebral Microglial Activation in Parkinson's Disease', *Journal of Neuroimaging*, 28(5), pp. 496–505. doi: 10.1111/jon.12519.

Kanthasamy, A. G. *et al.* (2005) 'Dieldrin-induced neurotoxicity: Relevance to Parkinson's disease pathogenesis', *NeuroToxicology*, 26(4 SPEC. ISS.), pp. 701–719. doi: 10.1016/j.neuro.2004.07.010.

Karalija, N. *et al.* (2019) 'High long-term test-retest reliability for extrastriatal 11C-raclopride binding in healthy older adults.', *Journal of cerebral blood flow and metabolism : official journal of the International Society of Cerebral Blood Flow and Metabolism*, p. 271678X19874770. doi: 10.1177/0271678X19874770.

Kas, A. *et al.* (2009) 'Decrease of nicotinic receptors in the nigrostriatal system in Parkinson's

disease', *Journal of Cerebral Blood Flow and Metabolism*, 29(9), pp. 1601–1608. doi: 10.1038/jcbfm.2009.74.

Kempuraj, D. *et al.* (2016) 'Neuroinflammation Induces Neurodegeneration.', *Journal of neurology, neurosurgery and spine*, 1(1), pp. 1–15. Available at: http://www.ncbi.nlm.nih.gov/pubmed/28127589%0Ahttp://www.pubmedcentral.nih.gov/articlerender.fcgi?artid=PMC5260818.

Khan, M. S. *et al.* (2019) 'Dietary Supplementation of the Antioxidant Curcumin Halts Systemic LPS-Induced Neuroinflammation-Associated Neurodegeneration and Memory/Synaptic Impairment via the JNK/NF- κ B/Akt Signaling Pathway in Adult Rats', *Oxidative Medicine and Cellular Longevity*, 2019. doi: 10.1155/2019/7860650.

Kiely, A. P. *et al.* (2013) 'α-Synucleinopathy associated with G51D SNCA mutation: a link between Parkinson's disease and multiple system atrophy?', *Acta Neuropathologica*, 125(5), pp. 753–769. doi: 10.1007/s00401-013-1096-7.

Kikuchi, T. *et al.* (2017) 'Human iPS cell-derived dopaminergic neurons function in a primate Parkinson's disease model.', *Nature*, 548(7669), pp. 592–596. doi: 10.1038/nature23664.

Kilbourn, M. R. *et al.* (2007) 'Pharmacokinetics of [18F]fluoroalkyl derivatives of dihydrotetrabenazine in rat and monkey brain', *Nuclear Medicine and Biology*, 34(3), pp. 233–237. doi: 10.1016/j.nucmedbio.2007.01.007.

Kilbourn, M. R. and Koeppe, R. A. (2019) 'Classics in Neuroimaging: Radioligands for the Vesicular Monoamine Transporter 2', *ACS Chemical Neuroscience*. American Chemical Society, 10(1), pp. 25–29. doi: 10.1021/acschemneuro.8b00429.

Kim, R. H. *et al.* (2005) 'Hypersensitivity of DJ-1-deficient mice to 1-methyl-4-phenyl-1,2,3,6-tetrahydropyrindine (MPTP) and oxidative stress', *Proceedings of the National Academy of Sciences*, 102(14), pp. 5215–5220. doi: 10.1073/pnas.0501282102.

Kim, W. G. *et al.* (2000) 'Regional difference in susceptibility to lipopolysaccharide-induced neurotoxicity in the rat brain: role of microglia.', *The Journal of neuroscience : the official journal of the Society for Neuroscience*, 20(16), pp. 6309–16. Available at: http://www.ncbi.nlm.nih.gov/pubmed/10934283.

Kim, Y. J. *et al.* (2009) 'Neuroprotective effects of human mesenchymal stem cells on dopaminergic neurons through anti-inflammatory action', *Glia*, 57(1), pp. 13–23. doi: 10.1002/glia.20731.

Kim, Y. S. and Joh, T. H. (2006) 'Microglia, major player in the brain inflammation: their roles in the pathogenesis of Parkinson's disease.', *Experimental & molecular medicine*, 38(4), pp. 333–47. doi: 10.1038/emm.2006.40.

Kirik, D. *et al.* (2002) 'Parkinson-like neurodegeneration induced by targeted overexpression of alpha-synuclein in the nigrostriatal system.', *The Journal of neuroscience : the official journal of the Society for Neuroscience*, 22(7), pp. 2780–91. doi: 20026246.

Kitada, T. *et al.* (1998) 'Mutations in the parkin gene cause autosomal recessive juvenile parkinsonism.', *Nature*, 392(6676), pp. 605–8. doi: 10.1038/33416.

Kitada, T. *et al.* (2007) 'Impaired dopamine release and synaptic plasticity in the striatum of PINK1-deficient mice.', *Proceedings of the National Academy of Sciences of the United States of America*, 104(27), pp. 11441–6. doi: 10.1073/pnas.0702717104.

Kobayashi, J. *et al.* (2019) 'Extracellular α-synuclein enters dopaminergic cells by modulating flotillin-1-assisted dopamine transporter endocytosis.', *FASEB journal : official publication of the Federation of American Societies for Experimental Biology*, 33(9), pp. 10240–10256. doi: 10.1096/fj.201802051R.

Kobayashi, T. *et al.* (1997) 'EFFECTS OF L-DOPA AND BROMOCRIPTINE ON HALOPERIDOL-INDUCED MOTOR DEFICITS IN MICE', *Life Sciences*, 61(26), pp. 2529–2538. doi: 10.1016/S0024-3205(97)01007-2.

Konnova, E. A. and Swanberg, M. (2018) *Animal Models of Parkinson's Disease*, *Parkinson's Disease: Pathogenesis and Clinical Aspects*. Codon Publications. doi: 10.15586/CODONPUBLICATIONS.PARKINSONSDISEASE.2018.CH5.

Kordower, J. H. *et al.* (2006) 'Failure of proteasome inhibitor administration to provide a model of Parkinson's disease in rats and monkeys', *Annals of Neurology*, 60(2), pp. 264–268. doi: 10.1002/ana.20935.

Kordower, J. H., Chu, Y., Hauser, R. A., Freeman, T. B., *et al.* (2008) 'Lewy body-like pathology in long-term embryonic nigral transplants in Parkinson's disease.', *Nature medicine*, 14(5), pp. 504–6. doi: 10.1038/nm1747.

Kordower, J. H., Chu, Y., Hauser, R. A., Olanow, C. W., *et al.* (2008) 'Transplanted dopaminergic neurons develop PD pathologic changes: A second case report', *Movement Disorders*, 23(16), pp. 2303–2306. doi: 10.1002/mds.22369.

Kouli, A., Torsney, K. M. and Kuan, W.-L. (2018) *Parkinson's Disease: Etiology, Neuropathology, and Pathogenesis*, *Parkinson's Disease: Pathogenesis and Clinical Aspects*. Available at: http://www.ncbi.nlm.nih.gov/pubmed/30702842.

Kowall, N. W. *et al.* (2000) 'MPTP induces alpha-synuclein aggregation in the substantia nigra of baboons', *NeuroReport*, 11(1), pp. 211–213. doi: 10.1097/00001756-200001170-00041.

Kristensen, K. and Nørbygaard, E. (1984) *Safety and efficacy of radiopharmaceuticals*. Edited by K. Kristensen and E. Nørbygaard. Dordrecht: Springer Netherlands. doi: 10.1007/978-94-009-6753-3.

Krüger, R. *et al.* (1998) 'Ala3OPro mutation in the gene encoding α-synuclein in Parkinson's disease', *Nature Genetics*, 18(2), pp. 106–108. doi: 10.1038/ng0298-106.

Kuhnast, B. *et al.* (2012) '[ 18F]DPA-714, [ 18F]PBR111 and [ 18F]FEDAA1106-Selective radioligands for imaging TSPO 18kDa with PET: Automated radiosynthesis on a TRACERLAb FX-FN synthesizer and quality controls', *Applied Radiation and Isotopes*, 70(3), pp. 489–497. doi: 10.1016/j.apradiso.2011.10.015.

Kulkarni, S. K., Bishnoi, M. and Chopra, K. (2009) 'In vivo microdialysis studies of striatal level of neurotransmitters after haloperidol and chlorpromazine administration.', *Indian journal of experimental biology*, 47(2), pp. 91–7. Available at: http://www.ncbi.nlm.nih.gov/pubmed/19374163.

Kung, M. P. *et al.* (2007) 'Characterization of optically resolved 9-fluoropropyl-dihydrotetrabenazine as a potential PET imaging agent targeting vesicular monoamine transporters', *Nuclear Medicine and Biology*, 34(3), pp. 239–246. doi: 10.1016/j.nucmedbio.2006.12.005.

Kuwahara, T. *et al.* (2006) 'Familial Parkinson mutant alpha-synuclein causes dopamine neuron dysfunction in transgenic Caenorhabditis elegans.', *The Journal of biological chemistry*. American Society for Biochemistry and Molecular Biology, 281(1), pp. 334–40. doi: 10.1074/jbc.M504860200.

Kuwahara, T. *et al.* (2008) 'A systematic RNAi screen reveals involvement of endocytic pathway in neuronal dysfunction in α-synuclein transgenic C . elegans', *Human Molecular Genetics*, 17(19), pp. 2997–3009. doi: 10.1093/hmg/ddn198.

Kyono, K. *et al.* (2011) 'Use of [18F]FDOPA-PET for in vivo evaluation of dopaminergic dysfunction in unilaterally 6-OHDA-lesioned rats.', *EJNMMI research*, 1(1), p. 25. doi: 10.1186/2191-219X-1-25.

Lam, C. S., Korzh, V. and Strahle, U. (2005) 'Zebrafish embryos are susceptible to the dopaminergic neurotoxin MPTP', *European Journal of Neuroscience*, 21(6), pp. 1758–1762. doi: 10.1111/j.1460-9568.2005.03988.x.

Lammertsma AA and Hume SP (1996) 'Simplified reference tissue model for PET receptor studies', *Neuroimage*, 4(4), pp. 153–158. Available at: http://dx.doi.org/10.1006/nimg.1996.0066.

Lang, A. E. and Marras, C. (2014) 'Initiating dopaminergic treatment in Parkinson's disease.', *Lancet (London, England)*, 384(9949), pp. 1164–6. doi: 10.1016/S0140-6736(14)60962-4.

Langston, J. W. *et al.* (1983) 'Chronic Parkinsonism in humans due to a product of meperidine-analog synthesis.', *Science (New York, N.Y.)*, 219(4587), pp. 979–80. Available at: http://www.ncbi.nlm.nih.gov/pubmed/6823561 (Accessed: 28 March 2019).

Langston, J. W. *et al.* (1999) 'Evidence of active nerve cell degeneration in the substantia nigra of humans years after 1-methyl-4-phenyl-1,2,3,6-tetrahydropyridine exposure.', *Annals of neurology*, 46(4), pp. 598–605. doi: 10.1002/1531-8249(199910)46:4<598::aid-ana7>3.0.co;2-f.

Langston, J. W. (2017) 'The MPTP Story', *Journal of Parkinson's Disease*. IOS Press, 7(s1), pp. S11–S19. doi: 10.3233/JPD-179006.

Langston, J. W., Langston, E. B. and Irwin, I. (1984) 'MPTP-induced parkinsonism in human and non-human primates--clinical and experimental aspects.', *Acta neurologica Scandinavica. Supplementum*, 100, pp. 49–54. Available at: http://www.ncbi.nlm.nih.gov/pubmed/6333134 (Accessed: 28 March 2019).

Larsen, K. E. *et al.* (2002) 'Methamphetamine-induced degeneration of dopaminergic neurons involves autophagy and upregulation of dopamine synthesis.', *The Journal of neuroscience : the official journal of the Society for Neuroscience*, 22(20), pp. 8951–60. Available at: http://www.ncbi.nlm.nih.gov/pubmed/12388602.

de Lau, L. M. L. and Breteler, M. M. B. (2006) 'Epidemiology of Parkinson's disease.', *The Lancet. Neurology*, 5(6), pp. 525–35. doi: 10.1016/S1474-4422(06)70471-9.

Lavicky, J. and Dunn, A. J. (1995) 'Endotoxin administration stimulates cerebral catecholamine release in freely moving rats as assessed by microdialysis.', *Journal of neuroscience research*, 40(3), pp. 407–13. doi: 10.1002/jnr.490400316.

Lavisse, S. *et al.* (2012) 'Reactive Astrocytes Overexpress TSPO and Are Detected by TSPO Positron Emission Tomography Imaging', *Journal of Neuroscience*, 32(32), pp. 10809–10818. doi: 10.1523/JNEUROSCI.1487-12.2012.

Lavisse, S., Inoue, K., *et al.* (2015) '[18F]DPA-714 PET imaging of translocator protein TSPO (18 kDa) in the normal and excitotoxically-lesioned nonhuman primate brain.', *European journal of nuclear medicine and molecular imaging*, 42(3), pp. 478–94. doi: 10.1007/s00259-014-2962-9.

Lavisse, S., García-Lorenzo, D., *et al.* (2015) 'Optimized Quantification of Translocator Protein Radioligand $^{18}$F-DPA-714 Uptake in the Brain of Genotyped Healthy Volunteers.', *Journal of nuclear*

*medicine : official publication, Society of Nuclear Medicine*, 56(7), pp. 1048–54. doi: 10.2967/jnumed.115.156083.

Lawson, L. J. *et al.* (1990) 'Heterogeneity in the distribution and morphology of microglia in the normal adult mouse brain.', *Neuroscience*, 39(1), pp. 151–70. doi: 10.1016/0306-4522(90)90229-w.

Lazarou, M. *et al.* (2013) 'PINK1 drives Parkin self-association and HECT-like E3 activity upstream of mitochondrial binding.', *The Journal of cell biology*, 200(2), pp. 163–72. doi: 10.1083/jcb.201210111.

Lee, C. S. *et al.* (2000) 'In vivo positron emission tomographic evidence for compensatory changes in presynaptic dopaminergic nerve terminals in Parkinson's disease.', *Annals of neurology*, 47(4), pp. 493–503. doi: 10.1002/1531-8249(200004)47:4<493::AID-ANA13>3.0.CO;2-4.

Lee, J.-W. *et al.* (2015) 'Behavioral, neurochemical, and pathologic alterations in bacterial artificial chromosome transgenic G2019S leucine-rich repeated kinase 2 rats.', *Neurobiology of aging*, 36(1), pp. 505–18. doi: 10.1016/j.neurobiolaging.2014.07.011.

Lee, S. *et al.* (2012) 'The synaptic function of LRRK2', *Biochemical Society Transactions*, 40(5), pp. 1047–1051. doi: 10.1042/BST20120113.

Lelos, M. J. *et al.* (2016) 'Direct Comparison of Rat- and Human-Derived Ganglionic Eminence Tissue Grafts on Motor Function.', *Cell transplantation*, 25(4), pp. 665–75. doi: 10.3727/096368915X690297.

Lemaire, C. *et al.* (2015) 'Automated production at the curie level of no-carrier-added 6-[ 18 F]fluoro- l -dopa and 2-[ 18 F]fluoro- l -tyrosine on a FASTlab synthesizer', *Journal of Labelled Compounds and Radiopharmaceuticals*, 58(7), pp. 281–290. doi: 10.1002/jlcr.3291.

Lerner, A. and Bagic, A. (2008) 'Olfactory pathogenesis of idiopathic parkinson disease revisited', *Movement Disorders*, 23(8), pp. 1076–1084. doi: 10.1002/mds.22066.

Leroy, E. *et al.* (1998) 'The ubiquitin pathway in Parkinson's disease', *Nature*, 395(6701), pp. 451–452. doi: 10.1038/26652.

Leung, K. (2004) *[11C]N,N-Dimethyl-2-(2-amino-4-cyanophenylthio)benzylamine*, *Molecular Imaging and Contrast Agent Database (MICAD)*. Available at: http://www.ncbi.nlm.nih.gov/pubmed/20641586.

Lewis, T. B. (2018) *Study of OXB-102 (AXO-Lenti-PD) in Patients With Bilateral, Idiopathic Parkinson's Disease (SUNRISE-PD)*, *ClinicalTrials.gov*. Available at: https://clinicaltrials.gov/ct2/show/NCT03720418.

Li, C. T. *et al.* (2014) 'A dual-tracer study of extrastriatal 6-[18F]fluoro-m-tyrosine and 6-[18F]-fluoro-l-dopa Uptake in Parkinson's disease', *Synapse*, 68(8), pp. 325–331. doi: 10.1002/syn.21745.

Li, J.-Q., Tan, L. and Yu, J.-T. (2014) 'The role of the LRRK2 gene in Parkinsonism', *Molecular Neurodegeneration*, 9(1), p. 47. doi: 10.1186/1750-1326-9-47.

Li, J.-Y. *et al.* (2008) 'Lewy bodies in grafted neurons in subjects with Parkinson's disease suggest host-to-graft disease propagation', *Nature Medicine*, 14(5), pp. 501–503. doi: 10.1038/nm1746.

Liddelow, S. A. *et al.* (2017) 'Neurotoxic reactive astrocytes are induced by activated microglia.', *Nature*, 541(7638), pp. 481–487. doi: 10.1038/nature21029.

Lin, C.-Y. *et al.* (2011) 'Dose-Response Relationship Between Cumulative Mercury Exposure Index and Specific Uptake Ratio in the Striatum on Tc-99m TRODAT SPECT', *Clinical Nuclear Medicine*, 36(8), pp.

689–693. doi: 10.1097/RLU.0b013e3181e9fa93.

Lin, K. J. *et al.* (2013) 'Brain Imaging of Vesicular Monoamine Transporter Type 2 in Healthy Aging Subjects by 18F-FP-(+)-DTBZ PET', *PLoS ONE*, 8(9), pp. 1–7. doi: 10.1371/journal.pone.0075952.

Lin, S. C. *et al.* (2014) 'In vivo detection of monoaminergic degeneration in early parkinson disease by 18F-9-fluoropropyl-(1)-dihydrotetrabenzazine PET', *Journal of Nuclear Medicine*, 55(1), pp. 73–79. doi: 10.2967/jnumed.113.121897.

Lin, X. *et al.* (2009) 'Leucine-Rich Repeat Kinase 2 Regulates the Progression of Neuropathology Induced by Parkinson's-Disease-Related Mutant α-synuclein', *Neuron*, 64(6), pp. 807–827. doi: 10.1016/j.neuron.2009.11.006.

Lindvall, O. *et al.* (1990) 'Grafts of fetal dopamine neurons survive and improve motor function in Parkinson's disease.', *Science (New York, N.Y.)*, 247(4942), pp. 574–7. doi: 10.1126/science.2105529.

Liu, B. *et al.* (2017) 'Vagotomy and Parkinson disease', *Neurology*, 88(21), pp. 1996–2002. doi: 10.1212/wnl.0000000000003961.

Liu, M. and Bing, G. (2011) 'Lipopolysaccharide Animal Models for Parkinson's Disease', *Parkinson's Disease*, 2011, pp. 1–7. doi: 10.4061/2011/327089.

Liu, Z. *et al.* (2008) 'A Drosophila model for LRRK2-linked parkinsonism.', *Proceedings of the National Academy of Sciences of the United States of America*, 105(7), pp. 2693–8. doi: 10.1073/pnas.0708452105.

Logan, J. *et al.* (1990) 'Graphical Analysis of Reversible Radioligand Binding from Time—Activity Measurements Applied to [ N - 11 C-Methyl]-(−)-Cocaine PET Studies in Human Subjects', *Journal of Cerebral Blood Flow & Metabolism*, 10(5), pp. 740–747. doi: 10.1038/jcbfm.1990.127.

Logan, J. *et al.* (1996) 'Distribution volume ratios without blood sampling from graphical analysis of PET data.', *Journal of cerebral blood flow and metabolism : official journal of the International Society of Cerebral Blood Flow and Metabolism*, 16(5), pp. 834–40. doi: 10.1097/00004647-199609000-00008.

Lopes, P. C. (2016) 'LPS and neuroinflammation: a matter of timing.', *Inflammopharmacology*, 24(5), pp. 291–293. doi: 10.1007/s10787-016-0283-2.

Lorenc-Koci, E. *et al.* (2004) 'Effect of 1,2,3,4,-tetrahydroisoquinoline administration under conditions of CYP2D inhibition on dopamine metabolism, level of tyrosine hydroxylase protein and the binding of [3H]GBR 12,935 to dopamine transporter in the rat nigrostriatal, dopaminergic sy', *Brain Research*, 1009(1–2), pp. 67–81. doi: 10.1016/j.brainres.2004.02.044.

Lu, X.-H. *et al.* (2009) 'Bacterial Artificial Chromosome Transgenic Mice Expressing a Truncated Mutant Parkin Exhibit Age-Dependent Hypokinetic Motor Deficits, Dopaminergic Neuron Degeneration, and Accumulation of Proteinase K-Resistant -Synuclein', *Journal of Neuroscience*, 29(7), pp. 1962–1976. doi: 10.1523/JNEUROSCI.5351-08.2009.

Lücking, C. B. *et al.* (2000) 'Association between Early-Onset Parkinson's Disease and Mutations in the Parkin Gene', *New England Journal of Medicine*, 342(21), pp. 1560–1567. doi: 10.1056/NEJM200005253422103.

Luk, K. C. *et al.* (2012) 'Pathological α-synuclein transmission initiates Parkinson-like neurodegeneration in nontransgenic mice.', *Science (New York, N.Y.)*, 338(6109), pp. 949–53. doi: 10.1126/science.1227157.

Ma, Y. *et al.* (2002) 'Parametric mapping of [18F]FPCIT binding in early stage Parkinson's disease: a PET study.', *Synapse (New York, N.Y.)*, 45(2), pp. 125–33. doi: 10.1002/syn.10090.

Ma, Y. *et al.* (2007) 'Abnormal metabolic network activity in Parkinson's disease: test-retest reproducibility.', *Journal of cerebral blood flow and metabolism : official journal of the International Society of Cerebral Blood Flow and Metabolism*, 27(3), pp. 597–605. doi: 10.1038/sj.jcbfm.9600358.

Ma, Y. *et al.* (2012) 'Abnormal metabolic brain networks in a nonhuman primate model of parkinsonism', *Journal of Cerebral Blood Flow and Metabolism*, 32(4), pp. 633–642. doi: 10.1038/jcbfm.2011.166.

Ma, Y. *et al.* (2015) 'Reproducibility of a Parkinsonism-related metabolic brain network in non-human primates: A descriptive pilot study with FDG PET', *Movement disorders : official journal of the Movement Disorder Society*, 30(9), pp. 1283–1288. doi: 10.1002/mds.26302.

Macedo, M. G. *et al.* (2003) 'The DJ-1L166P mutant protein associated with early onset Parkinson's disease is unstable and forms higher-order protein complexes.', *Human molecular genetics*, 12(21), pp. 2807–16. doi: 10.1093/hmg/ddg304.

Mach, R. H. and Luedtke, R. R. (2018) 'Challenges in the development of dopamine D2- and D3-selective radiotracers for PET imaging studies', *Journal of Labelled Compounds and Radiopharmaceuticals*, 61(3), pp. 291–298. doi: 10.1002/jlcr.3558.

Maia, S. *et al.* (2012) 'Longitudinal and parallel monitoring of neuroinflammation and neurodegeneration in a 6-hydroxydopamine rat model of Parkinson's disease', *Synapse*, 66(7), pp. 573–583. doi: 10.1002/syn.21543.

Maillet, A. *et al.* (2016) 'The prominent role of serotonergic degeneration in apathy, anxiety and depression in de novo Parkinson's disease.', *Brain : a journal of neurology*, 139(Pt 9), pp. 2486–502. doi: 10.1093/brain/aww162.

Maj, J. *et al.* (1997) 'The behavioural effects of pramipexole, a novel dopamine receptor agonist', *European Journal of Pharmacology*, 324(1), pp. 31–37. doi: 10.1016/S0014-2999(97)00066-6.

Malek, N. (2019) 'Deep Brain Stimulation in Parkinson's Disease', *Neurology India*, 67(4), pp. 968–978. doi: 10.4103/0028-3886.266268.

Mann, T. *et al.* (2018) '[18F]fallypride-PET/CT Analysis of the Dopamine $D_2/D_3$ Receptor in the Hemiparkinsonian Rat Brain Following Intrastriatal Botulinum Neurotoxin A Injection.', *Molecules (Basel, Switzerland)*, 23(3). doi: 10.3390/molecules23030587.

Manning-Bog, A. B. *et al.* (2002) 'The Herbicide Paraquat Causes Up-regulation and Aggregation of α-Synuclein in Mice', *Journal of Biological Chemistry*, 277(3), pp. 1641–1644. doi: 10.1074/jbc.C100560200.

Manning-Boğ, A. B. *et al.* (2006) 'Lack of nigrostriatal pathology in a rat model of proteasome inhibition', *Annals of Neurology*, 60(2), pp. 256–260. doi: 10.1002/ana.20938.

Männistö, P. T. (1998) 'Catechol O-methyltransferase: characterization of the protein, its gene, and the preclinical pharmacology of COMT inhibitors.', *Advances in pharmacology (San Diego, Calif.)*, 42, pp. 324–8. doi: 10.1016/s1054-3589(08)60755-3.

Mariani, S. *et al.* (2013) 'Fe and Cu do not differ in Parkinson's disease: A replication study plus meta-analysis', *Neurobiology of Aging*, 34(2), pp. 632–633. doi: 10.1016/j.neurobiolaging.2012.05.015.

Marin, O. *et al.* (1997) *Basal Ganglia Organization in Amphibians: Development of Striatal and Nucleus Accumbens Connections With Emphasis on the Catecholaminergic Inputs*, *J. Comp. Neurol*. Wiley-Liss, Inc.

Marks, W. J. *et al.* (2008) 'Safety and tolerability of intraputaminal delivery of CERE-120 (adeno-associated virus serotype 2-neurturin) to patients with idiopathic Parkinson's disease: an open-label, phase I trial', *The Lancet Neurology*, 7(5), pp. 400–408. doi: 10.1016/S1474-4422(08)70065-6.

Marks, W. J. *et al.* (2010) 'Gene delivery of AAV2-neurturin for Parkinson's disease: A double-blind, randomised, controlled trial', *The Lancet Neurology*, 9(12), pp. 1164–1172. doi: 10.1016/S1474-4422(10)70254-4.

Maroteaux, L., Campanelli, J. and Scheller, R. (1988) 'Synuclein: a neuron-specific protein localized to the nucleus and presynaptic nerve terminal', *The Journal of Neuroscience*, 8(8), pp. 2804–2815. doi: 10.1523/JNEUROSCI.08-08-02804.1988.

Marsden, C. D. (1990) 'Parkinson's disease', *The Lancet*, 335(8695), pp. 948–949. doi: 10.1016/0140-6736(90)91006-V.

Mastroeni, D. *et al.* (2009) 'Microglial responses to dopamine in a cell culture model of Parkinson's disease', *Neurobiology of Aging*, 30(11), pp. 1805–1817. doi: 10.1016/j.neurobiolaging.2008.01.001.

Mattammal, M. B. *et al.* (1993) 'Confirmation of a dopamine metabolite in parkinsonian brain tissue by gas chromatography—mass spectrometry', *Journal of Chromatography B: Biomedical Sciences and Applications*, 614(2), pp. 205–212. doi: 10.1016/0378-4347(93)80310-Z.

Matthews, D. C. *et al.* (2018) 'FDG PET Parkinson's disease-related pattern as a biomarker for clinical trials in early stage disease', *NeuroImage: Clinical*. Elsevier, 20(August), pp. 572–579. doi: 10.1016/j.nicl.2018.08.006.

McCormack, A. L. *et al.* (2002) 'Environmental risk factors and Parkinson's disease: selective degeneration of nigral dopaminergic neurons caused by the herbicide paraquat.', *Neurobiology of disease*, 10(2), pp. 119–27. doi: https://doi.org/10.1006/nbdi.2002.0507.

McCoy, M. K. and Cookson, M. R. (2012) 'Mitochondrial quality control and dynamics in Parkinson's disease.', *Antioxidants & redox signaling*, 16(9), pp. 869–82. doi: 10.1089/ars.2011.4019.

McGeer, P. L. *et al.* (1988) 'Reactive microglia are positive for HLA-DR in the substantia nigra of Parkinson's and Alzheimer's disease brains', *Neurology*, 38(8), pp. 1285–1285. doi: 10.1212/WNL.38.8.1285.

McNaught, Kevin St P. *et al.* (2002) 'Impairment of the ubiquitin-proteasome system causes dopaminergic cell death and inclusion body formation in ventral mesencephalic cultures', *Journal of Neurochemistry*, 81(2), pp. 301–306. doi: 10.1046/j.1471-4159.2002.00821.x.

McNaught, Kevin St. P. *et al.* (2002) 'Proteasome inhibition causes nigral degeneration with inclusion bodies in rats', *Neuroreport*, 13(11), pp. 1437–1441. doi: 10.1097/00001756-200208070-00018.

McNaught, K. S. P. *et al.* (2004) 'Systemic exposure to proteasome inhibitors causes a progressive model of Parkinson's disease', *Annals of Neurology*, 56(1), pp. 149–162. doi: 10.1002/ana.20186.

Meamar, R. *et al.* (2016) 'Assessing of plasma levels of iron, zinc and copper in Iranian Parkinson's disease', *Advanced Biomedical Research*, 5(1), p. 31. doi: 10.4103/2277-9175.178788.

Melega, W. P. *et al.* (1991) 'L-6-[18F]fluoro-dopa metabolism in monkeys and humans: biochemical

parameters for the formulation of tracer kinetic models with positron emission tomography.', *Journal of cerebral blood flow and metabolism : official journal of the International Society of Cerebral Blood Flow and Metabolism*, 11(6), pp. 890–7. doi: 10.1038/jcbfm.1991.154.

Meles, S. K. *et al.* (2017) 'Metabolic Imaging in Parkinson Disease.', *Journal of nuclear medicine : official publication, Society of Nuclear Medicine*, 58(1), pp. 23–28. doi: 10.2967/jnumed.116.183152.

Meles, S. K. *et al.* (2020) 'Abnormal pattern of brain glucose metabolism in Parkinson's disease: replication in three European cohorts', *European Journal of Nuclear Medicine and Molecular Imaging*. European Journal of Nuclear Medicine and Molecular Imaging, 47(2), pp. 437–450. doi: 10.1007/s00259-019-04570-7.

Melia, K. R. *et al.* (1994) 'Detection and regulation of tyrosine hydroxylase mRNA in catecholaminergic terminal fields: possible axonal compartmentalization.', *Experimental neurology*, 130(2), pp. 394–406. doi: 10.1006/exnr.1994.1219.

Melki, R. (2018) 'Alpha-synuclein and the prion hypothesis in Parkinson's disease', *Revue Neurologique*. doi: 10.1016/j.neurol.2018.08.002.

Migdalska-Richards, A. and Schapira, A. H. V (2016) 'The relationship between glucocerebrosidase mutations and Parkinson disease.', *Journal of neurochemistry*, 139 Suppl, pp. 77–90. doi: 10.1111/jnc.13385.

Millan, M. J. *et al.* (2002) 'Differential Actions of Antiparkinson Agents at Multiple Classes of Monoaminergic Receptor. I. A Multivariate Analysis of the Binding Profiles of 14 Drugs at 21 Native and Cloned Human Receptor Subtypes', *Journal of Pharmacology and Experimental Therapeutics*, 303(2), pp. 791–804. doi: 10.1124/jpet.102.039867.

Miller, P. W. *et al.* (2008) 'Synthesis of 11C, 18F, 15O, and 13N radiolabels for positron emission tomography.', *Angewandte Chemie (International ed. in English)*, 47(47), pp. 8998–9033. doi: 10.1002/anie.200800222.

Millot, M. *et al.* (2020) 'Prior MDMA administration aggravates MPTP-induced Parkinsonism in macaque monkeys.', *Neurobiology of disease*. Elsevier, 134(July 2019), p. 104643. doi: 10.1016/j.nbd.2019.104643.

MohanKumar, S. M., MohanKumar, P. S. and Quadri, S. K. (1999) 'Lipopolysaccharide-induced changes in monoamines in specific areas of the brain: blockade by interleukin-1 receptor antagonist.', *Brain research*, 824(2), pp. 232–7. doi: 10.1016/s0006-8993(99)01206-8.

Moore, D. J. *et al.* (2003) 'A missense mutation (L166P) in DJ-1, linked to familial Parkinson's disease, confers reduced protein stability and impairs homo-oligomerization.', *Journal of neurochemistry*, 87(6), pp. 1558–67. doi: 10.1111/j.1471-4159.2003.02265.x.

Moore, D. J., Dawson, V. L. and Dawson, T. M. (2006) 'Lessons from Drosophila models of DJ-1 deficiency.', *Science of aging knowledge environment : SAGE KE*, 2006(2), p. pe2. doi: 10.1126/sageke.2006.2.pe2.

Mori, S. *et al.* (1988) 'Immunohistochemical evaluation of the neurotoxic effects of 1-methyl-4-phenyl-1,2,3,6-tetrahydropyridine (MPTP) on dopaminergic nigrostriatal neurons of young adult mice using dopamine and tyrosine hydroxylase antibodies', *Neuroscience Letters*, 90(1–2), pp. 57–62. doi: 10.1016/0304-3940(88)90786-0.

Moriarty, N. *et al.* (2019) 'Encapsulation of young donor age dopaminergic grafts in a GDNF-loaded collagen hydrogel further increases their survival, reinnervation, and functional efficacy after

intrastriatal transplantation in hemi-Parkinsonian rats.', *The European journal of neuroscience*, 49(4), pp. 487–496. doi: 10.1111/ejn.14090.

Moriarty, N., Pandit, A. and Dowd, E. (2017) 'Encapsulation of primary dopaminergic neurons in a GDNF-loaded collagen hydrogel increases their survival, re-innervation and function after intra-striatal transplantation.', *Scientific reports*, 7(1), p. 16033. doi: 10.1038/s41598-017-15970-w.

Mukherjee, J. *et al.* (1995) 'Fluorinated benzamide neuroleptics--III. Development of (S)-N-[(1-allyl-2-pyrrolidinyl)methyl]-5-(3-[18F]fluoropropyl)-2, 3-dimethoxybenzamide as an improved dopamine D-2 receptor tracer.', *Nuclear medicine and biology*, 22(3), pp. 283–96. doi: 10.1016/0969-8051(94)00117-3.

Mukherjee, J. *et al.* (1997) 'Evaluation of d-amphetamine effects on the binding of dopamine D-2 receptor radioligand, 18F-fallypride in nonhuman primates using positron emission tomography', *Synapse*, 27(1), pp. 1–13. doi: 10.1002/(SICI)1098-2396(199709)27:1<1::AID-SYN1>3.0.CO;2-9.

Mukherjee, J. *et al.* (1999) 'Preliminary assessment of extrastriatal dopamine D-2 receptor binding in the rodent and nonhuman primate brains using the high affinity radioligand, 18F-fallypride', *Nuclear Medicine and Biology*, 26(5), pp. 519–527. doi: 10.1016/S0969-8051(99)00012-8.

Mukherjee, S. and Thrasher, A. J. (2013) 'Gene therapy for PIDs: Progress, pitfalls and prospects', *Gene*. Elsevier B.V., 525(2), pp. 174–181. doi: 10.1016/j.gene.2013.03.098.

Mulcahy, P. *et al.* (2012) 'Development and characterisation of a novel rat model of Parkinson's disease induced by sequential intranigral administration of AAV-α-synuclein and the pesticide, rotenone', *Neuroscience*. Elsevier Inc., 203, pp. 170–179. doi: 10.1016/j.neuroscience.2011.12.011.

Mulcahy, P. *et al.* (2013) 'The behavioural and neuropathological impact of intranigral AAV-α-synuclein is exacerbated by systemic infusion of the Parkinson's disease-associated pesticide, rotenone, in rats', *Behavioural Brain Research*. Elsevier B.V., 243(1), pp. 6–15. doi: 10.1016/j.bbr.2012.12.051.

Muramatsu, S. I. *et al.* (2010) 'A phase i study of aromatic l-amino acid decarboxylase gene therapy for parkinson's disease', *Molecular Therapy*. The American Society of Gene & Cell Therapy, 18(9), pp. 1731–1735. doi: 10.1038/mt.2010.135.

Musacchio, J. M. (1975) 'Enzymes Involved in the Biosynthesis and Degradation of Catecholamines', in Iversen, L. L., Iversen, S. D., and Snyder, S. H. (eds) *Biochemistry of Biogenic Amines*. Boston, MA: Springer US, pp. 1–35. doi: 10.1007/978-1-4684-3171-1_1.

Nagatsu, T. *et al.* (2000) 'Cytokines in Parkinson's disease.', *Journal of neural transmission. Supplementum*, (58), pp. 143–51. Available at: http://www.ncbi.nlm.nih.gov/pubmed/11128604.

Nalls, M. A. *et al.* (2019) 'Identification of novel risk loci, causal insights, and heritable risk for Parkinson's disease: a meta-analysis of genome-wide association studies.', *The Lancet. Neurology*, 18(12), pp. 1091–1102. doi: 10.1016/S1474-4422(19)30320-5.

Nandhagopal, R. *et al.* (2008) 'Progression of dopaminergic dysfunction in a LRRK2 kindred: A multitracer PET study', *Neurology*, 71(22), pp. 1790–1795. doi: 10.1212/01.wnl.0000335973.66333.58.

Napieczynska, H. *et al.* (2018) 'Impact of the arterial input function recording method on kinetic parameters in small-animal PET', *Journal of Nuclear Medicine*, 59(7), pp. 1159–1164. doi: 10.2967/jnumed.117.204164.

Nass, R. *et al.* (2002) 'Neurotoxin-induced degeneration of dopamine neurons in Caenorhabditis elegans', *Proceedings of the National Academy of Sciences*, 99(5), pp. 3264–3269. doi: 10.1073/pnas.042497999.

Navntoft, C. A. and Dreyer, J. K. (2016) 'How compensation breaks down in Parkinson's disease: Insights from modeling of denervated striatum.', *Movement disorders : official journal of the Movement Disorder Society*, 31(3), pp. 280–9. doi: 10.1002/mds.26579.

Ness, D. *et al.* (2013) 'Leucine-Rich Repeat Kinase 2 (LRRK2)-Deficient Rats Exhibit Renal Tubule Injury and Perturbations in Metabolic and Immunological Homeostasis', *PLoS ONE*, 8(6). doi: 10.1371/journal.pone.0066164.

Nicklas, W. J., Vyas, I. and Heikkila, R. E. (1985) 'Inhibition of NADH-linked oxidation in brain mitochondria by 1-methyl-4-phenyl-pyridine, a metabolite of the neurotoxin, 1-methyl-4-phenyl-1,2,5,6-tetrahydropyridine', *Life Sciences*. Pergamon, 36(26), pp. 2503–2508. doi: 10.1016/0024-3205(85)90146-8.

Nikolaus, S. *et al.* (2003) 'Bilateral increase in striatal dopamine D2 receptor density in the 6-hydroxydopamine-lesioned rat: a serial in vivo investigation with small animal PET.', *European journal of nuclear medicine and molecular imaging*, 30(3), pp. 390–5. doi: 10.1007/s00259-002-1056-2.

Nikolaus, S. *et al.* (2014) 'Relationship between L-DOPA-induced reduction in motor and exploratory activity and degree of DAT binding in the rat', *Frontiers in Behavioral Neuroscience*, 8(DEC), pp. 1–16. doi: 10.3389/fnbeh.2014.00431.

Nimmerjahn, A., Kirchhoff, F. and Helmchen, F. (2005) 'Resting microglial cells are highly dynamic surveillants of brain parenchyma in vivo.', *Science (New York, N.Y.)*, 308(5726), pp. 1314–8. doi: 10.1126/science.1110647.

Nolan, Y. *et al.* (2000) 'Lipopolysaccharide administration produces time-dependent and region-specific alterations in tryptophan and tyrosine hydroxylase activities in rat brain', *Journal of Neural Transmission*, 107(12), pp. 1393–1401. doi: 10.1007/s007020070003.

Norris, E. H. *et al.* (2007) 'Pesticide exposure exacerbates alpha-synucleinopathy in an A53T transgenic mouse model.', *The American journal of pathology*, 170(2), pp. 658–66. doi: 10.2353/ajpath.2007.060359.

Noyce, A. J. *et al.* (2012) 'Meta-analysis of early nonmotor features and risk factors for Parkinson disease', *Annals of Neurology*, 72(6), pp. 893–901. doi: 10.1002/ana.23687.

Offen, D. *et al.* (2007) 'Intrastriatal transplantation of mouse bone marrow-derived stem cells improves motor behavior in a mouse model of Parkinson's disease.', *Journal of neural transmission. Supplementum*, (72), pp. 133–43. doi: 10.1007/978-3-211-73574-9_16.

Okamura, N. *et al.* (2010) 'In vivo measurement of vesicular monoamine transporter type 2 density in Parkinson disease with 18F-AV-133', *Journal of Nuclear Medicine*, 51(2), pp. 223–228. doi: 10.2967/jnumed.109.070094.

Okun, M. S. (2012) 'Deep-brain stimulation for Parkinson's disease.', *The New England journal of medicine*, 367(16), pp. 1529–38. doi: 10.1056/NEJMct1208070.

Olanow, C. W. *et al.* (2004) 'Lewy-body formation is an aggresome-related process: A hypothesis', *Lancet Neurology*, 3(8), pp. 496–503. doi: 10.1016/S1474-4422(04)00827-0.

Olanow, C. W., Jenner, P. and Brooks, D. (1998) 'Dopamine agonists and neuroprotection in

Parkinson's disease.', *Annals of neurology*, 44(3 Suppl 1), pp. S167-74. doi: 10.1002/ana.410440725.

Olsson, M. *et al.* (1995) 'Forelimb akinesia in the rat Parkinson model: differential effects of dopamine agonists and nigral transplants as assessed by a new stepping test.', *The Journal of neuroscience : the official journal of the Society for Neuroscience*, 15(5 Pt 2), pp. 3863–75. Available at: http://www.ncbi.nlm.nih.gov/pubmed/7751951.

Ory, D. *et al.* (2015) 'PET imaging of TSPO in a rat model of local neuroinflammation induced by intracerebral injection of lipopolysaccharide', *Nuclear Medicine and Biology*, 42(10), pp. 753–761. doi: 10.1016/j.nucmedbio.2015.06.010.

Ory, D. *et al.* (2016) 'Quantification of TSPO overexpression in a rat model of local neuroinflammation induced by intracerebral injection of LPS by the use of [18F]DPA-714 PET', *European Journal of Nuclear Medicine and Molecular Imaging*, 43(1), pp. 163–172. doi: 10.1007/s00259-015-3172-9.

Ouchi, Y. *et al.* (2005) 'Microglial activation and dopamine terminal loss in early Parkinson's disease.', *Annals of neurology*, 57(2), pp. 168–75. doi: 10.1002/ana.20338.

Owen, D. R. J. and Matthews, P. M. (2011) 'Imaging Brain Microglial Activation Using Positron Emission Tomography and Translocator Protein-Specific Radioligands', in, pp. 19–39. doi: 10.1016/B978-0-12-387718-5.00002-X.

De Pablos, R. M. *et al.* (2005) 'Dopamine-dependent neurotoxicity of lipopolysaccharide in substantia nigra', *The FASEB Journal*, 19(3), pp. 407–409. doi: 10.1096/fj.04-2153fje.

Palermo, G. *et al.* (2020) 'Dopamine Transporter, Age, and Motor Complications in Parkinson's Disease: A Clinical and Single-Photon Emission Computed Tomography Study.', *Movement disorders : official journal of the Movement Disorder Society*. doi: 10.1002/mds.28008.

Palfi, S. *et al.* (2014) 'Long-term safety and tolerability of ProSavin, a lentiviral vector-based gene therapy for Parkinson's disease: a dose escalation, open-label, phase 1/2 trial.', *Lancet (London, England)*, 383(9923), pp. 1138–46. doi: 10.1016/S0140-6736(13)61939-X.

Palfi, S. *et al.* (2018) 'Long-Term Follow-Up of a Phase I/II Study of ProSavin, a Lentiviral Vector Gene Therapy for Parkinson's Disease', *Human Gene Therapy Clinical Development*, 29(3), pp. 148–155. doi: 10.1089/humc.2018.081.

Pan-Montojo, F. *et al.* (2010) 'Progression of Parkinson's disease pathology is reproduced by intragastric administration of rotenone in mice', *PLoS ONE*, 5(1). doi: 10.1371/journal.pone.0008762.

Pannell, M. *et al.* (2020) 'Imaging of translocator protein upregulation is selective for pro-inflammatory polarized astrocytes and microglia.', *Glia*, 68(2), pp. 280–297. doi: 10.1002/glia.23716.

Panneton, W. M. *et al.* (2010) 'The neurotoxicity of DOPAL: Behavioral and stereological evidence for its role in Parkinson disease pathogenesis', *PLoS ONE*, 5(12), pp. 1–9. doi: 10.1371/journal.pone.0015251.

Di Paolo, T. *et al.* (2014) 'AQW051, a novel and selective nicotinic acetylcholine receptor α7 partial agonist, reduces l-Dopa-induced dyskinesias and extends the duration of l-Dopa effects in parkinsonian monkeys.', *Parkinsonism & related disorders*, 20(11), pp. 1119–23. doi: 10.1016/j.parkreldis.2014.05.007.

Papadopoulos, V. *et al.* (2006) 'Translocator protein (18kDa): new nomenclature for the peripheral-type benzodiazepine receptor based on its structure and molecular function.', *Trends in pharmacological sciences*, 27(8), pp. 402–9. doi: 10.1016/j.tips.2006.06.005.

Parkinson, F. E. *et al.* (2016) 'The Effect of Endogenous Adenosine on Neuronal Activity in Rats: An FDG PET Study.', *Journal of neuroimaging : official journal of the American Society of Neuroimaging*, 26(4), pp. 403–5. doi: 10.1111/jon.12349.

Parkinson, J. (2002) 'An essay on the shaking palsy. 1817.', *The Journal of neuropsychiatry and clinical neurosciences*, 14(2), pp. 223–236. doi: 10.1176/jnp.14.2.223.

Parkkinen, L. *et al.* (2011) 'Disentangling the Relationship between Lewy bodies and nigral neuronal loss in Parkinson's disease', *Journal of Parkinson's Disease*, 1(3), pp. 277–286. doi: 10.3233/JPD-2011-11046.

Pasanen, P. *et al.* (2014) 'Novel α-synuclein mutation A53E associated with atypical multiple system atrophy and Parkinson's disease-type pathology.', *Neurobiology of aging*, 35(9), pp. 2180.e1–5. doi: 10.1016/j.neurobiolaging.2014.03.024.

Pate, B. D. *et al.* (1993) 'Correlation of striatal fluorodopa uptake in the MPTP Monkey with dopaminergic indices', *Annals of Neurology*, 34(3), pp. 331–338. doi: 10.1002/ana.410340306.

Patlak, C. S. and Blasberg, R. G. (1985) 'Graphical Evaluation of Blood-to-Brain Transfer Constants from Multiple-Time Uptake Data. Generalizations', *Journal of Cerebral Blood Flow & Metabolism*, 5(4), pp. 584–590. doi: 10.1038/jcbfm.1985.87.

Patlak, C. S., Blasberg, R. G. and Fenstermacher, J. D. (1983) 'Graphical evaluation of blood-to-brain transfer constants from multiple-time uptake data.', *Journal of cerebral blood flow and metabolism : official journal of the International Society of Cerebral Blood Flow and Metabolism*, 3(1), pp. 1–7. doi: 10.1038/jcbfm.1983.1.

Patterson, J. R. *et al.* (2019) 'Time course and magnitude of alpha-synuclein inclusion formation and nigrostriatal degeneration in the rat model of synucleinopathy triggered by intrastriatal α-synuclein preformed fibrils', *Neurobiology of Disease*, 130(June). doi: 10.1016/j.nbd.2019.104525.

de Paulis, T. (2003) 'The discovery of epidepride and its analogs as high-affinity radioligands for imaging extrastriatal dopamine D(2) receptors in human brain.', *Current pharmaceutical design*, 9(8), pp. 673–96. doi: 10.2174/1381612033391135.

Paumier, K. L. *et al.* (2015) 'Intrastriatal injection of pre-formed mouse α-synuclein fibrils into rats triggers α-synuclein pathology and bilateral nigrostriatal degeneration.', *Neurobiology of disease*, 82(1), pp. 185–199. doi: 10.1016/j.nbd.2015.06.003.

Paxinos, G. and Watson, C. (1998) *The Rat Brain in Stereotaxic Coordinates*. 4th edn. Academic Press.

PD Med Collaborative Group *et al.* (2014) 'Long-term effectiveness of dopamine agonists and monoamine oxidase B inhibitors compared with levodopa as initial treatment for Parkinson's disease (PD MED): a large, open-label, pragmatic randomised trial.', *Lancet (London, England)*. Elsevier Ltd, 384(9949), pp. 1196–205. doi: 10.1016/S0140-6736(14)60683-8.

Peelaerts, W. *et al.* (2015) 'α-Synuclein strains cause distinct synucleinopathies after local and systemic administration', *Nature*, 522(7556), pp. 340–344. doi: 10.1038/nature14547.

Pendleton, R. G. *et al.* (2002) 'Effects of Pharmacological Agents upon a Transgenic Model of Parkinson's Disease in Drosophila melanogaster', *Journal of Pharmacology and Experimental Therapeutics*, 300(1), pp. 91–96. doi: 10.1124/jpet.300.1.91.

Penney, J. *et al.* (2016) 'LRRK2 regulates retrograde synaptic compensation at the Drosophila neuromuscular junction', *Nature Communications*. Nature Publishing Group, 7. doi:

10.1038/ncomms12188.

Perez, F. A. and Palmiter, R. D. (2005) 'Parkin-deficient mice are not a robust model of parkinsonism.', *Proceedings of the National Academy of Sciences of the United States of America*, 102(6), pp. 2174–9. doi: 10.1073/pnas.0409598102.

Perlow, M. J. *et al.* (1979) 'Brain grafts reduce motor abnormalities produced by destruction of nigrostriatal dopamine system.', *Science (New York, N.Y.)*, 204(4393), pp. 643–7. doi: 10.1126/science.571147.

Van der Perren, A. *et al.* (2015) 'Longitudinal follow-up and characterization of a robust rat model for Parkinson's disease based on overexpression of alpha-synuclein with adeno-associated viral vectors.', *Neurobiology of aging*, 36(3), pp. 1543–58. doi: 10.1016/j.neurobiolaging.2014.11.015.

Peters, A. M. (1994) 'Graphical analysis of dynamic data: the Patlak-Rutland plot.', *Nuclear medicine communications*, 15(9), pp. 669–72. doi: 10.1097/00006231-199409000-00001.

Peyronneau, M.-A. *et al.* (2013) 'Metabolism and Quantification of [ 18 F]DPA-714, a New TSPO Positron Emission Tomography Radioligand', *Drug Metabolism and Disposition*, 41(1), pp. 122–131. doi: 10.1124/dmd.112.046342.

Peyronneau, M. A. *et al.* (2012) 'Difficulties in dopamine transporter radioligand PET analysis: The example of LBT-999 using [18F] and [11C] labelling. Part II: Metabolism studies', *Nuclear Medicine and Biology*. Elsevier Inc., 39(3), pp. 347–359. doi: 10.1016/j.nucmedbio.2011.09.006.

Pfeiffer, R. F. (2003) 'Gastrointestinal dysfunction in Parkinson's disease.', *The Lancet. Neurology*, 2(2), pp. 107–16. doi: 10.1016/s1474-4422(03)00307-7.

Phan, J. A. *et al.* (2017) 'Early synaptic dysfunction induced by α-synuclein in a rat model of Parkinson's disease', *Scientific Reports*. Springer US, 7(1), pp. 1–17. doi: 10.1038/s41598-017-06724-9.

Phelps, M. E. (2000) 'Positron emission tomography provides molecular imaging of biological processes', *Proceedings of the National Academy of Sciences of the United States of America*, 97(16), pp. 9226–9233. doi: 10.1073/pnas.97.16.9226.

Pienaar, I. S., Götz, J. and Feany, M. B. (2010) 'Parkinson's disease: Insights from non-traditional model organisms', *Progress in Neurobiology*, 92(4), pp. 558–571. doi: 10.1016/j.pneurobio.2010.09.001.

Pike, V. W. (2009) 'PET radiotracers: crossing the blood-brain barrier and surviving metabolism', *Trends in Pharmacological Sciences*, 30(8), pp. 431–440. doi: 10.1016/j.tips.2009.05.005.

PMOD (2009a) *Ichise's Non- Invasive Plot (MRTM0)*.

PMOD (2009b) *Logan's Reference Tissue Model based on Average k2'*.

PMOD (2009c) *Logan Plot*.

PMOD (2009d) *Patlak Plot*.

Poewe, W. *et al.* (2017) 'Parkinson disease', *Nature Reviews Disease Primers*, 3(1), p. 17013. doi: 10.1038/nrdp.2017.13.

Poletti, M. *et al.* (2013) 'A single-center, cross-sectional prevalence study of impulse control disorders in Parkinson disease: association with dopaminergic drugs.', *Journal of clinical psychopharmacology*,

33(5), pp. 691–4. doi: 10.1097/JCP.0b013e3182979830.

Polymeropoulos, M. H. *et al.* (1997) 'Mutation in the alpha-synuclein gene identified in families with Parkinson's disease.', *Science (New York, N.Y.)*, 276(5321), pp. 2045–7. doi: 10.1126/science.276.5321.2045.

Postuma, R. B. *et al.* (2012) 'Identifying prodromal Parkinson's disease: Pre-Motor disorders in Parkinson's disease', *Movement Disorders*, 27(5), pp. 617–626. doi: 10.1002/mds.24996.

Pottier, G. *et al.* (2017) 'PET imaging of cannabinoid type 2 receptors with [ 11 C]A-836339 did not evidence changes following neuroinflammation in rats', *Journal of Cerebral Blood Flow and Metabolism*, 37(3), pp. 1163–1178. doi: 10.1177/0271678X16685105.

Poulopoulos, M., Levy, O. A. and Alcalay, R. N. (2012) 'The neuropathology of genetic Parkinson's disease.', *Movement disorders : official journal of the Movement Disorder Society*, 27(7), pp. 831–42. doi: 10.1002/mds.24962.

Proukakis, C. *et al.* (2013) 'A novel a-synuclein missense mutation in Parkinson disease', *Neurology*, 80(11), pp. 1062–1064. doi: 10.1212/WNL.0b013e31828727ba.

Quik, M. *et al.* (2013) 'Nicotine reduces established levodopa-induced dyskinesias in a monkey model of Parkinson's disease.', *Movement disorders : official journal of the Movement Disorder Society*, 28(10), pp. 1398–406. doi: 10.1002/mds.25594.

Rahman, M. K., Nagatsu, T. and Kato, T. (1981) 'Aromatic L-amino acid decarboxylase activity in central and peripheral tissues and serum of rats with L-DOPA and L-5-hydroxytryptophan as substrates.', *Biochemical pharmacology*, 30(6), pp. 645–9. doi: 10.1016/0006-2952(81)90139-8.

Ransom, B. R. *et al.* (1987) 'Astrocytes convert the parkinsonism inducing neurotoxin, MPTP, to its active metabolite, MPP+', *Neuroscience Letters*. Elsevier, 75(3), pp. 323–328. doi: 10.1016/0304-3940(87)90543-X.

Raub, T. J. (2006) 'P-glycoprotein recognition of substrates and circumvention through rational drug design.', *Molecular pharmaceutics*, 3(1), pp. 3–25. doi: 10.1021/mp0500871.

Recasens, A. *et al.* (2014) 'Lewy body extracts from Parkinson disease brains trigger α-synuclein pathology and neurodegeneration in mice and monkeys', *Annals of Neurology*, 75(3), pp. 351–362. doi: 10.1002/ana.24066.

Rey, N. L. *et al.* (2016) 'Widespread transneuronal propagation of α-synucleinopathy triggered in olfactory bulb mimics prodromal Parkinson's disease', *The Journal of Experimental Medicine*, 213(9). doi: 10.1084/jem.20160368.

Riachi, N. J., LaManna, J. C. and Harik, S. I. (1989) 'Entry of 1-methyl-4-phenyl-1,2,3,6-tetrahydropyridine into the rat brain.', *Journal of Pharmacology and Experimental Therapeutics*, 249(3).

Riemensperger, T. *et al.* (2011) 'Behavioral consequences of dopamine deficiency in the Drosophila central nervous system.', *Proceedings of the National Academy of Sciences of the United States of America*. National Academy of Sciences, 108(2), pp. 834–9. doi: 10.1073/pnas.1010930108.

Rink, E. and Wullimann, M. F. (2001) 'The teleostean (zebrafish) dopaminergic system ascending to the subpallium (striatum) is located in the basal diencephalon (posterior tuberculum)', *Brain Research*, 889(1–2), pp. 316–330. doi: 10.1016/S0006-8993(00)03174-7.

Rink, E. and Wullimann, M. F. (2002) 'Connections of the ventral telencephalon and tyrosine hydroxylase distribution in the zebrafish brain (Danio rerio) lead to identification of an ascending dopaminergic system in a teleost', *Brain Research Bulletin*, 57(3–4), pp. 385–387. doi: 10.1016/S0361-9230(01)00696-7.

Ritz, B. *et al.* (2007) 'Pooled Analysis of Tobacco Use and Risk of Parkinson Disease', *Archives of Neurology*, 64(7), p. 990. doi: 10.1001/archneur.64.7.990.

Ritz, B. *et al.* (2014) 'Parkinson disease and smoking revisited: Ease of quitting is an early sign of the disease', *Neurology*, 83(16), pp. 1396–1402. doi: 10.1212/WNL.0000000000000879.

Rizek, P., Kumar, N. and Jog, M. S. (2016) 'An update on the diagnosis and treatment of Parkinson disease.', *CMAJ : Canadian Medical Association journal = journal de l'Association medicale canadienne*, 188(16), pp. 1157–1165. doi: 10.1503/cmaj.151179.

Van Rompuy, A.-S. *et al.* (2014) 'Long-Term Overexpression of Human Wild-Type and T240R Mutant Parkin in Rat Substantia Nigra Induces Progressive Dopaminergic Neurodegeneration', *Journal of Neuropathology & Experimental Neurology*, 73(2), pp. 159–174. doi: 10.1097/NEN.0000000000000039.

Roodveldt, C., Christodoulou, J. and Dobson, C. M. (2008) 'Immunological features of α-synuclein in Parkinson's disease', *Journal of Cellular and Molecular Medicine*, 12(5B), pp. 1820–1829. doi: 10.1111/j.1582-4934.2008.00450.x.

Rosenbloom, B. *et al.* (2011) 'The incidence of Parkinsonism in patients with type 1 Gaucher disease: Data from the ICGG Gaucher Registry', *Blood Cells, Molecules, and Diseases*. Elsevier Inc., 46(1), pp. 95–102. doi: 10.1016/j.bcmd.2010.10.006.

Ruottinen, H. M. *et al.* (1995) 'Striatal [18F]fluorodopa utilization after COMT inhibition with entacapone studied with PET in advanced Parkinson's disease', *Journal of Neural Transmission - Parkinson's Disease and Dementia Section*, 10(2–3), pp. 91–106. doi: 10.1007/BF02251225.

Ryan, R. E. *et al.* (2001) 'Dose-related neuroprotective effects of chronic nicotine in 6-hydroxydopamine treated rats, and loss of neuroprotection in alpha4 nicotinic receptor subunit knockout mice.', *British journal of pharmacology*, 132(8), pp. 1650–6. doi: 10.1038/sj.bjp.0703989.

Saba, W. *et al.* (2006) '[18F]LBT-999, a new radioligand to study the dopamine transporter with PET: Characterization in baboons', *Medecine Nucleaire*, 32(2).

Sabri, O. *et al.* (2015) 'Florbetaben PET imaging to detect amyloid beta plaques in Alzheimer's disease: phase 3 study.', *Alzheimer's & dementia : the journal of the Alzheimer's Association*, 11(8), pp. 964–74. doi: 10.1016/j.jalz.2015.02.004.

Saha, A. R. *et al.* (2000) 'Induction of neuronal death by alpha-synuclein.', *The European journal of neuroscience*, 12(8), pp. 3073–7. doi: 10.1046/j.1460-9568.2000.00210.x.

Sahin, G. *et al.* (2014) 'Differential dopamine receptor occupancy underlies L-DOPA-induced dyskinesia in a rat model of Parkinson's disease.', *PloS one*, 9(3), p. e90759. doi: 10.1371/journal.pone.0090759.

Samii, A., Nutt, J. G. and Ransom, B. R. (2004) 'Parkinson's disease.', *Lancet (London, England)*, 363(9423), pp. 1783–93. doi: 10.1016/S0140-6736(04)16305-8.

Sanchez-Guajardo, V. *et al.* (2010) 'Microglia acquire distinct activation profiles depending on the degree of α-synuclein neuropathology in a rAAV based model of Parkinson's disease', *PLoS ONE*, 5(1).

doi: 10.1371/journal.pone.0008784.

Sanna, G. *et al.* (2012) 'LRRK2 and vesicle trafficking', *Biochemical Society Transactions*, 40(5), pp. 1117–1122. doi: 10.1042/BST20120117.

Santangelo, B. (2018) *Modelling arterial input functions using data acquired with an MR- compatible sampler: a validation study using [18F]GE-179*, *NRM2018*.

Santiago-Ribeiro, M.-J. *et al.* (2017) 'A simplified method for the diagnosis of striatal dopaminergic dysfunction using PET with a new fluorine DAT tracer, the 18F-LBT-999', *Journal of Nuclear Medicine*. Society of Nuclear Medicine, 58(supplement 1), pp. 413–413. Available at: http://jnm.snmjournals.org/cgi/content/short/58/supplement_1/413 (Accessed: 19 March 2020).

Sauer, H. and Oertel, W. H. (1994) 'Progressive degeneration of nigrostriatal dopamine neurons following intrastriatal terminal lesions with 6-hydroxydopamine: A combined retrograde tracing and immunocytochemical study in the rat', *Neuroscience*. Pergamon, 59(2), pp. 401–415. doi: 10.1016/0306-4522(94)90605-X.

Schallert, T. *et al.* (2000) 'CNS plasticity and assessment of forelimb sensorimotor outcome in unilateral rat models of stroke, cortical ablation, parkinsonism and spinal cord injury.', *Neuropharmacology*, 39(5), pp. 777–87. doi: 10.1016/s0028-3908(00)00005-8.

Scheperjans, F., Derkinderen, P. and Borghammer, P. (2018) 'The gut and Parkinson's disease: Hype or hope?', *Journal of Parkinson's Disease*, 8(s1), pp. S31–S39. doi: 10.3233/JPD-181477.

Schiffer, W. K. *et al.* (2006) 'Serial microPET measures of the metabolic reaction to a microdialysis probe implant', *Journal of Neuroscience Methods*, 155(2), pp. 272–284. doi: 10.1016/j.jneumeth.2006.01.027.

Schou, M. *et al.* (2009) 'Synthesis, radiolabeling and preliminary in vivo evaluation of [18F]FE-PE2I, a new probe for the dopamine transporter.', *Bioorganic & medicinal chemistry letters*, 19(16), pp. 4843–5. doi: 10.1016/j.bmcl.2009.06.032.

Schrag, A. and Schott, J. M. (2006) 'Epidemiological, clinical, and genetic characteristics of early-onset parkinsonism', *Lancet Neurology*, 5(4), pp. 355–363. doi: 10.1016/S1474-4422(06)70411-2.

Schuldiner, S. (1994) 'A molecular glimpse of vesicular monoamine transporters.', *Journal of neurochemistry*, 62(6), pp. 2067–78. doi: 10.1046/j.1471-4159.1994.62062067.x.

Schwarting, R. K. W. and Huston, J. P. (1996) *THE UNILATERAL 6-HYDROXYDOPAMINE LESION MODEL IN BEHAVIORAL BRAIN RESEARCH. ANALYSIS OlF FUNCTIONAL DEFICITS, RECOVERY AND TREATMENTS Introduction 2. Behavioral effects 2.1. Turning behavior 2.1.1. Turning in the undrugged animal 2.1.1.1. IRole of lesion placement 2.1.1.2. IFunctional recovery 2.1.1.3. Other variables 2.1.1.4. ljummary*, *Progress in Neurobiology*.

Seelig, A. (2007) 'The role of size and charge for blood-brain barrier permeation of drugs and fatty acids', *Journal of Molecular Neuroscience*, 33(1), pp. 32–41. doi: 10.1007/s12031-007-0055-y.

Semchuk, K. M., Love, E. J. and Lee, R. G. (1993) 'Parkinson's disease: A test of the multifactorial etiologic hypothesis', *Neurology*, 43(6), pp. 1173–1173. doi: 10.1212/WNL.43.6.1173.

Sérrière, S. *et al.* (2014) 'In vivo PET quantification of the dopamine transporter in rat brain with [18F]LBT-999', *Nuclear Medicine and Biology*, 41(1), pp. 106–113. doi: 10.1016/j.nucmedbio.2013.09.007.

Sérrière, S. *et al.* (2015) 'Assessment of the Protection of Dopaminergic Neurons by an α7 Nicotinic Receptor Agonist, PHA 543613 Using [(18)F]LBT-999 in a Parkinson's Disease Rat Model.', *Frontiers in medicine*, 2, p. 61. doi: 10.3389/fmed.2015.00061.

Session, A. M. *et al.* (2016) 'Genome evolution in the allotetraploid frog Xenopus laevis', *Nature*, 538(7625), pp. 336–343. doi: 10.1038/nature19840.

Sgroi, S., Kaelin-Lang, A. and Capper-Loup, C. (2014) 'Spontaneous locomotor activity and L-DOPA-induced dyskinesia are not linked in 6-OHDA parkinsonian rats', *Frontiers in Behavioral Neuroscience*, 8(OCT), pp. 1–9. doi: 10.3389/fnbeh.2014.00331.

Shaikh, K. T. *et al.* (2015) 'Transgenic LRRK2R1441G rats-a model for Parkinson disease?', *PeerJ*, 2015(5), pp. 5–10. doi: 10.7717/peerj.945.

Shannon, K. M. *et al.* (2012) 'Alpha-synuclein in colonic submucosa in early untreated Parkinson's disease', *Movement Disorders*, 27(6), pp. 709–715. doi: 10.1002/mds.23838.

Sharma, N. and Nehru, B. (2015) 'Characterization of the lipopolysaccharide induced model of Parkinson's disease: Role of oxidative stress and neuroinflammation.', *Neurochemistry international*, 87, pp. 92–105. doi: 10.1016/j.neuint.2015.06.004.

Shendelman, S. *et al.* (2004) 'DJ-1 is a redox-dependent molecular chaperone that inhibits alpha-synuclein aggregate formation.', *PLoS biology*. Edited by Huda Y. Zoghbi, 2(11), p. e362. doi: 10.1371/journal.pbio.0020362.

Sherer, T. B. *et al.* (2003) 'Selective microglial activation in the rat rotenone model of Parkinson's disease', *Neuroscience Letters*, 341(2), pp. 87–90. doi: 10.1016/S0304-3940(03)00172-1.

Shimizu, K. *et al.* (2001) 'Carrier-mediated processes in blood–brain barrier penetration and neural uptake of paraquat', *Brain Research*, 906(1–2), pp. 135–142. doi: 10.1016/S0006-8993(01)02577-X.

Shimozawa, A. *et al.* (2017) 'Propagation of pathological α-synuclein in marmoset brain', *Acta neuropathologica communications*. Acta Neuropathologica Communications, 5(1), p. 12. doi: 10.1186/s40478-017-0413-0.

Shimura, H. *et al.* (2000) 'Familial Parkinson disease gene product, parkin, is a ubiquitin-protein ligase', *Nature Genetics*, 25(3), pp. 302–305. doi: 10.1038/77060.

Shumay, E., Fowler, J. S. and Volkow, N. D. (2010) 'Genomic features of the human dopamine transporter gene and its potential epigenetic states: Implications for phenotypic diversity', *PLoS ONE*, 5(6). doi: 10.1371/journal.pone.0011067.

Sidransky, E. *et al.* (2009) 'Multicenter analysis of glucocerebrosidase mutations in Parkinson's disease.', *The New England journal of medicine*, 361(17), pp. 1651–61. doi: 10.1056/NEJMoa0901281.

Silva, M. A. *et al.* (1997) 'Increased neostriatal dopamine activity after intraperitoneal or intranasal administration of L-DOPA: on the role of benserazide pretreatment.', *Synapse (New York, N.Y.)*, 27(4), pp. 294–302. doi: 10.1002/(SICI)1098-2396(199712)27:4<294::AID-SYN3>3.0.CO;2-7.

Silvestri, L. *et al.* (2005) 'Mitochondrial import and enzymatic activity of PINK1 mutants associated to recessive parkinsonism', *Human Molecular Genetics*, 14(22), pp. 3477–3492. doi: 10.1093/hmg/ddi377.

Simon-Sanchez, J. *et al.* (2009) 'Genome-Wide Association Study reveals genetic risk underlying

Parkinson's disease HHS Public Access Author manuscript', *Nat Genet*, 41(12), pp. 1308–1312. doi: 10.1038/ng.487.

Singleton, A. B. *et al.* (2003) 'alpha-Synuclein locus triplication causes Parkinson's disease.', *Science (New York, N.Y.)*, 302(5646), p. 841. doi: 10.1126/science.1090278.

Sloan, M. *et al.* (2016) 'LRRK2 BAC transgenic rats develop progressive, L-DOPA-responsive motor impairment, and deficits in dopamine circuit function', *Human Molecular Genetics*, 25(5), pp. 951–963. doi: 10.1093/hmg/ddv628.

Smith, W. W. *et al.* (2006) 'Kinase activity of mutant LRRK2 mediates neuronal toxicity.', *Nature neuroscience*, 9(10), pp. 1231–3. doi: 10.1038/nn1776.

Snead, D. and Eliezer, D. (2014) 'Alpha-synuclein function and dysfunction on cellular membranes.', *Experimental neurobiology*, 23(4), pp. 292–313. doi: 10.5607/en.2014.23.4.292.

Snyder, S. H. and D'Amato, R. J. (1985) 'Neurology: Predicting Parkinson's disease', *Nature*, 317(6034), pp. 198–199. doi: 10.1038/317198a0.

Sofroniew, M. V. (2015) 'Astrocyte barriers to neurotoxic inflammation.', *Nature reviews. Neuroscience*. Nature Publishing Group, 16(5), pp. 249–63. doi: 10.1038/nrn3898.

Sossi, V. *et al.* (2009) 'Dopamine transporter relation to levodopa-derived synaptic dopamine in a rat model of Parkinson's: an in vivo imaging study.', *Journal of neurochemistry*, 109(1), pp. 85–92. doi: 10.1111/j.1471-4159.2009.05904.x.

Spector, S., Sjoerdsma, A. and Udenfriend, S. (1965) 'BLOCKADE OF ENDOGENOUS NOREPINEPHRINE SYNTHESIS BY ALPHA-METHYL-TYROSINE, AN INHIBITOR OF TYROSINE HYDROXYLASE.', *The Journal of pharmacology and experimental therapeutics*, 147, pp. 86–95. Available at: http://www.ncbi.nlm.nih.gov/pubmed/14255166.

Spillantini, M. G. *et al.* (1997) 'a-Synuclein in Lewy bodies', *Nature*, 388(28), pp. 839–840. doi: 10.1038/42166.

Sridharan, S. *et al.* (2017) 'Comparative Evaluation of Three TSPO PET Radiotracers in a LPS-Induced Model of Mild Neuroinflammation in Rats.', *Molecular imaging and biology*, 19(1), pp. 77–89. doi: 10.1007/s11307-016-0984-3.

Stark, A. J., Smith, C. T., Petersen, K. J., *et al.* (2018) '[18F]fallypride characterization of striatal and extrastriatal D2/3 receptors in Parkinson's disease.', *NeuroImage. Clinical*. Elsevier, 18(January), pp. 433–442. doi: 10.1016/j.nicl.2018.02.010.

Stark, A. J., Smith, C. T., Lin, Y.-C., *et al.* (2018) 'Nigrostriatal and Mesolimbic D2/3 Receptor Expression in Parkinson's Disease Patients with Compulsive Reward-Driven Behaviors.', *The Journal of neuroscience : the official journal of the Society for Neuroscience*, 38(13), pp. 3230–3239. doi: 10.1523/JNEUROSCI.3082-17.2018.

Stewart, H. J. *et al.* (2016) 'Optimizing Transgene Configuration and Protein Fusions to Maximize Dopamine Production for the Gene Therapy of Parkinson's Disease.', *Human gene therapy. Clinical development*, 27(3), pp. 100–10. doi: 10.1089/humc.2016.056.

Stocchi, F. *et al.* (2013) 'AFQ056 in Parkinson patients with levodopa-induced dyskinesia: 13-week, randomized, dose-finding study.', *Movement disorders : official journal of the Movement Disorder Society*, 28(13), pp. 1838–46. doi: 10.1002/mds.25561.

Stoessl, A. J. (2007) 'Positron emission tomography in premotor Parkinson's disease.', *Parkinsonism & related disorders*, 13 Suppl 3, pp. S421-4. doi: 10.1016/S1353-8020(08)70041-5.

Stoker, T. B. (2018) *Stem Cell Treatments for Parkinson's Disease*, *Parkinson's Disease: Pathogenesis and Clinical Aspects*. Available at: http://www.ncbi.nlm.nih.gov/pubmed/30702846.

Stoker, T. B., Torsney, K. M. and Barker, R. A. (2018) 'Pathological Mechanisms and Clinical Aspects of GBA1 Mutation-Associated Parkinson's Disease.', in *Parkinson's Disease: Pathogenesis and Clinical Aspects*. Available at: https://www.ncbi.nlm.nih.gov/books/NBK536716/.

Stott, S. R. W. and Barker, R. A. (2014) 'Time course of dopamine neuron loss and glial response in the 6-OHDA striatal mouse model of Parkinson's disease', *European Journal of Neuroscience*, 39(6), pp. 1042–1056. doi: 10.1111/ejn.12459.

Streit, W. J., Walter, S. A. and Pennell, N. A. (1999) 'Reactive microgliosis.', *Progress in neurobiology*, 57(6), pp. 563–81. doi: 10.1016/s0301-0082(98)00069-0.

Sulzer, D., Maidment, N. T. and Rayport, S. (1993) 'Amphetamine and Other Weak Bases Act to Promote Reverse Transport of Dopamine in Ventral Midbrain Neurons', *Journal of Neurochemistry*, 60(2), pp. 527–535. doi: 10.1111/j.1471-4159.1993.tb03181.x.

Sveinbjornsdottir, S. (2016) 'The clinical symptoms of Parkinson's disease.', *Journal of neurochemistry*, 139 Suppl, pp. 318–324. doi: 10.1111/jnc.13691.

Svensson, E. *et al.* (2015) 'Vagotomy and subsequent risk of Parkinson's disease.', *Annals of neurology*, 78(4), pp. 522–9. doi: 10.1002/ana.24448.

Symes, A. L., Lal, S. and Soukes, T. L. (1976) 'Time-course of apomorphine in the brain of the immature rat after apomorphine injection.', *Archives internationales de pharmacodynamie et de therapie*, 223(2), pp. 260–4. Available at: http://www.ncbi.nlm.nih.gov/pubmed/1033736.

Takahashi, K. *et al.* (2007) 'Induction of Pluripotent Stem Cells from Adult Human Fibroblasts by Defined Factors', *Cell*, 131(5), pp. 861–872. doi: 10.1016/j.cell.2007.11.019.

Tanaka, M. *et al.* (2004) 'Aggresomes formed by alpha-synuclein and synphilin-1 are cytoprotective.', *The Journal of biological chemistry*, 279(6), pp. 4625–31. doi: 10.1074/jbc.M310994200.

Tanner, C. M. *et al.* (2011) 'Rotenone, paraquat, and Parkinson's disease', *Environmental Health Perspectives*, 119(6), pp. 866–872. doi: 10.1289/ehp.1002839.

Tansey, M. G. and Goldberg, M. S. (2010) 'Neuroinflammation in Parkinson's disease: Its role in neuronal death and implications for therapeutic intervention', *Neurobiology of Disease*. Elsevier Inc., 37(3), pp. 510–518. doi: 10.1016/j.nbd.2009.11.004.

Terada, T. *et al.* (2016) 'Extrastriatal spreading of microglial activation in Parkinson's disease: a positron emission tomography study.', *Annals of nuclear medicine*, 30(8), pp. 579–87. doi: 10.1007/s12149-016-1099-2.

Terry, R. D. (2000) 'Do neuronal inclusions kill the cell?', *Journal of neural transmission. Supplementum*, 59, pp. 91–3. doi: 10.1007/978-3-7091-6781-6_12.

Thakur, P. *et al.* (2017) 'Modeling Parkinson's disease pathology by combination of fibril seeds and α-synuclein overexpression in the rat brain', *Proceedings of the National Academy of Sciences*, 114(39), pp. E8284–E8293. doi: 10.1073/pnas.1710442114.

Thiele, S. L., Warre, R. and Nash, J. E. (2012) 'Development of a unilaterally-lesioned 6-OHDA mouse

model of Parkinson's disease.', *Journal of visualized experiments : JoVE*, (60). doi: 10.3791/3234.

Thiruchelvam, M. *et al.* (2000) 'The nigrostriatal dopaminergic system as a preferential target of repeated exposures to combined paraquat and maneb: Implications for Parkinson's disease', *Journal of Neuroscience*, 20(24), pp. 9207–9214. doi: 10.1523/jneurosci.20-24-09207.2000.

Thirumalai, V. and Cline, H. T. (2008) 'Endogenous Dopamine Suppresses Initiation of Swimming in Prefeeding Zebrafish Larvae', *Journal of Neurophysiology*. American Physiological Society, 100(3), pp. 1635–1648. doi: 10.1152/jn.90568.2008.

Thobois, S., Guillouet, S. and Broussolle, E. (2001) 'Contributions of PET and SPECT to the understanding of the pathophysiology of Parkinson's disease.', *Neurophysiologie clinique = Clinical neurophysiology*, 31(5), pp. 321–40. doi: 10.1016/s0987-7053(01)00273-8.

Thomson, J. A. *et al.* (1998) 'Embryonic stem cell lines derived from human blastocysts.', *Science (New York, N.Y.)*, 282(5391), pp. 1145–7. doi: 10.1126/science.282.5391.1145.

Tieu, K. (2011) 'A guide to neurotoxic animal models of Parkinson's disease', *Cold Spring Harbor Perspectives in Medicine*, 1(1). doi: 10.1101/cshperspect.a009316.

Tinakoua, A. *et al.* (2015) 'The impact of combined administration of paraquat and maneb on motor and non-motor functions in the rat', *Neuroscience*, 311, pp. 118–129. doi: 10.1016/j.neuroscience.2015.10.021.

Tolosa, E. *et al.* (1998) 'History of levodopa and dopamine agonists in Parkinson's disease treatment', *Neurology*, 50(Issue 6, Supplement 6), pp. S2–S10. doi: 10.1212/WNL.50.6_Suppl_6.S2.

Tompkins, M. M. and Hill, W. D. (1997) 'Contribution of somal Lewy bodies to neuronal death', *Brain Research*, 775(1–2), pp. 24–29. doi: 10.1016/S0006-8993(97)00874-3.

Tournier, B. B. *et al.* (2019) 'Fluorescence-activated cell sorting to reveal the cell origin of radioligand binding', *Journal of Cerebral Blood Flow & Metabolism*, p. 0271678X1986040. doi: 10.1177/0271678X19860408.

Trenkwalder, C., Berg, D., *et al.* (2016) 'A Placebo-Controlled Trial of AQW051 in Patients With Moderate to Severe Levodopa-Induced Dyskinesia', *Movement Disorders*, 31(7), pp. 1049–1054. doi: 10.1002/mds.26569.

Trenkwalder, C., Stocchi, F., *et al.* (2016) 'Mavoglurant in Parkinson's patients with l-Dopa-induced dyskinesias: Two randomized phase 2 studies', *Movement Disorders*, 31(7), pp. 1054–1058. doi: 10.1002/mds.26585.

Trétiakoff, C. (1919) *Contribution a l'etude l'anatomie pathologique du locus Niger de soemmering: avec quelques déductions relatives à la pathogénie des troubles du tonus musculaire et de la maladie de Parkinson*.

Trošt, M., Perovnik, M. and Pirtošek, Z. (2019) 'Correlations of Neuropsychological and Metabolic Brain Changes in Parkinson's Disease and Other α-Synucleinopathies', *Frontiers in Neurology*, 10(November), pp. 1–10. doi: 10.3389/fneur.2019.01204.

Trulson, M. E. *et al.* (1985) 'Effects of chronic methamphetamine on the nigral-striatal dopamine system in rat brain: Tyrosine hydroxylase immunochemistry and quantitative light microscopic studies', *Brain Research Bulletin*, 15(6), pp. 569–577. doi: 10.1016/0361-9230(85)90206-0.

Trzaska, K. A., Kuzhikandathil, E. V. and Rameshwar, P. (2007) 'Specification of a Dopaminergic

Phenotype from Adult Human Mesenchymal Stem Cells', *Stem Cells*, 25(11), pp. 2797–2808. doi: 10.1634/stemcells.2007-0212.

Uhl, G. R. *et al.* (1994) 'Dopamine transporter messenger RNA in Parkinson's disease and control substantia nigra neurons.', *Annals of neurology*, 35(4), pp. 494–8. doi: 10.1002/ana.410350421.

Ungerstedt, U. (1968) '6-hydroxy-dopamine induced degeneration of central monoamine neurons', *European Journal of Pharmacology*. Elsevier, 5(1), pp. 107–110. doi: 10.1016/0014-2999(68)90164-7.

Uversky, V. N., Li, J. and Fink, A. L. (2001) 'Metal-triggered Structural Transformations, Aggregation, and Fibrillation of Human α-Synuclein', *Journal of Biological Chemistry*, 276(47), pp. 44284–44296. doi: 10.1074/jbc.M105343200.

Varrone, A. *et al.* (2009) 'In vitro autoradiography and in vivo evaluation in cynomolgus monkey of [18F]FE-PE2I, a new dopamine transporter PET radioligand.', *Synapse (New York, N.Y.)*, 63(10), pp. 871–80. doi: 10.1002/syn.20670.

Varrone, A. and Pellecchia, M. T. (2018) 'SPECT Molecular Imaging in Familial Parkinson's Disease.', *International review of neurobiology*, 142, pp. 225–260. doi: 10.1016/bs.irn.2018.09.004.

Vasquez, V. *et al.* (2020) 'A multi-faceted genotoxic network of alpha-synuclein in the nucleus and mitochondria of dopaminergic neurons in Parkinson's disease: Emerging concepts and challenges.', *Progress in neurobiology*, 185, p. 101729. doi: 10.1016/j.pneurobio.2019.101729.

Ved, R. *et al.* (2005) 'Similar Patterns of Mitochondrial Vulnerability and Rescue Induced by Genetic Modification of α-Synuclein, Parkin, and DJ-1 in Caenorhabditis elegans', *Journal of Biological Chemistry*, 280(52), pp. 42655–42668. doi: 10.1074/jbc.M505910200.

Venkataramana, N. K. *et al.* (2010) 'Open-labeled study of unilateral autologous bone-marrow-derived mesenchymal stem cell transplantation in Parkinson's disease', *Translational Research*. Mosby, Inc., 155(2), pp. 62–70. doi: 10.1016/j.trsl.2009.07.006.

Venneti, S., Lopresti, B. J. and Wiley, C. A. (2006) 'The peripheral benzodiazepine receptor (Translocator protein 18 kDa) in microglia: From pathology to imaging', *Progress in Neurobiology*, 80(6), pp. 308–322. doi: 10.1016/j.pneurobio.2006.10.002.

Vetel, S. *et al.* (2019) 'Extensive exploration of a novel rat model of Parkinson's disease using partial 6-hydroxydopamine lesion of dopaminergic neurons suggests new therapeutic approaches.', *Synapse (New York, N.Y.)*, 73(3), p. e22077. doi: 10.1002/syn.22077.

Vezoli, J. *et al.* (2014) 'Increased DAT binding in the early stage of the dopaminergic lesion: A longitudinal [11C]PE2I binding study in the MPTP-monkey', *NeuroImage*. Elsevier B.V., 102(P2), pp. 249–261. doi: 10.1016/j.neuroimage.2014.07.059.

Vieira, I. F. *et al.* (2018) 'Volume-of-interest-based supervised cluster analysis for pseudo-reference region selection in [18F]DPA-714 PET imaging of the rat brain', *EJNMMI Research*. EJNMMI Research, 8(1), p. 112. doi: 10.1186/s13550-018-0467-4.

Visanji, N. P. *et al.* (2013) 'The prion hypothesis in Parkinson's disease: Braak to the future.', *Acta neuropathologica communications*, 1(1), p. 2. doi: 10.1186/2051-5960-1-2.

Volpicelli-Daley, L. A. *et al.* (2016) 'How can rAAV-α-synuclein and the fibril α-synuclein models advance our understanding of Parkinson's disease?', *Journal of neurochemistry*, 139 Suppl, pp. 131–155. doi: 10.1111/jnc.13627.

Wagner, G. C., Seiden, L. S. and Schuster, C. R. (1979) 'Methamphetamine-induced changes in brain catecholamines in rats and guinea pigs', *Drug and Alcohol Dependence*, 4(5), pp. 435–438. doi: 10.1016/0376-8716(79)90076-0.

Wakabayashi, K. *et al.* (1988) 'Parkinson's disease: the presence of Lewy bodies in Auerbach's and Meissner's plexuses.', *Acta neuropathologica*, 76(3), pp. 217–221. doi: 10.1007/bf00687767.

Wakabayashi, K. *et al.* (2007) 'The Lewy body in Parkinson's disease: molecules implicated in the formation and degradation of alpha-synuclein aggregates.', *Neuropathology : official journal of the Japanese Society of Neuropathology*, 27(5), pp. 494–506. doi: 10.1111/j.1440-1789.2007.00803.x.

Walker, M. D., Dinelle, K., Kornelsen, R., McCormick, S., *et al.* (2013) 'In-vivo measurement of LDOPA uptake, dopamine reserve and turnover in the rat brain using [18F]FDOPA PET.', *Journal of cerebral blood flow and metabolism : official journal of the International Society of Cerebral Blood Flow and Metabolism*, 33(1), pp. 59–66. doi: 10.1038/jcbfm.2012.120.

Walker, M. D., Dinelle, K., Kornelsen, R., Lee, A., *et al.* (2013) 'Measuring dopaminergic function in the 6-OHDA-lesioned rat: a comparison of PET and microdialysis.', *EJNMMI research*, 3(1), p. 69. doi: 10.1186/2191-219X-3-69.

Walker, M. D. *et al.* (2014) 'Behavioral deficits and striatal DA signaling in LRRK2 p.G2019S transgenic rats: a multimodal investigation including PET neuroimaging.', *Journal of Parkinson's disease*, 4(3), pp. 483–98. doi: 10.3233/JPD-140344.

Wallings, R. L. and Tansey, M. G. (2019) 'LRRK2 regulation of immune-pathways and inflammatory disease.', *Biochemical Society transactions*, 47(6), pp. 1581–1595. doi: 10.1042/BST20180463.

Wang, D. *et al.* (2008) 'Dispensable role of Drosophila ortholog of LRRK2 kinase activity in survival of dopaminergic neurons.', *Molecular neurodegeneration*, 3(1), p. 3. doi: 10.1186/1750-1326-3-3.

Wang, J. L. *et al.* (2010) 'In vivo studies of the SERT-selective [18F]FPBM and VMAT2-selective [18F]AV-133 radiotracers in a rat model of Parkinson's disease', *Nuclear Medicine and Biology*. Elsevier Inc., 37(4), pp. 479–486. doi: 10.1016/j.nucmedbio.2010.01.006.

Wang, L. *et al.* (2002) 'Delayed delivery of AAV-GDNF prevents nigral neurodegeneration and promotes functional recovery in a rat model of Parkinson's disease.', *Gene therapy*, 9(6), pp. 381–9. doi: 10.1038/sj.gt.3301682.

Wang, Q. *et al.* (2020) 'Locus coeruleus neurons are most sensitive to chronic neuroinflammation-induced neurodegeneration.', *Brain, behavior, and immunity*. doi: 10.1016/j.bbi.2020.01.003.

Wang, Q., Liu, Y. and Zhou, J. (2015) 'Neuroinflammation in Parkinson's disease and its potential as therapeutic target', *Translational Neurodegeneration*. Translational Neurodegeneration, 4(1), pp. 1–9. doi: 10.1186/s40035-015-0042-0.

Wang, R. *et al.* (2017) 'Suite PET/CT neuroimaging for the diagnosis of Parkinson's disease: statistical parametric mapping analysis.', *Nuclear medicine communications*, 38(2), pp. 164–169. doi: 10.1097/MNM.0000000000000622.

Warren Olanow, C. *et al.* (2015) 'Gene delivery of neurturin to putamen and substantia nigra in Parkinson disease: A double-blind, randomized, controlled trial', *Annals of Neurology*, 78(2), pp. 248–257. doi: 10.1002/ana.24436.

Weber, B. *et al.* (2002) 'A femoral arteriovenous shunt facilitates arterial whole blood sampling in animals.', *European journal of nuclear medicine and molecular imaging*, 29(3), pp. 319–23. doi:

10.1007/s00259-001-0712-2.

Weintraub, D. *et al.* (2010) 'Impulse Control Disorders in Parkinson Disease: A Cross-Sectional Study of 3090 Patients', *Archives of Neurology*, 67(5), pp. 589–595. doi: 10.1001/archneurol.2010.65.

Weintraub, D. and Claassen, D. O. (2017) 'Impulse Control and Related Disorders in Parkinson's Disease.', *International review of neurobiology*, 133, pp. 679–717. doi: 10.1016/bs.irn.2017.04.006.

Weng, C.-C., Huang, S.-L., *et al.* (2017) '[18F]FP-(+)-DTBZ PET study in a lactacystin-treated rat model of Parkinson disease.', *Annals of nuclear medicine*, 31(7), pp. 506–513. doi: 10.1007/s12149-017-1174-3.

Weng, C.-C., Chen, Z.-A., *et al.* (2017) 'Quantitative analysis of the therapeutic effect of magnolol on MPTP-induced mouse model of Parkinson's disease using in vivo 18F-9-fluoropropyl-(+)-dihydrotetrabenazine PET imaging.', *PloS one*, 12(3), p. e0173503. doi: 10.1371/journal.pone.0173503.

Werry, E. L. *et al.* (2019) 'Recent developments in TSPO PET imaging as a biomarker of neuroinflammation in neurodegenerative disorders', *International Journal of Molecular Sciences*, 20(13), pp. 1–21. doi: 10.3390/ijms20133161.

West, R. J. H. *et al.* (2015) 'Neurophysiology of Drosophila models of Parkinson's disease', *Parkinson's Disease*, 2015. doi: 10.1155/2015/381281.

White, J. G. *et al.* (1986) 'The Structure of the Nervous System of the Nematode Caenorhabditis elegans', *Philosophical Transactions of the Royal Society B: Biological Sciences*, 314(1165), pp. 1–340. doi: 10.1098/rstb.1986.0056.

Whitworth, A. J., Wes, P. D. and Pallanck, L. J. (2006) 'Drosophila models pioneer a new approach to drug discovery for Parkinson's disease', *Drug Discovery Today*, 11(3–4), pp. 119–126. doi: 10.1016/S1359-6446(05)03693-7.

Wile, Daryl J *et al.* (2017) 'Serotonin and dopamine transporter PET changes in the premotor phase of LRRK2 parkinsonism: cross-sectional studies.', *The Lancet. Neurology*, 16(5), pp. 351–359. doi: 10.1016/S1474-4422(17)30056-X.

Wile, Daryl J. *et al.* (2017) 'Serotonin and dopamine transporter PET changes in the premotor phase of LRRK2 parkinsonism: cross-sectional studies', *The Lancet Neurology*, 16(5). doi: 10.1016/S1474-4422(17)30056-X.

Wilson, A. A. *et al.* (2000) 'Novel Radiotracers for Imaging the Serotonin Transporter by Positron Emission Tomography: Synthesis, Radiosynthesis, and in Vitro and ex Vivo Evaluation of 11 C-Labeled 2-(Phenylthio)araalkylamines', *Journal of Medicinal Chemistry*, 43(16), pp. 3103–3110. doi: 10.1021/jm000079i.

Wimberley, C. *et al.* (2018) 'Impact of endothelial 18-kDa translocator protein on the quantification of 18 F-DPA-714', *Journal of Nuclear Medicine*, 59(2), pp. 307–314. doi: 10.2967/jnumed.117.195396.

Winklhofer, K. F. and Haass, C. (2010) 'Mitochondrial dysfunction in Parkinson's disease', *Biochimica et Biophysica Acta (BBA) - Molecular Basis of Disease*, 1802(1), pp. 29–44. doi: 10.1016/j.bbadis.2009.08.013.

Wood, H. (2017) 'Parkinson disease: Caffeine and nicotine do not provide symptomatic relief in Parkinson disease', *Nature reviews. Neurology*, 13(12), p. 707. doi: 10.1038/nrneurol.2017.155.

Xi, Y. *et al.* (2010) 'Impaired dopaminergic neuron development and locomotor function in zebrafish with loss of pink1 function', *European Journal of Neuroscience*, 31(4), pp. 623–633. doi: 10.1111/j.1460-9568.2010.07091.x.

Xi, Y., Noble, S. and Ekker, M. (2011) 'Modeling Neurodegeneration in Zebrafish', *Current Neurology and Neuroscience Reports*, 11(3), pp. 274–282. doi: 10.1007/s11910-011-0182-2.

Yabuki, Y. *et al.* (2020) 'Fatty Acid Binding Protein 3 Enhances the Spreading and Toxicity of α-Synuclein in Mouse Brain', *International journal of molecular sciences*, 21(6), pp. 1–19. doi: 10.3390/ijms21062230.

Yang, D. *et al.* (2019) 'The Role of the Gut Microbiota in the Pathogenesis of Parkinson's Disease', *Frontiers in Neurology*, 10(November), pp. 1–13. doi: 10.3389/fneur.2019.01155.

Yang, Y. *et al.* (2005) 'Inactivation of Drosophila DJ-1 leads to impairments of oxidative stress response and phosphatidylinositol 3-kinase/Akt signaling', *Proceedings of the National Academy of Sciences*, 102(38), pp. 13670–13675. doi: 10.1073/pnas.0504610102.

Zaccai, J. *et al.* (2008) 'Patterns and stages of α-synucleinopathy', *Neurology*, 70(13), pp. 1042 LP – 1048. doi: 10.1212/01.wnl.0000306697.48738.b6.

Zahoor, I., Shafi, A. and Haq, E. (2018) *Pharmacological Treatment of Parkinson's Disease*, *Parkinson's Disease: Pathogenesis and Clinical Aspects*. Available at: http://www.ncbi.nlm.nih.gov/pubmed/30702845.

Zarranz, J. J. *et al.* (2004) 'The new mutation, E46K, of α-synuclein causes parkinson and Lewy body dementia', *Annals of Neurology*, 55(2), pp. 164–173. doi: 10.1002/ana.10795.

Zhang, G. *et al.* (2018) 'New Perspectives on Roles of Alpha-Synuclein in Parkinson's Disease', *Frontiers in Aging Neuroscience*, 10(November), pp. 1–20. doi: 10.3389/fnagi.2018.00370.

Zhang, J. *et al.* (2003) 'Manganese ethylene-bis-dithiocarbamate and selective dopaminergic neurodegeneration in rat: a link through mitochondrial dysfunction', *Journal of Neurochemistry*, 84(2), pp. 336–346. doi: 10.1046/j.1471-4159.2003.01525.x.

Zhang, L. *et al.* (2005) 'Mitochondrial localization of the Parkinson's disease related protein DJ-1: implications for pathogenesis', *Human Molecular Genetics*, 14(14), pp. 2063–2073. doi: 10.1093/hmg/ddi211.

Zhang, Y. *et al.* (2000) 'Parkin functions as an E2-dependent ubiquitin- protein ligase and promotes the degradation of the synaptic vesicle-associated protein, CDCrel-1', *Proceedings of the National Academy of Sciences*, 97(24), pp. 13354–13359. doi: 10.1073/pnas.240347797.

Zheng, X. *et al.* (2012) 'A study of non-invasive Patlak quantification for whole-body dynamic FDG-PET studies of mice', *Biomedical Signal Processing and Control*. Elsevier Ltd, 7(5), pp. 438–446. doi: 10.1016/j.bspc.2011.11.005.

Zhou, H. *et al.* (2011) 'Temporal expression of mutant LRRK2 in adult rats impairs dopamine reuptake', *International Journal of Biological Sciences*, 7(6), pp. 753–761. doi: 10.7150/ijbs.7.753.

Zhu, L. *et al.* (2012) 'Imaging of VMAT2 binding sites in the brain by 18F-AV-133: The effect of a pseudo-carrier', *Nuclear Medicine and Biology*. Elsevier Inc., 39(7), pp. 897–904. doi: 10.1016/j.nucmedbio.2012.05.002.

Zimprich, A. *et al.* (2004) 'Mutations in LRRK2 cause autosomal-dominant parkinsonism with

pleomorphic pathology.', *Neuron*, 44(4), pp. 601–7. doi: 10.1016/j.neuron.2004.11.005.

## Thesis summary in English

The cerebral pathology of Parkinson's disease is characterized by a progressive loss of dopaminergic neurons of the substantia nigra, and an accumulation of α-synuclein aggregates. neuroinflammation and genetic predisposition contribute to PD as the main confounding factors. In this PhD thesis, I aimed to evaluate, *in vivo* and *post-mortem*, the effects of three factors on the dopaminergic system: 1) α-synuclein overexpression, 2) α-synuclein and LRRK2 co-expression, and 3) mild neuroinflammation, on the dopaminergic system and dopaminergic neuronal cell loss.

To this end, positron emission tomography (PET) imaging and behavioural studies have been selected as the main *in vivo* tools. I have used [$^{18}$F]LBT999 and [$^{18}$F]FMT PET imaging to evaluate striatal levels of dopamine transporter (DAT) and the dopamine-synthesising AADC enzyme, respectively. To assess neuroinflammation, I have used [$^{18}$F]DPA714 to evaluate 18kDa TSPO binding. The *in vivo* data were validated by *post-mortem* techniques evaluating the expression of genes (RT-qPCR) and proteins (immunohistochemistry).

The results of my work show that overexpression of human WT-α-synuclein in the substantia nigra through viral vectors (AAV2/6-PGK-WT-α-synuclein) does not generate detectable neuronal loss in the substantia nigra, nor does it generate *in vivo* motor deficits or changes in the dopaminergic system as seen by in vivo PET imaging. On the other hand, I have demonstrated here that overexpression of A53T-α-synuclein in the substantia nigra, using an AAV2/6-PGK-A53T-α-synuclein viral vector approach, resulted in significant α-synuclein aggregation in the substantia nigra as soon as 8wpi, but not in the striatum. Quantitative microscopic analyses show that A53T-α-synuclein aggregation induced a mild but progressive degeneration of dopaminergic neurons in the substantia nigra. The loss of dopaminergic fibres in the striatum as detected by immunohistochemistry of tyrosine hydroxylase (TH) remains, however, moderate. DAT-PET imaging, but not AADC-PET imaging, was able to measure the progressive neuronal loss. Taken together, our *in vivo* and *post-mortem* data suggest that DAT-PET does not only reflect neuronal loss induced by α-synuclein accumulation, but also functional compensation mechanisms of the dopaminergic synapse. A reduction in DAT levels, combined with normal TH and AADC levels, could normalise the synaptic dopamine concentrations in the striatum. In addition, this dopaminergic neuronal loss coincided with in initially moderate, followed by a more pronounced microglial response. Finally, in a viral vector model of co-overexpression of AAV2/6-PGK-A53T-α-synuclein and AAV2/6-PGK-G2019S-LRRK2, we did not observe added neurotoxicity of G2019S mutated LRRK2 to A53T-α-synuclein toxicity.

In an acute neuroinflammatory model following LPS injection in the striatum, *post-mortem* analysis revealed the absence of dopaminergic neuronal loss in the substantia nigra and synaptic loss in the striatum. Nevertheless, I observed a significant inverse correlation between inflammation markers (TSPO-PET and IBA1 expression) and markers for dopamine production (TH) and storage (VMAT2). These data support the hypothesis that neuroinflammation may impair the functionality of the dopaminergic system, regardless of the presence dopaminergic neuron loss.

In summary, my thesis results confirm the interest of PET in demonstrating functional damage in vivo, which cannot be demonstrated *post-mortem* in animal models of PD.

## Thesis summary in French

La pathologie cérébrale de la maladie de Parkinson (MP) est caractérisée par une perte neuronale progressive des neurones dopaminergiques de la substance noire pars compacta (SNc) et une accumulation d'α-synucléine agrégée. L'inflammation et la prédisposition génétique contribuent à la MP en tant que facteurs principaux de comorbidité. Dans cette thèse, j'ai étudié, in vivo et post mortem, les effets de trois facteurs sur le système dopaminergique: 1) l'agrégation d'α-synucléine, 2) la toxicité additionnelle des mutations LRRK2 et 3) une neuroinflammation modérée. Pour ce faire, l'imagerie par Tomographie par Emission de Positons (TEP) et des tests comportementaux ont été utilisés. J'ai utilisé les radiotraceurs [18F]LBT-999 et [18F]FMT pour mesurer respectivement les taux cérébraux du Transporteur de la dopamine (DAT) et de l'AADC, l'enzyme de synthèse de la dopamine. Pour évaluer l'inflammation j'ai utilisé le [18F]DPA714, un radiotraceur de référence pour la neuroinflammation radioligand du TSPO 18kDa,. Les résultats obtenus ont été validés par des techniques post mortem évaluant l'expression des gènes (RT-qPCR) et des protéines (immunohistochimie).

Les résultats de mes travaux montrent que la surexpression de l'α-synucleine humaine « sauvage » obtenue par transduction de la substance noire par des vecteurs viraux (AAV2/6-PGK-WT-α-synuclein) ne génère ni perte neuronale détectable dans la substance noire, ni déficits moteur, ni changements majeurs du système dopaminergique observé par imagerie TEP in vivo. D'autre part, utilisant cette même stratégie d'expression par vecteur viral (AAV2/6-PGK-A53T-α-synucléine), j'ai démontré une agrégation significative de l'α-synucléine mutée (A53T) dans la substance noire dès 8 semaines post-injection, celle-ci restant très faible dans le striatum. Les analyses quantitatives en microscopie montrent que la surexpression de l'α-synucléine induit une dégénérescence modérée mais significative des neurones dopaminergiques, s'aggravant au cour du temps. La perte des fibres dopaminergiques détectées par l'immunohistochimie de la Tyrosine Hydroxylase (TH) reste cependant très modérée dans le striatum. Les résultats obtenus par imagerie TEP montrent une réduction du DAT dans le striatum, au contraire de l'AADC dont les niveaux restent stables. Ainsi, les données in vivo combinées aux observations *post-mortem* suggèrent que l'imagerie TEP du DAT ne reflète pas seulement la perte neuronale induite par l'α-synucléine, mais aussi une dérégulation fonctionnelle de la synapse dopaminergique. Celle-ci pourrait permettre, via la baisse du transporteur, et en présence de niveau normaux de TH et AADC le maintien des concentrations synaptiques de dopamine dans le striatum. J'ai également montré que cette perte neuronale coïncidait avec une réponse inflammatoire initialement modérée, suivie d'une réponse microgliale plus prononcée. Enfin, dans le modèle viral de co-expression des vecteurs AAV2/6-PGK-A53T-α-synucléine et AAV2/6-PGK-G2019S-LRRK2, nous n'avons pas observé que la présence de LRRK2 mutée augmentait la toxicité de l'α-synucléine.

Dans le modèle de neuroinflammation induite par l'injection de LPS, l'imagerie TEP et les analyses *post-mortem* montrent l'absence de perte des neurones dopaminergiques. Néanmoins, j'ai mis en évidence une corrélation inverse significative entre les marqueurs de sévérité de l'inflammation (l'imagerie TEP des TSPO, expression IBA1) et les marqueurs de production (TH) et de stockage (VMAT2) de la dopamine. Ces données renforcent l'hypothèse que la neuroinflammation altère la fonctionnalité du système dopaminergique, indépendamment de la perte neuronale dopaminergique.

# Thesis summary in Dutch

De cerebrale pathologie van de ziekte van Parkinson (PD) wordt gekenmerkt door een progressief verlies van de dopaminerge neuronen in de substantia nigra en de accumulatie van α-synucleïne-aggregaten. Neuroinflammatie en genetische aanleg zijn de belangrijkste comorbiditeitsfactoren voor PD. In dit proefschrift heb ik getracht om zowel *in vivo* als *post-mortem* de effecten van drie factoren op het dopaminerge systeem en dopaminerge neuronale overleving te evalueren: 1) α-synucleïne overexpressie, 2) co-overexpressie van α-synucleïne en LRRK2, en 3) milde neuroinflammatie. Daartoe zijn Positron Emissie Tomografie (PET) beeldvorming en gedragsstudies geselecteerd als de belangrijkste *in vivo* technieken. Ik heb [$^{18}$F]LBT-999 en [$^{18}$F]FMT PET beeldvorming gebruikt om dopamine transporter (DAT) en het dopamine-synthetiserend enzym AADC, respectievelijk, te evalueren in het striatum. Om de neuroinflammatie te evalueren, heb ik [$^{18}$F]DPA714 gebruikt om 18kDa TSPO binding in beeld te brengen. De *in vivo* resultaten werden vervolgens gevalideerd door *post-mortem* technieken die gen- (door RT-qPCR) en eiwitexpressie (door immunohistochemie) evalueren op dezelfde modellen.

In het resulterende werk heb ik aangetoond dat overexpressie van humane WT-α-syncleïne in de substantia nigra door middel van virale vectoren (AAV2/6-PGK-WT-α-synuclein) hier geen detecteerbaar verlies van dopaminerge neuronen genereert, noch *in vivo* motorische symptomen veroorzaakt of andere veranderingen in het dopaminerge systeem zoals in beeld gebracht met *in vivo* PET-beeldvorming. Anderzijds heb ik hier aangetoond dat overexpressie van A53T-α-synucleïne in de substantia nigra, met behulp van een AAV2/6-PGK-A53T-α-synuclein virale vector benadering, resulteerde in significante α-synucleïne-aggregatie in de substantia nigra reeds na 8 weken, maar niet in het striatum. Kwantitatieve microscopische analyse laat zien dat α-synucleïne-aggregatie een milde maar progressieve degeneratie van dopaminerge neuronen in de substantia nigra veroorzaakte. Het verlies van dopaminerge vezels in het striatum, zoals gezien met immunohistochemie van tyrosine hydroxylase (TH) bleef echter beperkt. PET-beeldvorming van DAT, maar niet van AADC, gaf een duidelijke aanwijzing voor progressief verlies van de dopaminerge neuron. De combinatie van de *in vivo* en *post-mortem* data suggereert dat DAT-PET-beeldvorming niet alleen het neuronaal verlies reflecteert, veroorzaakt door α-synucleïne accumulatie, maar ook beïnvloed wordt door functionele aanpassingsmechanismen van de dopaminerge synaps. Een vermindering van DAT expressie, in combinatie met normale TH en AADC expressie, zou de hoeveelheid dopamine in de synapse kunnen normaliseren. In parallel werd aanvankelijk een matige response waargenomen gevolgd door een meer uitgesproken microgliale respons. Daarnaast heb ik geen verergerd toxisch effect gemeten van co-overexpressie van G2019S gemuteerd LRRK2 en A53T-α-synucleïne op A53T-α-synucleïne toxiciteit.

In een acuut neuro-inflammatoir model geïnduceerd door intrastriatale LPS-injectie heb ik in *post-mortem* een afwezigheid van dopaminerge neuronaal verlies waargenomen in de substantia nigra alsmede een afwezigheid van synaptisch verlies in het striatum. Desalniettemin heb ik een significante inverse correlatie waargenomen tussen inflammatiemarkers (TSPO-PET en IBA1 expressie) en markers voor dopamine productie (TH) en opslag (VMAT2). Deze data ondersteunen de hypothese dat neuroinflammatie de functionaliteit van dopaminerge markers kan veranderen, ongeacht de aanwezigheid van neuronaal verlies.

Samengevat laat mijn thesis dus zien dat er een belang is voor het gebruik van PET beeldvorming om functionele schade aan het dopaminerge systeem weer te geven in vivo, die niet aangetoond kan worden door middel van *post-mortem* technieken in PD diermodellen.

université PARIS-SACLAY

**ECOLE DOCTORALE N°568**
Signalisations et réseaux intégratifs en biologie (Biosigne)

**Titre :** Évaluation du système dopaminergique en utilisant l'imagerie TEP in vivo et des analyses post mortem dans le contexte d'un mod PD neurodégénératif et neuroinflammatoire léger

**Mots clés :** La maladie de Parkinson, dopamine, neuroimagerie, compensation, système nigrostriatal

**Résumé :** La maladie de Parkinson (MP) est caractérisée par l'agrégation de l'α-synucléine, la perte des neurones qui synthétisent la dopamine (neurone DA), et une inflammation cérébrale.

Pendant ma thèse, j'ai évalué les effets de l'α-synucléine et de l'inflammation modérée sur les neurones DA dans des modèles animaux de la MP. J'ai utilisé une méthode d'imagerie nucléaire, la tomographie d'émission de positons (TEP) et des analyses post mortem évaluant l'expression de différents gènes et protéines dans ces modèles.

J'ai démontré que l'α-synucléine mutée induit une mort des neurones DA, et une faible réponse inflammatoire. À l'inverse, l'inflammation modérée n'entraîne pas la mort de ces neurones. Dans les deux cas, la TEP montre de plus des atteintes fonctionnelles des neurones DA, qui ne sont pas détectées par les analyse post mortem, soulignant l'intérêt crucial de cette méthode non invasive pour mieux caractériser la dégénérescence dans les modèles animaux de la MP.

**Title :** Evaluation of the dopaminergic system using in vivo PET imaging and post-mortem analyses in the context of mild neurodegenerative and neuroinflammatory PD models

**Keywords :** Parkinson's disease, dopamine, neuroimaging, compensation, nigrostriatal system

**Abstract :** Parkinson's disease (PD) is characterised by the aggregation of α-synuclein, a progressive loss of the dopamine-producing neurons, and the presence of neuroinflammation

During my PhD studies, I evaluated the impact of α-synuclein aggregation and moderate neuroinflammation on dopaminergic neurons in animal models of PD. To this end, I have used a nuclear imaging method, positron emission tomography (PET), and *post-mortem* analyses to assess the expression of different genes and proteins in these models.

I have demonstrated that mutated α-synuclein induces mild progressive death of dopamine neurons, coupled with a weak inflammatory response. Conversely, mild neuroinflammation did not lead to loss of dopamine neurons. PET imaging showed functional damage to the dopamine neurons, which was not detectable by *post-mortem* analyses. This highlights the crucial interest PET imaging to better characterise neurodegeneration in animals models of PD.